

Starch nanoparticles: Isolation, characterization and applications

by

Mariana Pérez Herrera

A thesis submitted in partial fulfillment of the requirements for the degree of

Doctor of Philosophy

in

Food Science and Technology

Department of Agricultural, Food and Nutritional Science
University of Alberta

© Mariana Pérez Herrera, 2016

ABSTRACT

Starch nanoparticles (SNP) were isolated by acid hydrolysis from starches varying in amylose content and crystalline type, and physicochemically characterized in terms of their morphology, particle size, crystallinity, molecular size distribution, chain length distribution, amylase resistance and thermal and rheological properties. Scanning electron microscopy and dynamic light scattering studies revealed that the SNP varied in size (50-500 nm) and shape (elliptical, oval, irregular, polygonal) according to the starch type. X-ray diffraction confirmed a crystalline transformation from B-type to A-type in B-type SNP, while A-type SNP remained the same as the native starch. The data indicated a positive correlation between the amylose content and SNP yield. A model for the release of SNP as individual amylopectin blocklets and the formation of recrystallized short chain amylose spherulites during the acid hydrolysis treatment was postulated. The average molecular weight and linear chain length distribution of SNP were determined by high performance size exclusion chromatography and high performance anion exchange chromatography with pulsed amperometric detector, respectively. Different eluting profiles and detectable degrees of polymerization were observed between waxy, normal, hylon V and hylon VII starches. The resistance of maize SNP towards amylolysis followed the order: hylon VII > hylon V > normal > waxy. The data showed the potential amylose involvement in the SNP structure of B-type high amylose maize starches. A rheological study confirmed that the variations in the starch source, morphology and thermal stability of SNP influence their viscosity and viscoelastic properties as a function of shear rate, frequency and temperature. Regardless of the starch source, all SNP suspensions at 5% (w/v) exhibited a viscosity profile similar to that of lyotropic liquid crystal polymers like cellulose nanocrystals. The data suggested that processing

conditions such as heating temperature and shearing can alter the functional properties of SNP. The potential application of SNP as a texture modifier in different gum systems (λ -carrageenan, xanthan) was also investigated. Binary blends consisting of 0.5% (w/v) gum and different concentrations of SNP (waxy and hylon VII) were prepared. The effect of SNP source and concentration on the viscosity and viscoelastic behaviour varied with gum type. The addition of SNP helped maintain a stable viscoelastic behaviour in particular in gum systems with low viscosity and elasticity such as λ -carrageenan, whereas it did not significantly change the rheological behaviour of a high viscosity system like xanthan gum.

PREFACE

This research was financially supported by the Natural Sciences and Engineering Research Council (NSERC) of Canada and a graduate student scholarship by Alberta Innovates -Technology Futures (AITF) and Alberta Enterprise and Advanced Education.

The following journal papers have been published from the work completed in this thesis.

Chapter 3 was published as Perez Herrera, M., Vasanthan, T. and Hoover, R. 2016. Characterization of maize starch nanoparticles prepared by acid hydrolysis. *Cereal Chemistry*, volume 93, 323-330.

Chapter 4 has been accepted for publication as Perez Herrera, M., Vasanthan, T., Hoover, R. and Izydorczyk, M. 2016. Molecular size distribution and amylase-resistance of maize starch nanoparticles prepared by acid hydrolysis. *Cereal Chemistry*, DOI:10.1094/CCHEM-02-16-0028-R

Chapter 5 has been accepted for publication as Perez Herrera, M., Vasanthan, T. and Chen, L. 2016. Rheology of starch nanoparticles as influenced by particle size, concentration and temperature. *Food Hydrocolloids*, DOI:10.1016/J.FOODHYD.2016.11.026

In the majority of the projects, I was responsible for the experimental work, data analysis and manuscript composition. Thava Vasanthan (supervisory author) and Ratnajothi Hoover, assisted with scientific discussions and idea development, manuscript edits and composition. In the collaborative projects, Marta Izydorczyk (Research scientist, Canadian Grain Commission) and Lingyun Chen (University of Alberta) provided insightful experimental planning, manuscript revisions and analysis equipment.

Part of the work completed during the beginning of my graduate studies, prior to transferring to my PhD program focused on oat grain quality. The study investigated how environmental

growing conditions and cultivar type influence the composition and physicochemical properties (viscosity and solubility) of oat cultivars grown in Canada. As this is not directly related to the thesis research on starch nanoparticles, the work is presented in the Appendix I. In this project, I was responsible for the experimental work and manuscript composition, while all collaborators assisted in data analysis and manuscript edits. The work completed was published as Herrera, M. P., Gao, J., Vasanthan, T., Temelli, F., & Henderson, K. 2016. β -Glucan content, viscosity, and solubility of Canadian grown oat as influenced by cultivar and growing location. *Canadian Journal of Plant Science*, volume 96, 183-196.

ACKNOWLEDGEMENTS

I would like to begin by thanking my supervisor Dr. Thava Vasanthan for giving me the opportunity to develop my research skills, for his guidance and for always pushing me to strive for more. To both members of my supervisory committee, Dr. Feral Temelli and Dr. Michael Gänzle for their valuable experience and willingness to help. I thank my collaborators, Dr. Ratnajothi Hoover (Memorial University of Newfoundland) for his time and invaluable critical review of my manuscripts; Dr. Marta Izydorczyk (Canadian Grain Commission) and Dr. Lingyun Chen for their help with experimental planning and for providing valuable experimental equipment. My appreciation is also extended to Nataly Lopez and Naguleswaran Sabaratnam for being part of excellent research discussions and long working days and to Jun Gao, Nathan Gerein, Sharon Bazin and Yi Xiang Wang for their extensive technical assistance. To the staff in our department, Jody Forslund, Holly Horvath, Robin Miles, Urmila Basu, Susan Gibson, for all their day to day work in helping students. I would like to thank my friends for making me feel at home, away from home. To Sean Molesky for his complete support and encouragement during the highs and lows and for always having time to help and listen. Lastly, I would like to thank my parents (Estela Herrera Carlón and Mariano Pérez Vivanco) and sister (Jimena Pérez Herrera) for their unconditional love and support in this journey away from home.

TABLE OF CONTENTS

Chapter 1 Introduction and objectives	1
1.1. INTRODUCTION	1
1.2. RESEARCH OBJECTIVES AND HYPOTHESIS	3
Chapter 2 Literature review	5
2.1. GRAIN STRUCTURE AND COMPOSITION	5
2.2. STARCH	6
2.2.1. Granule morphology.....	7
2.2.2. Granule architecture	11
2.2.3. Gelatinization and retrogradation.....	20
2.2.4. Acid hydrolysis.....	21
2.2.4.1 Effect of acid type and starch source on the rate of hydrolysis.....	22
2.2.4.2 Acid-treated starches.....	25
2.3. STARCH NANOPARTICLES.....	26
2.3.1. Isolation and preparation methods.....	28
2.3.1.1 Acid hydrolysis	29
2.3.1.2 Enzymatic hydrolysis.....	31
2.3.1.3 Physical treatments	33
2.3.2. Characterization	36
2.3.2.1 Morphology.....	36
2.3.2.2 Crystallinity	38
2.3.2.3 Molecular structure	39
2.3.2.4 Thermal stability	40
2.3.2.5 Rheological properties.....	41

2.3.3. Current uses and potential applications	43
2.3.3.1 Non-food applications	43
2.3.3.2 Food applications.....	46
Chapter 3 Characterization of maize starch nanoparticles prepared by acid hydrolysis.....	48
3.1. INTRODUCTION	48
3.2. MATERIALS AND METHODS	49
3.2.1. Materials.....	49
3.2.2. Chemical composition	50
3.2.3. Acid hydrolysis of native starches and fractionation of hydrolyzed starch residues..	50
3.2.4. Scanning electron microscopy.....	52
3.2.5. X-ray diffraction	52
3.2.6. Turbidity.....	53
3.2.7. Statistical analysis.....	53
3.3. RESULTS AND DISCUSSION.....	53
3.3.1. Solubilization patterns.....	53
3.3.2. Fractionation of acid hydrolyzed starch	55
3.3.3. Turbidity measurements	58
3.3.4. Mass balance of fractions 1, 2 and 3.....	60
3.3.5. Morphology of native starch and their acid hydrolyzed fractions 2 and 3	62
3.3.6. X-ray diffraction	64
3.4. CONCLUSIONS	70
Chapter 4 Molecular size distribution and amylase-resistance of maize starch nanoparticles prepared by acid hydrolysis.....	71
4.1. INTRODUCTION	71

4.2. MATERIALS AND METHODS	73
4.2.1. Materials.....	73
4.2.2. Acid hydrolysis and isolation of SNP	73
4.2.3. Weight average molecular weight (M_w) of SNP	73
4.2.3.1 Gelatinization and solubilization of SNP.....	73
4.2.3.2 Preparation of debranched SNP	74
4.2.3.3 HPSEC-MALLS-RI System.....	74
4.2.4. Linear chain length distribution of SNP	75
4.2.4.1 HPAEC-PAD System.....	75
4.2.5. Resistant starch content of SNP	75
4.2.6. SEM of the RS residues of SNP from hylon V and VII	76
4.2.7. M_w and linear chain length distribution of RS residues from hylon V and VII	76
4.2.8. Statistical analysis.....	76
4.3. RESULTS AND DISCUSSION.....	77
4.3.1. HPSEC profiles of SNP before debranching.....	77
4.3.2. HPSEC profiles of SNP after debranching.....	79
4.3.3. HPAEC profiles and linear chain length distribution of SNP.....	82
4.3.4. Amylolysis of SNP by pancreatic α -amylase	84
4.3.5. Morphology, M_w and linear chain length distribution of the SNP RS residue	85
4.4. CONCLUSIONS	90
Chapter 5 Rheology of starch nanoparticle suspensions as influenced by particle size, concentration and temperature	91
5.1. INTRODUCTION	91
5.2. MATERIALS AND METHODS	94

5.2.1. Materials.....	94
5.2.2. Isolation of SNP by acid hydrolysis	95
5.2.3. Field emission scanning electron microscopy (FE-SEM)	95
5.2.4. Dynamic light scattering (DLS).....	95
5.2.5. Static and dynamic rheological properties.....	96
5.2.6. Statistical analysis.....	97
5.3. RESULTS AND DISCUSSION.....	97
5.3.1. Morphology and particle size distribution	97
5.3.2. Thermal stability of SNP suspensions by DLS	101
5.3.3. Viscosity of SNP suspensions.....	106
5.3.4. Dynamic rheological properties as a function of frequency	110
5.3.5. Dynamic rheological properties as a function of temperature.....	112
5.4. CONCLUSIONS	117
Chapter 6 Rheological characterization of gum and starch nanoparticle blends	118
6.1. INTRODUCTION	118
6.2. MATERIALS AND METHODS	122
6.2.1. Materials.....	122
6.2.2. Isolation of SNP by acid hydrolysis	122
6.2.3. Preparation of SNP suspensions and gum-SNP blends	122
6.2.4. Static and dynamic rheological properties.....	123
6.3. RESULTS AND DISCUSSION.....	125
6.3.1. Viscosity of SNP suspensions as a function of concentration	125
6.3.2. Rheological properties of CAR-SNP blends	128
6.3.3. Rheological properties of XAN-SNP blends	134

6.4. CONCLUSIONS	139
Chapter 7 General conclusions	140
7.1. SUMMARY AND SIGNIFICANCE OF RESEARCH.....	140
7.2. RECOMMENDATIONS FOR FUTURE WORK	144
References	145
APPENDIX I	158
APPENDIX II	185
APPENDIX III	192

LIST OF TABLES

Table 3.1 Light transmittance of fraction 2 in suspension form	59
Table 3.2 Mass balance of the acid hydrolyzed starch fractions.....	61
Table 4.1 Average molecular weight (M_w) and relative content (%) of high and low molecular weight fractions in solubilized SNP	79
Table 4.2 Average molecular weight (M_w) and relative content (%) of four different fractions present in solubilized and debranched SNP	81
Table 4.3 Chain length distributions of SNP after debranching with isoamylase	84
Table 4.4 Resistant starch content of SNP from maize starches.....	85
Table 5.1 Particle size of SNP determined by FE-SEM at room temperature and DLS after incubation at different temperatures.....	100
Table 6.1 Preparation of binary blends of SNP suspensions and gums	123

LIST OF FIGURES

Figure 2.1 Scanning electron microscopy images of native starch granules from (A) wheat, (B) corn, (C) potato and (D) pea.	8
Figure 2.2 Molecular structure of A) amylose and B) amylopectin.....	10
Figure 2.3 Schematic representation of the starch granule structural hierarchy.....	12
Figure 2.4 Basic labelling of A, B and C chains in amylopectin clusters.	13
Figure 2.5 Alternative models of amylopectin cluster organisation.	15
Figure 2.6 Crystalline structures of A- and B-type polymorphs.	17
Figure 2.7 X-ray diffraction patterns of A-, B-, and C-type starches with their d-spacings (Å).	18
Figure 2.8 Mechanism of acid hydrolysis of starch.	23
Figure 2.9 Transmission electron microscopy images of waxy maize SNC (scale bar = 50 nm). .	29
Figure 2.10 Formation of sulfate esters and formic and levulinic acids on the surface of SNC...	32
Figure 3.1 Protocol for acid hydrolysis and fractionation of the hydrolyzed starch residues.	51
Figure 3.2 Acid hydrolysis profile of native starches in 3.16 M of H ₂ SO ₄ at 40°C.	54
Figure 3.3 Scanning electron microscopy image showing surface granule pores in native normal maize starch.	56
Figure 3.4 Suspensions of fraction 2 obtained after (A) 1, (B) 3 and (C) 6 days of acid hydrolysis.	57
Figure 3.5 Scanning electron microscopy images of native starch granules and fractions 2 and 3 collected after 6 days of acid hydrolysis.....	63
Figure 3.6 Scanning electron microscopy images of fraction 3 suspension of waxy maize collected after 6 days of acid hydrolysis.	65

Figure 3.7 X- ray diffraction patterns and relative crystallinity (RC) of (A) native starch, (B) fraction 2 and (C) fraction 3 collected after 6 days of acid hydrolysis.....	66
Figure 3.8 Sequence of events leading to the released of individual blocklets and the formation of retrograded amylose (AM) chains during acid hydrolysis of normal and high amylose maize starches.	69
Figure 4.1 HPSEC profiles of solubilized SNP from maize starches of varying amylose content. 78	
Figure 4.2 HPSEC profiles of solubilized and debranched SNP from maize starches of varying amylose content.	80
Figure 4.3 Chromatograms of isoamylase debranched SNP from maize starches analyzed by HPAEC-PAD.	83
Figure 4.4 Field emission scanning electron microscopy images of SNP from hylon V and hylon VII.	86
Figure 4.5 HPSEC profiles of the RS residue obtained from SNP of hylon V and hylon VII, (A) before and (B) after debranching.	88
Figure 4.6 Chromatograms of isoamylase debranched RS residue obtained from SNP of hylon V and hylon VII analyzed by HPAEC-PAD.	89
Figure 5.1 Scanning electron microscopy images of SNP from (A) wheat, (B) oat, (C) barley and (D) potato isolated by acid hydrolysis.	98
Figure 5.2 Particle size distribution of SNP suspensions after incubation at: (A) 25°C and (B) 80°C, respectively.	103
Figure 5.3 Schematic diagram showing the network formation of SNP suspensions from amylose containing starches.	105

Figure 5.4 SNP aqueous suspensions: (A), 1% w/v, liquid-like behaviour; and (B), 5% w/v, gel-like behaviour.	106
Figure 5.5 Apparent viscosity of 1% and 5% SNP suspensions as a function of shear rate.	108
Figure 5.6 Storage modulus (G') and loss modulus (G'') of 5% SNP suspensions as a function of frequency at 25°C. The solid symbols represent G' and the open symbols represent G''	111
Figure 5.7 Storage modulus (G') and loss modulus (G'') of 5% SNP suspensions from (A) wheat, (B) oat, (C) barley and (D) potato as a function of temperature. The solid symbols represent G' and the open symbols represent G''	113
Figure 5.8 Complex viscosity of 5% SNP suspensions as a function of temperature.	116
Figure 6.1 Apparent viscosity of waxy and hylon VII SNP suspensions at various concentrations as a function of shear rate.	127
Figure 6.2 Apparent viscosity of CAR-SNP blends as a function of shear rate.	129
Figure 6.3 Storage modulus (G') and loss modulus (G'') of CAR-SNP blends as a function of frequency. The solid symbols represent G' and the open symbols represent G''	131
Figure 6.4 Storage modulus (G') and loss modulus (G'') of CAR-SNP blends as a function of temperature. The solid symbols represent G' and the open symbols represent G''	132
Figure 6.5 Apparent viscosity of XAN-SNP blends as a function of shear rate.	135
Figure 6.6 Storage modulus (G') and loss modulus (G'') of XAN-SNP blends as a function of frequency. The solid symbols represent G' and the open symbols represent G''	136
Figure 6.7 Storage modulus (G') and loss modulus (G'') of XAN-SNP blends as a function of temperature. The solid symbols represent G' and the open symbols represent G''	138

LIST OF SYMBOLS AND ABBREVIATIONS

Å	Angstrom
ADP	Adenosine Diphosphate
<i>ae</i>	Amylose-Extender
AFM	Atomic Force Microscopy
AM	Amylose
AP	Amylopectin
CL	Chain Length
CNC	Cellulose nanocrystals
DLS	Dynamic Light Scattering
DMSO	Dimethyl Sulfoxide
DP	Degree of Polymerization
DSC	Differential Scanning Calorimetry
FE-SEM	Field Emission Scanning Electron Microscope
G^*	Complex Modulus
G'	Storage Modulus
G''	Loss Modulus
GBSS	Granule Bound Starch Synthase
GOPOD	Glucose Oxidase Peroxidase
HCl	Hydrochloric Acid
HNO ₃	Nitric Acid

H ₂ SO ₄	Sulfuric Acid
H ₃ PO ₄	Phosphoric Acid
HPAEC-PAD	High Performance Anion Exchange Chromatography with Pulsed Amperometric Detector
HPSEC	High Performance Size Exclusion Chromatography
HV	Hylon V Maize
HVII	Hylon VII Maize
MALLS	Multi Angle Laser Light Scattering
M _w	Weight Average Molecular Weight
NM	Normal Maize
PSD	Particle Size Distribution
RC	Relative Crystallinity
RI	Refractive Index
RS	Resistant Starch
SEM	Scanning Electron Microscopy
SNC	Starch Nanocrystals
SNP	Starch Nanoparticles
T _c	Conclusion Temperature
T _c - T _o	Transition Temperature Range
T _o	Onset Temperature
T _p	Peak Temperature
TEM	Transmission Electron Microscopy

T%	Light Transmittance
WM	Waxy Maize
Wt%	Weight Percent
ω	Angular Frequency
η^*	Complex Viscosity
ΔH	Enthalpy of Gelatinization
θ	Theta

CHAPTER 1 Introduction and objectives

1.1. INTRODUCTION

Starch is a natural biopolymer of alpha-D-glucose that can be isolated from cereals, legumes, tubers and roots. It is extensively used as a food and non-food ingredient due to its renewable and biodegradable nature, vast abundance and cheap market price. In food, starch is commonly used for its thickening, gelling, emulsifying, encapsulation and fat replacement functionalities. In non-food applications it has been used for the production of starch based bioethanol, bioplastics (polylactic acid, thermoplastic starch), as a paper coating material and more recently as a reinforcing agent in polymer nanocomposites and nanogels. Research has shown that the morphology, molecular characteristics and granule architecture of starch determine its functional and physicochemical properties such as swelling capacity, solubility, gelatinization and retrogradation, crystallinity, rheology and digestibility. In most commercial applications, chemical modifications such as cross-linking and substitution play a significant role in improving the functional properties of native starches.

Over the past decade, research in the area of starch nanotechnology has been gaining momentum in the food and biomaterial industry. Particularly a great deal of interest has emphasized the development of new ingredients and nanomaterials. Starch nanocrystals (SNC) and starch nanoparticles (SNP) are commonly prepared by acid hydrolysis and have been successfully used as a filler in polymer matrices to improve the mechanical and barrier properties (Angellier et al. 2005a). SNC and SNP are crystalline structures resulting from the disruption of the amorphous regions of the starch granules by acid hydrolysis (Le Corre and Angellier-Coussy

2014). To date, the majority of the research on SNP has focused on one type of starch, namely waxy maize. Waxy maize is genetically modified to contain high amounts of amylopectin in comparison to regular starches and thus more crystalline material is available for isolation. Previous research has shown that starches obtained from different botanical origins vary in their functional properties (Hoover and Ratnayake 2002). Yet it remains an open question as to whether or not at the nanoscale all these structures have a common building block. Furthermore, despite the vast amount of research conducted over the past decade with regard to the isolation, characterization and potential applications of SCN and SNP, the relationship between structure and function of SNP, in particular in amylose containing starches is not well understood.

Historically, the study of starch has always been motivated by cellulose research and this thesis research follows the same logic. Cellulose nanocrystals (CNC) were first isolated in the 1950s by a controlled acid hydrolysis process using sulfuric acid (Rånby and Ribi 1950). Previous research has shown that the geometrical dimensions (length and width) of CNC, which vary according to the cellulosic material and the acid hydrolysis conditions play an important role in the strengthening and mechanical properties of this material. Before SNP can be used as an alternative source to CNC, more research is needed to determine how the starch source (morphology, amylose content, crystalline type, etc.) and molecular characteristics of SNP influence their physicochemical and functional properties. This thesis research is geared towards understanding how variations in the starch molecular composition and botanical origins would influence the SNP properties and thus provide a guideline in selecting the appropriate starch type for a target functionality. The outcome of this thesis research, may also provide fundamental information with regard to the starch granular structure, in particular to the presence and

location of amylose molecules within the crystalline and amorphous regions of different starch types.

1.2. RESEARCH OBJECTIVES AND HYPOTHESIS

The overall objective of this thesis was to investigate the isolation of SNP by acid hydrolysis from starches varying in amylose content and crystalline type, and characterize their structural and physiochemical properties in order to understand how structure impacts their potential food and non-food applications. This study was also expected to further elucidate the role of amylose and amylopectin in the starch granular architecture, in particular to understand the role of amylose in A- and B- type crystallites. The specific objectives of this research were as follows:

Objective 1

Hypothesis: The yield, morphology, particle size and crystallinity of SNP significantly differ between waxy and amylose containing starches.

Objective: To investigate the impact of water washings on the extent of SNP isolation from the acid hydrolyzed residue containing unhydrolyzed and partially hydrolyzed starch granules and determine whether varying the amylose content among waxy (0% amylose), normal (21.6% amylose), hylon V (47.0% amylose) and hylon VII (71.0% amylose) maize starches influences the yield, morphology, particle size and crystallinity of the SNP (Chapter 3).

Objective 2

Hypothesis: The molecular characteristics of SNP significantly differ between waxy and amylose containing starches, where the crystalline structure and molecular composition of high amylose maize SNP provides acid and enzymatic resistance.

Objective: To characterize the weight average molecular weight and chain length distribution of SNP from maize starches varying in amylose content and crystalline type, to determine the susceptibility of SNP from waxy, normal and high amylose starches to hydrolysis by porcine pancreatic α -amylase and to characterize the morphology, weight average molecular weight and chain length distribution of the amylase-resistant SNP residues from high amylose maize starches (Chapter 4).

Objective 3

Hypothesis: The starch source, morphology and crystalline type will significantly influence the thermal stability of SNP and their viscosity and viscoelastic behaviour in suspension form.

Objective: To compare the temperature effect on particle size of SNP isolated from native starches of different botanical origins (wheat, oat, barley, potato), showing comparable amylose contents but different crystalline types and to understand the static and dynamic rheological properties of aqueous SNP suspensions as a function of shear rate, frequency and temperature (Chapter 5).

Objective 4

Hypothesis: The viscosity and viscoelastic behaviour of the binary blends of gums and SNP will vary according to the gum type and SNP source and concentration.

Objective: To investigate how the SNP source and concentration influence the rheological properties of common food gums (λ -carrageenan and xanthan) as a function of shear rate, frequency and temperature (Chapter 6).

CHAPTER 2 Literature review

2.1. GRAIN STRUCTURE AND COMPOSITION

In the taxonomy of plants, grain crops primarily belong to two families known as *Gramineae* and *Leguminosae*. The family *Gramineae* includes all major cereals such as wheat, corn, oat, barley, rice, rye, whereas the family *Leguminosae* includes pulses like field pea, lentil, chickpea, dry beans, etc. Cereal and pulse grains share compositional similarities in the hull, bran, endosperm, germ and cotyledon. However, the extent to which each tissue layer develops is different. Cereal grains are comprised of a hull or husk (13-25 wt %), the bran layer (6-15 wt %), a germ or embryo (2-12 wt %) and an endosperm (63-86 wt %) (Evers and Millar 2002). The husk is the outermost layer which is composed of cellulose, hemicellulose and lignin. In some grains (wheat and rye) the husk is not adhered to the fruit coat and can be easily removed; however, other cereals including oats and barley require mechanical removal. The bran layer found between the husk and the endosperm is made up of the pericarp, seed coat, aleurone and sub-aleurone layers. The germ contains the cotyledon and is rich in lipids and protein, while in the endosperm, starch is embedded in a protein matrix. In comparison, pulse grains have a well-developed cotyledon that acts as the major storage organ for starch and protein, a very small endosperm and are devoid of aleurone and sub-aleurone layers in the bran.

Cereal grains have a characteristic composition which is high in carbohydrates and low in protein, while pulses have significantly higher protein content. Cereals are composed of starch (56-73 wt %), fiber (2-13 wt %), protein (7-12 wt %), lipids (1-7 wt %) and minor amounts of vitamins and minerals (Koehler and Wieser 2013). The chemical composition of cereal grains can

vary by variety (genotypes) and growing conditions (temperature and water). According to Kim et al. (2003), the total starch, crude protein, soluble and insoluble fibre contents of three different wheat varieties grown in high, medium and low rainfall conditions significantly varied. Rainfall correlated to the total starch content, while the harvest year had a strong influence in the overall chemical composition. Similar observations have been reported for other cereal grains including barley (Ehrenbergerová et al. 2008) and oats (Doehlert and Simsek 2012; Redaelli et al. 2013). However, variations in the chemical composition of oats and barley have focused primarily in the β -glucan content and its physicochemical properties. My research contribution to this topic is included in Appendix I.

2.2. STARCH

Starch is a biopolymer that exists as a storage material in most cereal and pulse grains, as well as in tubers and roots. It is synthesized during tissue development and maturation by amyloplast enzymes such as ADP-glucose pyrophosphorylase, starch synthase and starch branching enzymes. Starch occurs in the form of granules, which vary in shape and size according to their botanical origin. Native starch granules represent a unique model of molecular architecture, which includes the whole granule, growth rings, blocklets, amorphous and crystalline lamellae and linear (amylose) and branched (amylopectin) chains. The granules are semi-crystalline in nature and almost entirely composed of two glucose polysaccharides, amylose and amylopectin. Aside from amylose and amylopectin, the starch granule contains very small amounts of protein, lipid and phosphorous. Protein is present in the form of enzymes such as granule-bound starch synthase (GBSS), while the lipids are associated with amylose molecules to

form a complex and phosphorous is found in the phospholipids and as phosphate monoesters (Pérez and Bertoft 2010).

2.2.1. Granule morphology

Microscopy techniques such as scanning electron microscopy (SEM), transmission electron microscopy (TEM), atomic force microscopy (AFM) and confocal laser scanning microscopy (CLSM) have been commonly used to study the surface and interior morphology of starch granules. Native starch granules differ in their surface morphology according to the botanical origin and plant maturity. Granules can occur in different shapes (round, spherical, polygonal, lenticular, and filamentous) and a wide range of sizes (2-100 μm). Most cereal starches like wheat, rye and barley have a bimodal size distribution with small and large granules. For example, wheat starch is composed of large lenticular and small round starch granules (Figure 2.1A). Corn starch granules on the other hand have a unimodal size distribution with round, spherical and polygonal shapes and diameters in the range of 5 to 18 μm (Figure 2.1B). Granules from tuber and legume starches such as potato and pea, are larger in size and spherical or irregular disc shaped, respectively (Figure 2.1C-D). In comparison to cereal starches, tuber starches have a smoother outer surface and lower number of pore cavities, whereas legume starches have a large number of indentations (Figure 2.1D). CLSM in combination with fluorescent staining can be used to visualize the starch granule pores and channels and detect the presence of granule bound proteins and phospholipids (Naguleswaran et al. 2011).

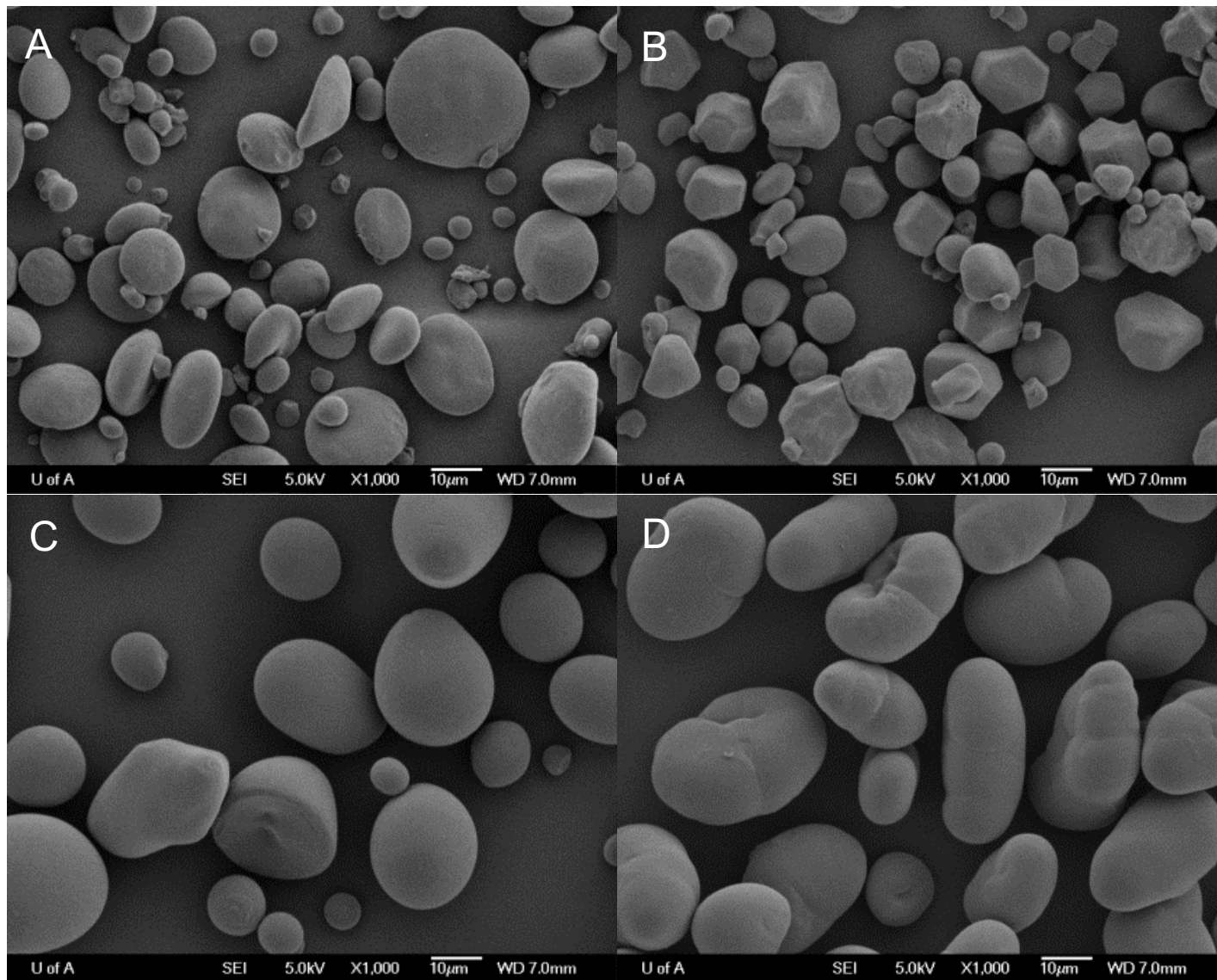


Figure 2.1 Scanning electron microscopy images of native starch granules from (A) wheat, (B) corn, (C) potato and (D) pea.

Starch granules are composed of two types of anhydroglucose polymers, amylose (Figure 2.2A) and amylopectin (Figure 2.2B). Amylose is a relatively long, linear molecule with few branches, containing 99% α - (1 \rightarrow 4) and up to 1% α - (1 \rightarrow 6) linkages and differing in size and structure depending on botanical origin. The molecular weight and degree of polymerization (DP) of amylose generally range from 10^5 to 10^6 and 700 to 5000 anhydroglucose units, respectively (Hizukuri 1996). About 25 to 55% of the total amylose (mole basis) is branched with 4-18 branch points per molecule and branch chain length (CL) of 4 to over 100 (Hizukuri et al. 1981). The apparent and total amylose content can be quantitatively determined by the iodine affinity of native and defatted starches, respectively, and the blue color formed by the amylose-iodine complex (Morrison and Laignelet 1983). Although this principle is commonly used, the presence of lipids, which form complexes with amylose and the ability of some amylopectin chains to also complex with iodine may lead to incorrect measurements. Other methods currently used include high performance size exclusion chromatography and a colorimetric assay using concanavalin A precipitation and enzymatic hydrolysis, developed by Megazyme International (Ireland).

Amylopectin, consists of α -D glucopyranose residues linked by α - (1 \rightarrow 4) linkages with a greater proportion (5-6%) of α - (1 \rightarrow 6) linkages, which gives it a highly branched structure. The number average DP, weight average molecular weight (M_w) and the average chain length of amylopectin are in the range 4800-15900, 10^7 - 10^8 and 18-27, respectively (Vamadevan and Bertoft 2015). The ratio of amylose and amylopectin varies according to the botanical origin of the starch. Normal starches consist of 20-30% amylose and 70-80% amylopectin. The waxy starches, which lack GBSS activity, contain less than 15% amylose, and high amylose starches (*ae* mutants) contain greater than 40% (Tester et al. 2004). Intermediate materials, which are

branched polyglucans with molecular size intermediate to amylose and amylopectin have been reported in wrinkled pea (Bertoft et al. 1993) and maize mutant starches (Yuan et al. 1993). Intermediate materials have been described to have lower iodine affinity than linear amylose chains. Furthermore, amylopectin in high amylose starches have a lower degree of branching, higher average chain length and a larger proportion of long chains than those in waxy and normal starches (Cheetham and Tao 1997).

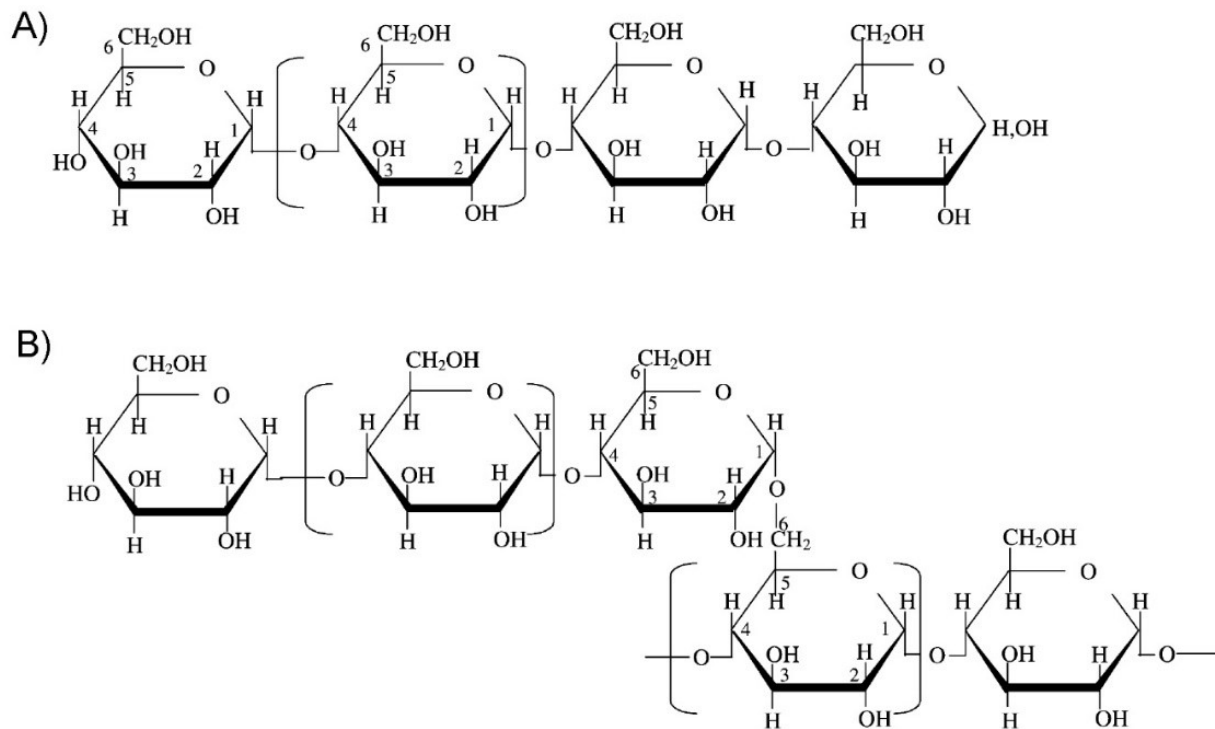


Figure 2.2 Molecular structure of A) amylose and B) amylopectin. Adapted and modified from Tester et al. (2004), with permission of Elsevier Ltd.

2.2.2. Granule architecture

The native starch granule structure can be divided into five different length scales: 1) whole granule architecture (1-100 μm), 2) growth rings (120-400 nm), 3) blocklets (20-500 nm), 4) amorphous and crystalline lamellae (9 nm) and 5) amylose and amylopectin chains (Figure 2.3). The inner architecture of native starch granule is characterized by concentric alternating amorphous (soft) and semi-crystalline (hard) growth rings, originating from the hilum, or the growth center of the granule. Due to their radial orientation, when starch granules are observed under a polarized light microscope they exhibit a Maltese cross referred to as birefringence. The growth rings are composed of spherical structures, called blocklets, which stack on top of each other and have sizes between 20 and 500 nm in diameter, depending on the starch source and location in the granule (Gallant et al. 1997). Semi-crystalline rings contain large blocklets of about 100 nm in diameter, compared to 20 to 50 nm blocklets in less organized amorphous rings.

The size of the blocklets at a granule surface depth of 10 μm are smaller in cereal (80-120 nm) than in tuber and pulse starches (200-500 nm) (Gallant et al. 1997). The blocklet model was first evident from images obtained by SEM and AFM (Gallant et al. 1997; Baldwin et al. 1998; Baker et al. 2001), which suggested that a high order of crystalline organization exists between the lamellae and the growth rings. Individual blocklets are thought to be the semi-crystalline ultrastructure of amylopectin composed of a single or several clusters (Szymonska and Krok 2003).

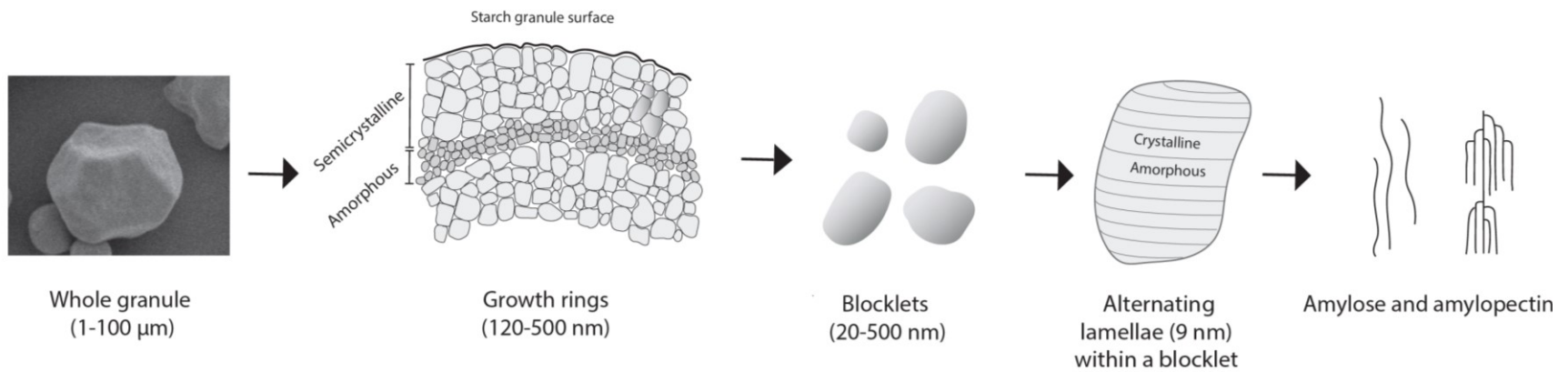


Figure 2.3 Schematic representation of the starch granule structural hierarchy.

The granule is made up of concentric semi-crystalline and amorphous growth rings starting from the center of the granule. The growth rings are composed of structures called blocklets which stack on top of each other. Individual blocklets have alternating amorphous and crystalline lamellae consisting mainly of amylopectin (branched chain) and in some cases amylose (linear chain) molecules.

Amylopectin is found in the form of clusters, which consist of three types of chains, A-, B- and C-chains (Figure 2.4). A-chains do not carry any other chains and are connected by α - (1 \rightarrow 6) linkages to the rest of the macromolecule, while B-chains are substituted and carry one or more chains. Each amylopectin cluster contains a single C-chain, which carries the reducing end (Figure 2.4). The semi-crystalline regions are formed by alternating crystalline and amorphous lamellae, with a periodicity of 9-10 nm. Within the lamella, amylopectin double helices pack into a crystalline lattice, and the amorphous layers contain amylopectin branching points and amylose and amylopectin molecules in a disordered conformation.

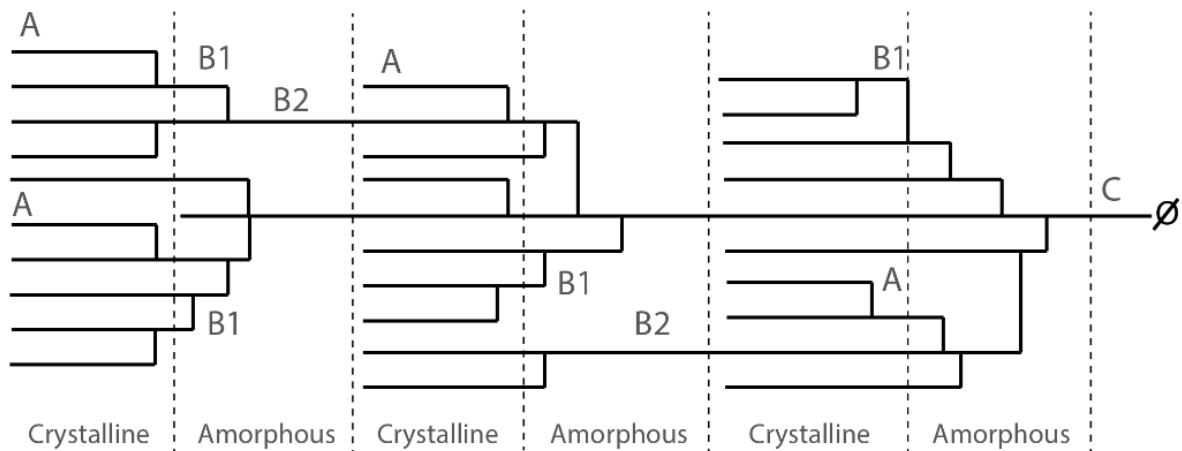
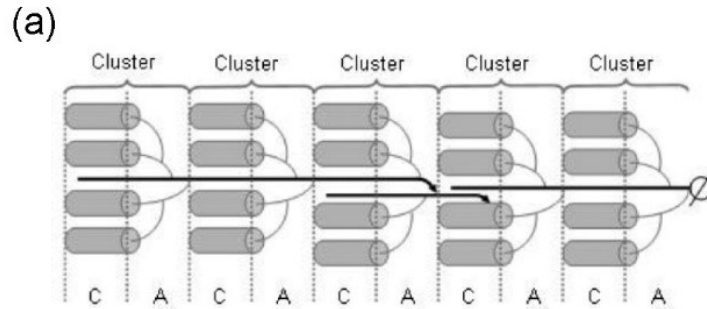


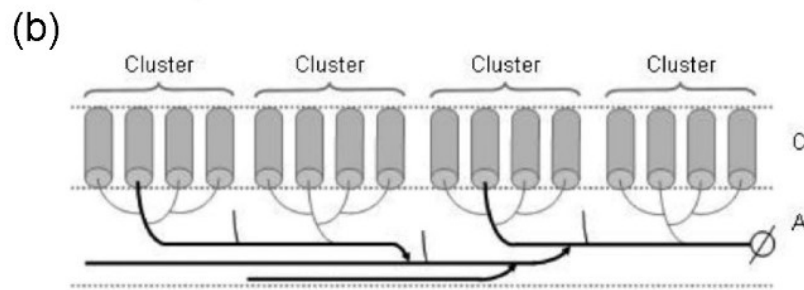
Figure 2.4 Basic labelling of A, B and C chains in amylopectin clusters. Horizontal lines represent (1 \rightarrow 4) linkages, perpendicular lines (1 \rightarrow 6) linkages, and Ø is the reducing end. Adapted and modified from Hizukuri (1986), with permission of Elsevier Ltd.

To date, many models have been proposed to explain the amylopectin ultrastructure and the organization of clusters within the crystalline and amorphous lamellae (Hizukuri 1986; Bertoft 2004b; 2007; Laohaphatanaleart et al. 2010). The cluster model proposed by Hizukuri (1986) and the backbone model by Bertoft (2007) have received the most acceptance (Figure 2.5). According to the cluster model, the amylopectin branch chains follow a polymodal distribution with 5 different fractions designated as A, B1, B2, B3 and B4 (Figure 2.4). A single cluster is made up of A and B1 chains (shortest chains) containing 27-28 glucosyl units equivalent to a length of 9.7 nm. The B2, B3 and B4 chains extend into 2, 3 or 4 clusters and therefore are present in both the crystalline and amorphous regions. All branches are connected by α - (1 \rightarrow 6) linkages and each amylopectin molecule has only one C-chain with the reducing end. Based on this model, the amylopectin chain length distribution of different starch sources was further classified by Hanashiro et al. (1996) using high performance anion exchange chromatography. Accordingly, the chain length distributions or degree of polymerization (DP) were separated as follows: A chains (DP 6-12), B1 chains (DP 13-24), B2 chains (DP 25-36) and B3 chains (DP > 37).

The cluster model shows all amylopectin chains arranged parallel to each other with alternating amorphous and crystalline regions (Figure 2.5a); however, the backbone model predicts that the cluster chains in the amorphous regions are perpendicular to the direction of the crystalline chains (Figure 2.5b). In the backbone model, shorter chains (A and B1) make up the crystalline regions and the longer interconnecting chains (B2 and B3) are found in the amorphous region. This lamellae organization is possible because in acid treated starches the long B-chains are removed by acid completely due to their amorphous nature, while the more crystalline sections remain intact (Bertoft 2004a).



The cluster model



The backbone model

Figure 2.5 Alternative models of amylopectin cluster organisation.

(a) The cluster model by Hizukuri (1986), shows long chains integrated as part of the clusters.

(b) The backbone model by Bertoft (2007), shows shorter B2-chains in the crystalline lamellae and long chains in the amorphous lamellae. Long chains (black, bold lines), short chains (grey, thin lines), the reducing end (\emptyset) and the amorphous (A) and crystalline (C) lamellae.

Adapted and modified from Perez and Bertoft (2010), with permission of John Wiley & Sons Inc.

Two types of crystalline structures have been identified in native starch according to the arrangement of the amylopectin chains, namely A- and B-type (Figure 2.6). The A-type polymorph is commonly found in cereal starches and corresponds to a monoclinic left-handed parallel stranded double helix (Figure 2.6a) with 12 water molecules (Figure 2.6b). The B-type polymorph is common in tuber and high amylose starches and is composed of six hexagonally arranged left handed parallel stranded double helices with 36 water molecules (Figure 2.6c). Pulse and legume starches are characteristics of a C-type structure comprised of a mixture of both A- and B-type crystallites, located in the periphery and near the center of the granule, respectively (Bogracheva et al. 1998).

X-ray diffraction is commonly used to determine the crystalline type along with the relative crystallinity of the native starch granules which can range between 15 and 45%. Native starches exhibiting the A-type polymorph will show a diffraction pattern with peaks centered at 15° , 17° , 18° and 23° 2θ whereas those with a B-type polymorph pattern will have peaks centered at 5.6° , 15° , 17° , 22° and 24° 2θ (Figure 2.7). The C-type polymorph diffraction pattern shows peaks centered at 5.6° , 15° , 17° , 23° 2θ (Figure 2.7). Moreover, a peak located at 20° 2θ reflects the lipid complexed amylose chains or the amylose single helical structures known as V-complexes. The V-type pattern is only common in native high amylose maize starches.

Native starch granules can undergo a polymorphic transition during different processing conditions such as heat moisture treatment, annealing and acid hydrolysis. Generally, the type of crystallite formed depends on the processing conditions; under cool and wet conditions B-type crystals are more likely to form whereas under warm and dry conditions A-type crystals may form.

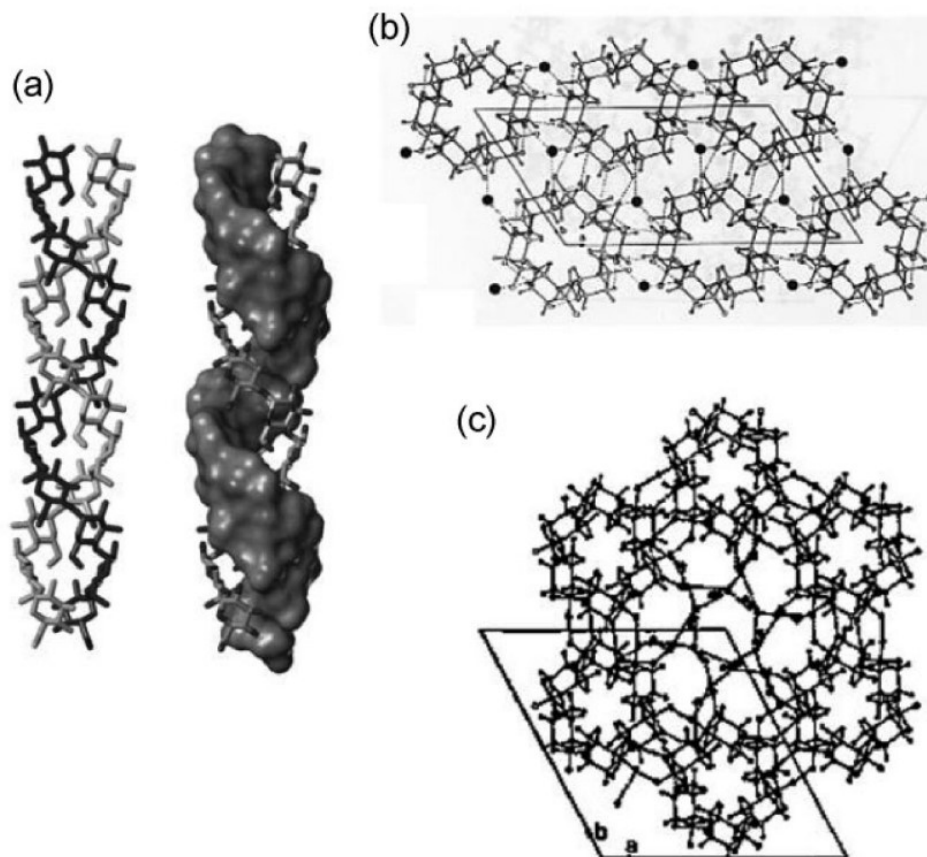


Figure 2.6 Crystalline structures of A- and B-type polymorphs.

(a) Left handed and parallel stranded double helices, (b) A-type polymorph is a monoclinic lattice with twelve water molecules located in between the helices, (c) B-type polymorph is a hexagonal lattice with thirty six water molecules, tightly bound to the double helices or forming a complex network in the center region. The water molecules are indicated as black dots and hydrogen bonds as broken lines. Adapted and modified from Perez and Bertoft (2010), with permission of John Wiley & Sons Inc.

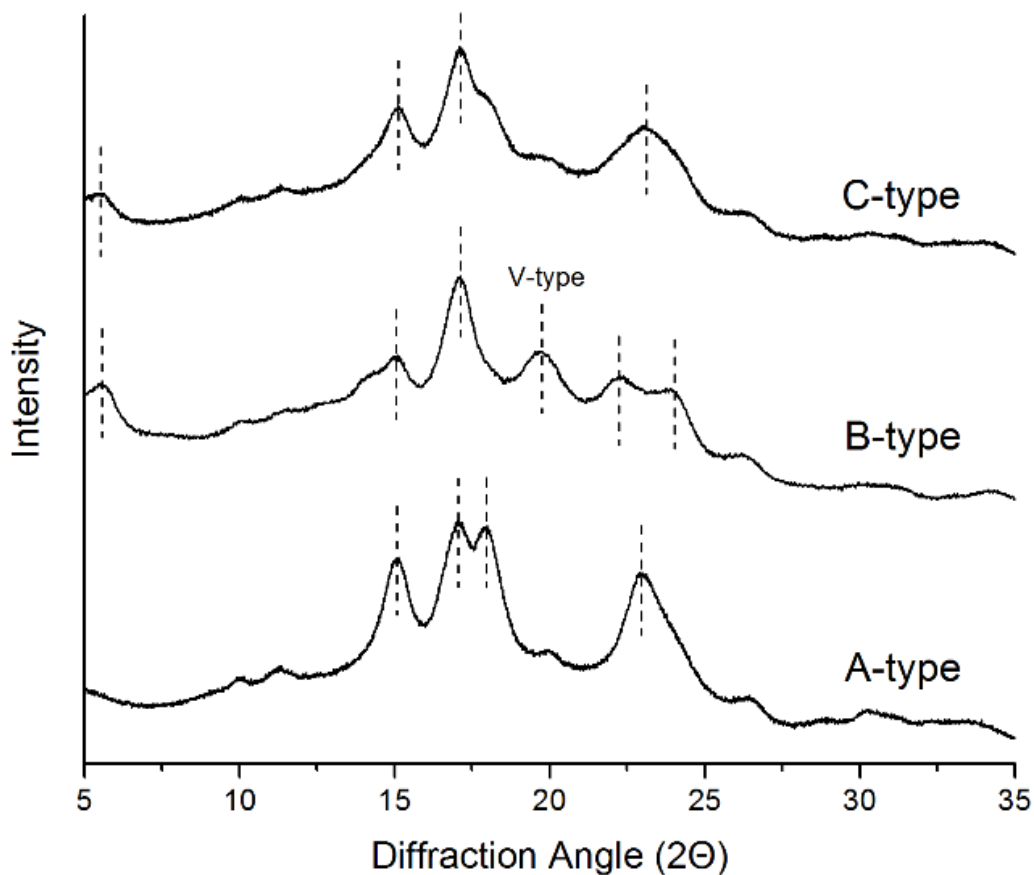


Figure 2.7 X-ray diffraction patterns of A-, B-, and C-type starches with their d-spacings (Å). The peak locations for each crystalline type are marked by the dash lines. A-type polymorph will show peaks centered at 15° ($d=5.8\text{Å}$), 17° ($d=5.2\text{Å}$), 18° and 23° ($d=3.8\text{Å}$) 2θ . B-type polymorph at 5.6° ($d=15.8\text{-}16\text{Å}$), 15° ($d=5.9\text{Å}$), 17° ($d=5.2\text{Å}$), 22° ($d=4.0\text{Å}$) and 24° ($d=3.7\text{Å}$) 2θ . C-type polymorph at 5.6°, 15°, 17°, 23° 2θ . The peak at 20° ($d=4.4\text{Å}$) 2θ is known as the V-complex (Zobel, 1988; Vasanthan and Bhattu, 1996; Cheetam and Tao, 1998).

The transition from one crystalline type to another indicates a molecular reorganization in the amylopectin double helices. For example, in heat-moisture treatments, an irreversible transition from B- to A-type has been reported for potato and yam starches due to a change in the crystalline orientation of the double helices (Gunaratne and Hoover 2002). Furthermore, Wang et al. (2013) reported a polymorphic transition from A- to B-type in annealed pea starch from reordering the double helices and the introduction of water molecules during the hydrothermal treatment.

Although the exact location of amylose within the starch granules remains unclear, various models have been proposed. Amylose may be randomly interspersed as individual molecules in both the amorphous and crystalline regions of the granule, co-crystallized with amylopectin molecules (Kasemsuwan and Jane 1994; Jenkins and Donald 1995) or may be present as tie chains, which pass through both the crystalline and amorphous lamellae (Kozlov et al. 2007). Amylose molecules present as tie chains are embedded within the blocklets or in the surface of the blocklets in amylose containing starches. According to Ridout et al. (2003), the blocklet structure and surrounding matrix between the wild type and the *r* mutant pea starch containing 35% and 65% amylose, respectively, were reported to vary. The wild type starch had asymmetrical blocklets of 130 nm diameter, which were embedded in a soft matrix composed of amylose, while the *r* mutant had bigger blocklets (250 nm) surrounded by a hard matrix believed to be crystalline amylose.

Amylose chains may also play a critical role in the assembly of the crystalline lamellae in B-type crystallites of high amylose maize starches and potato starch (Gérard et al. 2002; Saibene and Seetharaman 2010). Park et al. (2011) investigated the surface morphology of starch granules

using a novel in situ atomic force microscopy imaging technique. The authors reported the presence of linear “hairy-like” structures (between 1.5-2.5 nm in length) on the surface of corn and potato blocklets (100-200nm), which were able to complex with iodine vapor. The presence of amylose linear chains within the blocklets in amylose containing starches is expected to play an important role in the functional and physicochemical properties of starch, particularly when native starch granules are hydrolyzed into their subunits.

2.2.3. Gelatinization and retrogradation

Native starch granules are insoluble in cold water due to their compact and highly organized semi-crystalline structure. However, when heated above a critical temperature in the presence of water, native starch experiences an irreversible phase transition called gelatinization. During gelatinization the starch granules undergo hydration and swelling of the amorphous regions, crystallite melting, dissociation of the double helices, loss of birefringence and amylose leaching (French 1984). The partial or complete disruption of the native starch granules forms a viscous paste, made up of solubilized amylose and amylopectin molecules and granule ghosts.

The gelatinization and swelling properties of starch depend primarily on the amylopectin molecular structure (chain length, degree of branching, molecular weight, polydispersity), the starch composition (amylose-to-amylopectin ratio, amylose-lipid complexes) and the granule architecture (crystalline-to-amorphous ratio) (Tester 1997; Hoover and Ratnayake 2002). However, the precise relations and correlations between these factors are not yet clearly established. Differential scanning calorimetry is one of the most common methods used to investigate the melting and gelatinization properties [onset temperature (T_o), peak temperature (T_p), conclusion temperature (T_c) and melting enthalpy (ΔH)] of starch. The endothermic

transitions, initial gelatinization and temperature range ($T_o - T_c$), can vary according to the starch-to-water ratio, starch source and granule heterogeneity. For example, high amylose maize starches have a higher T_o and broader gelatinization range (up to 58°C) than waxy and normal maize (10°C) (Jane et al. 1999). Furthermore, when native starches are heat-moisture treated, annealed or partially acid hydrolyzed there is an increase in their gelatinization temperature and broadening temperature range (Hoover and Vasanthan 1994a; Hoover 2000).

During cooling and storage, the solubilized amylose and amylopectin molecules from the gelatinized starch can partially re-associate into a more organized structure, in a process called retrogradation. Retrogradation is time and temperature dependent and can vary depending on the starch source and composition (amylose-to-amylopectin ratio) (Liu 2005). Retrograded starch forms an elastic gel with increased turbidity and firmness compared to the gelatinized starch. Linear amylose molecules recrystallize very quickly by forming double helices, whereas branched amylopectin recrystallization occurs more slowly upon association of the outermost branches (Hoover and Sosulski 1991). Retrograded starch (particularly retrograded amylose) has been shown to be acid and enzyme resistant (Jane and Robyt 1984).

2.2.4. Acid hydrolysis

Acid hydrolysis has been widely used to understand the starch granule structure as well as in commercial applications to produce soluble and acid-modified (thin boiling) starches. When starch is acid treated, hydrolysis of the glycosidic linkages in both amylose and amylopectin chains leads to the degradation of the native starch granular structure. The rate of acid hydrolysis and the acid resistant end product vary depending on the acid type (HCl, H₂SO₄, HNO₃, H₃PO₄), concentration, time, temperature and the starch granular and molecular properties.

Native starch (or glucose chains) undergo acid hydrolysis by the mechanism presented in Figure 2.8. When starch is added to an acid solution, the hydrolysis process begins by the hydronium ion (H_3O^+) carrying out an electrophilic attack on the oxygen atom of the α - (1 \rightarrow 4) glycosidic linkage between two glucose units (Figure 2.8A). Next, the electron from one of the carbon-oxygen bonds move onto the oxygen atom (Figure 2.8B) to generate an unstable, high energy carbocation intermediate (Figure 2.8C). The carbocation intermediate is a Lewis acid, so it subsequently reacts with water (Figure 2.8D), leading to the release of one glucose molecule and the regeneration of a hydroxyl group (Figure 2.8E) (Hoover 2000). Due to the continuous regeneration process of the hydroxyl groups, removal of the acid by water washing or neutralization is needed to stop the hydrolysis reaction.

2.2.4.1 Effect of acid type and starch source on the rate of hydrolysis

Native starches will undergo acid solubilization at different rates depending on the acid type and starch source; however, all starches exhibit a two-stage hydrolysis pattern. According to Robin et al. (1975), acid hydrolysis with 2.2N HCl has been shown to consist of an initial fast step due to hydrolysis of the amorphous regions of the granule followed by a second slower step, due to hydrolysis of the crystalline regions. To account for the slower rate of hydrolysis of the crystalline domains, two hypotheses (French 1984) have been proposed. First, the dense packing of starch chains within the starch crystallites does not readily allow the penetration of H_3O^+ into these regions. Second, the chair \rightarrow half chair transformation, required for hydrolysis of the glucosidic bond, occurs very slowly due to immobilization of the sugar conformation within the starch crystallites.

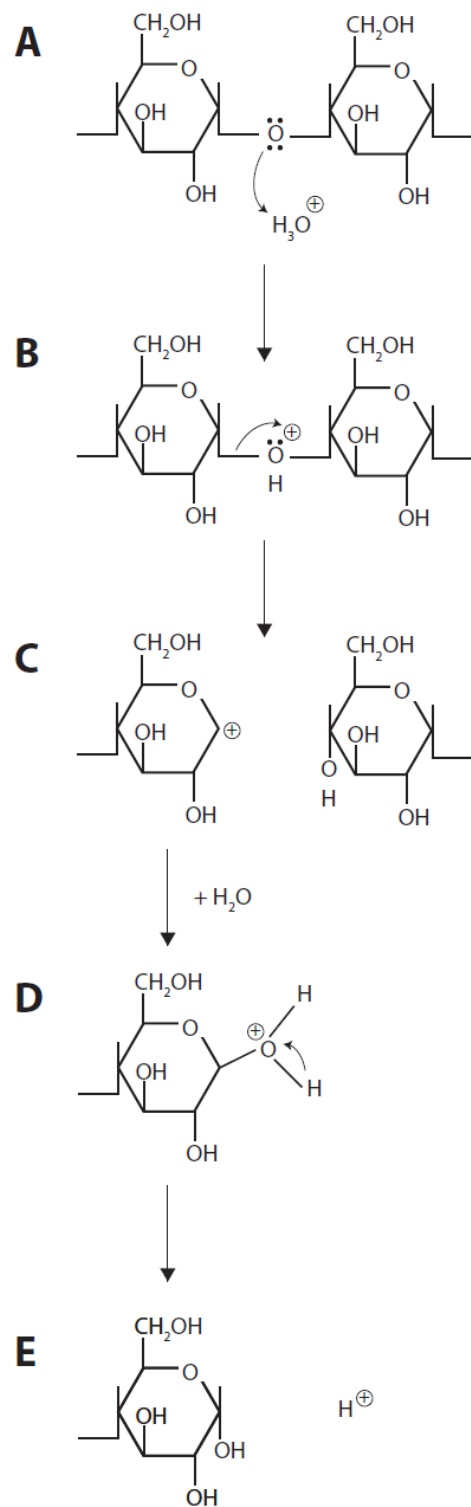


Figure 2.8 Mechanism of acid hydrolysis of starch.
Adapted from Hoover (2000), with permission of Taylor & Francis.

The effect of acid type is closely related to the dissociation constants of each acid, which is proportional to their proton releasing capacity. Monobasic acids (HCl and HNO₃) have very high dissociation constants as compared to dibasic (H₂SO₄) and tribasic (H₃PO₄) acids. According to Singh and Ali (2008), the higher dissociation constant and monobasic nature of HCl and HNO₃ leads to the production of thinner acid-modified starches than H₂SO₄. Moreover, weak acids produce less amount of acid solubles, which have lower molecular weight compared to those produced by strong acids.

Under similar treatment conditions, the susceptibility of native starch granules to acid hydrolysis also depends on factors such as: 1) the presence of pores on the granule surface, 2) the granule size (Vasanthan and Bhatta 1996; Singh and Ali 2008), 3) the amount of α (1 \rightarrow 6) linkages (Inouchi et al. 1987), 4) the amount and nature of lipid complexed amylose chains (Jayakody and Hoover 2002), 5) the extent to which amylose chains are co-crystallized with amylopectin and/or are buried within the crystalline lamellae (Vamadevan et al. 2014), 6) the packing density of amylose chains within the amorphous regions (Hoover and Manuel 1996) and 7) the polymorphic type of the native starch (Jane et al. 1997; Nagahata et al. 2013). A-type starches are typically hydrolyzed to a greater extent than B-type starches although the degree of hydrolysis of each starch type is due to the interplay of the factors listed above. For example, waxy maize starch has a higher susceptibility to acid hydrolysis than high-amylose maize starches. This may be due to the restricted swelling behaviour in high-amylose starches, which can limit the acid penetration (Nakazawa and Wang 2003). Furthermore, smaller starch granules from rice and millet, conventionally expected to be hydrolyzed faster due to their larger surface area, show

higher resistance to acid hydrolysis than bigger starch granules from potato, wheat and corn (Singh and Ali 2008).

2.2.4.2 Acid-treated starches

Acid-treated starches have been extensively used for food and paper industrial applications. In comparison to native starches, acid-treated starches have different functional properties including: 1) no swelling power, 2) shift in melting temperature and broadening endotherm, 3) accelerated retrogradation, 4) increase in pasting temperature and 5) decreased viscosity (Hoover 2000; Wang and Copeland 2015). The properties listed above are closely related to structural changes that occur during acid hydrolysis at the molecular and surface length scales. These changes include: 1) decrease in amylose content due to the preferential hydrolysis of the amorphous regions, 2) change in the amylopectin chain length distribution (Biliaderis et al. 1981), 3) increase in double helical structures (Morrison et al. 1993), 4) increase in relative crystallinity and polymorphic transition (McPherson and Jane 1999; Gérard et al. 2002), 5) increase in pores and channels (Wang et al. 2012) and 6) decrease in granule size and disruption of the granule into smaller subunits, including platelet nanocrystals and nanoparticles (Putaux et al. 2003; LeCorre et al. 2011).

Treatment of native potato starch in water with 15% H₂SO₄ for 30 days at room temperature results in an acid-resistant fraction that is readily soluble in water, called Nægeli amyloextrin. Nægeli amyloextrins are a mixture of low molecular weight, linear, and branched dextrins, with an average degree of polymerization (DP) of 25-30 (Nægeli 1874). However, treatment of starch with 2.2 N HCl at temperatures in the range of 30-40°C produces lintnerized starch (Lintner 1886). Lintnerized starch consists of the following fractions: a) linear amylose

chains with a DP ranging from 13 to 15, b) singly branched amylose chains (DP 25), c) multiply branched chains, d) retrograded amylose and e) amylose-lipid complexes (Watanabe and French 1980; Morrison et al. 1993). Lintnerized starch and Nageli amyloextrins from different starch sources have been widely studied in order to understand the amylopectin branch structure and chain length distribution (Jane et al. 1997; Srichuwong et al. 2005), the amylose involvement in the crystalline structure of B-type starches (Gerard et al. 2002; Jiang et al. 2010), the acid resistance of the amylose-lipid complex (Morrison et al. 1993), the molecular structure of retrograded amylose (Jane and Robyt 1984; Perera et al. 2001) and the effect of annealing and heat-moisture treatments on the amorphous and crystalline lamellae (Gunaratne and Hoover 2002; Nakazawa and Wang 2003). Moreover, recently Nagahata et al. (2013) studied the formation of resistant starch in maize starches during a mild acid hydrolysis treatment. The authors concluded that resistant starch can be generated due to the formation of amylose double helices or the co-crystallization between longer amylopectin chains and amylose molecules released during the hydrolysis process. A similar mechanism was previously proposed by Morrison et al. (1993), who attributed the higher number of double helices in non-waxy barley starches to the retrogradation of amylose chains. Lastly, over the past decade acid hydrolysis has been used for the isolation of starch nanocrystals and starch nanoparticles to be discussed in further detail in the following sections.

2.3. STARCH NANOPARTICLES

Interest in the use of starch nanocrystals (SNC) and starch nanoparticles (SNP) in applications like polymer nanocomposites, drug delivery, paper binding and food additives has promoted new research in this area. Although in most of the literature the terms SNC and SNP

are used interchangeably, it is important to note that according to some researchers a structural difference exists between these two. SNC are defined as the crystalline nanoplatelets resulting from the disruption of the amorphous and semi-crystalline structure of starch granules by the acid hydrolysis, while SNP are not solely the crystalline regions but also include amorphous material (Le Corre and Angellier-Coussy 2014). The different structure between SNC and SNP is either due to the degree of acid hydrolysis (SNC requiring more than SNP), or due to the isolation and preparation process. Although by definition SNC are considered to be the crystalline region of amylopectin molecules, it is important to note that neither SNC nor SNP are 100% crystalline. In this literature review, the terms SNC and SNP will be used according to how they were presented by the original authors, and may in some cases be used interchangeably.

Much research has focused on the isolation of SNC and SNP from waxy maize starch and very few studies have included other starch sources. Preparation of SNC and SNP from starches other than waxy maize have only been reported by LeCorre et al. (2011), Kim et al. (2012) and Xu et al. (2014). Furthermore, research has been solely concentrated on the study of the acid-resistant residues collected after hydrolysis with 3.16 M H₂SO₄ at 40 °C for 5 days (Angellier et al. 2004). SNP have been found to vary in length (40-150 nm), shape (platelet, round edges, grape like aggregates, square) and yield according to the acid type, acid concentration, hydrolysis time, temperature and starch source (Putaux et al. 2003; Angellier et al. 2004; LeCorre et al. 2011; Kim et al. 2012; Wei et al. 2014b).

To date, several review articles have been published, which describe the preparation, characterization and applications of SNC and SNP (Le Corre et al. 2010; Lin et al. 2011a; Le Corre and Angellier-Coussy 2014; Kim et al. 2015). Le Corre et al. (2010) focused on the preparation of

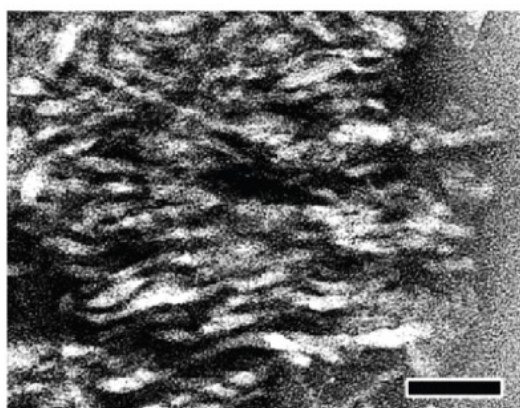
SNC using different acid hydrolysis conditions, their characterization and application as a reinforcing material in polymer matrices. Later, Lin et al. (2011a) described the use of SNC in nanomaterials with a particular emphasis in their chemical modifications and applications. More recently, different methods for preparing SNP and their reinforcing effect in polymer nanocomposites have been reviewed (Le Corre and Angellier-Coussy 2014). Lastly, Kim et al. (2015) compared the different methods of isolating and synthesizing SNP including acid, enzymatic and physical methods. The authors also describe the physicochemical characteristics of SNP and their potential use in food and biomedical applications.

2.3.1. Isolation and preparation methods

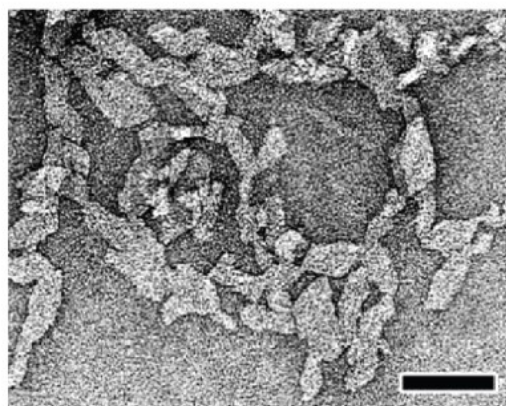
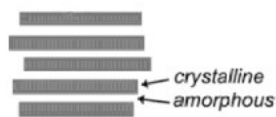
The production of SNP is classified into “top-down” and “bottom-up” methods. Top-down methods like acid hydrolysis and ultrasonication imply that the SNP are obtained by the selective hydrolysis or disruption of a part of the original structure into smaller subunits. While bottom-up refers to the opposite, where single molecules are carefully manipulated to bind and form larger particles. Currently, the most commonly used method for the isolation of SNC and SNP is the acid hydrolysis process optimized by Angellier et al. (2004). However, new technologies and environmental awareness has led to the rise of enzymatic and physical techniques such as enzymatic hydrolysis with debranching enzymes, ultrasonication and high pressure homogenization. These methods have the advantage of producing little to no waste compared to acid hydrolysis where large volumes of water are required to wash away the acid and for the neutralization process.

2.3.1.1 Acid hydrolysis

As previously mentioned, acid hydrolysis is the most commonly used method for isolating SNC and SNP from different starch sources. By definition, SNC are the highly crystalline amylopectin residues, which can resist acid hydrolysis (Putaux et al. 2003; Angellier et al. 2004; Angellier-Coussy et al. 2009; LeCorre et al. 2011; Wei et al. 2014a). Crystalline nanoplatelets also known as nanocrystals were first observed by Putaux et al. (2003). After incubating native waxy maize starch in 2.2 N HCl at 36°C for 40 days, the authors isolated individual parallelepipedal blocks with 60-65° acute angles, a length of 20-40 nm and a width of 15-30 nm. Longitudinal and planar views of these fragments confirmed the presence of the crystalline lamellae and individual platelets, which separated after hydrolyzing the amylopectin branching points (Figure 2.9).



Longitudinal view



Planar view



Figure 2.9 Transmission electron microscopy images of waxy maize SNC (scale bar = 50 nm). Adapted and modified from Putaux et al. (2003), with permission of American Chemical Society.

The process of isolating SNC with acid was further optimized by Angellier et al. (2004), as follows: Similar SNC as those obtained previously with HCl were collected after only 5 days with 3.16 M H₂SO₄ at 40°C, followed by several water washings and centrifugation cycles until the washed water was at or near neutrality. The authors reported that SNC were present in the final residue after repeated water washings. Due to the shorter preparation time (5 vs 40 days) and higher yield (15% vs 5% w/w) compared to HCl, many studies have used this process for the isolation of SNC. Furthermore, due to the high amylopectin content (almost 100%) in waxy maize starch, most of the acid hydrolysis studies have been carried out using this starch source (Angellier-Coussy et al. 2009; LeCorre et al. 2011; 2012a; Li et al. 2014; Wei et al. 2014a; Xu et al. 2014) and only a few studies have investigated other sources like regular corn, potato, wheat, mungbean, tapioca, barley and chickpea starches (LeCorre et al. 2011; Kim et al. 2012; Xu et al. 2014).

Acid hydrolysis with H₂SO₄ was also reported to produce nanosuspensions with better colloidal stability than HCl, due to the presence of negative surface charge and sulfate groups, which promote electrostatic repulsion (Angellier et al. 2005a; Wei et al. 2014b). The surface chemical composition of SNP isolated by using different types of acids was determined by X-ray photoelectron spectroscopy (Wei et al. 2014b). Waxy maize SNC prepared with HCl and H₂SO₄ showed the presence of carboxyl groups in both samples and sulfate esters only in the samples hydrolyzed by H₂SO₄ (Wei et al. 2014b). The extent of substitution was found to be dependent on the acid type, concentration and hydrolysis time (Wei et al. 2014b; Romdhane et al. 2015). The authors proposed the following reactions are occurring during acid hydrolysis: 1) the formation of sulfate esters on the surface of SNC and 2) glucose is degraded to formic and

levulinic acids, which also adsorb to the surface of SNC making them negatively charged (Figure 2.10). Therefore, when SNC and SNP are suspended in water, the surface charge and counter ions (NaCl, CaCl₂) in solution produce an electric double layer around the particles, which enhances their colloidal stability. The pH is also an important parameter to determine the colloidal stability of SNC. Wei et al. (2014a) recently reported that the pH of the aqueous medium affects the aggregation behaviour of waxy maize SNC. A stable suspension occurs between pH 7.44 and 9.45, while a more acidic solution allows the SNC to aggregate and settle. Although acid hydrolysis continues to be the most common method, the low recovery and waste production have promoted the use of other more environmentally friendly and cost efficient techniques.

2.3.1.2 Enzymatic hydrolysis

Only two methods have been described using enzymatic hydrolysis for the isolation and production of SNC and SNP. LeCorre et al. (2012b) first described the use of α -amylase, β -amylase or glucoamylase enzymes as a pre-treatment to reduce the acid hydrolysis time. According to LeCorre et al. (2012b), the sequential use of glucoamylase enzyme and acid resulted in a decrease in hydrolysis time from 5 days to 45 hours with a similar yield (15 wt %) of SNC obtained. During the pre-treatment, enzymes promote the formation of pores inside the starch granule, which allow the acid to diffuse at a faster rate than compared to the native starch granules. Enzymes are capable of hydrolyzing both the amorphous and crystalline regions, although due to their tightly packed structure the crystalline lamella is more likely to resist enzymatic hydrolysis. In contrast, Sun et al. (2014) prepared waxy maize SNP using a “bottom-up” method, through enzymolysis by pullulanase (debranching enzyme) and recrystallization of linear chains.

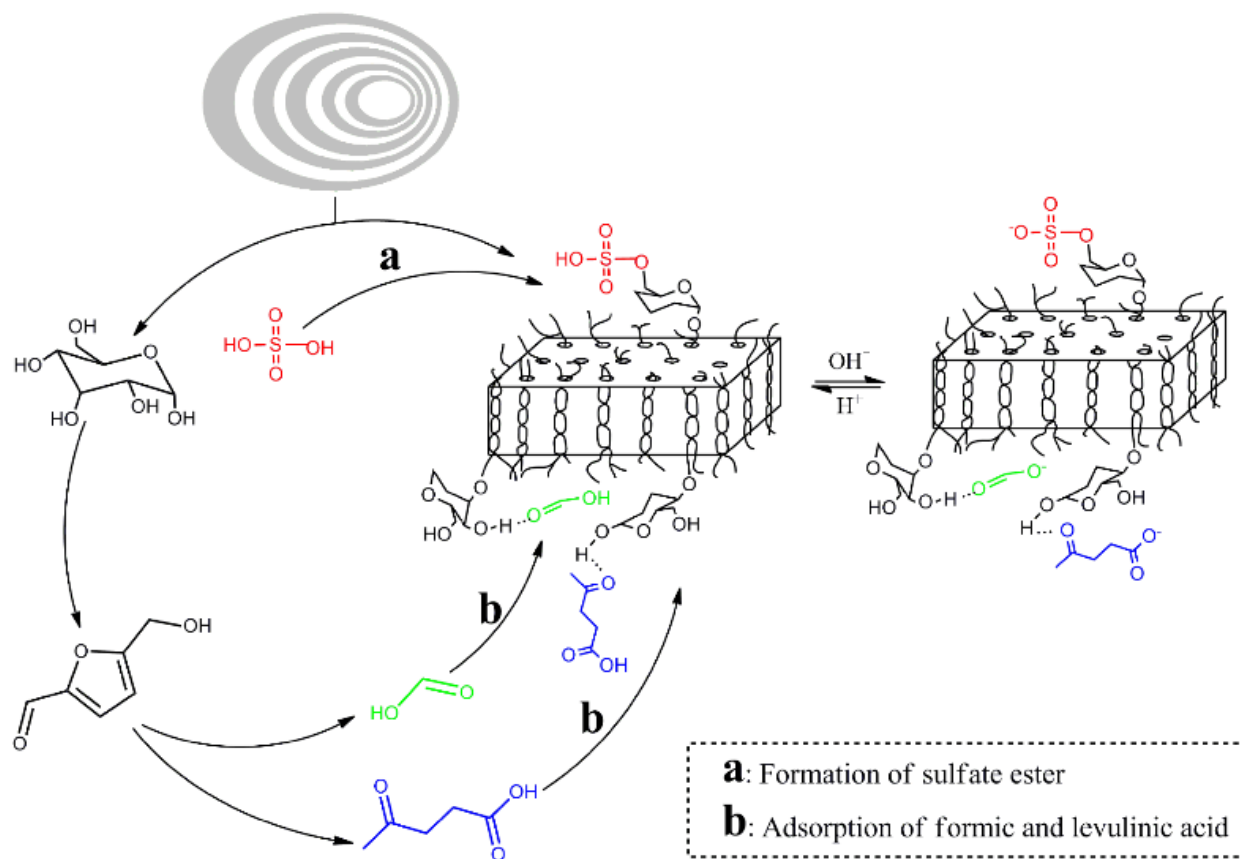


Figure 2.10 Formation of sulfate esters and formic and levulinic acids on the surface of SNC.
Adapted from Wei, et al. (2014), open-access article.

In this method, native waxy maize starch was cooked in order to fully gelatinize the starch, cooled and incubated with pullulanase in order to de-branch the amylopectin chains by hydrolyzing the α -1 \rightarrow 6 linkages. The solution containing the debranched chains was further stored at 4°C to promote the self-assembly and recrystallization of linear chains. Sun et al. (2014) obtained SNP (60-120 nm) with irregular shapes from the retrogradation of linear chains (DP 12-60), which formed double helices and further clusters.

2.3.1.3 Physical treatments

Most of the physical treatments available for the preparation of SNP are classified as “top-down” methods. Compared to acid hydrolysis, these methods are more environmentally friendly and time saving. Via physical treatments such as ultrasonication, reactive extrusion and high pressure homogenization, the starch granule structure is precisely disrupted to yield nanoparticles that can be then purified and collected. The information presented in this section describes the current methodologies which have successfully isolated SNP.

During ultrasonication, native starch undergoes degradation and shattering, leading to the recovery of smaller particles. Using this method, starch is immersed in water and subjected to very high frequencies (15-20 kHz) for short periods of time (up to 75 min). The principle behind this method is the formation of cavitation bubbles in the liquid medium, which collapse during compression and release high energy and pressure near the material surface, thus causing damage and disruption. For example, ultrasound treatment of potato starch for short periods of time (30 min) and under controlled temperature conditions resulted in changes to the cluster structure (crystalline regions) and damage to the starch granule surface (Zhu et al. 2012). More recently, ultrasonication was used to isolate SNP from waxy maize (Haaj et al. 2013). A suspension

of waxy maize starch was immersed in a water bath at 8°C in order to prevent plasticization and sonicated for a longer period of time (75 min) at 20 kHz. SNP between 30-100 nm were recovered; however, these had lower crystallinity than those obtained by acid hydrolysis. Kim et al. (2013a) also studied the effect of combining both acid hydrolysis (3.16 M H₂SO₄ at 40°C) and subsequent ultrasonic treatments for the preparation of SNP from waxy maize. The authors suggested that ultrasound would decrease the amount of particle-particle aggregation and thus change the particle size distribution of the acid hydrolysate from micro to nano size. When ultrasound was applied to the starch suspensions during acid hydrolysis (5-7 days), a longer ultrasonic time and higher amplitudes resulted in smaller SNP (Kim et al. 2013a). The process to isolate SNP was further improved by reducing the amount of acid hydrolysis time to 2 days and using a post-ultrasonic treatment (60% amplitude, 3 min) (Kim et al. 2013a). One major drawback of using ultrasonication is the disruption of the crystalline material and recovery of SNP with low crystallinity (less than 30%). In order to minimize crystalline disruption, Kim et al. (2013b) used a combination of cold acid hydrolysis and ultrasonication. Acid hydrolysis followed the method of Angellier et al. (2004) with the incubation temperature at 4°C instead of 40°C and ultrasonication was performed at 60% amplitude for 3 min. When starch was hydrolyzed at 4°C, the low temperature facilitated the association of chains, forming new crystalline structures and increasing the recovery yield from 15% (acid hydrolysis) to 78%. The SNP had similar crystallinity to the native starch and were globular shaped ranging in size between 50-90 nm (Kim et al. 2013b).

Other mechanical methods less commonly used are high pressure homogenization (Liu et al. 2009) and reactive extrusion (Song et al. 2011). High pressure homogenization was utilized to

break down the native granules of high-amylose maize starch from 3-6 μm to 10-20 nm particles (Liu et al. 2009). A 5% starch slurry was passed through a microfluidizer up to 20 times at a pressure of 270 MPa. In the microfluidizer, the product stream reached very high velocities thus creating high shearing and a reduction in the particle size. Although this technique was considered a good alternative to acid and enzymatic treatments due to the high recovery yields (almost 100%), X-ray diffraction showed that after 10 homogenizing cycles the SNP were devoid of any crystalline material (Liu et al. 2009). Using reactive extrusion, SNP ranging in size from 100-200 nm were produced (Song et al. 2011). Native starch was exposed to high shear, pressure and heat, which caused gelatinization, melting and disruption of the native structure to produce SNP. Native corn starch premixed with water and glycerol was extruded at a screw speed range of 100-360 rpm and temperatures within 55-100°C. The extruded material was immersed in water and then homogenized in solution to disperse the SNP. Similar to the results presented for high pressure homogenization, the SNP produced via reactive extrusion were also almost completely amorphous (Song et al. 2011).

Nanoprecipitation has also been investigated as a “bottom-up” approach to producing SNP. With nanoprecipitation, polymer chains are dissolved in solution and precipitated when mixed with an organic solvent. Ma et al. (2008), fabricated SNP by precipitating a corn starch paste with ethanol. Due to the complete gelatinization of the starch prior to precipitation, the native crystalline structure (A-type) was destroyed and the fabricated SNP, which ranged between 50-100 nm exhibited a V-type crystalline structure. Nanoprecipitation has also been used to produce starch based nanospheres, which can be used as encapsulating agents (Tan et al. 2009).

2.3.2. Characterization

A variety of techniques have been used to characterize SNC and SNP isolated from different starch sources. Their morphology has been previously investigated using SEM (Song et al. 2008), TEM (Namazi and Dadkhah 2008; Kim et al. 2012) or field emission scanning electron microscopy (FE-SEM) (LeCorre et al. 2011; 2012a; Wei et al. 2014a; Xu et al. 2014). Their crystalline type and relative crystallinity have been determined by X-ray diffraction (LeCorre et al. 2011; Kim et al. 2012; Xu et al. 2014) using the same methodologies as for native starch. Little information is available with regard to the molecular composition and structure of SNC and SNP. The molecular size distribution of a few starch sources was investigated by gel permeation chromatography (GPC) (Kim et al. 2012), while only the molecular structure of waxy maize SNC has been demonstrated by high performance anion-exchange chromatography with pulsed amperometric detection system (HPAEC-PAD) (Angellier-Coussy et al. 2009). In addition, with respect to their thermal properties, differential scanning calorimetry (Kim et al. 2012; LeCorre et al. 2012a; Xu et al. 2014) and thermogravimetric analysis (LeCorre et al. 2012a; Xu et al. 2014) data have been reported. Lastly, only the rheological properties of SNP from a few starch sources including soluble potato starch (Shi et al. 2012a; b; Shi et al. 2013) and waxy maize (Jiang et al. 2016) have been previously investigated.

2.3.2.1 Morphology

The morphology and size of SNP have been found to vary according to the starch source and the isolation method used. With acid hydrolysis, the shape of the SNP represent the original structures present in native starches, whereas with other methods, the morphology (shape and size) can be controlled by altering the isolating conditions. Using acid hydrolysis, LeCorre et al.

(2011), reported a link between the shape of SNC from five different starches (waxy maize, normal maize, high amylose maize, potato and wheat) and the crystalline type (amylopectin double helical packing) of their native starches. SNC from A-type starches had a square shape while those from B-type starches were round. Furthermore, the authors found no correlation between the particle size and crystalline type or amylose content of the native starches. For example, when the amylose contents were nearly similar, wheat SNC (100 nm) were almost twice the size of normal maize SNC (58 nm) and when the crystalline types differed between potato and normal maize starches, the average particle size of SNC (52 and 58 nm, respectively) did not differ significantly. Additionally, round and oval shaped SNP, ranging from 40-70 nm were reported following acid hydrolysis of maize, potato and mungbean starches (Kim et al. 2012). The SNP tended to aggregate into clusters, which made it difficult to precisely determine the morphology and particle size. SNP from B- and C-type starches were larger than those from A-type starches, which indicated a possible correlation between particle size and resistance to acid hydrolysis. Similar to the previous observation, Xu et al. (2014) found that the SNP average size varied significantly with starch source and those from A-type starches tended to be smaller in size. Moreover, the authors reported all SNP had a similar spherical shape regardless of the starch source. This finding is contradictory to the correlation shown between SNC shape and crystalline type by LeCorre et al. (2011).

When SNP were synthesized by pullulanase hydrolysis with a controlled self-assembly process, they were observed to be spherical in shape and ranging in size from 200-300 nm (Jiang et al. 2016) or irregularly shaped with a width of 50-100 nm and length of 80-120 nm (Sun et al. 2014; Ji et al. 2015). In comparison to acid and enzymatic hydrolysis, using physical treatments

such as ultrasonication and high pressure homogenization leads to a wide range of SNP size distribution where higher amplitudes and pressures, and longer times result in smaller SNP. Globular shaped SNP from ultrasonicated waxy maize starch between 30-100 nm (Haaj et al. 2013) and 50-90 nm (Kim et al. 2013b) have been recovered. Lastly, waxy maize SNP did not change in size and shape when exposed to a heat-moisture treatment (Ji et al. 2015).

2.3.2.2 Crystallinity

The ability of SNP to act as a reinforcing material in polymer matrices is closely related to their crystalline nature. The starch source and isolation method both play a very important role in the relative crystallinity and crystalline type of SNP. With acid hydrolysis, disruption of the amorphous material leads to SNP with higher relative crystallinity than their respective native starches, which contain between 15 and 45% crystalline material. LeCorre et al. (2011) found that SNC from different botanical origins and crystalline type had comparable degree of crystallinity. The authors attributed the increase in relative crystallinity to the amount of amylopectin in the native starch, and not the crystalline type. Furthermore, SNC and SNP from waxy maize, which is almost entirely composed of amylopectin had the highest relative crystallinity (48-79%) compared to those from amylose containing starch sources (35-51%) (LeCorre et al. 2011; Xu et al. 2014). Similar X-ray diffraction patterns have been reported between SNC and SNP and their corresponding native starches. However, Kim et al. (2012) demonstrated an increase in peak intensities of A-type starches and a decrease in some peak intensities of B-type starches. SNP obtained by ultrasonication have lower crystallinity (less than 30%) than those obtained by acid hydrolysis, possibly due to the disruption of both amorphous and crystalline material (Kim et al. 2013a; Kim et al. 2013b).

When SNP are produced by pullulanase hydrolysis and self-assembly of short linear chains, a transformation in the crystalline type from A-type to B-type and the formation of V-complexes (amylose crystals) have been demonstrated (Sun et al. 2014). During this process, the A-type crystals are first completely disrupted during gelatinization and debranching, followed by the formation of new crystalline structures by recrystallization and retrogradation of linear chains at low temperatures. Ji et al. (2015) also observed a change in crystalline type from B- to A-type when SNP were subjected to a heat-moisture treatment. This transition is due to a change in the crystalline orientation of the double helices at high temperature and low moisture conditions. These results are in agreement with those reported for B-type potato and yam native starches (Gunaratne and Hoover 2002).

2.3.2.3 Molecular structure

Little information is available with regard to the molecular structure of SNC and SNP. In 2009, a detailed investigation, which discussed the use of debranching enzymes (isoamylase and pullulanase) and β -amylase in combination with anion-exchange chromatography, characterized the molecular profile of waxy maize SNC (Angellier-Coussy et al. 2009). Waxy maize SNC was composed of two major dextrin populations, one with a high DP (23-85) and another with a low DP (9-22), corresponding to branched and linear dextrans, respectively. The authors also reported a similar amount of branched chains in both the high and low DP populations, thus concluding homogeneity in their molecular structure. Waxy maize SNC was found to be mostly composed of the low DP chains and the average DP of 14.2 (length of 5 nm) was attributed to the thickness of the crystalline lamellae. According to the above findings, acid hydrolysis of native starch granules leads to the disruption of the amorphous regions and thus the isolation of the crystalline

lamellae. More recently, the chain length distribution of SNP from waxy, normal, high amylose maize, potato and mungbean starches was investigated using gel permeation chromatography (Kim et al. 2012). Kim et al. (2012), reported a decrease in the proportion of long amylopectin chains in waxy maize and the disappearance of the amylose peak in amylose containing starches due to the acid hydrolysis treatment. The SNP from waxy maize were composed of short (B1 and A) chains while those from amylose containing starches also contained longer B chains. Kim et al. (2012), concluded that short (B1 and A) chains are more resistant to acid hydrolysis than long chains because they exist mostly in the crystalline lamellae.

2.3.2.4 Thermal stability

Native starch granules undergo melting and gelatinization when heated in the presence of water. Their endothermic transitions [temperature onset (T_o), temperature peak (T_p), temperature conclusion (T_c) and melting enthalpy] vary according to the starch source and processing (wet or dry) conditions. Since SNP are isolated from native starch granules, they may be susceptible to thermal degradation. Therefore, special attention should be given to preserve their structure and crystalline nature, in order to target their functionality in different applications. For example, in the production of nanocomposite and food packaging films, techniques such as hot-pressing, compression molding and extrusion employ high temperatures, which may cause melting of SNP and therefore change their reinforcing effect (Kim et al. 2015).

The thermal properties of SNC and SNP have been previously investigated using differential scanning calorimetry and thermogravimetric analysis (Kim et al. 2012; LeCorre et al. 2012a; Xu et al. 2014). In comparison to native starches, SNC and SNP are more heat stable possibly due to one of the following reasons: 1) their increased crystallinity, 2) more tightly

packed and perfect crystals or 3) a decrease in the plasticizer (amylose) content (LeCorre et al. 2012a). By investigating the thermal properties of waxy, normal, high amylose maize, wheat and potato SNC, LeCorre et al. (2012a) found no correlation between the melting temperature and botanical origin. However, the B-type starches began melting at temperatures above 82°C, whereas those from A-type starches began melting at lower temperatures (54-67°C). When SNC are heated in excess water, two thermal transitions due to crystallite melting are observed, one from unpacking and the other from unwinding of the double helices (LeCorre et al. 2012a). Furthermore, the thermal stability of SNC changes with processing conditions. In wet processes, SNC should remain at temperatures lower than 80-100°C, while in dry conditions they can be subjected too much higher temperatures (150-200°C). Similar results were also reported by Kim et al. (2012), Kim et al. (2013b) and Xu et al. (2014). After acid hydrolysis the T_o , T_p , T_c and melting enthalpy of SNC increased compared to their native starches and this increase positively correlated with the hydrolysis temperature and time. Ji et al. (2015) also studied the thermal properties of waxy maize SNP produced by an enzymatic pullulanase treatment followed by a heat-moisture treatment. T_o , T_p , T_c and the melting enthalpy of SNP increased when the temperature and moisture content increased from 90 to 100°C and 20 to 30%, respectively. Ji et al. (2015) suggested that these conditions promote the formation of intermolecular hydrogen bonds with highly ordered crystalline structures that require higher energy to melt.

2.3.2.5 Rheological properties

Static and dynamic rheological properties can be used to investigate how SNP suspensions behave under shear, temperature and frequency conditions. When SNP are suspended into a liquid medium their particle-particle interactions and associations with the continuous phase

under different processing conditions can provide useful information with regard to their functional properties. To date, only the rheological properties of SNC or SNP from maize, wheat and potato starches (LeCorre et al. 2011; Shi et al. 2012a; b; Shi et al. 2013; Jiang et al. 2016) have been investigated.

LeCorre et al. (2011) found a positive correlation between the viscosity and concentration of SNC. At concentrations between 2.5 and 10%, all SNC suspension from different starch sources displayed a shear-thinning behaviour. Furthermore, they reported no particular relationship between the viscosity and SNC size, thickness and surface area; however, the SNC with the lowest viscosities had similar morphologies. In a series of studies, Shi et al. (2012b) reported the effects of spray drying and freeze drying on the re-dispersibility of soluble potato SNP in aqueous suspension, and the influence of NaCl concentration on the aqueous rheological properties of SNP obtained by the two different drying methods. Their findings indicated that both the drying method and NaCl concentration affected the interactions of SNP in an aqueous solution. In the presence of NaCl, the apparent viscosity of SNP produced by the two drying methods exhibited opposite trends, where those from freeze drying had increased viscosity with salt concentration (Shi et al. 2013). Furthermore, the thermal stability as determined by the dynamic rheological properties as a function of temperature (25-90°C) indicated that addition of salt results in suspensions with better thermal stability.

More recently, the rheological behaviours of waxy maize SNC and SNP as a function of ionic strength were compared (Jiang et al. 2016). The effect of temperature, frequency and ionic strength on the dynamic rheological properties varied between SNC and SNP, which were prepared by acid hydrolysis and by a controlled self-assembly of short linear chains, respectively.

All SNP suspensions showed a shear-thinning behaviour regardless of the salt concentration. In another study, the pasting properties of normal corn SNP obtained by precipitating a starch paste solution with ethanol were also investigated using a rapid visco analyzer (Ma et al. 2008). In comparison to the native starch, SNP did not show the characteristic pasting curve (increase in viscosity with temperature). At low concentrations, the viscosity of SNP solutions remained unchanged during heating and showed similar properties to pregelatinized starch, whereas, at higher concentrations, heating induced melting of SNP, which was accompanied by a slight increase in viscosity.

2.3.3. Current uses and potential applications

2.3.3.1 Non-food applications

SNC and SNP have attracted a lot of attention due to their potential use in applications including polymer nanocomposites, biomedical materials and binding or paper coating. SNP are obtained from an inexpensive and abundant raw material, and in comparison to other synthetic nanomaterials, they are biodegradable, natural and non-toxic. For these reasons, the use of SNP has dramatically increased over the past 10 years. In particular, significant amount of research has been devoted to their use as a reinforcing filler in polymer matrices also known as nanocomposites. In biomedical applications, nanospheres may regulate drug release and due to their biodegradable nature these can also serve as implant materials (Santander-Ortega et al. 2010). Furthermore, in the paper industry SNP are a suitable alternative to cooked starch for paper binding and coating because of their high binding capacity and low paste viscosity (Kim et al. 2015).

The reinforcing effects of SNC and SNP have been tested in natural and synthetic polymers, including natural rubber (Angellier et al. 2005a), polylactic acid (Yu et al. 2008), pullulan (Kristo and Biliaderis 2007), soy protein isolate (Zheng et al. 2009), polyvinyl alcohol (Chen et al. 2008) and polybutylene succinate (Lin et al. 2011b). According to the above mentioned studies, polymer films containing SNC and SNP have higher tensile strength and elongation at break, due to the homogenous dispersion of the nanoparticles and the strong interfacial interactions with the polymer matrix. The presence of surface hydroxyl groups in SNC and SNP make these nanoparticles hydrophilic in nature and thus they exhibit a low affinity to hydrophobic polymer matrices. In order to minimize this problem, various surface modification techniques including grafting and cross-linking have been extensively studied. This information is outside of the scope of this thesis and not discussed further. For more details, the reader is referred to the following reviews, which explain in detail the preparation and chemical modifications of SNC materials (Lin et al. 2012; Le Corre and Angellier-Coussy 2014).

Nanocomposite films are commonly produced by the casting and water evaporation method in order to prevent exposure to high pressures and temperatures that can damage the crystalline structure of SNC. The basic procedure for preparing nanocomposites consists of; 1) combining the SNC suspension and polymer material, 2) mixing and vacuum degassing to avoid the formation of bubbles and 3) casting and water evaporation above the glass transition temperature of the polymer (Le Corre and Angellier-Coussy 2014). Other techniques, including hot-pressing and compression molding with extrusion can also be used to prepare polymer nanocomposites; however, these can cause melting of SNC and therefore change their reinforcing effect (Kim et al. 2015).

The production of nanocomposite films by casting and water evaporation using natural rubber latex as the matrix and an aqueous suspension of waxy maize SNC as the reinforcing agent was investigated by Angellier et al. (2005a). X-ray diffraction showed no damage was done to the crystalline SNC structure during the preparation method. A decrease in the water vapor permeability and oxygen diffusion was observed with increasing SNC content from 2 to 50%. Scanning electron micrographs of the films confirmed the filler was evenly distributed within the polymer matrix and thus the authors postulated that the platelet structure of waxy maize SNC plays a significant role in its barrier properties. In another study, the combination of a natural nanoparticle filler (pea SNC) into a synthetic polymer (polyvinyl alcohol PVA) was investigated (Chen et al. 2008). The films prepared by the non-thermal casting and water evaporation method and containing up to 30% pea SNC had very similar transparency to the pure PVA films. Moreover, films with 5 to 10% pea SNC had higher tensile strength, elongation at break and lower moisture uptake than the pure PVA films. More recently, the reinforcing effect of wheat SNC and cellulose whiskers into a plasticized starch matrix were compared (Nasseri and Mohammadi 2014). Both fillers were extracted by the same process and the films produced in a similar fashion for better comparison. The authors reported a higher reinforcement effect in spherical SNC than those containing rod-like cellulose whiskers. This finding was contradictory to previous findings that nanoparticles with a higher aspect ratio (cellulose whiskers) have better reinforcing effect (de Rodriguez et al. 2006; Jiang et al. 2007).

To date, only two commercial products with SNP are available. A collaboration project between Goodyear and Novamont produced BioTRED tires, which replaced some of the carbon

black and silica with nanoparticles from corn starch. In contrast, Ecosynthetix developed a starch-based biolates (Eco-Sphere) used for paper coating or tissue complexing.

2.3.3.2 Food applications

Several reviews are available, which discuss the potential impact of nanotechnology in the food industry (Bouwmeester et al. 2014; Mihindukulasuriya and Lim 2014; Rossi et al. 2014; Warriner et al. 2014). These reviews emphasize the implications and future trends for the food sector (Rossi et al. 2014), the development of nanosensors for food safety (Warriner et al. 2014), the safety and risk assessment of nanomaterials in food production (Bouwmeester et al. 2014) and the development of food packaging materials (Mihindukulasuriya and Lim 2014). With respect to food packaging, the incorporation of nanomaterials (silicate and clay) into synthetic polymer based nanocomposites have been shown to enhance the mechanical and barrier properties of these materials. However, new concerns with the environmental impact of these materials demand more sustainable and environmentally friendly alternatives.

Films from biodegradable materials such as thermoplastic starch and the incorporation of biodegradable SNP into natural polymers are currently being investigated. In the presence of SNP, natural rubber films have been shown to have enhanced barrier properties (Angellier et al. 2005a). Similar results were also found by Kristo and Biliaderis (2007) who reported a significant decrease in the water vapor permeability of sorbitol-plasticized pullulan film with the addition 30-40% waxy maize SNC. Developing ways to improve or control the barrier properties of food packages is of significant importance to the food industry due to the saving costs associated with increasing the product shelf life and product quality.

To date, SNP have not been incorporated into any commercial food products; however, based on their functional properties they are a promising candidate as a thickening, bulking, and texturizing agent, fat replacer, emulsion stabilizer, etc. For example, research has shown that SNP in solution increase the viscosity of the aqueous system with a positive correlation between the viscosity and SNC concentration (LeCorre et al. 2011). Furthermore, at high concentrations, SNP suspension have a similar rheological behaviour to gelatinized starch, a common thickening agent used in foods. Their ability to modify texture also make these a suitable fat replacer. Currently, the fat content in a food product can be reduced by the incorporation of modified starches and gums, which provide a similar functionality with a lower caloric intake.

Lastly, the use of SNC as an oil-in-water emulsion stabilizer for their potential use in food and cosmetic applications were recently investigated by Li et al. (2012) and Li et al. (2014). The emulsions of 1:1 water to paraffin, were stabilized by the incorporation of different waxy maize SNC concentrations (0.2 - 60 mg/ml), and showed no coalescence after 5 months and 1 year of storage. Their stability was due to the presence of negative surface charges (sulfate ester groups), and their stabilizing effect was reduced by decreasing the pH or adding salt to the emulsions. During heating, Li et al. (2012) observed a stable emulsion at less than 60°C whereas at 80°C the emulsion phase separated possibly due to SNC melting. Prior to the use of SNP in food systems, more research is needed in the area of safety and risk assessment in order to understand how these ingredients influence human physiology.

CHAPTER 3 Characterization of maize starch nanoparticles prepared by acid hydrolysis

3.1. INTRODUCTION

Acid hydrolysis has been used to modify the starch granule structure and produce soluble starch for many years. However, more recently, starch nanocrystals (SNC) and starch nanoparticles (SNP) have been prepared with acid hydrolysis, which are being used as fillers in polymeric matrices to improve their mechanical and/or barrier properties (Angellier et al. 2005a). SNC and SNP are crystalline structures resulting from the disruption of the semi-crystalline structure of starch granules by the acid hydrolysis of the amorphous regions (Le Corre and Angellier-Coussy 2014). SNP have been found to vary in length, shape and yield according to the acid type, acid concentration, hydrolysis time, and starch source. SNC are defined as the highly crystalline amylopectin residues, which can resist acid hydrolysis (Putaux et al. 2003; Angellier et al. 2004; Angellier-Coussy et al. 2009; LeCorre et al. 2011; Wei et al. 2014) and thus have been mainly isolated from waxy maize. However, their isolation from different botanical origins have also been reported by LeCorre et al. (2011), Kim et al. (2012) and Xu et al. (2014). In these studies, SNP were prepared by hydrolysis of starches with 3.16 M H₂SO₄ at 40°C for 5 days followed by several water washings and centrifugal cycles until the washed water was at or near neutrality. The authors reported that the final residue after repeated water washings contained SNC or SNP.

*A version of this chapter was published in *Cereal Chemistry*, 2016, 93:323-330.

A preliminary study using waxy and high amylose (hylon VII) maize starch revealed that the final residues after acid hydrolysis of the starches were composed of a mixture of both nanoparticles and unhydrolyzed or partially hydrolyzed starch granules. Furthermore, repeated water washing of the hylon VII residue removed most of the SNP fraction into the wash water, specifically in the wash water collected after washes 9-15. When the same washing protocol was implemented on the waxy maize (WM) starch residue, SNP did not separate into the wash water. This finding suggests that the SNP isolated from waxy starches may show different properties compared to those obtained from amylose containing starches. Research on SNP has been solely concentrated on the study of the morphology and properties of the residues remaining after completion of the washing cycles. However, the characteristics of the SNP isolated from the wash water of amylose containing starches and the mechanism of amylose involvement in SNP formation have not been reported.

The objectives of this study were twofold: 1) to investigate the impact of water washings on the extent of SNP separation from the acid hydrolyzed residue, containing unhydrolyzed and partially hydrolyzed starch granules of maize starches varying in amylose content, and 2) to determine whether varying the amylose content among waxy (0% amylose), normal (21.6% amylose), hylon V (47.0% amylose) and hylon VII (71.0% amylose) maize starches influences the yield, morphology, and crystallinity of the nanoparticles in the separated fractions.

3.2. MATERIALS AND METHODS

3.2.1. Materials

Waxy maize (Amioca), normal maize (Melojel) and high amylose maize (hylon V and hylon VII) (>95% purity) were provided by Ingredion Incorporated (Westchester, IL, U.S.A). All other

chemicals were of ACS-certified grade. Pure amylose and amylopectin were obtained from Sigma-Aldrich (Saint Louis, MO, USA).

3.2.2. Chemical composition

Apparent amylose content was determined by the colorimetric procedure (Hoover and Ratnayake 2001). A detailed protocol is given in the Appendix II. Apparent amylose content was calculated from the standard curve obtained with pure potato amylose and amylopectin mixtures, over the range of 0-100%.

3.2.3. Acid hydrolysis of native starches and fractionation of hydrolyzed starch residues

The acid hydrolysis process followed the methodology reported by Angellier et al. (2004) with modifications (Figure 3.1). Native starch (4 g) was mixed with a solution of 3.16 M of H₂SO₄ (starch concentration in the slurry was ~14.7% w/v) and incubated at 40°C in a water bath for 1-6 days with frequent vortex mixing. The hydrolysate suspension was centrifuged (12,000 x g for 15 min) and the supernatant was discarded. The starch residue was then washed 15 times with distilled water (30 ml), and the supernatants from the washings 2-8 and 9-15 were pooled and designated as fraction 1 and fraction 2, respectively (Figure 3.1). At the 15th wash, the starch slurry (acid hydrolyzed starch residue and water) was homogenized at 15,200 rpm for 3 min (Heidolph Diax 900, Heidolph Instruments, Schwabach, Germany) to aid dispersion and centrifuged at 12,000 x g for 15 min. Fraction 2 representing the pooled supernatants 9-15, was filtered using a glass microfiber filter with a 1 µm pore size (GF/B Whatman, GE Healthcare, Little Chalfont, U.K.) and lyophilized.

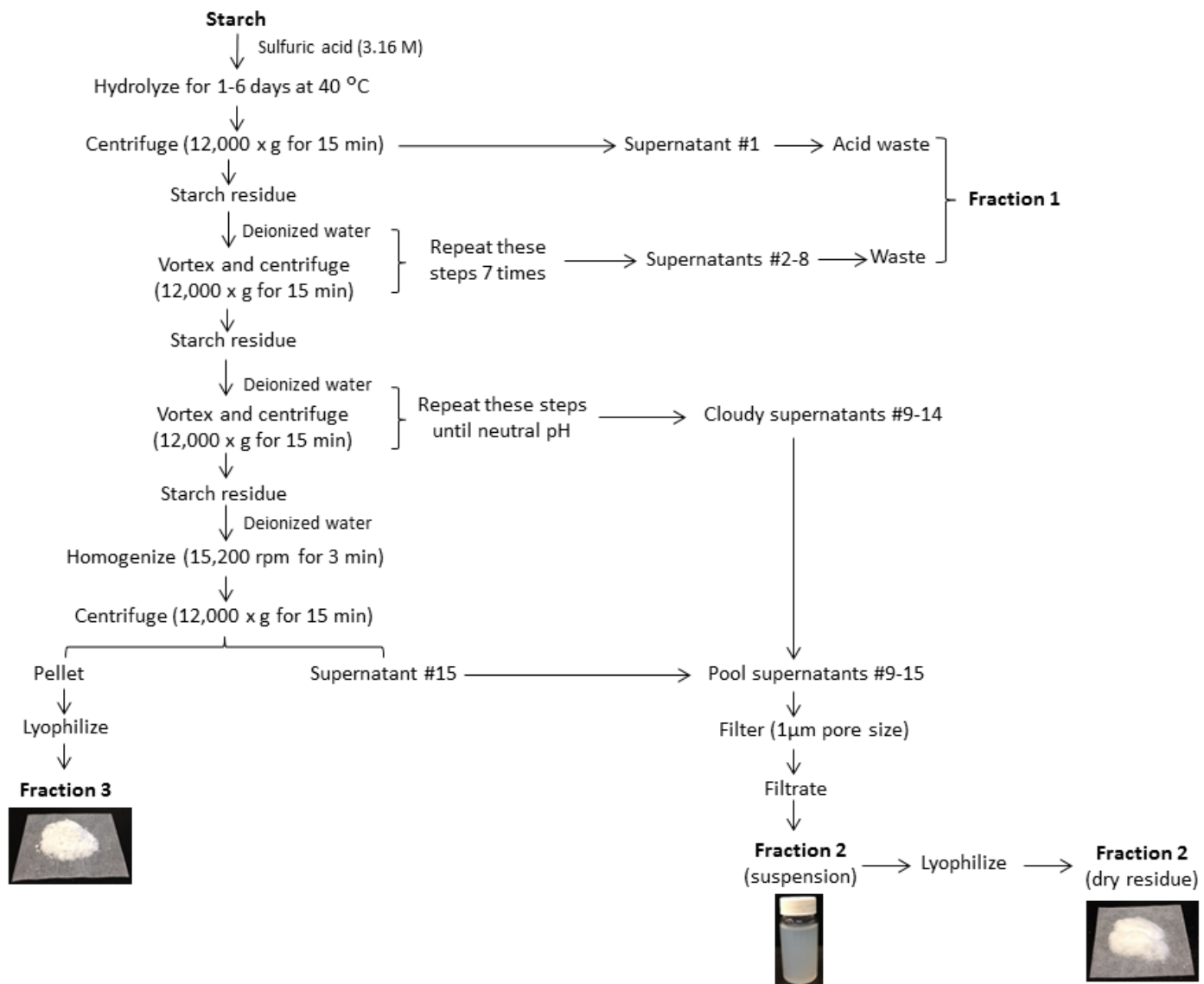


Figure 3.1 Protocol for acid hydrolysis and fractionation of the hydrolyzed starch residues.

The final starch residue obtained after the 15th wash was also lyophilized and designated as fraction 3 (Figure 3.1). The extent of acid solubilized starch was calculated as the percentage of starch solubilized in fraction 1, based on the initial starch weight. The fractionation protocol was replicated.

3.2.4. Scanning electron microscopy

Native starch granules were mounted on circular aluminum stubs with double-sided sticky tape and coated with 12 nm thickness of gold. Fractions 2 and 3 were mounted on glass cover slips, coated with a 10 nm thickness of chromium and then examined in the lyophilized state and after addition of water and air drying by scanning electron microscopy (model JSM 6301, JOEL, Tokyo, Japan) at an accelerating voltage of 5 kV.

3.2.5. X-ray diffraction

X-ray diffraction was determined based on the methodology of Naguleswaran et al. (2013) with modifications. Before X-ray analyses, the moisture contents of all samples were equilibrated to ~20% by keeping them in a desiccator over saturated K₂SO₄ solution (water activity = 0.98 at 25°C) for 12 days. X-ray diffractograms were obtained with cross beam optics technology of Rigaku Ultima IV multipurpose X-ray diffractometer (Rigaku America, Woodlands, TX, U.S.A). The starch powder was scanned through the 2 θ range of 5-40°, using a Co-K α X-ray tube with a D/teX Ultra counter operating at the following conditions: target voltage, 38 kV; target current, 38 mA; scan speed, 1.0°/min; divergence slit width, 1 cm; scatter slit width, 1.3 cm; and receiving slit width, 1.3 cm. All data files were converted from cobalt (1.78899 Å) to copper (1.54059 Å) by changing the radiation wavelength. Relative crystallinity was measured

based on the method of Lopez-Rubio et al. (2008), using the Origin 9.1 software (OriginLab Northampton, MA, U.S.A.).

3.2.6. Turbidity

The extent of cloudiness of the aqueous suspensions of fraction 2 (pooled supernatants 9-15) were determined by measuring the % light transmittance (%T) (Perera and Hoover 1999). Triplicate samples were placed in cuvettes and the turbidity was determined by measuring transmittance at 640 nm against a water blank with a Jenway UV/Vis Spectrophotometer (6320D spectrophotometer, Bibby Scientific, Stone, U.K.).

3.2.7. Statistical analysis

The SNP isolation was replicated twice and all determinations were done in triplicates where the mean and standard deviations are reported. Analysis of variance was performed, and the mean comparisons were determined by Tukey's HSD test at $P < 0.05$ with Origin 9.1 software (OriginLab).

3.3. RESULTS AND DISCUSSION

3.3.1. Solubilization patterns

The acid solubilization patterns of native starches are presented in Figure 3.2. All starches exhibited a relatively high rate of hydrolysis (WM > normal maize [NM] > hylon V > hylon VII) during the first 6 days, corresponding mainly to the degradation of the amorphous regions of the granule. Acid hydrolysis of starch with 2.2N HCl has been shown (Robin et al. 1975) to consist of an initial fast step owing to the hydrolysis of the amorphous regions of the granule followed by a second slower step owing to the hydrolysis of the crystalline regions.

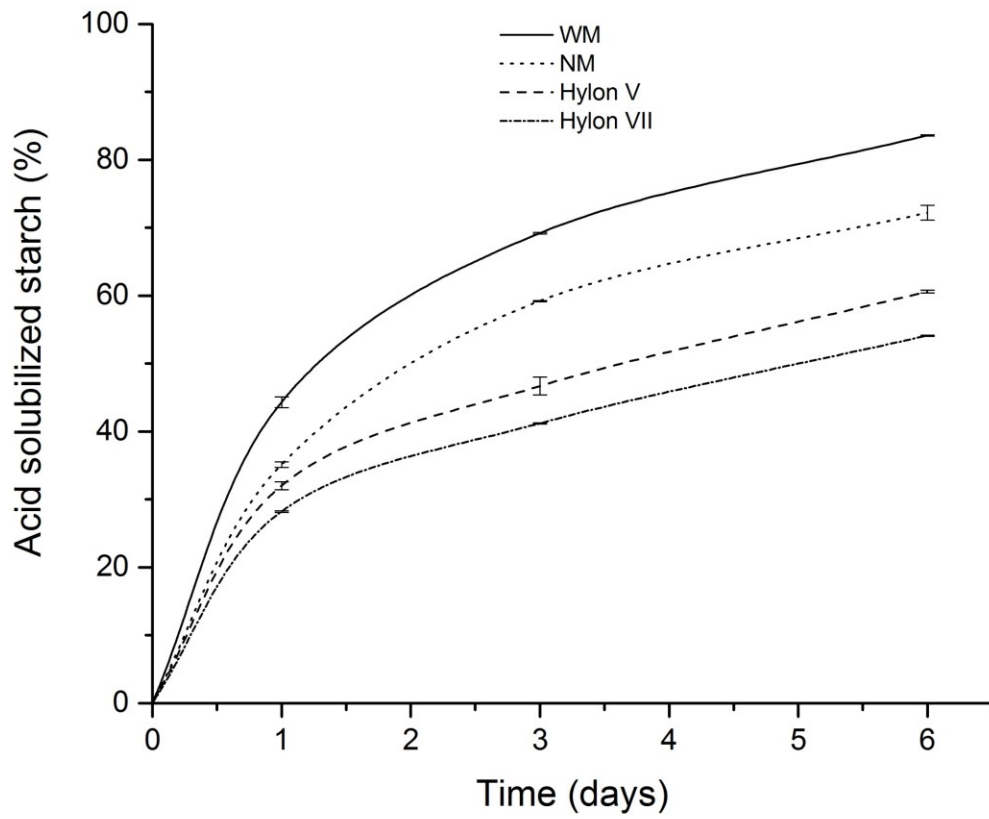


Figure 3.2 Acid hydrolysis profile of native starches in 3.16 M of H_2SO_4 at 40°C.

To account for the slower rate of hydrolysis of the crystalline domains of the starch granule, two hypotheses (French 1984) have been proposed. First, the dense packing of starch chains within the starch crystallites does not readily allow the penetration of H_3O^+ into these regions. Second, the chair to half chair transformation, required for hydrolysis of the glucosidic bond, occurs very slowly owing to immobilization of the sugar conformation within the starch crystallites. Differences in the rate and extent of hydrolysis among the starches were more pronounced after the first 3 days. At the end of the sixth day, WM, NM, hylon V and hylon VII were hydrolyzed to the extent of 83.5, 72.2, 60.6 and 54.1%, respectively. These differences in the kinetics of hydrolysis can be attributed to the interplay among the following factors: 1) amount of lipid complexed amylose chains (hylon VII > hylon V > NM > WM) (Jayakody and Hoover 2002), 2) pores on the granule surface (hylon V > NM > WM) (Figure 3.3), 3) granule size (NM > hylon V ~ WM > hylon VII), 4) extent to which amylose chains are co-crystallized with amylopectin and/or are buried within the crystalline lamellae (hylon VII > hylon V > NM) (Vamadevan et al. 2014) and 5) packing density of amylose chains within the amorphous regions (hylon VII > hylon V > NM) (Hoover and Manuel 1996).

3.3.2. Fractionation of acid hydrolyzed starch

Multiple water washing cycles were used to separate the SNP from unhydrolyzed and partially hydrolyzed starch granules according to the protocol in Figure 3.1. The native starch hydrolysate was separated into fractions 1, 2 and 3. During repeated washings, waxy and non-waxy starches behaved differently. The supernatants of all starches from each of the 8 initial washes were clear. However, supernatants from washings 9-15 appeared cloudy in NM, hylon V and hylon VII, but remained clear in WM (Figure 3.4).

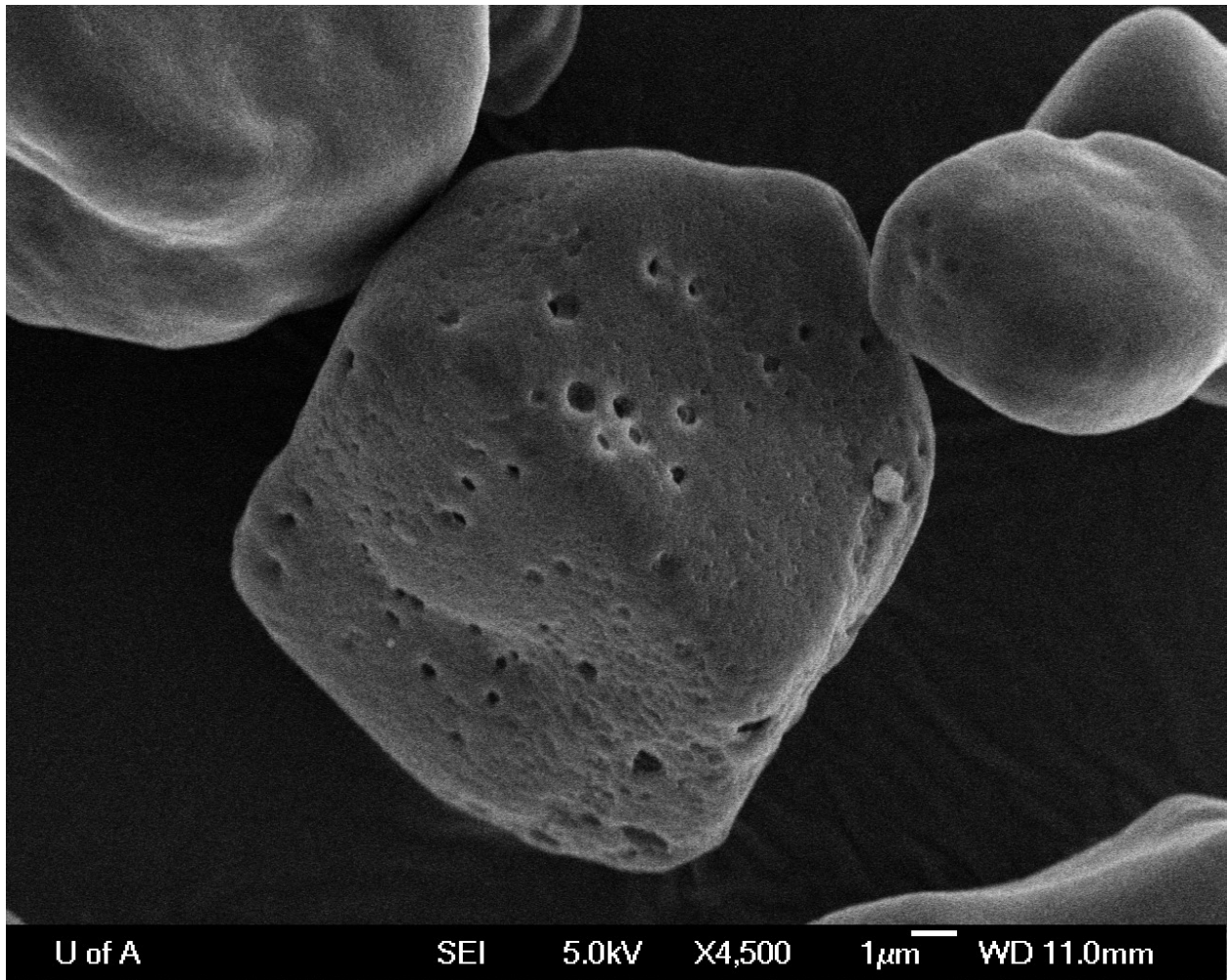


Figure 3.3 Scanning electron microscopy image showing surface granule pores in native normal maize starch.

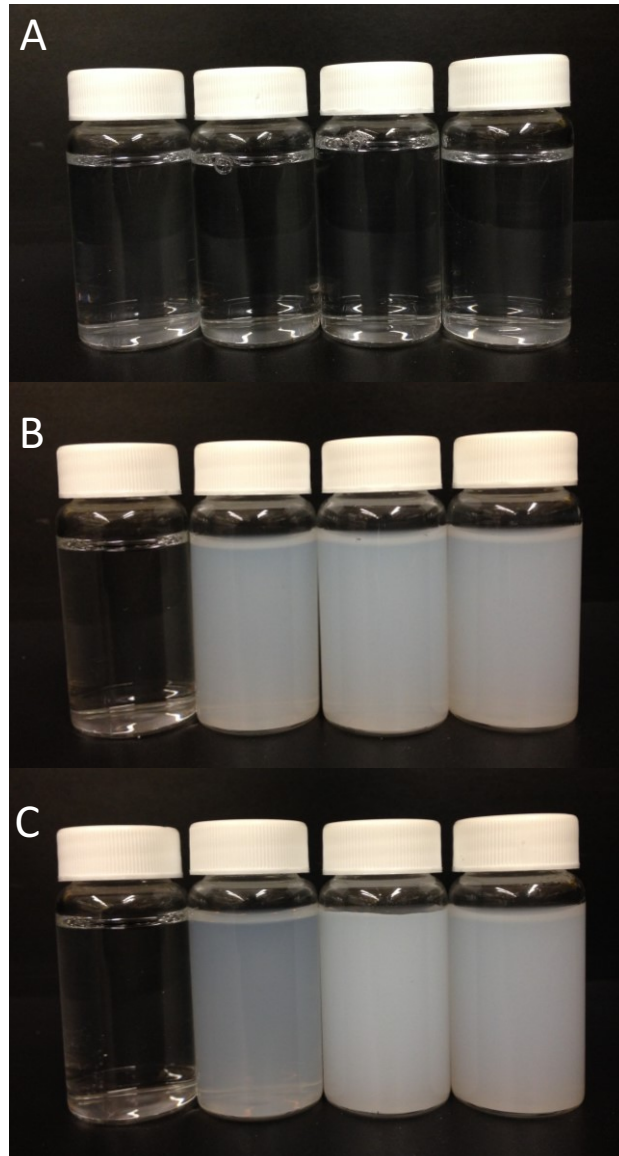


Figure 3.4 Suspensions of fraction 2 obtained after (A) 1, (B) 3 and (C) 6 days of acid hydrolysis. Vial left to right represent waxy maize, normal maize, hylon V, and hylon VII starches.

Consequently, supernatant 1 and the clear supernatants 2-8 were collected separately and pooled as fraction 1. The cloudy supernatants (9-15) were pooled as fraction 2 and the starch residue in the pellet collected as fraction 3 (Figure 3.1). The cloudiness that first appeared at wash 9 (average pH 4.8) was indicative of the presence of particulate material with colloidal stability. It is likely that hydrolysis with sulfuric acid results in the addition of negative sulfate ester groups (SO_3^-) to the particulate material, which remain aggregated together with the hydrolyzed residue at a low pH and then became dislodged when the pH exceeded 4.8 due to electrostatic repulsion. This observation seems plausible, because these particles remained suspended in solution for over 45 days at room temperature (22°C). The extent of cloudiness in fraction 2 increased with hydrolysis time (Figure 3.4) and was more pronounced in hylon V and hylon VII (hylon VII > hylon V) than in NM (Table 3.1). Because the presence of particulate material in fraction 2 was only observed in amylose-containing starches, the involvement of amylose linear chains in this fraction was proposed. The absence of particulates in fraction 2 of WM is in agreement with the current protocol (Angellier et al. 2004) used for the preparation of SNC, in which extensive water washings and centrifugation cycles are not utilized. In WM, all of the starch residues left after acid hydrolysis and repeated water washing were collected as a pellet in fraction 3.

3.3.3. Turbidity measurements

The extent of cloudiness in fraction 2 of WM, NM, hylon V and hylon VII at different stages of hydrolysis determined by measuring %T is presented in Table 3.1. Turbidity effects have their origin in refractive index fluctuations over a distance scale comparable to the wavelength of observation (Gidley and Bulpin 1989).

Table 3.1 Light transmittance of fraction 2 in suspension form

Fig 3.4	Hydrolysis time (days)	% Light Transmittance			
		WM	NM	Hylon V	Hylon VII
A	1	99.2±0.2a	99.9±0.1a	99.6±0.1a	97.1±0.3a
B	3	98.9±0.2a	47.9±0.2b	30.4±0.1b	21.4±0.2b
C	6	99.5±0.4a	73.6±0.2c	8.23±0.1c	10.3±0.1c

Values followed by the same letter in the same column are not significantly different ($P < 0.05$), based on Tukey's HSD test. WM = waxy maize, and NM= normal maize.

In a polymer-solvent system, refractive index fluctuations are caused by density fluctuations over the same distance scale and are most likely owing to extensive polymer-polymer chain aggregation. During the first 3 days of hydrolysis (Table 3.1), %T remained unchanged in WM; however, it decreased rapidly in the other starches (hylon VII > hylon V > NM). Thereafter, %T increased in NM, but continued to decrease in hylon V and hylon VII starches and remained unchanged in WM. The decrease in %T, which correlates with the amylose content, could be attributed to the formation and aggregation of double helices resulting from the interaction between hydrolyzed amylose chains, which grew sufficiently to show a particulate nature. It is also likely that the decrease in %T could reflect the presence of amylopectin blocklets that may have been dislodged from their orderly arrangement within the crystalline growth rings owing to hydrolysis of amylose tie chains present in between the amylopectin blocklets. This mechanism is plausible because 1) %T remained unchanged in WM, and 2) the extent of decrease in %T increased with increase in amylose content (Table 3.1). The decrease in %T on day 3, and the subsequent increase in %T on day 6 seen with NM (Table 3.1) are indicative of the rate and extent

of aggregation of hydrolyzed amylose chains of NM being slower and weaker owing to lower amylose content and longer chain length [NM (DP_n 990), hylon V (DP_n 660), hylon VII (DP_n 740)] (Takeda et al. 1988; Takeda et al. 1993). Consequently, it is possible that aggregated amylose chains of NM formed during the first 3 days of hydrolysis may have been partially hydrolyzed, resulting in an increased %T on day 6.

3.3.4. Mass balance of fractions 1, 2 and 3

The mass balance (yield) of the three fractions obtained at different days of acid hydrolysis following the protocol in Figure 3.1 is presented in Table 3.2. The yield of fraction 1 was calculated by subtracting the pooled dry weight of fractions 2 and 3 from the dry weight of the native starches. During the progress of hydrolysis, the yield of fraction 1 decreased in the following order: WM (83.5%) > NM (72.2%) > hylon V (60.6%) > hylon VII (54.1%). The yield of fraction 2 decreased in WM (from 2.1 to 0.9%), but increased in the other starches (hylon VII [from 0.4 to 26.6%] > hylon V [from 0.5 to 19.9%] > NM [from 1.1 to 10.3%]) with an increase in hydrolysis time from day 1 to day 6. At the end of day 6, the amount of fraction 2, representing the dislodged blocklets and retrograded crystalline amylose, followed the order: hylon VII > hylon V > NM > WM. This order followed the extent of decrease in %T (hylon VII > hylon V > NM) on day 6 as reported in the turbidity measurements (Table 3.1). Furthermore, at the end of day 6, WM was composed mostly of fraction 3 (15.6%) and non-waxy starches contained a mixture of fraction 2 and fraction 3 corresponding to 10.3% and 17.5% for NM, 19.9% and 19.5% for hylon V, 26.6% and 19.3% for hylon VII, respectively. Earlier researchers reported no correlation between the yield of SNC and amylose content from starches of different botanical origins and stated SNC are composed of amylopectin side chains (LeCorre et al. 2011; Xu et al. 2014).

Table 3.2 Mass balance of the acid hydrolyzed starch fractions

Sample	Fraction	% Yield		
		1 Day	3 Days	6 Days
WM	1	44.3 ± 0.8e	69.2 ± 0.0a	83.5 ± 0.0a
	2	2.15 ± 0.1i	1.93 ± 0.1j	0.86 ± 0.0k
	3	53.6 ± 0.7d	28.9 ± 0.1g	15.6 ± 0.0i
NM	1	35.1 ± 0.4f	59.3 ± 0.1b	72.2 ± 1.1b
	2	1.06 ± 0.2j	12.9 ± 0.3i	10.3 ± 0.2j
	3	63.8 ± 0.2c	27.8 ± 0.4g	17.5 ± 0.9hi
Hylon V	1	32.0 ± 0.6g	46.7 ± 1.3c	60.6 ± 0.2c
	2	0.46 ± 0.1k	17.5 ± 1.0h	19.9 ± 0.1f
	3	67.6 ± 0.5b	35.8 ± 0.4f	19.5 ± 0.1g
Hylon VII	1	28.2 ± 0.0h	41.2 ± 0.1e	54.1 ± 0.1d
	2	0.35 ± 0.1l	16.7 ± 1.0h	26.6 ± 0.2e
	3	71.4 ± 0.1a	42.1 ± 1.0d	19.3 ± 0.3gh

Protocol for obtaining fractions is shown in Figure 3.1. Values followed by the same letter in the same column are not significantly different ($P < 0.05$), based on Tukey's HSD test. Values reported are on % dry basis of the original starch weight. WM= waxy maize, and NM= normal maize.

In this study, a positive correlation between the yield of fraction 2 in non-waxy starches and the amylose content of the native starches was found. This result may be indicative of the amylose participation in the particulate material collected as fraction 2. Is it possible that during acid hydrolysis, disruption of the starch granules led to the release of hydrolyzed amylose chains which retrograded and recrystallized to form aggregates with a particulate nature. According to Ring et al. (1987) and Cai and Shi (2013), short chain amylose can be recrystallized to form starch spherulites, which vary in their crystalline type due to the temperature of recrystallization.

3.3.5. Morphology of native starch and their acid hydrolyzed fractions 2 and 3

The granule morphology of native starches is presented in Figure 3.5A-D. The granules of WM were angular and irregular in shape and ranged in size between 4 and 12 μm (Figure 3.5A). NM granules were spherical, round or irregular in shape with diameters in the range 5-18 μm (Figure 3.5B). Some granules of NM were smooth, and others exhibited surface pores. The granules of hylon V with diameters in the range of 5-15 μm were oval to spherical to irregular to rod shaped (Figure 3.5C). The surfaces of hylon V granules were rough with pores and fissures (Figure 3.5C). The granules of hylon VII were of the same shape (Figure 3.5D) as those of hylon V (Figure 3.5C). However, hylon VII granules were smaller (6-10 μm) with smooth surfaces.

The morphology of fractions 2 & 3, obtained after 6 days of acid hydrolysis, are presented in Figure 3.5E-G and H-K, respectively. The morphology of fraction 2 was examined in the form of a suspension that was allowed to air dry on the stub. In a suspension form, NM (Figure 3.5E) exhibited SNP (50 to 200 nm) that were oval to irregular in shape. However, those of hylon V (Figure 3.5F) and hylon VII (Figure 3.5G) were oval to round (40-50 nm) and square to round to polygonal (50-100 nm), respectively. All starch sources showed different morphological characteristics for fraction 3 (Figure 3.5H-K) despite being hydrolyzed for the same time period. The freeze-dried fraction 3 of WM (Figure 3.5H) showed sheet-like fragments that ranged in size from 50 to 300 μm , which may have resulted from the aggregation of acid-resistant SNP with hydrolyzed amorphous material. In contrast, fraction 3 from NM (Figure 3.5I), hylon V (Figure 3.5J) and hylon VII (Figure 3.5K) exhibited intact (hylon VII \sim hylon V > NM) and partially hydrolyzed granules (NM).

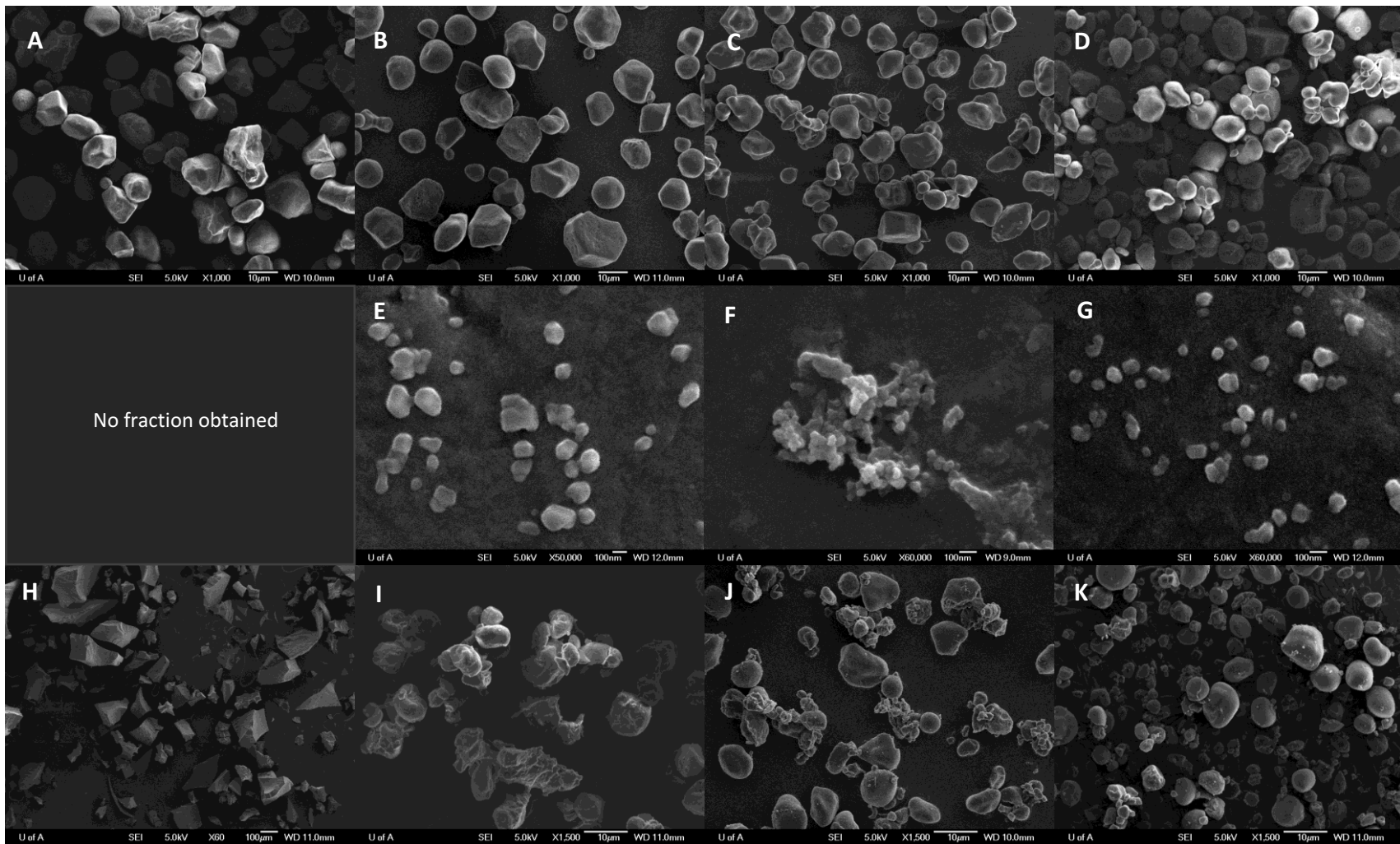


Figure 3.5 Scanning electron microscopy images of native starch granules and fractions 2 and 3 collected after 6 days of acid hydrolysis. A-D, native starch granules of waxy maize (WM), normal maize (NM), hylon V and hylon VII, respectively (scale bar = 10 μ m). E-G, fraction 2 suspensions of NM, hylon V and hylon VII, respectively (scale bar = 100 nm). H-K, fraction 3 suspensions of WM, NM, hylon V and hylon VII, respectively (scale bar = 10 μ m), that were subjected to freeze drying.

The morphology of the WM suspension obtained after 6 days of hydrolysis (fraction 3) is presented in Figure 3.6. In a suspension form, WM exhibited flat ellipsoidal SNP, 150 nm width x 500 nm length, with an approximate thickness of 20-30 nm (Figure 3.6). The SEM images revealed morphological differences between the starch types, suggesting the nanoparticles may be composed of different entities, which make up the granular rings. The particle size distribution of the native starch granules and their acid hydrolyzed fractions 2 and 3 collected after 6 days of acid hydrolysis can be found in the Appendix II.

3.3.6. X-ray diffraction

X-ray diffraction patterns and relative crystallinity (RC) of native starches and their hydrolyzed fractions 2 and 3 obtained after day 6 of hydrolysis are presented in Figure 3.7. Native WM and NM starches exhibited A-type polymorphic patterns with peaks centered at 15, 17, 18 and 23° 2 θ and 15, 17, 18, 20 and 23° 2 θ , respectively. Native hylon V and hylon VII exhibited B-type polymorphic patterns centered at 5.6, 15, 17, 22 and 24° 2 θ . The X-ray pattern of fraction 2 NM (A-type) was nearly similar to that of native NM. However, X-ray intensities and RC in fraction 2 NM were higher. In contrast, the X-ray diffractograms of fraction 2 of hylon V and hylon VII were different from that of their native counterparts with respect to 1) change in X-ray pattern (B to A + B), 2) absence of the peak centered at 5.6° 2 θ (reflects a decrease in double helical chain length forming the B-type crystallites), 3) decrease in the intensity of the peak centered at 20° 2 θ (reflects a decrease in the proportion of lipid complexed amylose chains and/or hydrolysis of ordered V6-type single helical structures) (Gidley and Bociek 1985; Waduge et al. 2014), 4) merging of the doublets centered at 22-24° 2 θ , 5) appearance of peaks centered at 10° and 11.5° 2 θ and 6) higher RC (Figure 3.7B).

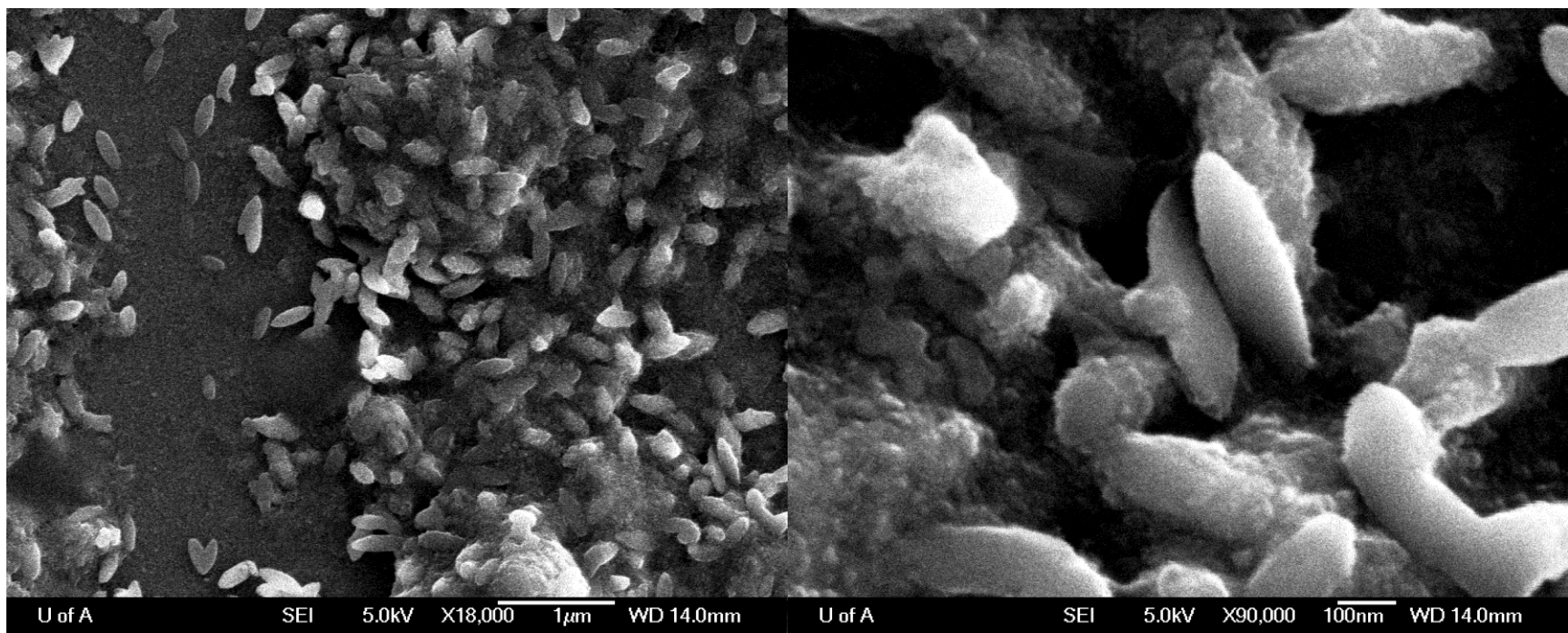


Figure 3.6 Scanning electron microscopy images of fraction 3 suspension of waxy maize collected after 6 days of acid hydrolysis.

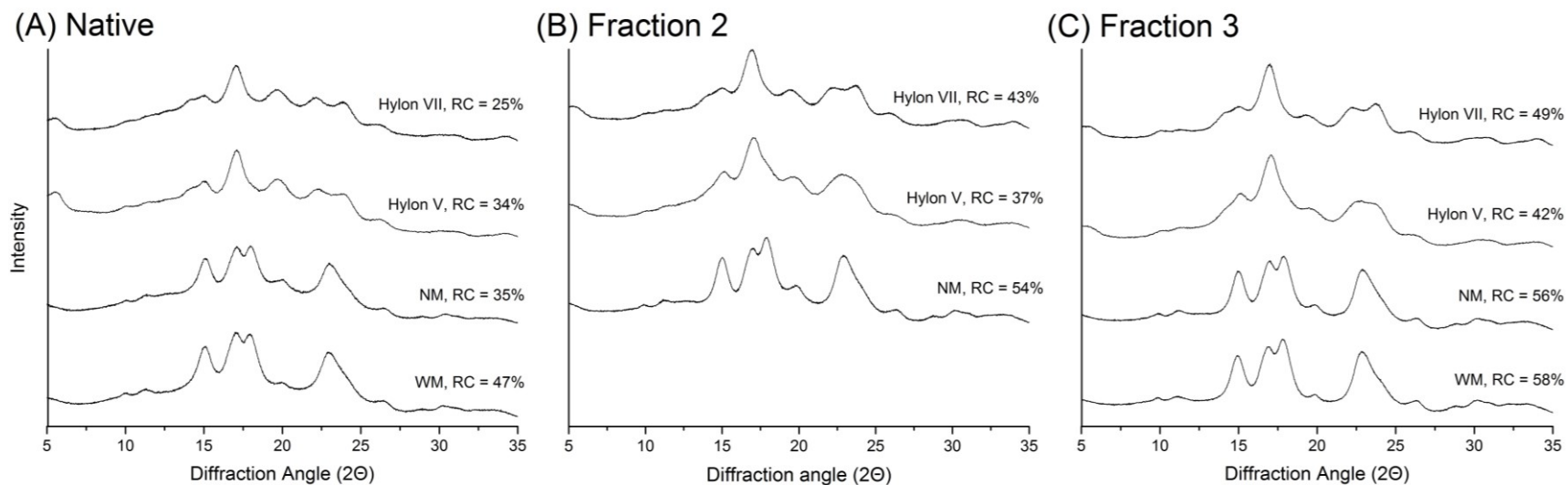


Figure 3.7 X- ray diffraction patterns and relative crystallinity (RC) of (A) native starch, (B) fraction 2 and (C) fraction 3 collected after 6 days of acid hydrolysis

Merging of the doublets were more complete in hylon V than in hylon VII, because double helices forming the B-type crystallites were more extensively hydrolyzed in hylon V (Figure 3.2). The A-type X-ray pattern of fraction 3 WM (Figure 3.7C) was almost identical to that of native WM (Figure 3.7A). However, X-ray intensities and RC of fraction 3 WM were higher. Likewise, the A-type X-ray pattern of fraction 3 NM (Figure 3.7C) was almost identical to that of fraction 2 NM (Figure 3.7B) and native NM (Figure 3.7A). However, with the exception of the peak centered at $20^\circ 2\theta$, the intensities of all other peaks and the RC of fraction 3 NM were higher than those of fraction 2 NM and native NM.

The X-ray patterns (A+B) of fraction 3 hylon V and hylon VII (Figure 3.7C) were similar to those of fraction 2 hylon V and hylon VII (Figure 3.7B). However RC of the fraction 3 hylon V and hylon VII was higher. The differences in RC between fraction 3 WM, fraction 3 NM, fraction 2 NM and their respective native counterparts mainly reflect hydrolysis of the amorphous domains. Differences in RC between fraction 2 hylon V, fraction 2 hylon VII, fraction 3 hylon V, fraction 3 hylon VII and their respective native counterparts reflect both hydrolysis of amorphous domains and formation of double helical structures arranged in a crystalline array. These findings result from interactions and aggregation between hydrolyzed amylose chains, and can be explained considering the following reasons: 1) differences in X-ray patterns, intensities, and RC of fraction 2 and fraction 3 of hylon V and hylon VII starches and their respective native counterparts were more pronounced than those between fraction 2 and fraction 3 of NM and native NM starch, and 2) RC differences between fraction 3 of hylon VII and native hylon VII was much higher than that between fraction 3 of hylon V and native hylon V owing to higher extent of retrogradation between hydrolyzed amylose chains of hylon VII.

The X-ray data when considered along with the data obtained from fractionation, turbidity and morphology (shape and dimensions) suggest that the fraction 3 of WM consists mainly of SNP composed of amylopectin crystallites in the form of ellipsoidal blocklets (Figure 3.6), and fraction 2 of NM, hylon V and hylon VII consist mainly of SNP composed of amylopectin blocklets and retrograded crystalline amylose possibly in the form of starch spherulites. To explain the origin of morphological differences between waxy and non-waxy SNP, a model (Figure 3.8) is proposed based on the work reported by Atkin et al. (1998), on the sequence of events that occur during starch gelatinization. These authors showed by microscopy the presence of ellipsoidal particles, composed of single units of amylopectin clusters, in WM starch granules in excess water at ambient temperatures. These particles of 200-400 nm length and 60 nm width were shown to swell to spherical particles upon application of heat. During swelling, the amylopectin units in WM starch remained aligned along granular rings prior to a slow separation from the granular rings. Furthermore, the separation of 400 nm particles was instantaneous in amylose-containing starches and occurred at the onset of tangential swelling. This was attributed to the disruption of intermolecular interactions between amylopectin chains by amylose chains present between amylopectin molecules. Thus, according to this model (Figure 3.8), during acid hydrolysis and water washings, hydrolysis of amylose tie chains (Kozlov et al. 2007), present within the amorphous and crystalline lamellae of NM, hylon V and hylon VII starches may have disrupted the ordered amylopectin blocklets from their location within the growth rings, resulting in the release of nanoparticles, previously formed by disrupted amylopectin blocklets into fraction 2.

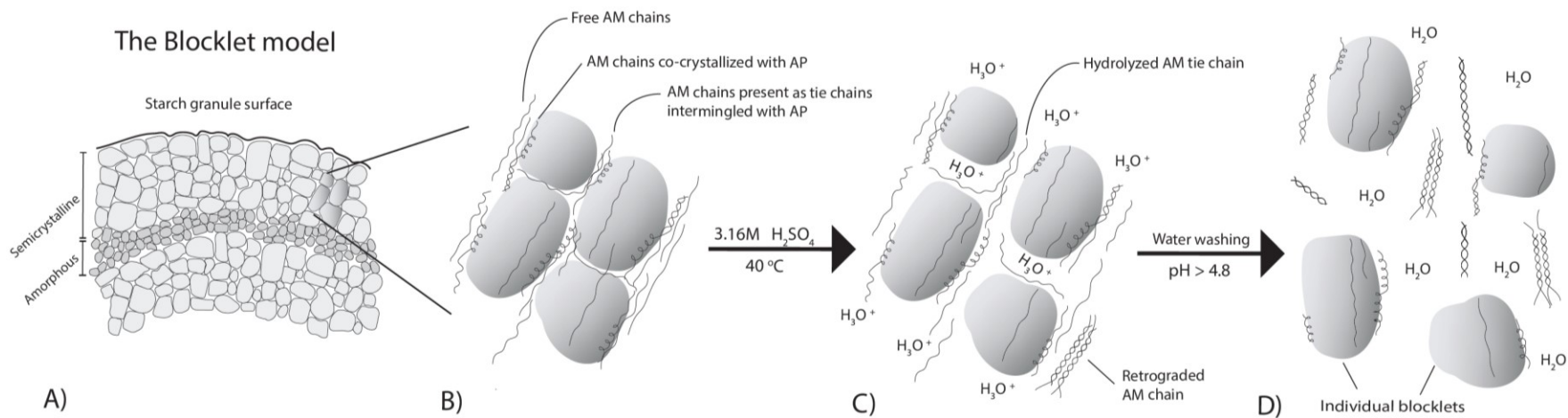


Figure 3.8 Sequence of events leading to the released of individual blocklets and the formation of retrograded amylose (AM) chains during acid hydrolysis of normal and high amylose maize starches.

Overview of the blocklet model (A). Close-up of the blocklet arrangement (B) within the native starch granule. AM is present as the interconnecting material within the blocklets as linear chains, co-crystallized with amylopectin (AP), or as tie chains. Hydrolysis of AM chains present in between blocklets in native normal and high-AM starches (C) will result in blocklets being dislodged from their ordered arrangement within the crystalline growth rings. Dislodged individual blocklets and retrograded AM chains in the fraction 2 (D) of normal and high-AM maize starches.

While it is also likely that fraction 2 contains nanoparticles made from retrograded amylose chains, resulting from interactions between amylose chains during hydrolysis (Figure 3.8). Therefore, when SNP are isolated from non-waxy starches using the acid hydrolysis and fractionation protocol described in Figure 3.1, it is expected that mechanisms of SNP formation, both “top-down” and “bottom-up”, are occurring simultaneously.

3.4. CONCLUSIONS

A modified acid hydrolysis protocol for SNP isolation from both waxy and non-waxy starches has been investigated. In waxy maize, the SNP concentrated in the water-washed acid-resistant starch residue, whereas in non-waxy starches, the SNP appeared in the water washings used in the removal of excess acid from the acid-resistant starch residues. Variation in amylose content among native starches influenced the yield, morphology and crystalline properties of SNP, which is expected to provide guidance in the selection of starch types for different SNP applications. Further research and improvements to the SNP isolation protocol in regard to minimizing the time of hydrolysis and water usage are warranted in order to make the protocol commercially appealing. This study expands the basic knowledge of starch nanotechnology, with the specific aim to better understand the role of amylose involvement in SNP formation and separation using the modified isolation protocol. SNP from non-waxy maize starches consisted mainly of disrupted round, irregular and polygonal amylopectin blocklets and retrograded crystalline amylose (spherulites). In contrast, SNP from waxy maize were composed mainly of elliptical amylopectin blocklets and/or crystallites.

CHAPTER 4 Molecular size distribution and amylase-resistance of maize starch nanoparticles prepared by acid hydrolysis

4.1. INTRODUCTION

The extent of hydrolysis of a starch granule is dependent on the acid type, acid concentration and hydrolysis time. An extensive hydrolysis over 15-30 days with sulfuric (15%) or hydrochloric (2.2 N) acids has been shown to yield Nageli amyloextrins and Lintnerized starch, respectively (Nageli 1874; Lintner 1886). Whereas, a shorter hydrolysis period of 5-7 days with sulfuric acid results in starch nanocrystals (SNC) and starch nanoparticles (SNP) composed mostly of the crystalline lamellae. Much of the research on SNC and SNP has focused on characterizing the morphology, crystallinity and thermal properties, however, little information is available regarding their molecular structures. Angellier-Coussy et al. (2009) previously investigated the molecular structure of waxy maize SNC and found it was mostly composed of low DP chains in the range of 9-22 with an average DP of 14.2. The authors attributed the average DP to the thickness of the crystalline lamellae; thus, concluding that nanocrystals correspond to the crystalline lamellae present in the native starch. The chain length distribution of SNP from maize, potato and mungbean was also determined by gel permeation chromatography (Kim et al. 2012). Kim et al. (2012) reported an increase in the proportion of short chains, resulting from hydrolysis of long amylose and amylopectin chains in the amorphous regions of native starches.

*A version of this chapter was accepted for publication in *Cereal Chemistry*, DOI:10.1094/CCHEM-02-16-0028-R

In Chapter 3, SNP isolated from waxy and non-waxy (normal, hylon V and hylon VII) maize starches through acid hydrolysis showed that the extent of SNP separation during fractionation was influenced to a large extent by the amylose content. Furthermore, variation in the amylose content was also shown to influence the yield, morphology and crystallinity of SNP. The results showed that SNP are composed of blocklets, which are released when amylose tie chains are hydrolyzed by acid; and spherulites made from the recrystallization of amylose chains during the acid hydrolysis treatment. The relative crystallinity followed the order: waxy (58%) > normal (54%) > hylon VII (43%) > hylon V (37%). Waxy and normal maize SNP had an A-type crystalline structure while both high amylose starches (hylon V and hylon VII) exhibited a change in their diffraction pattern from B-type to a mixture of A- and B-types (Chapter 3).

The present study was designed to investigate the molecular composition of waxy and non-waxy maize SNP. The objectives were: 1) to determine the weight average molecular weight and chain length distribution of SNP resulting from acid hydrolysis (3.16 M H₂SO₄) of maize starches varying in amylose (0-71%) content; 2) to determine the susceptibility of SNP from waxy, normal and high amylose starches to hydrolysis by pancreatic α -amylase; and 3) to characterize the morphology, molecular size and chain length distribution of the amylase-resistant SNP residues from high amylose maize starches. This study was intended to show how the molecular structure and enzyme resistance of SNP differing in crystalline type and amylose content are influenced by the presence of recrystallized short chain amylose and amylose tie chains co-crystallized with the amylopectin crystalline lamellae.

4.2. MATERIALS AND METHODS

4.2.1. Materials

Waxy maize (Amioca), normal maize (Melojel) and high amylose maize (hylon V and hylon VII) (>95% purity) were provided by Ingredion Incorporated (Westchester, IL, U.S.A.). All other chemicals were of ACS certified grade.

4.2.2. Acid hydrolysis and isolation of SNP

The acid hydrolysis and isolation protocol was performed according to the methodology reported in section 3.2.3 in Chapter 3.

4.2.3. Weight average molecular weight (M_w) of SNP

4.2.3.1 Gelatinization and solubilization of SNP

Starch nanoparticles were gelatinized and then purified with 90% dimethyl sulfoxide (DMSO) and ethanol precipitation as stipulated by the method of Jane and Chen (1992). Briefly, SNP in 90% DMSO were heated in a boiling bath for 1 h and then cooled to 30°C. The purified starch was precipitated with 4 volumes of 95% ethanol with constant stirring, then placed in an ice bath for 30 min and left overnight at 4°C. A pellet was collected after centrifugation (7000 rpm for 20 min). The pellet was dispersed in 95% ethanol, then washed further with ethanol and acetone on a 0.45 µm Pall HVLP filter, and left to dry overnight. These samples are referred to as gelatinized starch. To aid in dispersion, 100 µl of 95% ethanol was added to the gelatinized starch followed by 1 N NaOH until dissolved. The starch solution was then diluted with water, neutralized with 1 N HCl and autoclaved for 20 min at 121°C. These samples are referred to as solubilized starch. The solubilized starch solution was filtered through 0.45 µm syringe filter and

then injected into a high performance size exclusion chromatography system with multi angle laser light scattering and refractive index detectors (HPSEC-MALLS-RI).

4.2.3.2 Preparation of debranched SNP

The solubilized starch solution (3 ml), was incubated with 10 μ l isoamylase (Megazyme 1000u/ml) in 1 ml of acetate buffer (0.1 M, pH 3.5) overnight at 40°C. After incubation with the enzyme, the digested starch solution was neutralized with 1 N NaOH, heated in a boiling water bath for 5 min to stop enzyme activity, filtered through a 0.45 μ m syringe filter and then injected into HPSEC-MALLS-RI system.

4.2.3.3 HPSEC-MALLS-RI System

The weight-average molecular weight (M_w) of the SNP was determined with a high performance size exclusion chromatography (HPSEC-MALLS) system consisting of a Waters chromatography system, Alliance 2695, controlled by Waters Empower software (Waters Associates, Milford, MA, U.S.A.), and a Dawn Heleos II laser-light-scattering detector, ViscoStar-II Viscomoter, rEX, RI detector controlled by Astra software (Wyatt Technology, Santa Barbara, CA, U.S.A.). Separation was performed on two columns in series, SB803HQ and SB802.5HQ (300 x 7.8 mm; Shodex Showa Denko K.K. Tokyo, Japan) with a guard, OHPAKSB-G (50 x 6 mm; Shodex) maintained at 30°C. The samples (100 μ L injections) were analyzed using an effluent of 0.075 M sodium nitrate, 0.02% sodium azide buffer at a flow rate of 0.5 ml/min over 120 min. The M_w calculations were performed by the Astra software (Wyatt Technology) using the Zimm extrapolation method. The Wyatt light scattering detector was calibrated with toluene and beta-

glucan standards (Megazyme International, Ireland) with known M_w values to determine if the equipment was operating correctly.

4.2.4. Linear chain length distribution of SNP

4.2.4.1 HPAEC-PAD System

All samples were prepared as described in section 4.2.3.2 *Preparation of debranched SNP*. The high performance anion exchange chromatography (HPAEC) was performed using a Dionex system equipped with a gradient pump, DC column compartment heater, AS-AP autosampler, a pulsed amperometric detector (PAD) and a Dionex CarboPac PA-1 column (4 x 250 mm) with a PA-1 guard column (4 x 50 mm). The temperature of the column was controlled at 30°C. Eluent A was 150 mM sodium hydroxide and eluent B was 150 mM sodium hydroxide containing 500 mM sodium acetate. The eluents were degassed and stored under helium gas. The sample injection was 10 μ L and flow rate was 1.0 ml/min. The elution program was as follows: linear gradient; 1-15 min, 50% B; 15-45 min, 75% B; 45-60 min, 90% B; 60-72 min, 100% B; 72-92.5 min, equilibrate back to 25% B. A conventional gold electrode was used. Data collection and peak analysis was performed using the software Chromeleon 7.1 (Dionex). The DP of oligomers was assigned by running standards of G6 (maltohexose) and G7 (maltoheptose).

4.2.5. Resistant starch content of SNP

Megazyme assay kit for resistant starch (RS) was used to determine the amylase resistance of SNP (Megazyme International, Ireland). Briefly, the samples were incubated at 37°C with pancreatic α -amylase and amyloglucosidase in a sodium maleate buffer solution (100 mM, pH 6.0). After a 16 h incubation period, the enzymatic reaction was stopped with 4 ml of 99%

ethanol, the RS residue was washed twice with 50% ethanol and then hydrolyzed with 2 M KOH in a shaking ice bath. The hydrolyzed starch was incubated at 50°C with amyloglucosidase (3000 U/ml) enzyme and then with 3 ml of GOPOD reagent. The resistant starch content was determined by measuring the absorbance at 510 nm against a reagent blank.

4.2.6. SEM of the RS residues of SNP from hylon V and VII

SNP in suspension form were mounted on glass cover slips, allowed to air dry, coated with carbon using a Nanotek SEM prep 2 sputter coater and examined by field emission scanning electron microscopy (model Zeiss Sigma 300 VP-FESEM) at an accelerating voltage of 10 kV. The size of the particles in the FE-SEM micrographs were analyzed using the processing software ImageJ. The diameter of 200 particles (n=200) from each sample were measured to determine the particle size distribution.

4.2.7. M_w and linear chain length distribution of RS residues from hylon V and VII

The M_w and DP of the RS residue from nanoparticles were determined as described above. The residues were gelatinized, solubilized and debranched using isoamylase and then analyzed with HPSEC-MALLS-RI and HPAEC-PAD systems.

4.2.8. Statistical analysis

Analysis of variance was performed and the mean comparisons determined by Tukey's HSD test at $P < 0.05$ with Origin 9.1 software (OriginLab MA, USA). The isolation protocol was done in replicates and the mean and standard deviations of duplicates are reported.

4.3. RESULTS AND DISCUSSION

4.3.1. HPSEC profiles of SNP before debranching

The HPSEC elution profiles of solubilized SNP (Figure 4.1) differed depending on the starch type they were prepared from. The normal and high amylose SNP appeared to contain two populations of molecules: a minor high molecular weight population that eluted between 26 and 28 min (designated as Fraction I) and a major low molecular weight population that eluted between 28 and 34 min (designated as Fraction II). The relative proportion and the weight average molecular weight (M_w) of Fraction I increased with increasing amylose content in the native starches as shown in Table 4.1. This suggests that the minor Fraction I of normal and high amylose SNP contain some long linear amylose chains. Waxy SNP eluted in the low molecular weight region as a single and relatively symmetrical peak. The average M_w of Fraction II was 5,500 for waxy SNP and ranged from 6,000 to 6,500 (Table 4.1) for SNP from the amylose containing starches. It is likely that Fraction II contained a mixture of intermediate/short chains of amylopectin and low M_w segments of amylose chains, which resist acid hydrolysis. These acid resistant chains may have been closely associated within the native granule and/or may have retrograded during the time course of hydrolysis.

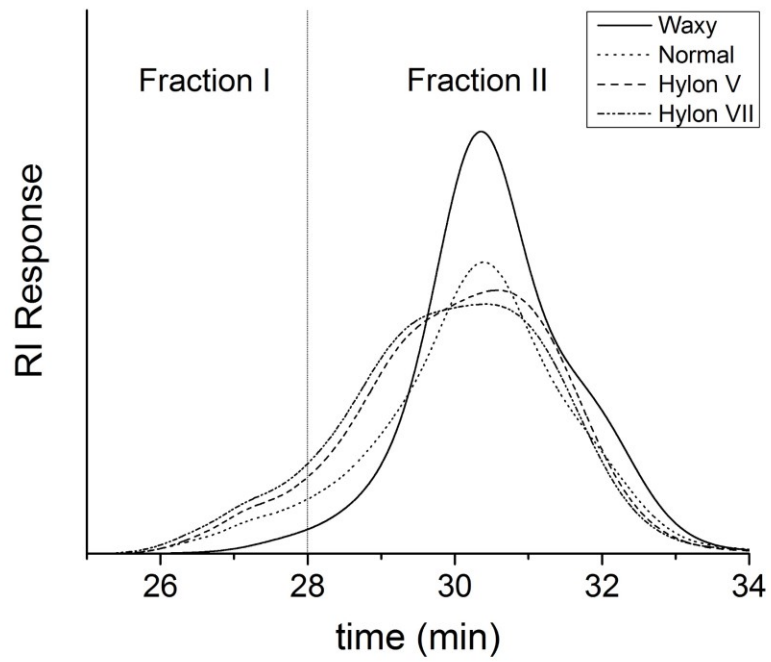


Figure 4.1 HPSEC profiles of solubilized SNP from maize starches of varying amylose content.

Table 4.1 Average molecular weight (M_w) and relative content (%) of high and low molecular weight fractions in solubilized SNP

Starch type	Fraction I (26-28 min)		Fraction II (28-34 min)	
	M_w ($\times 10^{-3}$)	Relative content (%)	M_w ($\times 10^{-3}$)	Relative content (%)
Waxy	nd	nd	$5.5 \pm 0.1a$	99.9
Normal	$17.7 \pm 1.6a$	7.1	$6.1 \pm 0.3a$	92.9
Hylon V	$16.2 \pm 0.4a$	8.0	$6.0 \pm 0.1a$	92.0
Hylon VII	$17.7 \pm 2.8a$	9.5	$6.5 \pm 0.5a$	90.5

Values followed by the same letter in the same column are not significantly different ($P < 0.05$), based on Tukey's HSD test. nd-none detected.

4.3.2. HPSEC profiles of SNP after debranching

The HPSEC elution profiles of debranched SNP for waxy and non-waxy starches are presented in Figure 4.2. All SNP contained the major low M_w peak eluting between 31.7 and 34 min. While the debranched SNP from waxy maize eluted in a single, relatively narrow peak between 31.7 and 34 min, the debranched SNP prepared from non-waxy starches exhibited a multimodal distribution of chains (Figure 4.2). Four populations of chains differing in molecular weight were detected in SNP prepared from hylon V and hylon VII as indicated in Table 4.2. Some differences were also noted between debranched SNP from normal and high amylose starches (Figure 4.2 and Table 4.2). The average M_w of linear chains generated by debranching waxy maize SNP was about 2,100 that corresponds to the average DP of 13 (Table 4.2). This indicates that SNP from waxy starch may contain both short A and B amylopectin chains. Non-waxy maize starches likely contained also much longer chains. The M_w of Fraction 1 in the debranched normal and high amylose starches SNP (Figure 4.2) were in the range of 16,700 to 18,700 (Table 4.2).

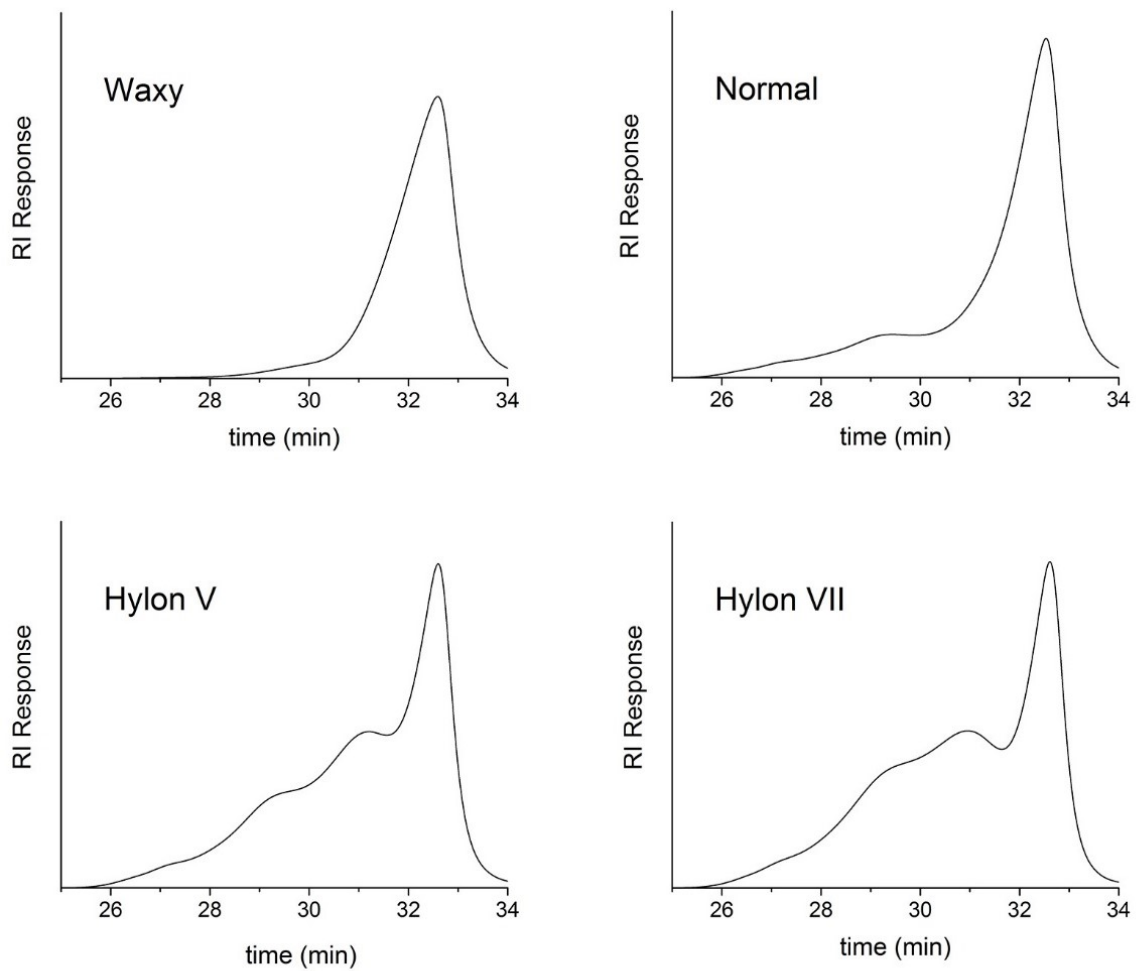


Figure 4.2 HPSEC profiles of solubilized and debranched SNP from maize starches of varying amylose content.

Table 4.2 Average molecular weight (M_w) and relative content (%) of four different fractions present in solubilized and debranched SNP

Starch type	Fraction 1 (26-28 min)		Fraction 2 (28-30 min)		Fraction 3 (30-31.7 min)		Fraction 4 (31.7-34 min)	
	M_w		M_w		M_w		M_w	
	($\times 10^{-3}$)	(%)	($\times 10^{-3}$)	(%)	($\times 10^{-3}$)	(%)	($\times 10^{-3}$)	(%)
Waxy	nd	nd	nd	nd	nd	nd	2.1 \pm 0.3a	96.6
Normal	18.7 \pm 2.3a	4.3	9.4 \pm 1.1a	15.6	nd	nd	2.1 \pm 0.2a	79.9
Hylon V	17.8 \pm 1.6a	5.2	8.4 \pm 0.4a	19.6	4.5 \pm 0.3a	28.7	1.2 \pm 0.0b	46.3
Hylon VII	16.7 \pm 0.8a	5.9	8.4 \pm 0.4a	22.9	4.9 \pm 0.2a	29.9	1.4 \pm 0.2ab	40.5

Values followed by the same letter in the same column are not significantly different ($P < 0.05$), based on Tukey's HSD test. nd- none detected.

These values are similar to those shown in Table 4.1 for the solubilized SNP without debranching and indicate the presence of long linear amylose chains. The relative content (%) of Fraction 2 and Fraction 3 in the non-waxy SNP was proportional to the amylose content in the native starches (hylon VII > hylon V > normal). The M_w of Fraction 2 ranged from 8,400 to 9,400, corresponding to the weight average DP of 52 to 58. SNP from hylon V and hylon VII had a population of intermediate chains (Fraction 3) with M_w of 4,500 and 4,900 that corresponded to a weight average DP of 28 and 30, respectively. The presence of Fraction 3 only in hylon V and hylon VII starches, suggests the involvement of amylose tie chains interspersed in the crystalline lamellae of B-type starches. The M_w data presented suggests that the crystalline lamellae of SNP from waxy and normal (A-type) maize starches are composed of short A and B amylopectin chains, while those of hylon V and hylon VII (B-type) starches also contain linear amylose chains that are co-crystallized with the short A and B amylopectin chains.

4.3.3. HPAEC profiles and linear chain length distribution of SNP

The chain length distribution in SNP prepared from maize starches was also investigated by HPAEC-PAD after debranching (Figure 4.3). SNP prepared from waxy maize contained relatively short linear chains with the majority of chains with DP < 25. In comparison, the non-waxy SNP contained linear chains with DP up to 60 corresponding to the longest detectable DP chain. The chain length distribution of SNP after debranching is presented in Table 4.3. The DP of the linear chains in waxy maize SNP ranged from 6 to 31 with the average chain length (\overline{CL}) of 14.4. This is in close agreement with Angellier-Coussy et al. (2009), who reported that the major dextrin population in waxy maize nanocrystals exhibited a DP in the range of 9 to 22, \overline{CL} of 14.2 and a peak position at 13. These authors attributed the \overline{CL} of 14.2 in waxy maize nanocrystals to a length of 5 nm and to the thickness of the crystalline lamellae (short A + B amylopectin chains). According to Kim et al. (2012), the intermediate and long amylopectin chains in the amorphous lamellae of waxy maize are preferentially hydrolysed thus increasing the proportions of shorter chains in the crystalline lamellae.

In non-waxy starches, the \overline{CL} increased with amylose content (Table 4.3). According to Cheetham and Tao (1997), high amylose maize starches have a higher \overline{CL} and a larger proportion of long chains than waxy and normal starch. The abundance of chains with DP > 25 in non-waxy SNP increased from 7.9% to 27.7% with increasing amylose content of the native starches (Table 4.3). The HPAEC elution profiles of the debranched SNP from non-waxy starches showed the presence of a second abundant population of chains with DP > 30. As proposed by Saibene and Seetharaman (2010), this population may originate from short amylose chains present within the B-type crystallites of hylon V and hylon VII. Furthermore, this population may also be due to

formation of amylose spherulites from the recrystallization of short chain amylose with a degree of polymerization > 25 (Ring et al. 1987).

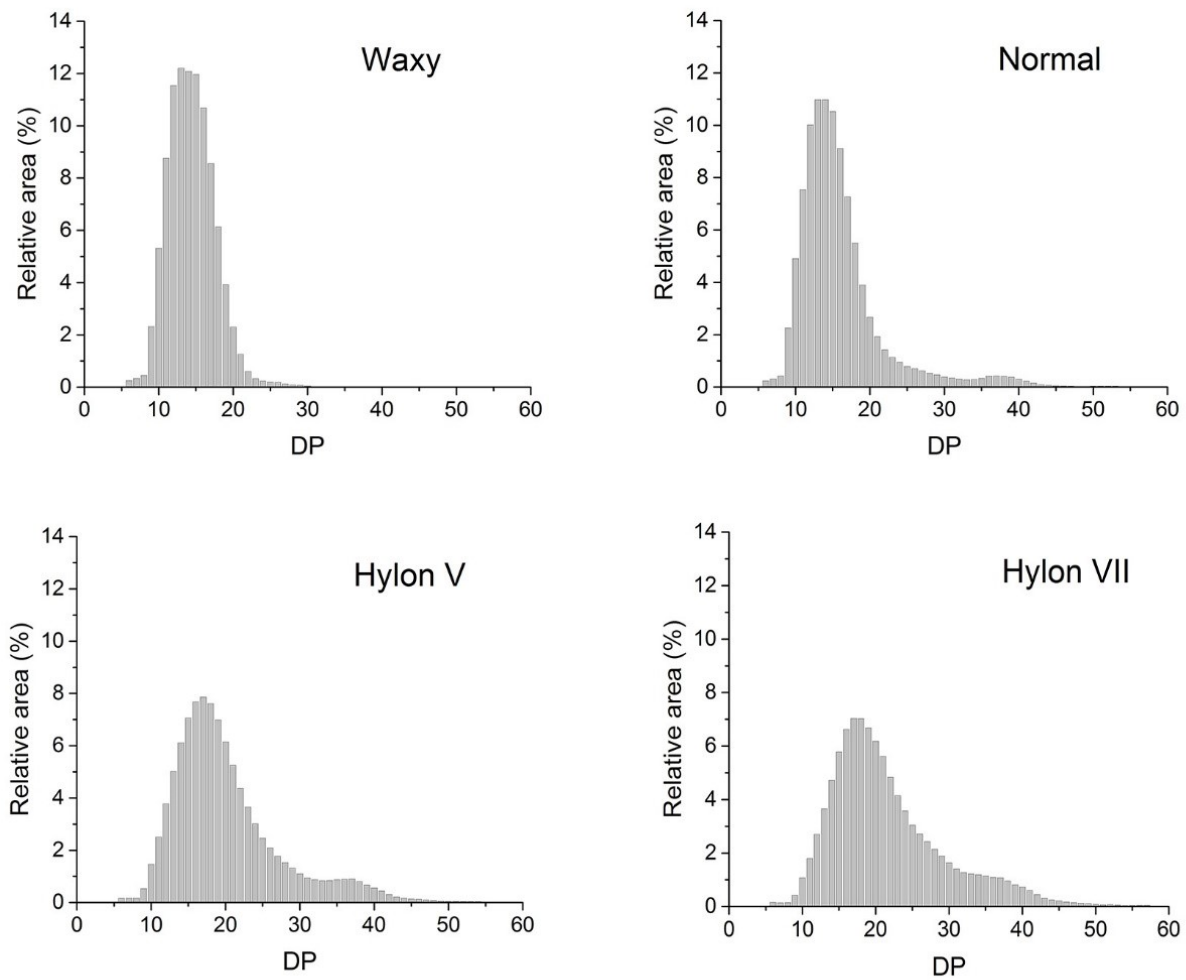


Figure 4.3 Chromatograms of isoamylase debranched SNP from maize starches analyzed by HPAEC-PAD.

Table 4.3 Chain length distributions of SNP after debranching with isoamylase

Starch type	Most abundant DP	Highest detectable DP	\overline{CL}	% Distribution		
				DP 6-12	DP 13-24	DP > 25
Waxy	13	31	14.4	29.0	70.3	0.70
Normal	13	55	16.1	25.7	66.4	7.90
Hylon V	16	57	20.2	8.80	70.8	20.4
Hylon VII	16	59	21.7	6.40	65.9	27.7

DP- Degree of polymerization; \overline{CL} - Average chain length

However, this does not explain why normal maize (A-type) starch also contains some chains with DP > 30. It is possible that in addition to what is observed in B-type starches, amylose may have retrograded during acid hydrolysis leading to the formation of aggregates in the form of nanoparticles. According to Perera et al. (2001), Nägeli dextrans from su2 corn starch (33% apparent amylose) collected after acid hydrolysis at 38°C, had chain length distribution peak at DP 34 after isoamylase debranching. These authors attributed this population to retrograded amylose. Retrograded amylose forms aggregates with crystalline regions (double helices), which have been shown to be acid and enzyme resistant (Jane and Robyt 1984).

4.3.4. Amylolysis of SNP by pancreatic α -amylase

The resistance of SNP towards amylolysis (Table 4.4) followed the order: hylon VII > hylon V > normal > waxy. Waxy maize was almost completely digested (>99%), while those from non-waxy starches showed different degrees of resistance. The resistance of SNP of the maize starches was proportional to amylose content. This suggests that co-crystallization of short amylose chains with amylopectin or the presence of retrograded amylose, may have contributed to amylase resistance.

Table 4.4 Resistant starch content of SNP from maize starches

Starch type	Resistant starch (% db)
Waxy	0.50 ± 0.0c
Normal	3.90 ± 0.1c
Hylon V	31.3 ± 1.1b
Hylon VII	38.9 ± 1.3a

Values followed by the same letter in the same column are not significantly different ($P < 0.05$), based on Tukey's HSD test.

4.3.5. Morphology, M_w and linear chain length distribution of the SNP RS residue

The resistant starch residue left after enzyme hydrolysis of the SNP was only collected from hylon V and hylon VII. This residue was further used to investigate the morphology and molecular composition of the chains, which are able to resist both acid and enzymatic hydrolysis. The morphology of SNP from hylon V and hylon VII before and after enzymatic hydrolysis are presented in Figure 4.4. Nanoparticles similar to those observed in the SNP collected after acid hydrolysis (Figure 4.4A-B) were also observed in the resistant starch residue (Figure 4.4C-D). The nanoparticles were oval to round in shape and ranged in size depending on the starch type. SNP from hylon V (Figure 4.4A) were between 42-105 nm while those from hylon VII (Figure 4.4B) ranged from 64-160 nm. The nanoparticles in the resistant starch residue for hylon V (Figure 4.4C) and hylon VII (Figure 4.4D) had larger particles ranging between 47-155 nm and 84-203 nm, respectively. Although a reduction in particle size after enzymatic hydrolysis was expected, this was not evident in the SEM micrographs. The increase in size after enzyme hydrolysis may be due to the ability of larger nanoparticles (smaller surface area) to resist hydrolysis, nanoparticle swelling and hydration during the enzyme hydrolysis conditions (incubation at 37°C) or due to the formation of aggregates during the sample preparation prior to SEM analysis.

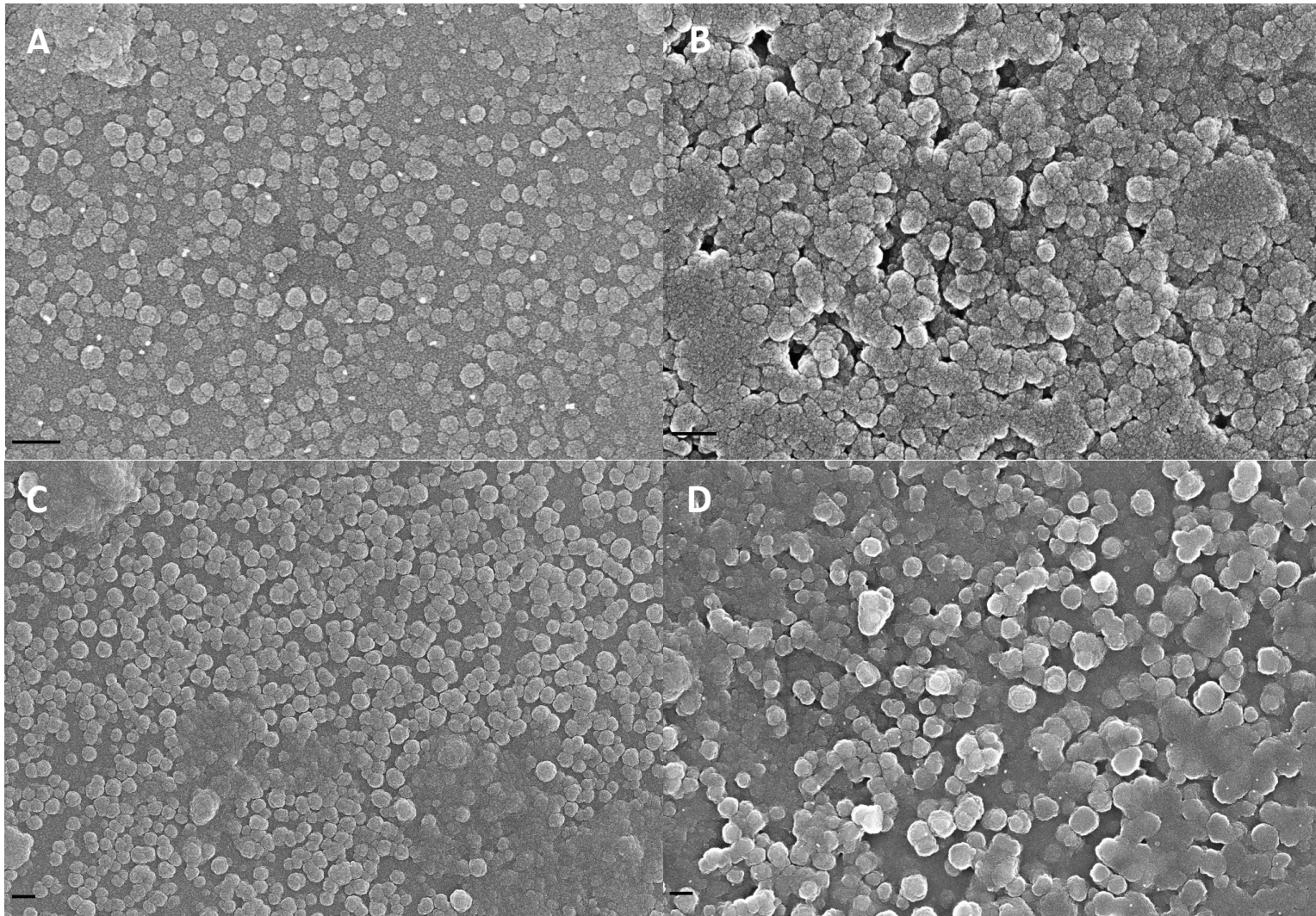


Figure 4.4 Field emission scanning electron microscopy images of SNP from hylon V and hylon VII.
A-B – nanoparticles of hylon V (A) and hylon VII (B) (x40000, scale bar = 200 nm).
C-D – nanoparticles of hylon V (C) and hylon VII (D) after enzymatic hydrolysis with pancreatic α -amylase (x20000, scale bar = 200 nm).

The HPSEC profiles of the resistant starch residue obtained from SNP of hylon V and hylon VII before and after debranching are presented in Figure 4.5. Before debranching, the RS residues of both hylon V and hylon VII eluted in a single peak, with the M_w comparable to that of the original SNP. The M_w of the resistant starch residue from hylon V was about 6,400 whereas from hylon VII about 6,000. After debranching, the linear chains of the resistant residue from hylon V and hylon VII eluted as two distinct populations, one eluting between 26 and 31.7 min and another between 31.7 and 34 min; designated as high and low M_w populations, respectively. The high M_w population of the linear chains (5,600-5,700), corresponding to the weight average DP of 34-35, may be attributed to the presence of retrograded amylose chains. Jane and Robyt (1984), ascribed an average DP 31 for Nageli dextrans obtained after acid hydrolysis of retrograded amylose from potato starch. Jiang et al. (2010) also showed the presence of long chains with DP > 25 (attributed to amylose double helices) in debranched Nageli dextrans from maize ae mutant starches. Moreover, the low M_w peak (retention time 31.7-34 min) observed in RS residues only after debranching may be indicative of the presence of short A and B amylopectin chains (Figure 4.5). A M_w of 1,100 in this population corresponded to a weight average DP value of 7 (Figure 4.5). The isoamylase debranched resistant starch residue from hylon V and hylon VII SNP was further analyzed by HPAEC-PAD. The chromatograms showed the presence of linear chains with a DP ranging from 6 to 50 (Figure 4.6). Based on these observations, the RS residues obtained from hylon V and hylon VII contain both low M_w linear and branched chains, which are resistant to both acid and enzyme hydrolysis.

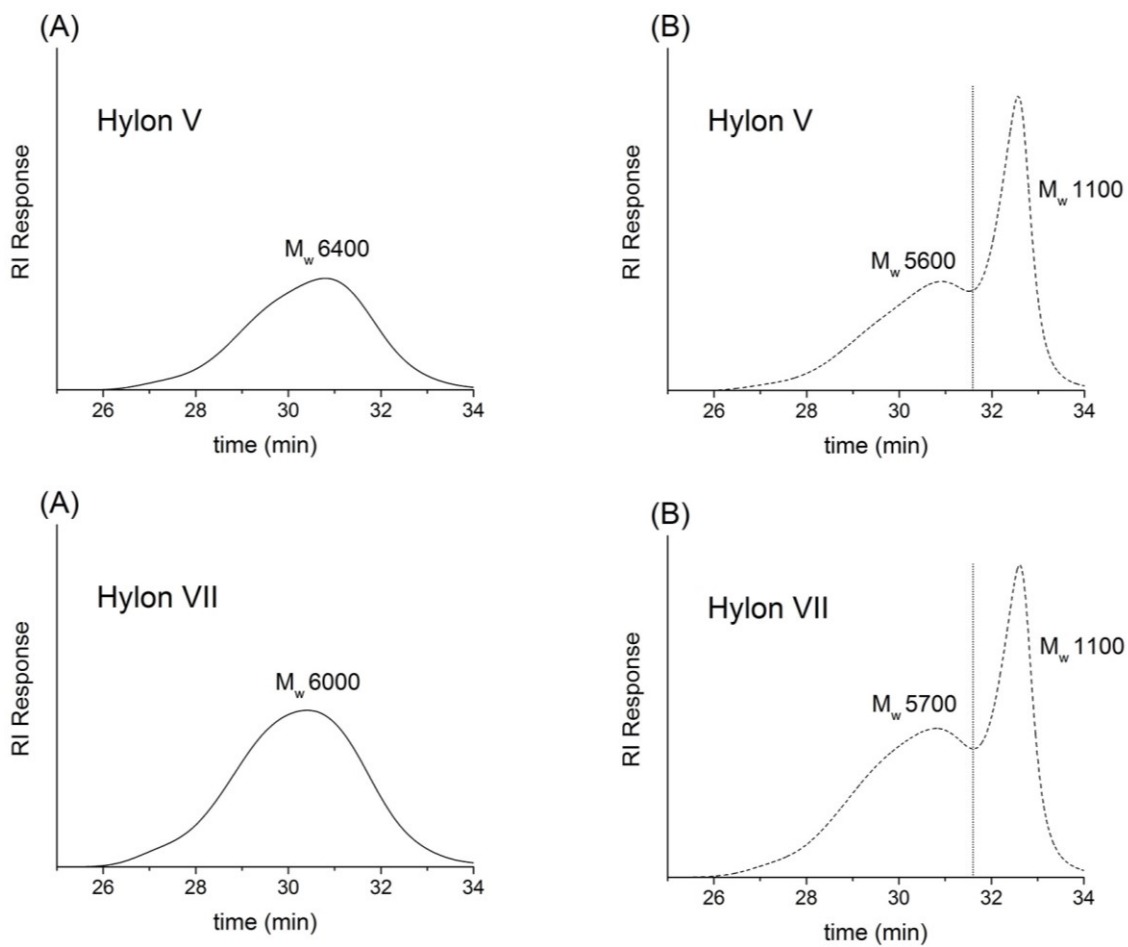


Figure 4.5 HPSEC profiles of the RS residue obtained from SNP of hylon V and hylon VII, (A) before and (B) after debranching.

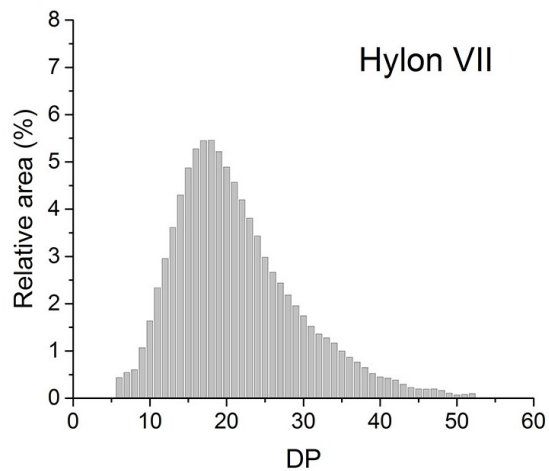
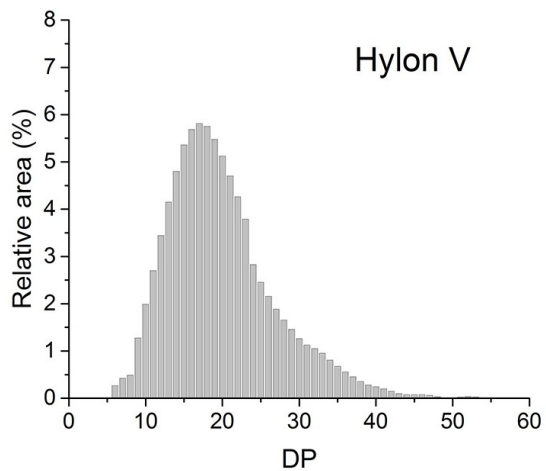


Figure 4.6 Chromatograms of isoamylase debranched RS residue obtained from SNP of hylon V and hylon VII analyzed by HPAEC-PAD.

4.4. CONCLUSIONS

The chromatography elution profiles, molecular size and chain length distribution of the SNP showed significant variations in the molecular composition of SNP prepared from waxy and non-waxy starches. For non-waxy SNP, the presence of amylose either co-crystallized with amylopectin short chains or as retrograded amylose crystals possibly in the form of spherulites was demonstrated. The molecular characteristics before and after isoamylase debranching, and the amylase resistance of SNP isolated from high amylose maize starches, both helped elucidate the presence of amylose in the crystalline lamellae (co-crystallization) of B-type starches. The SNP from high amylose starches are comprised of both low M_w linear and short A + B amylopectin chains, which are both acid and enzyme resistant. On the other hand, SNP from waxy and normal (A-type) starches are comprised primarily of short A + B amylopectin chains, which are acid resistant, but susceptible to amylase hydrolysis. The study overall established the nature of amylose involvement in A- and B-type crystals of SNP. Furthermore, the demonstrated difference in the molecular composition of SNP may explain variations in the rheological properties of SNP, especially when used in applications like polymer nanocomposites and nanogels.

CHAPTER 5 Rheology of starch nanoparticle suspensions as influenced by particle size, concentration and temperature

5.1. INTRODUCTION

SNC and SNP are the crystalline and semi-crystalline structures, respectively, resulting from the disruption of the amorphous structure of starch granules by acid hydrolysis (Le Corre and Angellier-Coussy 2014). Their morphology and size has been previously investigated using SEM (Song et al. 2008), TEM (Kim et al. 2012) or FE-SEM (LeCorre et al. 2011; Wei et al. 2014a; Xu et al. 2014). According to the aforementioned studies, SNC and SNP vary in length (40-150 nm) and shape (platelet, round edges, grape-like aggregates, square) depending on the starch source. More recently, nanoparticle and colloidal size measurements have been studied using dynamic light scattering (DLS) (Jin et al. 2015; Romdhane et al. 2015). DLS measures the Brownian motion of particles suspended in solution and determines the hydrodynamic diameter. In SNP aqueous suspensions, the surface charge and counter ions present in solution produce an electric double layer around the particles, which enhances colloidal stability. This stability has been attributed to the presence of a negative surface charge (SO_3^- groups) after sulfuric acid hydrolysis (Angellier et al. 2005a; Wei et al. 2014b).

*A version of this chapter was accepted for publication in *Food Hydrocolloids*, DOI:10.1016/J.FOODHYD.2016.11.026

SNC and SNP have attracted a lot of attention due to their potential use in various applications including biodegradable nanocomposites, food packaging films, binding and paper coating, emulsion stabilization, fat replacement and drug delivery. Their renewable, abundant and non-toxic nature make them excellent substitutes for synthetic materials; however, more research is needed to understand how their functional properties change under different processing conditions. For example, in the production of nanocomposite and food packaging films, knowing the thermal stability of SNC and SNP is very important to preserve the particulate nature and target functionality. Techniques such as hot-pressing, compression molding and extrusion employ high temperatures and pressures, which may cause melting of SNP and therefore change their reinforcing effect (Kim et al. 2015). Also, when SNP are added to oil-in-water emulsions, their stabilizing ability changes with temperature. Li et al. (2012) observed a stable emulsion at temperatures below 60°C, whereas at 80°C the emulsion phase separated due to nanoparticle melting. The rheological characterization of SNP is an area that lacks investigation. According to Mewis and Wagner (2009), rheological assessment provides information of the particle-particle interactions and the network properties of the continuous matrix in which these particles are suspended. Therefore, investigating the interaction of SNP among themselves in an aqueous system prior to being incorporated into other food and non-food matrices is important.

Although some information on the rheological properties of SNP is available, there is no study in the literature, which compares the static and dynamic rheology of SNP suspensions from different starch sources. This dearth in the literature formed the platform for the present study, which aimed to characterize the SNP that were isolated from regular starches but different

crystalline type (A-type: wheat, oat and barley starch and B-type: potato starch). In Chapter 3 and 4, SNP from maize starches (waxy, normal, hylon V and hylon VII) were found to vary in their morphology, crystallinity and molecular size distribution. In amylose containing starches with B-type crystalline structures, the presence of amylose either as retrograded amylose crystals or co-crystallized with amylopectin short chains was demonstrated, while SNP from waxy maize (A-type) were comprised of short A + B amylopectin chains. The difference in the molecular composition between A- and B-type starches is expected to play an important role in the rheological behaviour of aqueous SNP systems.

To date, only the rheological properties of SNC or SNP from maize, wheat and potato starches (LeCorre et al. 2011; Shi et al. 2012a; b; Shi et al. 2013; Jiang et al. 2016) have been investigated. LeCorre et al. (2011) found a positive correlation between the viscosity and concentration of SNC from different starch sources, while all suspensions displayed a shear-thinning behaviour. They reported no particular relationship between the viscosity and SNC size, thickness and surface area; however, the SNC with the lowest viscosities had similar morphologies. In a series of studies, Shi et al. (2012b) reported the effect of spray drying and freeze drying on the re-dispersibility of soluble potato SNP in aqueous suspension, and the influence of NaCl concentration on the aqueous rheological properties of SNP obtained by the two different drying methods. Their findings indicated that both the drying method and NaCl concentration affected the interaction of SNP in an aqueous solution. In the presence of NaCl, the apparent viscosity of SNP produced by the two drying methods exhibited opposite trends, where the viscosity of freeze dried SNP increased with salt concentration (Shi et al. 2013). Furthermore, the thermal stability as determined by the dynamic rheological properties as a

function of temperature (25-90°C) indicated that addition of salt results in suspensions with better thermal stability. More recently, the rheological behaviours of waxy maize SNC and SNP as a function of ionic strength were compared (Jiang et al. 2016). The effect of temperature, frequency and ionic strength on the dynamic rheological properties varied between SNC and SNP, which were prepared by acid hydrolysis and by a controlled self-assembly of short linear chains, respectively. All SNP suspensions showed a shear-thinning behaviour regardless of the salt concentration.

The present study was intended to demonstrate how the starch source and morphological characteristics influence the viscosity and viscoelastic behaviour of SNP suspensions measured at increasing shear rates, frequency and temperatures. The objectives were: 1) to compare the particle size distribution of SNP by solid state microscopy and dynamic light scattering methods, 2) to evaluate the effect of temperature on the particle size distribution of SNP in aqueous suspension and 3) to determine the static and dynamic rheological properties of SNP suspensions as a function of shear, frequency and temperature. The outcome of the study would enhance the understanding of how incorporating SNP isolated from different starch sources and exposure to processing conditions can affect their functionality.

5.2. MATERIALS AND METHODS

5.2.1. Materials

The wheat (hard red spring wheat), oat (HiFi) and barley (CDC Candle) grains were ground into flour using a mill (Model ZM 200, Retsch, Haan, Germany) equipped with a ring with an aperture size of 0.5 mm. Pure starch from wheat flour was isolated using a dough ball method as described by Kim and Huber (2008), while oat and barley starches were purified according to the

method of Gao et al. (2009). Detailed protocols are given in Appendix II. Potato starch was obtained from Avebe (Avebe Group, Veendam, Netherlands). All the starches had a purity > 92%. All other chemicals were of ACS certified grade.

5.2.2. Isolation of SNP by acid hydrolysis

The acid hydrolysis and isolation protocol was performed according to the methodology reported in section 3.2.3 in Chapter 3. All samples were prepared in duplicate and the SNP collected as Fraction 2 (pooled cloudy supernatants from washing 9-15).

5.2.3. Field emission scanning electron microscopy (FE-SEM)

SNP in suspension were mounted on glass cover slips, allowed to air dry, coated with carbon using a Nanotek SEM prep 2 sputter coater and examined by FE-SEM (Zeiss Sigma 300 VP-FESEM, Germany) at an accelerating voltage of 10 kV. The size of the particles in the microscopy images were analyzed using the processing software ImageJ. The diameter of 200 particles (n=200) from each sample were measured to determine the particle size distribution (PSD).

5.2.4. Dynamic light scattering (DLS)

The particle size and zeta potential of the SNP in suspension were determined with a Zetasizer (Nano S, Malvern Instruments, Worcestershire, U.K.). For the particle size measurements the SNP suspensions were diluted to 0.1% (w/v) with milliQ water and left to equilibrate at room temperature overnight. Measurements were conducted at a scattering angle of 173° in a temperature regulated cell at 25°C. Eleven measurements were determined for each run and the mean \pm standard deviation of triplicates are reported. In order to evaluate the effect of temperature on PSD, SNP suspensions were incubated at 25, 40, 60 and 80°C for 30 min,

allowed to cool and the particle size measurements for all SNP suspensions were conducted at 25°C. Zeta potential measurement were determined in the presence of 1 mM NaCl and a pH of 6.0.

5.2.5. Static and dynamic rheological properties

SNP suspensions of 1% and 5% (w/v) were prepared for the rheological tests. Lyophilized SNP were re-dispersed in milliQ water using a homogenizer at 15,200 rpm for 20 min (Heidolph DiAx 900, Schwabach, Germany). The rheological tests were performed using a rheometer (HR-3, TA Instrument, Delaware, U.S.A.) with a cone and plate (40 mm diameter, 53 μm gap). Instrument calibrations were performed to generate better quality data (Appendix III). The samples were allowed to equilibrate at 25°C for 2 min before each test. The continuous shear test was performed to determine the relationship between the apparent viscosity and the shear rate of the SNP suspensions. The shear rate range was from 0.01-100 s^{-1} and the constant temperature of 25°C. The frequency sweep test evaluated the changes in the viscoelastic modulus as a function of angular frequency (0.1-10 rad/s). The temperature was set at 25°C and oscillating strain of 2% was used. Preliminary amplitude sweep tests confirmed a 2% strain was within the linear viscoelastic region of all samples. The temperature ramp test was carried out to determine the relationship between viscoelastic modulus and temperature. The test was performed at a frequency of 1 rad/s, oscillating strain of 2% and a heating rate of 2°C/min from 25°C to 90°C. The gap temperature compensation feature was enabled in all temperature ramp tests, which allows the stage to move according to the expansion coefficient of the geometry as the temperature changes. A solvent trap geometry and solvent trap cover were used to create a thermally stable environment and prevent moisture loss from the samples during heating. Silica oil was placed in

the solvent well. All rheological measurements were carried out in duplicates and the mean is reported.

5.2.6. Statistical analysis

Analysis of variance was performed and the mean comparisons determined by Tukey's HSD test at $P < 0.05$ with Origin 9.1 software (OriginLab MA, USA).

5.3. RESULTS AND DISCUSSION

5.3.1. Morphology and particle size distribution

The morphology of SNP isolated from wheat, oat, barley and potato are presented in Figure 5.1A-D. In all starches, individual round, irregular particles (possibly starch blocklets or retrograded amylose crystals) and long oval aggregates (clusters of 2 or more blocklets or starch spherulites) were evident. These results are similar to those reported for amylose containing maize starches but differ from waxy maize. In Chapter 3, differences in the size and shape of SNP were reported according to the starch source and crystalline type. Acid hydrolysis of amylose containing starches led to the release of SNP composed of individual blocklets and recrystallized short chain amylose. In the native starch granules, amylose molecules are present as the interconnecting material between blocklets either as linear chains, co-crystallized with amylopectin or as tie chains. However, during the acid treatment, hydrolysis of amylose tie chains present within the amorphous and crystalline lamellae result in the disruption of the amylopectin blocklets from their ordered arrangement within the semi-crystalline and amorphous growth rings and their release into solution (Chapter 3).

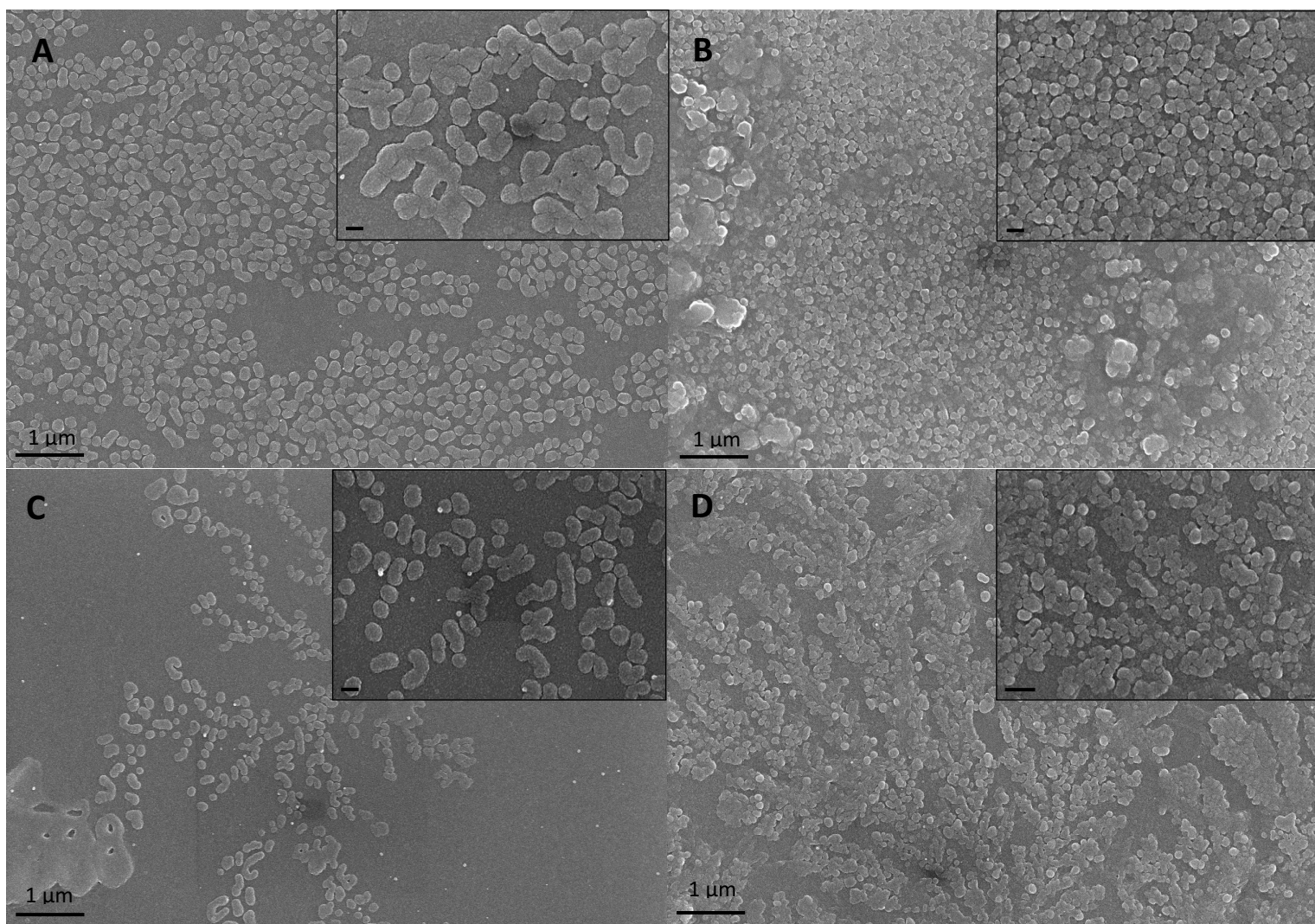


Figure 5.1 Scanning electron microscopy images of SNP from (A) wheat, (B) oat, (C) barley and (D) potato isolated by acid hydrolysis. The inserts in images A, B and C have a scale bar = 100 nm; whereas in image D the scale bar = 200 nm.

Simultaneously to acid hydrolysis occurring, it is possible that the hydrolyzed amylose chains are retrograding and recrystallizing to form nano-size starch spherulites (inserts in Figure 5.1A and C), through the sequential addition of glucose or low molecular weight linear chains. According to Ring et al. (1987), short chain amylose with a degree of polymerization of 22 can be recrystallized from an aqueous solution of hydrolyzed starch into starch spherulites. More recently, Cai and Shi (2013) concluded that the formation of starch spherulites from short chain amylose is due to the alignment of double helices into crystalline bundles and the radial orientation of these into spherulites.

In the present study, the size range of SNP in their dry state was determined from the microscopy images as reported in Table 5.1. SNP from wheat starch showed the biggest SNP ranging between 70-226 nm (Figure 5.1A), followed by barley (Figure 5.1C) (62-167 nm). SNP from oat and potato had the smallest size range distribution corresponding to 55-130 nm (Figure 5.1B) and 49-155 nm (Figure 5.1D), respectively. In the literature SNP are referred to as the blocklet structures present in native starch granules. Gallant et al. (1997) previously reported smaller blocklets in A-type starches (8-120 nm) and larger blocklets (200-500 nm) in tuber and pulse starches; however, the findings of this study showed that B-type starches had the smallest blocklets. Perhaps, this could be due to acid hydrolysis at sub-blocklet levels or the formation of nanoparticle (spherulites) from the recrystallization of short chain amylose.

Further characterization of the PSD of SNP in aqueous suspension was conducted using DLS. This technique determines the hydrodynamic diameter by taking into account the Brownian motion of the particles in solution. Table 5.1 summarizes the mean particle diameters measured by both methodologies, FE-SEM and DLS.

Table 5.1 Particle size of SNP determined by FE-SEM at room temperature and DLS after incubation at different temperatures

Starch source	FE-SEM			DLS			
	Diameter (nm)			Hydrodynamic Diameter (nm)			
	Min.	Max.	Mean \pm S.D.	25 °C	40 °C	60 °C	80 °C
Wheat	70	226	127 \pm 30a	226 \pm 2a	192 \pm 2a	177 \pm 2a	141 \pm 1a
Oat	55	130	87 \pm 13b	201 \pm 1b	148 \pm 1d	78 \pm 1d	81 \pm 1c
Barley	62	167	97 \pm 20c	199 \pm 3b	163 \pm 1c	143 \pm 1b	139 \pm 0b
Potato	49	155	88 \pm 19b	177 \pm 2c	176 \pm 4b	135 \pm 1c	50 \pm 1d

The values represent the mean \pm standard deviation of triplicates. Values followed by the same letter in the same column are not significantly different ($P < 0.05$), based on Tukey's HSD test.

FE-SEM: nanoparticles analyzed in solid state at 25°C.

DLS: all measurements were evaluated in a temperature regulated cell at 25°C after incubating at the different temperatures.

The size of SNP in dry state (FE-SEM) was substantially smaller than the hydrodynamic diameter, possibly due to the following reasons: 1) swelling of SNP due to hydration, and 2) the presence of the electrical double layer around the nanoparticles in solution. When native starch is hydrolyzed with sulfuric acid, negatively charged sulfonate esters and carboxyl groups are imparted on the surface of SNP (Angellier et al. 2005a; Wei et al. 2014b). In aqueous suspension, the surface charge and the inter particulate repulsion between the surface charge and the solution ions produce an electric double layer around the particles which increases the nanoparticle diameter and provides suspension stability (Boluk et al. 2011). The SNP suspensions from all starch sources had superior colloidal stability as shown by their zeta potential values between -24 and -32 mV (measured at a pH of 6.0) and their ability to remain suspended in solution for over 60 days. The average hydrodynamic diameter at room temperature varied significantly between the different starches and was the greatest in wheat (226 nm), followed by

oat (201 nm) and barley (199 nm), and was the lowest in potato (177 nm) (Table 5.1). The values reported in Table 5.1 for DLS are the mean values (hydrodynamic diameter) of a size distribution curve. According to Shafiei-Sabet et al. (2012), the rheological properties of cellulose nanocrystals are influenced by the particle size and shape, surface charge, electrical double layer and ionic strength. Therefore, variation in the PSD and ionic strength between different starch sources may play an important role in the dispersity and rheological behaviour of SNP in aqueous suspension.

5.3.2. Thermal stability of SNP suspensions by DLS

In order to evaluate the effect of temperature on SNP size distribution, aqueous suspensions were incubated in a water bath at 25, 40, 60 and 80°C for 30 min. The SNP from all starch sources showed low thermal stability (i.e. high heat sensitivity), as determined by a decrease in the mean particle size with an increase in temperature (Table 5.1). Within the same starch source, the comparison between the average hydrodynamic diameters at the different temperatures suggests that larger SNP are less resistant to elevated temperatures than smaller particles. This may be due to the preferential solubilization of larger SNP through melting of amylopectin crystallites and the resistance of smaller SNP (possibly recrystallized short chain amylose) to melting. A previous study showed waxy maize SNC in excess water have two thermal transitions due to crystallite melting, one from unpacking and the other from unwinding of the double helices, which begin melting at 55°C (LeCorre et al. 2012a). While according to Cai and Shi (2013) spherulites made from recrystallized short chain amylose have a higher melting temperature between 100-140°C.

In the present study, following incubation at 40°C, oat SNP showed the greatest decrease in size, followed by barley and wheat, and no change was observed for potato. When heated to 60 °C, all of the SNP diameters decreased and the extent of decrease followed the order: Oat > Potato > Barley > Wheat. For example, oat SNP had significantly smaller particles (78 nm), than the other starches (135-177 nm). Furthermore, after incubation at 80°C, the SNP diameter of potato was the lowest (50 nm), followed by oat (81 nm), barley (139 nm) and wheat (141 nm); the heat sensitivity of SNP varies according to the starch source. Between the different starch sources, the particle size distribution after incubation at 25°C and 80°C (Figure 5.2) suggests that the thermal stability was the greatest for wheat (lower % size reduction) while it was the least for potato. The thermal stability was the lowest for potato, while it was the highest for wheat (Figure 5.2). The thermal degradation of the SNP was also visually evident by a change from a cloudy to a more clear solution. Similar observations were reported by Wei et al. (2014a) and Romdhane et al. (2015). The authors attributed the transformation of waxy maize SNC solutions from opaque to clear to a decrease in particle size due to partial dissolution of SNC to dextrin or the breakdown of larger particles to smaller ones under alkaline conditions (pH > 10).

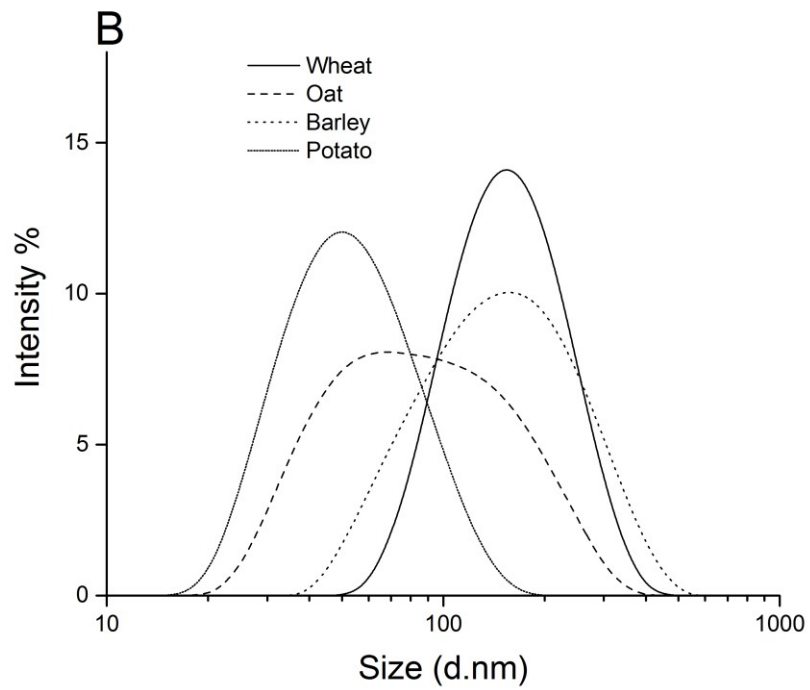
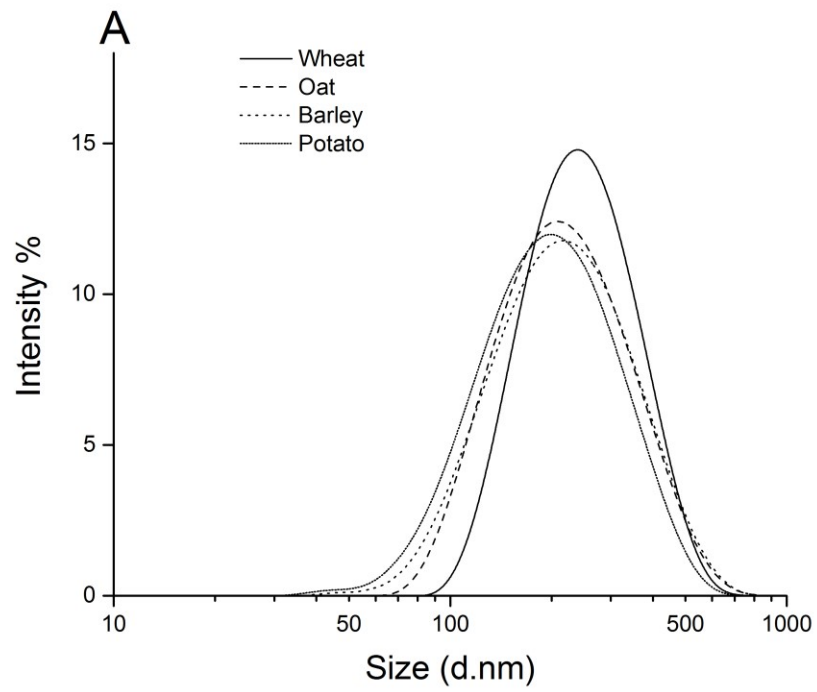


Figure 5.2 Particle size distribution of SNP suspensions after incubation at: (A) 25°C and (B) 80°C, respectively.

The differences observed in particle size before and after heating are expected to influence the rheological and functional properties of SNP suspensions. At room temperature, SNP (amylopectin blocklets and recrystallized short chain amylose) in a concentrated suspension can form a network composed of SNP interacting at their surface through water bridges (hydrogen bonds connecting the sulfonate groups and water molecules) (Figure 5.3A). Furthermore, SNP from amylose containing starches such as those presented here, can also contain retrograded crystalline amylose and co-crystallized amylose and amylopectin molecules (Figure 5.3A). Upon heating, the disruption of intermolecular hydrogen bonds through swelling and solubilization of a portion of SNP, leads to the release of acid depolymerized linear short chain amylose and branched amylopectin molecules into the solution (Figure 5.3B). Due to the different thermal stability between amylopectin crystals (low melting temperature $\sim 65^{\circ}\text{C}$) and retrograded amylose crystals (high melting temperature $\sim 140^{\circ}\text{C}$), the observed particle size reduction at temperatures above 60°C is more likely due to the melting of amylopectin SNP than retrograded amylose. Therefore, after heating, the suspension network is comprised of small heat resistant amylopectin SNP and recrystallized short chain amylose (spherulites) embedded within the solubilized linear, if any, and branched (possibly depolymerized amylopectin) molecules which along with water make up the continuous phase (Figure 5.3C). It is expected that the heat induced changes to the SNP (amylopectin blocklets and/or recrystallized short chain amylose) will modify the viscoelastic behaviour of SNP suspensions.

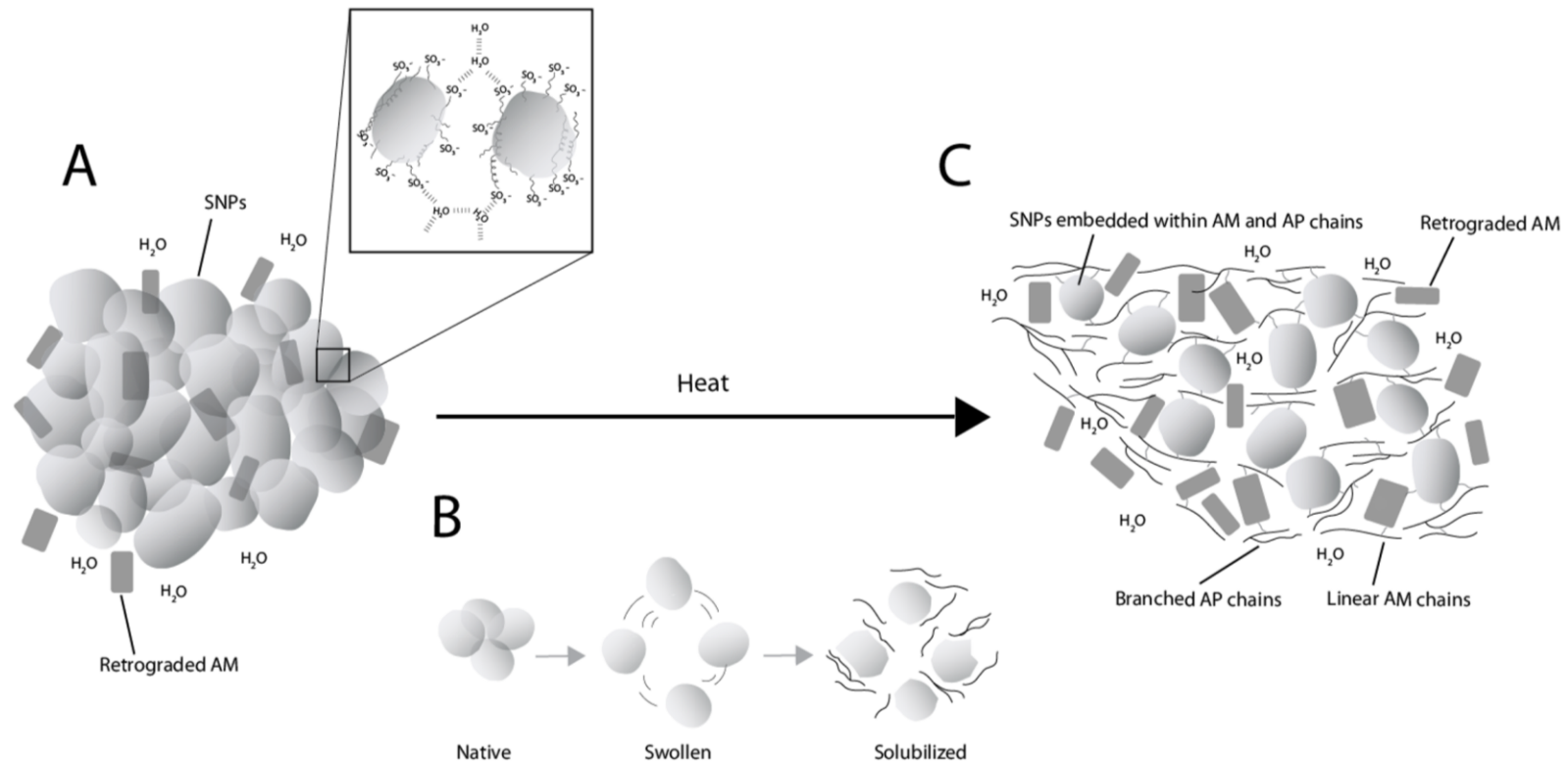


Figure 5.3 Schematic diagram showing the network formation of SNP suspensions from amylose containing starches. At room temperature **(A)**, the network is composed of SNP, retrograded amylose (AM) and water molecules interacting at their surface through hydrogen bonds (water bridges). During heating **(B)**, the intermolecular hydrogen bonds of SNP get disrupted through swelling and solubilization, leading to the release of depolymerized linear short chain amylose (AM) and branched amylopectin (AP) molecules. After heating **(C)**, the network is composed of linear AM and branched AP chains (continuous phase) and small heat resistant SNP and retrograded AM embedded internally (dispersed phase).

5.3.3. Viscosity of SNP suspensions

The effect of SNP concentration on aqueous viscosity at room temperature was first examined visually by comparing 1% and 5% (w/v) aqueous suspensions. At 1% concentration, the suspensions exhibited a thin liquid which can easily flow (Figure 5.4A), while increasing the concentration to 5% resulted in a gel-like material (Figure 5.4B). The liquid behaviour of SNP suspensions at low concentrations is due to the negative surface charge and repulsion of the electrical double layer between the nanoparticles. In colloidal suspensions, electroviscous effects are defined as the change in viscosity of a fluid primarily due to surface charged particles (Rubio-Hernandez et al. 2004). In the SNP suspensions, it is likely that both primary and secondary electroviscous effects are occurring due to the electrostatic repulsion within the electrical double layer of the particle and the fluid and to the overlap of double layers between two particles, respectively (Rubio-Hernandez et al. 2004).

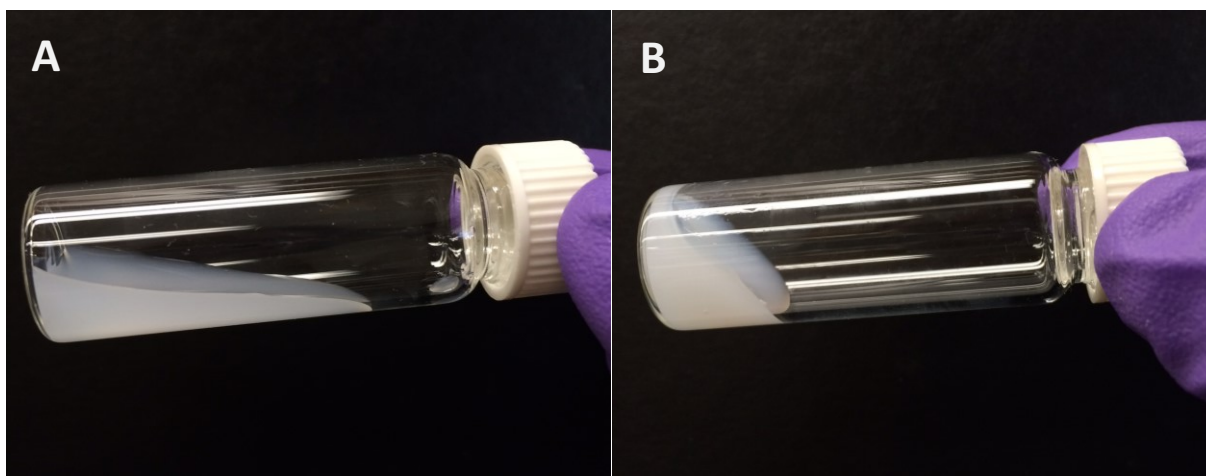


Figure 5.4 SNP aqueous suspensions: (A), 1% w/v, liquid-like behaviour; and (B), 5% w/v, gel-like behaviour.

A similar electroviscous behaviour was observed in cellulose nanocrystal suspensions of low concentrations (Boluk et al. 2011). At the higher concentration (5%), the gel-like appearance of SNP suspensions suggests the formation of a network possibly due to strong hydrogen bonding between the particles (Angellier et al. 2005b) and the presence of a higher number of nanoparticles. Suspensions of waxy maize SNP with concentrations higher than 9.6% (w/w) were also found to exhibit a gel-like consistency (Jin et al. 2015).

The continuous shear flow curves of 1% and 5% SNP suspensions from wheat, oat, barley and potato are presented in Figure 5.5. Due to the sensitivity limits of the rheometer at low shear rates, some data points for the 1% samples are not reported. At 1%, both wheat and potato SNP suspensions showed a shear-thinning behaviour with substantially greater viscosities than oat and barley (Figure 5.5). For 1% oat and barley, the viscosity remained unchanged with increasing shear rates from 10-100 s⁻¹, thus exhibiting a Newtonian behaviour.

At the higher concentration (5%), both the starch source and shear rate (0.01-100 s⁻¹) had a significant influence on the apparent viscosity. However, all SNP suspensions exhibited three distinct regions which are typical of lyotropic liquid crystal polymers (Srinivasarao 1995). The viscosity profile of lyotropic liquid crystal polymers consists of the following three regions: 1) a shear thinning behaviour at low shear rates, due to the alignment of chiral nematic liquid crystal domains; 2) a plateau region at intermediate shear rates, due to the orientation of the domains with the shear direction; and 3) a shear thinning behaviour at high shear rates, due to the disruption of the crystal domains and re-orientation along the shear flow direction (Shafiei-Sabet et al. 2012).

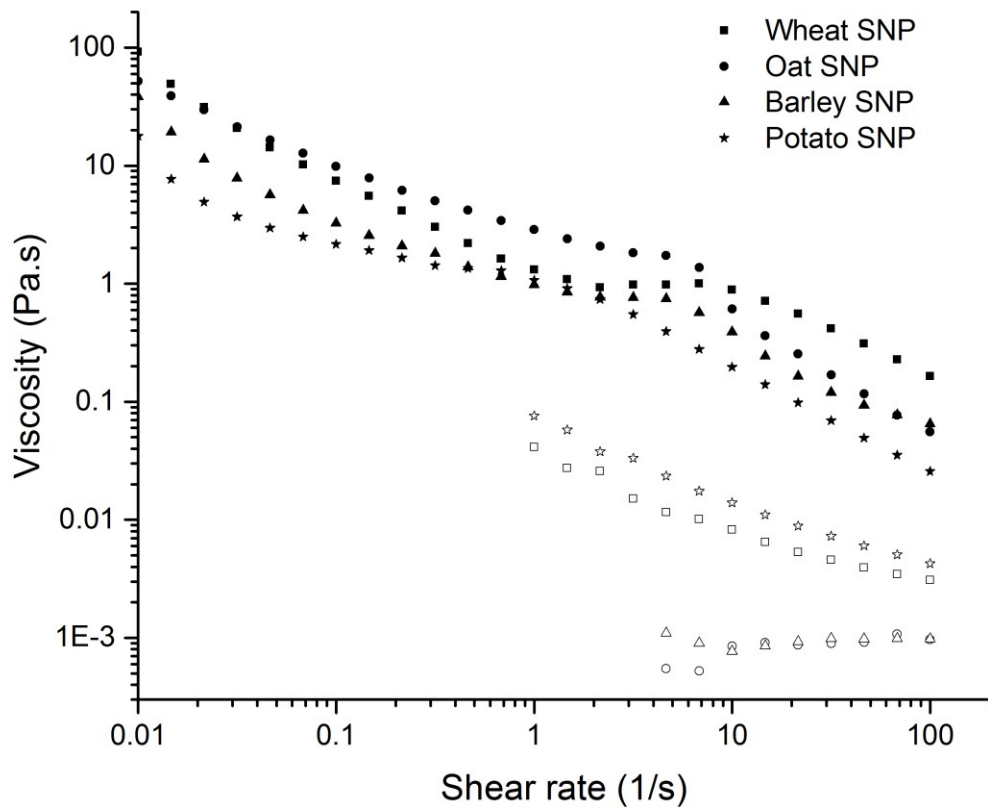


Figure 5.5 Apparent viscosity of 1% and 5% SNP suspensions as a function of shear rate. The open symbols correspond to 1% and the solid symbols to the 5% concentrations.

A viscosity profile similar to that of the 5% SNP suspensions was reported for sonicated cellulose nanocrystal rods in suspension (Shafiei-Sabet et al. 2012). Non-spherical particles such as rods, disks and spheroids exhibit hydrodynamic stresses, which depend on the shape and particle orientation (translational and rotational motion) during shear flow (Mewis and Wagner 2012). The similarity in the viscosity profile between the 5% SNP suspensions and cellulose rods may be due to the presence of long oval aggregates or clusters of two or more nanoparticles (Figure 5.1). At this concentration and 0.01 s^{-1} , the viscosity followed the order: wheat (92.1 Pa.s) > oat (51.8 Pa.s) > barley (38.3 Pa.s) > potato (17.8 Pa.s). This order is in agreement with the mean particle diameter, where the sample with the largest particles corresponds to the highest viscosities. Perhaps due to the ability of larger particles to occupy more volume than smaller particles at the same concentration. The plateau region at intermediate shear rates varied between all starches. For example, in wheat SNP this was between 2-10 Pa.s whereas in potato SNP it was between 0.3-0.7 Pa.s. This difference may be related to the orientation of the nanoparticles with the shear direction or to the amount of energy required to change the orientation of the domains. Furthermore, at 100 s^{-1} the 5% SNP suspensions of potato had the lowest viscosity (0.03 Pa.s) followed by oat (0.06 Pa.s), barley (0.07 Pa.s) and wheat SNP suspensions remained the highest viscosity (0.16 Pa.s). One possible explanation for the different viscosities observed (both at 1 and 5%) can be the degree of SNP sulfonation, which determines the surface charge density. Negative sulfate ester groups in the SNP surface can promote electrostatic repulsion between the SNP when they are suspended in a neutral solution and thus influence the viscosity behavior.

5.3.4. Dynamic rheological properties as a function of frequency

Figure 5.6 presents the storage modulus (G') and loss modulus (G'') of 5% SNP suspensions as a function of frequency (0.1-10 rad/s). For wheat and oat SNP, the loss modulus (G'') was higher than the storage modulus (G') over the entire frequency range, which corresponds to the viscous behaviour being dominant over the elastic behaviour. This behaviour was also reported for a 15% waxy maize SNP suspension within the same frequency range (Jiang et al. 2016). Barley and potato SNP on the other hand exhibited a more elastic behaviour. These suspensions behaved like a viscoelastic solid, indicative by a G' , which is significantly higher than G'' and independent of frequency (Figure 5.6). For example, the G' in barley was over 4 times higher than G'' . When compared to the particle size distribution and the continuous shear test data, the starches which showed a viscous behaviour (wheat and oat) had the highest apparent viscosities and hydrodynamic diameters, while those behaving like a viscoelastic solid (barley and potato) had the lowest apparent viscosities and hydrodynamic diameters. Since the effect of frequency was measured at a constant temperature (25°C), the different viscoelastic properties are attributed to changes in the three dimensional gel-like network formed by the nanoparticles (Figure 5.3A). It is proposed that SNP with smaller particle size (larger surface area) such as potato are capable of forming extensive inter-particulate associations and therefore providing a more elastic behaviour than larger SNP.

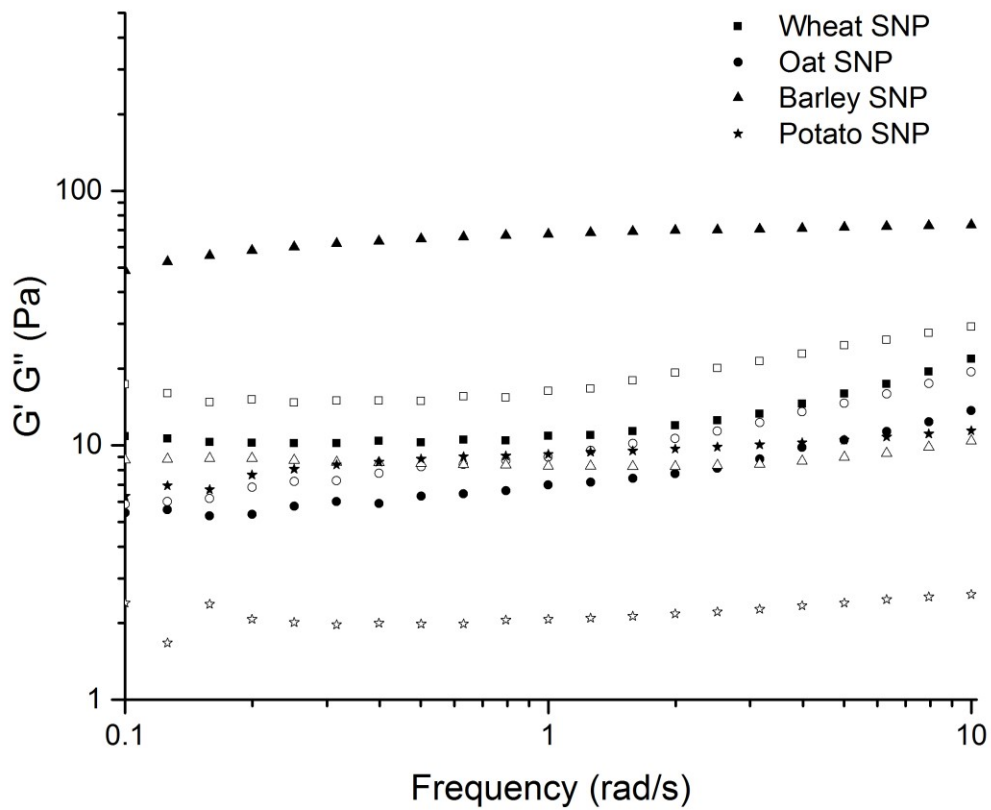


Figure 5.6 Storage modulus (G') and loss modulus (G'') of 5% SNP suspensions as a function of frequency at 25°C. The solid symbols represent G' and the open symbols represent G'' .

5.3.5. Dynamic rheological properties as a function of temperature

In order to further understand how temperature affects the aqueous nanoparticle network, the viscoelastic behaviour of 5% SNP suspensions as a function of temperature were investigated. The change in storage modulus (G') and loss modulus (G'') of SNP suspensions with temperature are presented in Figure 5.7. The suspensions of wheat, oat and barley SNP showed prominent crossover points ($G' = G''$) indicative of gel formation with an increase in temperature. At the beginning of the temperature ramp test (25°C), these suspensions behaved like a viscoelastic liquid ($G'' > G'$), which transitioned to an elastic gel ($G' > G''$). The transition temperature followed the order: oat (35°C) < wheat (43°C) < barley (49°C) (Figure 5.7 A, B and C).

Potato SNP suspension on the other hand behaved like an elastic gel ($G' > G''$) at all temperatures, although G' and G'' came close to each other and departed at ~ 60°C (Figure 5.7D). The above observations can be attributed to the phase transition behaviour of native starches as determined by differential scanning calorimetry. A-type starches (oat, wheat and barley) have lower T_o (onset), T_c (conclusion) and ΔH (enthalpy of gelatinization) than B-type potato starch. The sharp drop in G' between 55-70°C in both wheat (Figure 5.7A) and potato (Figure 5.7D), corresponds to a change in the internal structure, possibly due to crystal melting and solubilization of the SNP (LeCorre et al. 2012a; Li et al. 2012). As shown Table 5.1, incubation of SNP at 40 and 60°C, leads to a decrease in particle size distribution in both of these starches.

Barley SNP (Figure 5.7C) which showed the lowest decrease in the average hydrodynamic diameter upon heating (Table 5.1), also exhibited a drop in G' and G'' with an increase in temperature, however the decrease was more gradual than in wheat and potato.

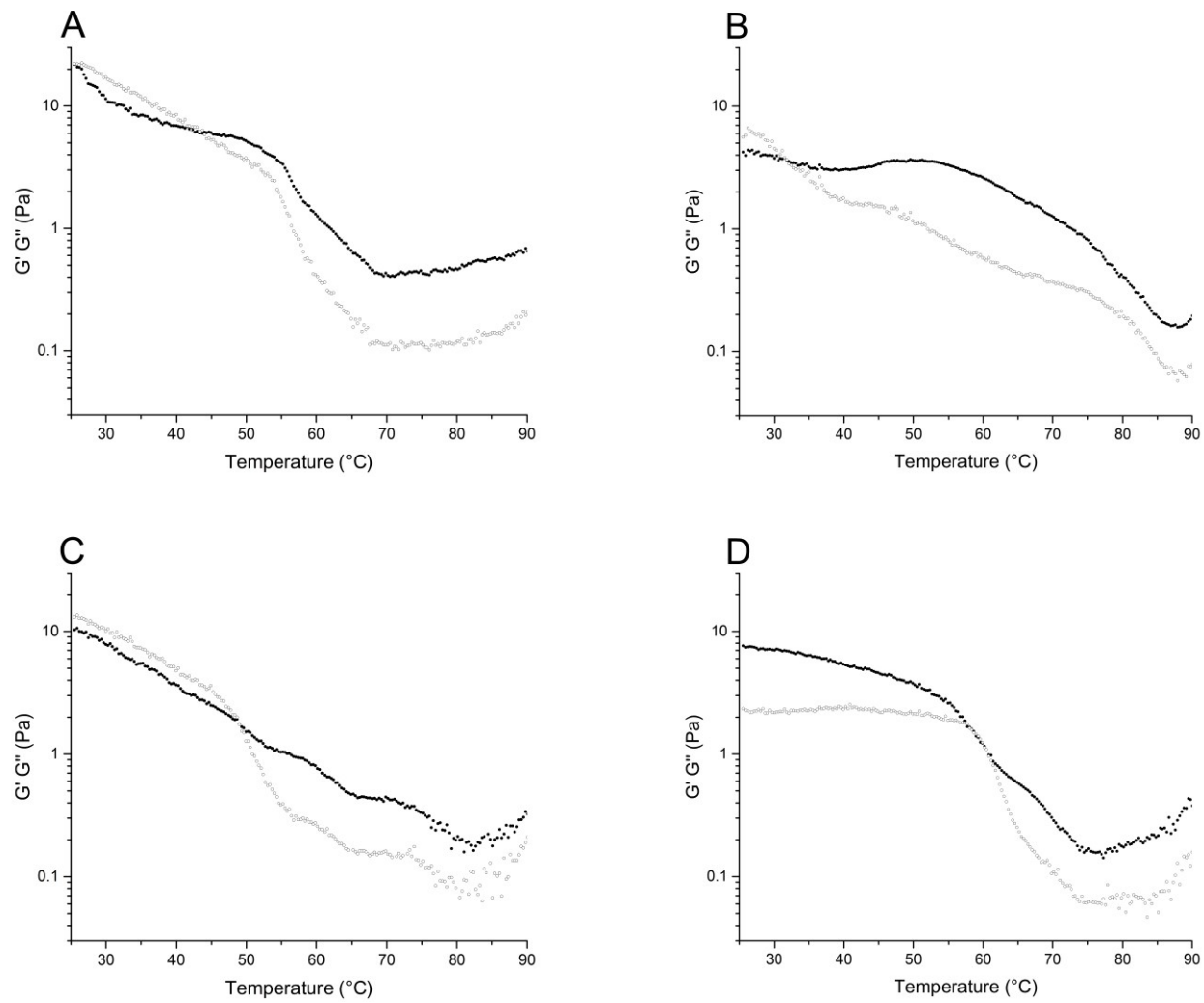


Figure 5.7 Storage modulus (G') and loss modulus (G'') of 5% SNP suspensions from (A) wheat, (B) oat, (C) barley and (D) potato as a function of temperature. The solid symbols represent G' and the open symbols represent G'' .

Oat SNP (Figure 5.7B) on the other hand exhibited a slight increase in G' at 40°C, which then decreased gradually above 53°C. Furthermore, in wheat and potato, G' increased above 70°C, while in oat and barley this increase was observed above 80°C. The increase in G' observed in all SNP, may have been due to the melting of SNP into their composing molecules (disruption of inter and intra molecular bonds) and the consequent increase in starch-water hydrogen bonding (Shi et al. 2013). According to Chung et al. (2007), a decrease and then an increase in G' when SNP are heated from 25-90°C corresponds to SNP swelling and perhaps melting.

A large variation in the temperature dependency of G' and G'' was observed among the SNP. In all samples the G' and G'' values were lower with increasing temperature than those initially recorded at 25°C. As discussed earlier (Figure 5.3), changes to the SNP structure during heating can modify the suspension network and thus their viscoelastic behaviours. At elevated temperatures, the decrease in G' and G'' may be due to a change from a particulate network to a network containing solubilized linear amylose and branched amylopectin chains (continuous phase) and small heat resistant SNP and nano-spherulites (retrograded amylose) embedded internally as the dispersed phase.

The complex viscosity of 5% SNP suspensions as a function of temperature is presented in Figure 5.8. Complex viscosity (η^*) in oscillation rheology is found by dividing the complex modulus (G^*) by the angular frequency (ω). For wheat and barley, an increase in temperature from 25 to 50°C corresponded to a sharp decrease in complex viscosity, which continued to decrease slightly thereafter. The complex viscosity of oat SNP exhibited a very different behaviour when compared to the other starch sources (Figure 5.8). With increasing temperature from 25 to 38°C, the complex viscosity of oat SNP decreased, then increased slightly between 38-

50°C, and decreased above 50°C. At temperatures above 38°C, the increase in complex viscosity may be due to particle swelling, while the decrease in complex viscosity above 50°C may be due to the disruption and melting of SNP (LeCorre et al. 2012a). Lastly, the complex viscosity of potato SNP decreased constantly with an increase in temperature. Although potato SNP showed the highest reduction in the hydrodynamic diameter (Table 5.1), the viscoelastic behaviour and complex viscosity data show that the potato (B-type) SNP network is more stable to temperature changes (particularly between 25-60°C) than the other A-type starches. Similar results were reported by LeCorre et al. (2012a), where the melting temperature in B-type starches shifted to higher temperatures than A-type starches. Based on the above findings, it is postulated that upon heating, the different viscoelastic behaviours as a function of temperature observed in all SNP are closely related to the changes in the particulate morphology, primarily due to swelling, partial melting and solubilization (Figure 5.3 B and C) and consequently the gel network nature (particulate network vs molecular network).

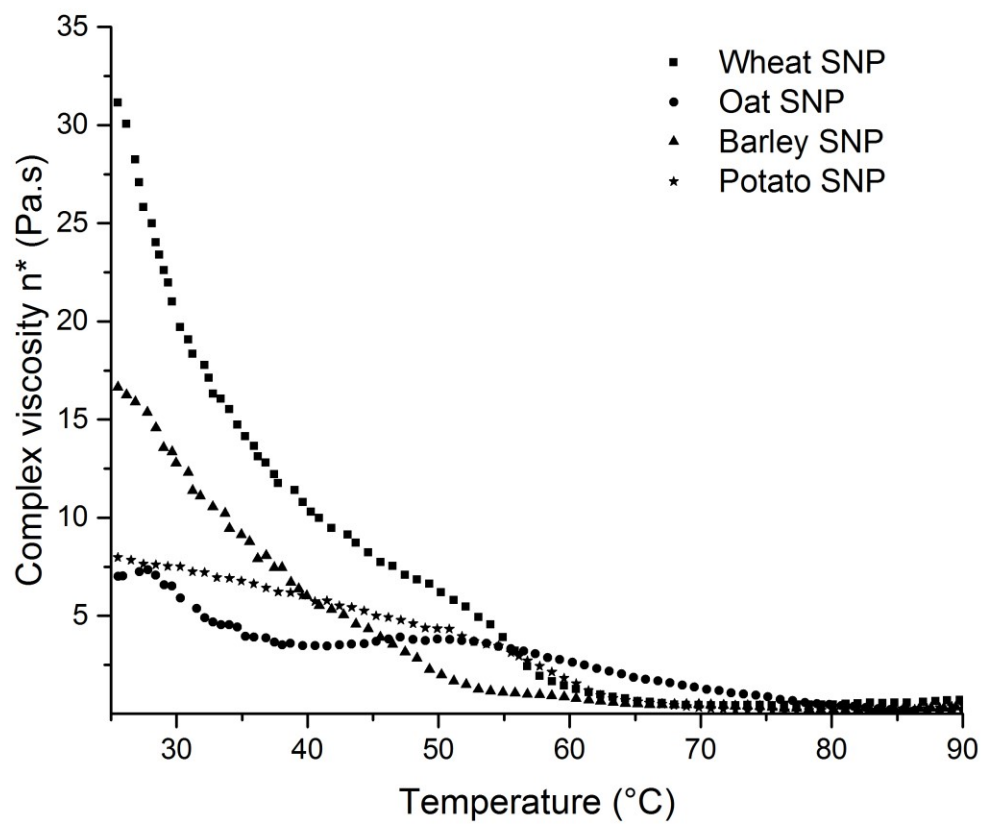


Figure 5.8 Complex viscosity of 5% SNP suspensions as a function of temperature.

5.4. CONCLUSIONS

The SNP isolated from A- and B- type regular native starches (wheat, oat, barley and potato) had significant variations in their particle size distribution, thermal stability and rheological properties. The thermal degradation of SNP in solution when compared within each starch source showed that larger particles were less heat resistance than smaller particles (i.e. reduction in the average hydrodynamic diameter). The starch source and SNP concentration influenced the viscosity behaviour of the aqueous SNP suspension. At 5% (w/v) concentration, the viscosity profile of all SNP suspensions was similar to that of lyotropic liquid crystal polymers like cellulose nanocrystals. In addition, at 5% (w/v), smaller SNP such as those in potato are capable of forming extensive inter-particulate associations and thus excel a more elastic behaviour than larger SNP, which exhibit a more viscous behaviour. Due to the growing demand for the use of SNP in food and non-food applications, understanding how processing conditions can alter the particulate nature and SNP network composition is of significant interest. In this respect, the present study demonstrated that during heating, the SNP network can undergo substantial changes due the susceptibility of a portion of SNP to swelling, melting and solubilisation. This suggested that the aqueous SNP suspensions at room temperature would be mainly composed of crystalline amylopectin blocklets (both small and large) and recrystallized short chain amylose (spherulites). However, after heating, the amylose and amylopectin from solubilized larger SNP would form the continuous phase, and the small heat resistant SNP (amylopectin blocklets and recrystallized amylose spherulites) would remain embedded in the dispersed phase.

CHAPTER 6 Rheological characterization of gum and starch nanoparticle blends

6.1. INTRODUCTION

Gums and hydrocolloids are commonly used as texturizing agents due to their ability to bind large volumes of water. This nature gives them the capacity to modify the functional and rheological properties of a food system. Carrageenan and xanthan are among the most common gums and are widely used for their thickening and gelling properties in dairy products, dessert gels, salad dressings and processed meats. Carrageenan is a naturally occurring polysaccharide obtained from red seaweed. It is classified in three main structural forms [κ (kappa), ι (iota) and λ (lambda)] depending on the extraction and purification method. Among these, λ -carrageenan contains the most sulfate (3 groups for every 2 galactose units), followed by ι - and κ -carrageenan with 2 and 1 sulfate groups, respectively. λ -Carrageenan is made up of repeating galactose units with little or no 3,6-anhydrogalactose, joined by alternating α -(1,3) and β -(1,4) glycosidic links and containing approximately 37% ester sulphate groups (Phillips and Williams 2009). λ -Carrageenan is a cold water soluble thickening agent, unable to form gels due to the electrostatic repulsion of its sulfate groups and structural conformation, which prevents the formation of double helices (Van de Velde et al. 2002). In comparison, both κ - and ι -carrageenan can form gel networks by undergoing a structural transition from coil (disordered state) to double helix (ordered state) conformation after heating and cooling (Rees et al. 1969). According to Campo et al. (2009), the viscosity and gel strength depends on the type of carrageenan, concentration, temperature, and the presence of cations, which can decrease the repulsion between the sulfate

groups. For the purpose of this study, only λ -carrageenan was investigated due to its synergistic effect with most starches.

Xanthan gum on the other hand is an extracellular polysaccharide produced through a fermentation process by the microorganism *Xanthomonas campestris*. It is composed of a linear β -(1,4)-D-glucose backbone and a trisaccharide side chain on every other glucose at C-3 with a glucuronic acid residue linked to two mannose units that connect to the backbone (Jansson et al. 1975). The presence of some pyruvic and acetic acid groups in the trisaccharide side chain make this a charged (anionic) polysaccharide. Xanthan gum is soluble in both cold and hot water. It has a double helical structure that can form a complex network thus exhibiting high viscosity and pseudoplastic behaviour along with excellent temperature and acid stability (Katzbauer 1998). According to Morris et al. (1977), the temperature at which xanthan gum is dissolved in solution significantly affects the gel viscosity due to a potential change in the structural conformation from a helix to a coil (ordered to disordered state).

In the past, much research has been done to understand the synergistic effects of blending more than one hydrocolloid together. Strong synergism has been reported between κ -carrageenan and locust bean gum or konjac glucomannan and by combining xanthan gum with galactomannans (guar, locust bean, cassia and tara gum) and glucomannans (Phillips and Williams 2009). For example, blending locust bean gum and κ -carrageenan increases the gel strength and elasticity and reduces syneresis. Furthermore, the interaction between xanthan gum and galactomannans depends on the degree of substitution of the mannose backbone with galactose side chains, where a stronger interaction forms with galactomannans with fewer galactose side chains as is the case for locust bean gum (Phillips and Williams 2009). Blends of

high purity β -glucan with xanthan, ι -carrageenan and carboxymethyl cellulose also result in viscosity synergism (Ghotra et al. 2009). The shear tolerant behaviour in the β -glucan and xanthan blend was attributed to increased molecular entanglements at high shear rates. Ghotra et al. (2009) concluded that such high viscosity blends could improve satiety when added to various food products.

Within hydrocolloids field of research, understanding the associations between starch and gums for their applications in food systems has been another focus of investigation. In particular, many studies have been conducted to determine how adding xanthan, guar, cassia and carboxymethyl cellulose to starch pastes can influence the paste and gel properties (BeMiller 2011). Kaur et al. (2008) investigated the microstructure of starch and cassia gum systems made from various starches and gum concentrations. The authors reported that the extent of interaction with cassia gum differed significantly between the different starch types, the amylose content and the granule size. In the presence of low gum concentrations, starch swelling may be restricted due to limited water availability, which can lead to changes in the viscosity and viscoelastic properties of the starch system. Similarly, Weber et al. (2009) compared the interactions of guar and xanthan gums with maize starches varying in amylose content. They found all starch pastes increased their viscosity with the addition of gum and concluded this was either due to the associations with soluble amylose and amylopectin or due to the competition for free water between the gum and the starch.

Currently, there is no study available focusing on the influence of starch nanoparticles (SNP) on the rheological properties of gums in a pure system. Only the rheological properties of aqueous suspensions of starch nanocrystals (SNC) and SNP from maize, wheat and potato

starches (LeCorre et al. 2011; Shi et al. 2012a; b; Shi et al. 2013; Jiang et al. 2016) have been investigated. LeCorre et al. (2011) found all SNC suspensions exhibit a shear-thinning behaviour regardless of the SNC concentration and starch source and no correlation was established between the viscosity and SNC size, thickness and surface area. In a series of studies, Shi et al. (2012b) compared the effect of two different drying methods on the re-dispersibility of soluble potato SNP, and the influence of NaCl concentration on the aqueous rheological properties of SNP. The authors found both the drying method and the NaCl concentration changed the properties of the SNP aqueous suspensions. In the presence of NaCl, the apparent viscosity of SNP obtained from freeze drying and spray drying showed opposite trends, where the viscosity of the freeze dried SNP increased with salt concentration (Shi et al. 2013). Furthermore, SNP suspensions containing NaCl had better thermal stability between 25-90°C than those without NaCl. More recently, Jiang et al. (2016) investigated the rheological properties of waxy maize SNC (prepared by acid hydrolysis) and SNP (prepared by enzymatic hydrolysis and a controlled self-assembly) as a function of ionic strength. Similar to the other studies, the SNP suspensions showed a shear-thinning behaviour which did not change with the addition of NaCl. Based on the current information available, research is warranted to better understand the rheological behaviour of SNP and their blends with commercial gums.

The present study was intended to demonstrate how the SNP source and concentration influence the rheology of common food gums such as λ -carrageenan (CAR) and xanthan (XAN) gums. These gums were selected due to their wide range of applications in different food systems. For this purpose, SNP from waxy (0% amylose) and high amylose maize (71% amylose) starches were isolated by acid hydrolysis. The objectives were: 1) to determine the effect of SNP

concentration on the viscosity of aqueous SNP suspensions, 2) to compare the static and dynamic rheological properties of binary blends consisting of 0.5% (w/v) gum and different SNP concentrations. This study is expected to provide a clear understanding of how SNP interact with the continuous phase of low and high elasticity gum systems.

6.2. MATERIALS AND METHODS

6.2.1. Materials

Waxy maize (amioca) and high amylose maize (hylon VII) (>95% purity) were provided by Ingredion Incorporated (Westchester, IL, U.S.A). λ -Carrageenan (Ticaloid 750) and xanthan (Tixacan pre-hydrated rapid-3) powders were provided by TIC Gums Inc. (White Marsh, MD, U.S.A). All other chemical were of ACS certified grade.

6.2.2. Isolation of SNP by acid hydrolysis

The acid hydrolysis and isolation protocol was performed in replicates according to the methodology reported in section 3.2.3 in Chapter 3.

6.2.3. Preparation of SNP suspensions and gum-SNP blends

Aqueous SNP suspensions, control samples (gum only) and their blends were prepared for the rheological tests. First, SNP suspensions with 0.5, 1.0 and 3.0% (w/v) concentrations were produced by mixing lyophilized SNP and MilliQ water, and homogenizing at 15,200 rpm for 20 min (Heidolph DiAx 900, Heidolph Instruments, Schwabach, Germany) to aid dispersion. Binary blends of gum-SNP were prepared according to Table 6.1, to achieve a 0.5% (w/v) total gum concentration. Appropriate amounts of CAR and XAN were added to the SNP suspension,

manually mixed until the gum fully solubilized and the samples appeared homogeneous. Control samples containing gum alone at 0.5% (w/v) concentration were prepared with MilliQ water.

Table 6.1 Preparation of binary blends of SNP suspensions and gums

Gum	+	SNP suspension	
Source		Source	Concentration
0.5% λ -Carrageenan	-		0% (control)
	Waxy		0.5%
			1.0%
	Hylon VII		0.5%
			1.0%
0.5% Xanthan	-		0% (control)
	Waxy		0.5%
			1.0%
	Hylon VII		0.5%
			1.0%

6.2.4. Static and dynamic rheological properties

Preliminary experiments were performed to select the geometry type and calibrate the rheometer (HR-3, TA Instrument, DE, U.S.A.) to generate better quality data. Details of this study are presented in Appendix III. Briefly, a comparative analysis between three different geometry types [cone and plate (40 mm, 2°, 53 μ m gap, steel), parallel plate (40 mm, 1000 μ m gap, steel) and cup and bob (concentric cylinder cup radius 15 mm, DIN rotor radius 14 mm, aluminium)] was conducted using low and high viscosity commercial gums, λ -carrageenan and xanthan, respectively. Results showed that cup and bob should be used for low viscosity systems (0.5% λ -carrageenan); however, this geometry demands a significant amount of sample for each measurement. Among the other two geometries, cone and plate gave more reproducible results

than the parallel plate, particularly for the low viscosity sample, while for the high viscosity sample the geometry type had no impact. Based on the results from this preliminary work and considering other factors such as sample size, the cone and plate geometry (40 mm, 2°, 53 μm gap, steel) was selected for all rheological testing. Rheometer and geometry calibrations included oscillatory mapping, rotational mapping, geometry inertia, and gap temperature compensation (Appendix III).

The continuous shear test was performed to determine the relationship between the apparent viscosity and the shear rate. The shear rate range was from 0.01-100 s^{-1} and the temperature was set at 25°C. Before each rheological test the samples were allowed to equilibrate at 25°C for 2 min. The frequency sweep test evaluated the changes in the viscoelastic modulus as a function of angular frequency (0.1-100 rad/s). The temperature was set at 25°C and oscillating strain of 2% was used. Preliminary amplitude sweep tests confirmed a 2% strain was within the linear viscoelastic region of all samples. The temperature ramp test was carried out to determine the relationship between viscoelastic modulus and temperature. The test was performed at a frequency of 1 rad/s, oscillating strain of 2% and a heating rate of 2°C/min from 25°C to 90°C. The gap temperature compensation feature was enabled in all temperature ramp tests, which allows the stage to move according to the expansion coefficient of the geometry as the temperature changes. A solvent trap geometry and solvent trap cover were used to create a thermally stable environment and prevent moisture loss from the samples during heating. Silica oil was placed in the solvent well. All rheological measurements were carried out in duplicates and the mean is reported.

6.3. RESULTS AND DISCUSSION

6.3.1. Viscosity of SNP suspensions as a function of concentration

SNP were isolated by acid hydrolysis from waxy and high amylose (hylon VII) maize starches varying in amylose content, 0% and 71%, respectively. Previous studies showed that waxy and hylon VII SNP differ in their morphology, particle size, crystallinity, molecular structure and amylase resistance (Chapter 3 and 4). SNP from waxy maize are larger in size (500 nm) and have a flat elliptical shape while those from hylon VII are round-polygonal with an average hydrodynamic diameter of 268 nm. The crystalline type of waxy SNP (A-type) was similar to its native starch, whereas for hylon VII there was a transformation observed from B-type to A-type after acid hydrolysis. Accordingly, SNP from high amylose maize starches are comprised of both low molecular weight linear chains and short A + B amylopectin chains, which are both acid and enzyme resistant, while those from waxy maize starch are comprised primarily of short A + B amylopectin chains that are only acid resistant, but susceptible to amylase hydrolysis. Variations in the above mentioned characteristics are expected to influence the functional properties of aqueous SNP suspensions alone and in combination with different food ingredients such as gums.

When SNP are suspended in solution, their viscous behaviour is dependent on the concentration, the electroviscous effects of the negative surface charges (Rubio-Hernandez et al. 2004) or the formation of strong particle-particle hydrogen bonds (Angellier et al. 2005a). Since the SNP were isolated with sulfuric acid, the presence of sulfate ester (SO_3^-) groups on the nanoparticle surface will impart a negative surface charge and ionic strength in solution. Thus the degree of SNP sulfonation can determine how much electrostatic repulsion exists between the SNP in solution and therefore the viscosity behavior.

The viscosity of aqueous SNP suspensions alone were investigated prior to being blended with different commercially available food gums. For all samples, the continuous shear rate tests were performed from 0.1 to 100 s⁻¹; however, due to the sensitivity limits of the rheometer at low shear rates, some data points are not reported (Figure 6.1). The viscosity profile of SNP suspensions varied according to the starch source and concentration. At 0.5%, both waxy and hylon VII SNP suspensions exhibited a Newtonian behaviour (Figure 6.1). Similar results were also reported for suspensions of acid modified waxy maize starch and cellulose nanocrystals (Wang et al. 2003; Shafiei-Sabet et al. 2012). When the concentration was increased to 1%, the viscosity of the SNP suspensions of waxy and hylon VII varied significantly. Waxy SNP continued behaving like a Newtonian liquid with a steady viscosity of ~0.001 Pa.s at increasing shear rates. However, the SNP suspension of hylon VII exhibited a shear thinning behaviour and greater viscosities. At the shear rate of 10 s⁻¹, the viscosity of 1% hylon VII (0.016 Pa.s) was 16 times greater than that of 1% waxy (0.001 Pa.s). Moreover, when the concentration of SNP was increased to 3%, the suspensions of both waxy and hylon VII had a gel-like appearance and showed shear thinning behaviour (Figure 6.1). The same behaviour was also reported for waxy SNP suspensions (>6%, w/v) in the presence and absence of NaCl (Shi et al. 2013; Jiang et al. 2016). Among the two SNP, hylon VII was around 10 times more viscous than waxy, possibly due to the presence of recrystallized short chain amylose in the form of spherulites or nanoparticles, which due to their smaller size have greater particle density and greater hydrodynamic interactions (larger surface area) than waxy SNP. According to Shafiei-Sabet et al. (2012), the rheological properties of cellulose nanocrystal suspension at different concentrations varied due to their size and shape, surface charge and ionic strength. Furthermore, other studies have shown the starch source

(Chapter 5), and isolation or drying method (Jiang et al. 2016) can also significantly influence the rheological behaviour of SNP suspensions.

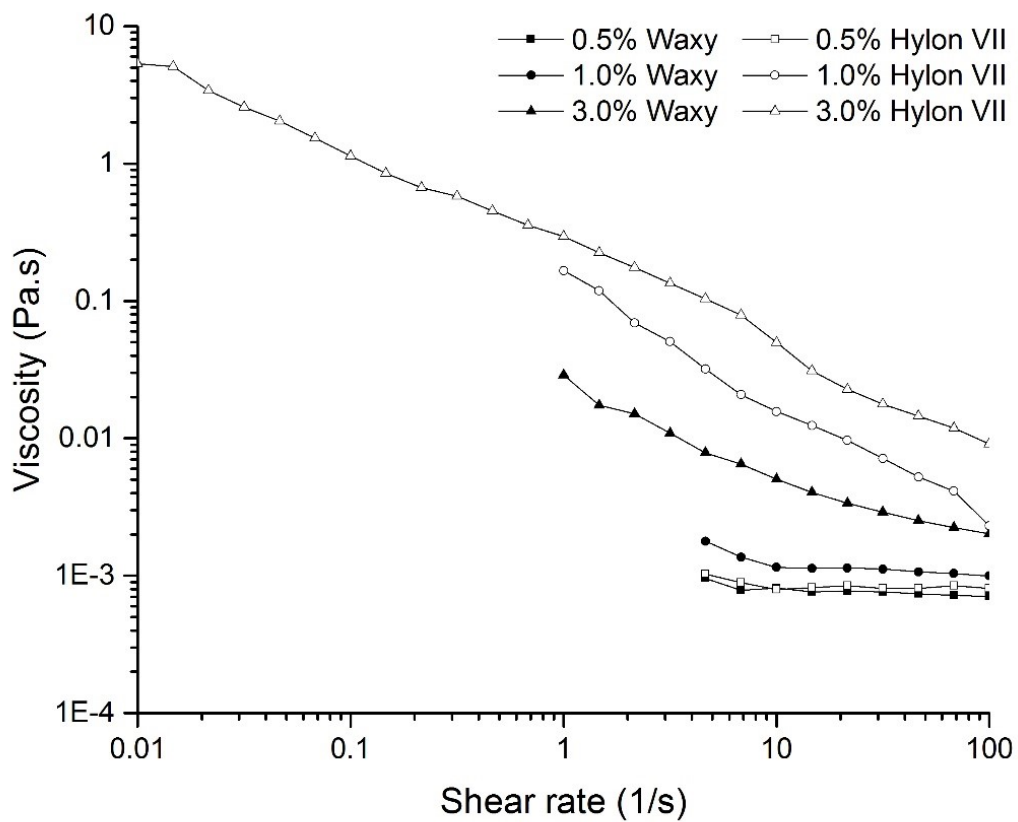


Figure 6.1 Apparent viscosity of waxy and hylon VII SNP suspensions at various concentrations as a function of shear rate.

6.3.2. Rheological properties of CAR-SNP blends

In order to understand how SNP influence the viscosity and viscoelastic properties of common food gums, binary blends of 0.5% (w/v) gum and different SNP concentrations were prepared and evaluated (Table 6.1). The apparent viscosity of the CAR-SNP blends as a function of shear rate showed that all samples exhibit a weak shear thinning behaviour regardless of the SNP source and concentration (Figure 6.2). Due to the sensitivity limits of the rheometer at low shear rates, the apparent viscosity of CAR alone and blended with SNP was evaluated at shear rates above 1 s^{-1} . An antagonistic interaction was expected between the SNP and CAR due to the repulsion of negatively charged sulfate groups (SO_3^-) present on the surface of both SNP (Angellier et al. 2005a; Wei et al. 2014) and the molecular structure of λ -carrageenan. However, in comparison to CAR alone, increasing the SNP concentration increased the viscosity slightly in all blends except one at 0.5% SNP. The greatest viscosities were for the binary blends with 1% SNP and no significant difference was observed between waxy and hylon VII despite their significant viscosity differences shown in Figure 6.1. The observed increase in viscosity could be due to the inclusion of SNP (dispersed phase) within the void spaces of the CAR coil structure (continuous phase) by a space filling mechanism, the formation of intermolecular interactions between the gum and SNP or simply due to an increase in the solid content.

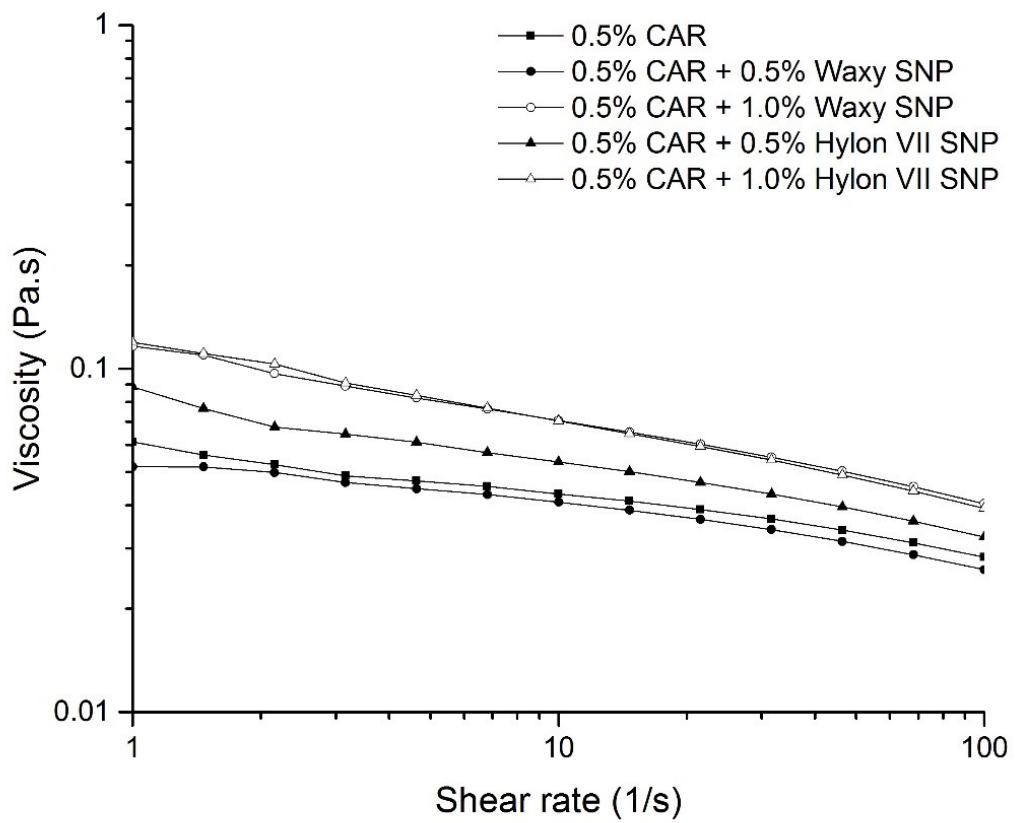


Figure 6.2 Apparent viscosity of CAR-SNP blends as a function of shear rate.

In order to further determine if SNP are interacting with the CAR, and thus modifying their viscoelastic behaviour, dynamic rheological properties of the CAR-SNP blends were also investigated. Figure 6.3 presents the storage modulus (G') and loss modulus (G'') as a function of frequency (0.1-100 rad/s). All samples showed a strong frequency dependency, which varied by SNP source. With the exception of the 1% hylon VII blend, all samples exhibited a more viscous than elastic behaviour, as shown by G'' being higher than the G' over the entire frequency range and having $\tan \delta$ values > 1 . On the other hand, the 1% hylon VII blend showed 2 crossover points ($G' = G''$), one at very low and one at very high frequencies. At frequencies below 1 rad/s, both blends containing 0.5% SNP were very unstable and had lower G' and G'' values than CAR alone, while at greater frequencies the samples behaved nearly similar. With the addition of 1% waxy and 1% hylon VII the G' and G'' values increased significantly and $\tan \delta$ values decreased in comparison to CAR alone. This is an indication that the CAR gum became slightly more elastic in nature with the incorporation of SNP, although it remained a viscous system.

The viscoelastic behaviour of CAR-SNP blends as a function of increasing temperature was also investigated and is shown in Figure 6.4. Special care was taken to prevent moisture loss in order to minimize data generated with this effect. At the initial temperature (25°C), all the blends and CAR alone behaved like a viscous liquid ($G'' > G'$), which transitioned to an elastic gel ($G' > G''$) at higher temperatures. This transition is known as thermal gelation and has been previously reported for globular proteins (Wang and Damodaran 1990) and methylcellulose in aqueous solutions (Li 2002). It is likely that the thermally induced gelation in CAR was due to the development of a cross-linked three dimensional network by hydrogen bonds and associations of the polymer chains (Li 2002).

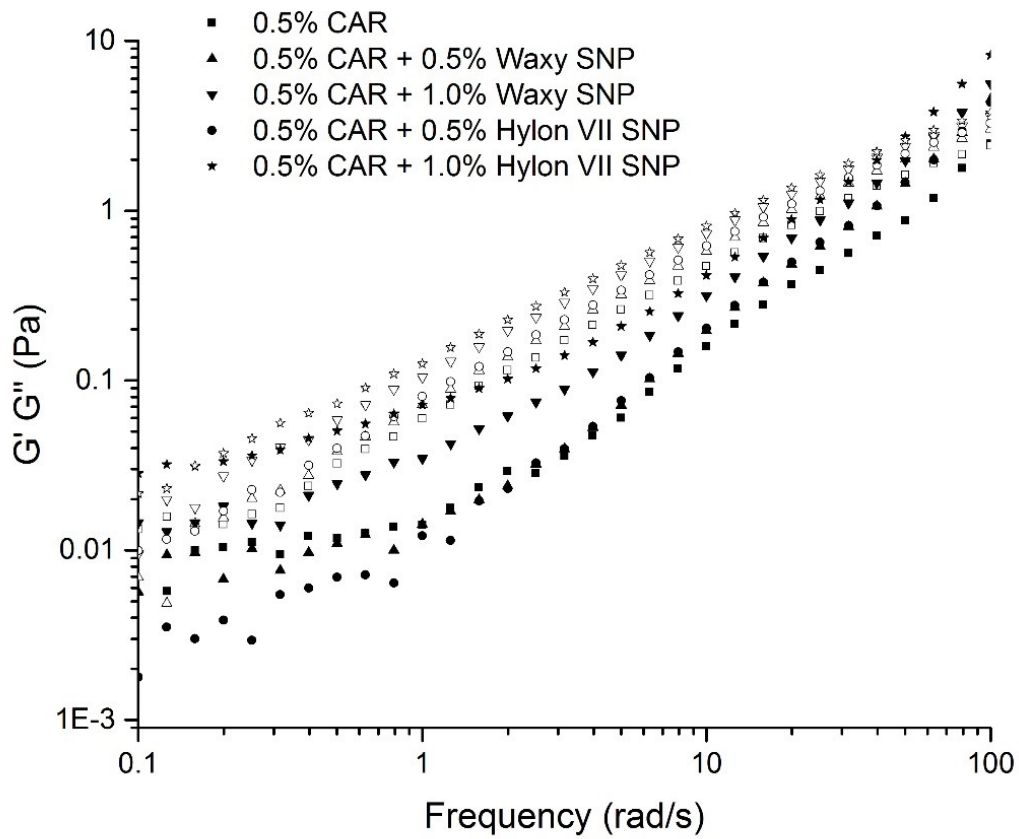


Figure 6.3 Storage modulus (G') and loss modulus (G'') of CAR-SNP blends as a function of frequency. The solid symbols represent G' and the open symbols represent G'' .

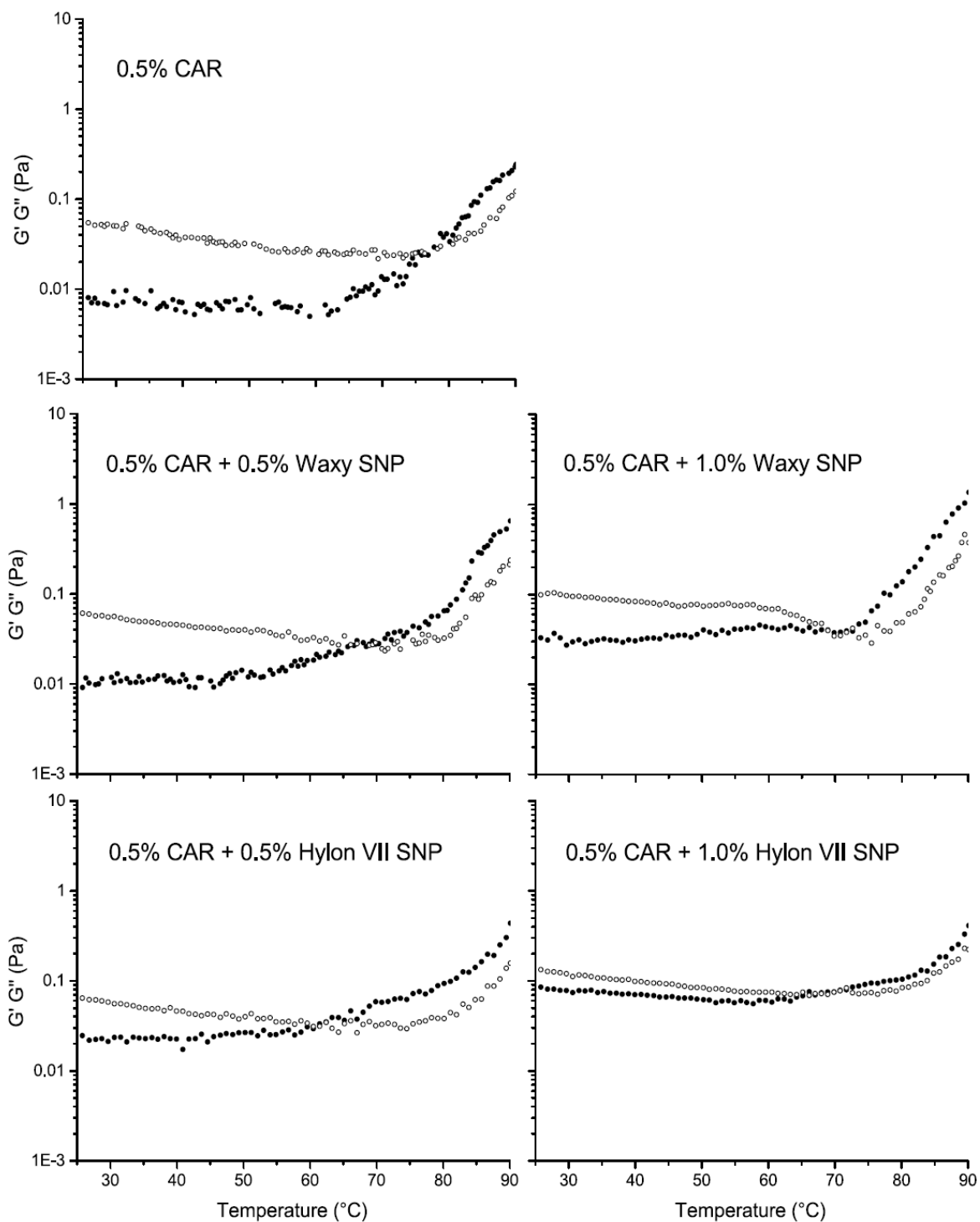


Figure 6.4 Storage modulus (G') and loss modulus (G'') of CAR-SNP blends as a function of temperature. The solid symbols represent G' and the open symbols represent G'' .

In comparison to CAR alone, the addition of SNP decreased the transition temperature and this differed by starch source and concentration (Figure 6.4). However, the viscoelastic behaviour remained nearly similar. Similar results have also been reported for methylcellulose and cellulose in solution (Li 2002; Weng et al. 2004). The incorporation of SNP increased the G' and G'' values, as well as decreased $\tan \delta$ and this followed the order: 0.5% waxy < 1% waxy < 0.5% hylon VII < 1% hylon VII.

Before the transition temperature, the viscoelastic behaviour of all samples remained somewhat stable as shown by the horizontal G' and G'' lines. However, beyond the transition temperature their behaviour changed depending on the SNP source (Figure 6.4). According to the results from Chapter 4, waxy and hylon VII SNP should differ in their thermal stabilities due to their different molecular composition. In the blends containing waxy SNP, variations in the viscoelastic properties with temperature can be due to changes in the particulate nature and composition of the dispersed phase (nanoparticles vs solubilized molecules) from melting of amylopectin crystallites. The sharp increase in G' and G'' above 70°C, observed in Figure 6.4 (0.5% CAR + 1.0% Waxy SNP), may correspond to the partial swelling and melting of the nanoparticles (Shi et al. 2013), which can lead to an increase in the starch-water-gum interactions. This same behaviour was not observed for the samples containing hylon VII SNP, perhaps due to the ability of a portion of SNP to withstand higher melting temperatures. According to Chapters 3 and 4, hylon VII SNP are composed of a mixture of amylopectin crystallites (low melting temperature ~ 55°C) and recrystallized short chain amylose possibly in the form of starch spherulites (higher melting temperature ~ 140°C), while waxy SNP are made up of amylopectin crystallites alone. Blending SNP with CAR gum did not provide any significant change to the viscous nature of the

system. However, results from the temperature ramp test revealed interesting information with regard to the potential melting behaviour of the different SNP. These results show that the addition of hylon VII SNP can help maintain similar viscoelastic properties (G' and G'' values) in spite of increasing temperatures, while this is not the case with waxy SNP.

6.3.3. Rheological properties of XAN-SNP blends

The apparent viscosity of XAN alone and blended with SNP was evaluated as a function of shear rate from 0.1-100 s^{-1} (Figure 6.5). In comparison to CAR, XAN gum has a greater viscosity and shear thinning behaviour attributed to its molecular rod-like conformation that can form a complex gel network (Choi and Yoo 2009). The addition of SNP did not substantially affect the viscosity and the shear thinning behaviour of XAN (Figure 6.5). For example, at 0.1 s^{-1} , the viscosity of 0.5% XAN alone increased from 9.5 to 12 Pa.s with the addition of 1% waxy or 1% hylon VII SNP.

XAN alone and the XAN-SNP blends showed a different viscoelastic behaviour when compared to CAR. Figure 6.6 presents the storage modulus (G') and loss modulus (G'') as a function of frequency (0.1-100 rad/s). All samples exhibited an elastic gel-like behaviour ($G' > G''$) over the entire frequency range. This behaviour is similar to that observed for a mixture of sweet potato starch and xanthan gum (Choi and Yoo 2009). In comparison to 0.5% XAN alone, increasing the SNP concentration increased the G' and G'' values which followed the order: 0.5% hylon VII < 0.5% waxy < 1% waxy < 1% hylon VII. The samples behaved similar to an ideal gel, as shown by a G' which is almost independent of frequency and $G' > G''$ (Tzoumaki et al. 2013). Furthermore, with the addition of SNP the $\tan \delta$ values did not change and remained in the range 0.3-0.9, indicating the elastic nature prevailed over the viscous behaviour.

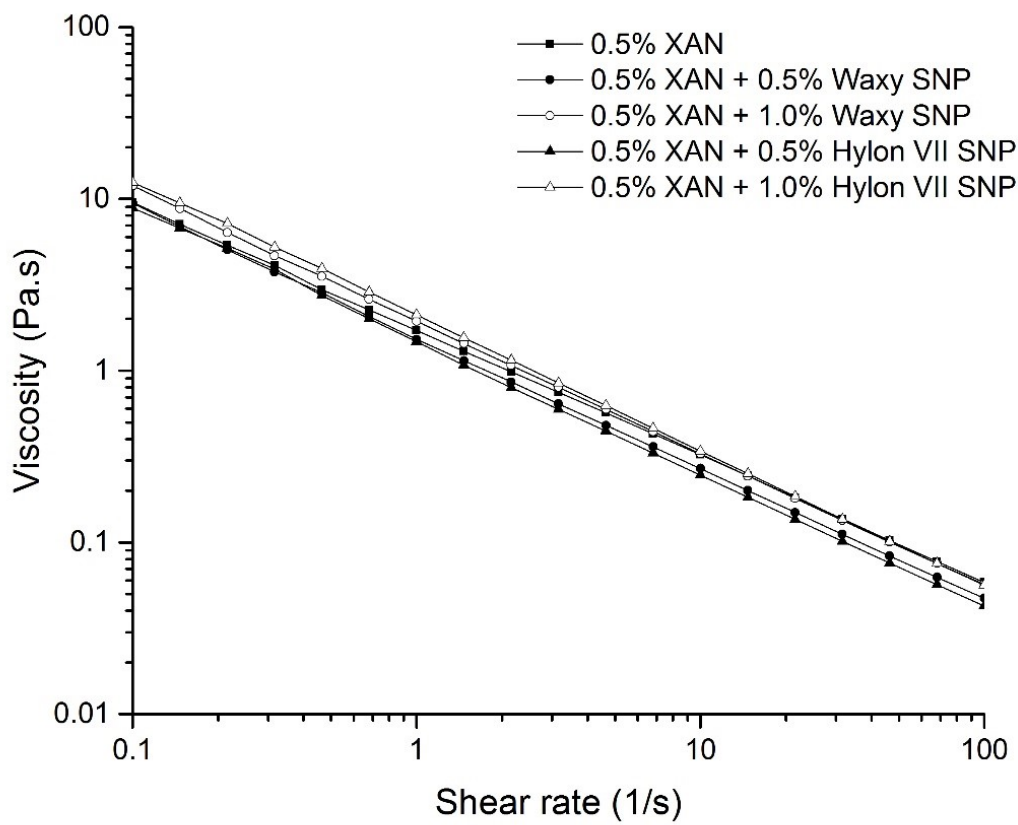


Figure 6.5 Apparent viscosity of XAN-SNP blends as a function of shear rate.

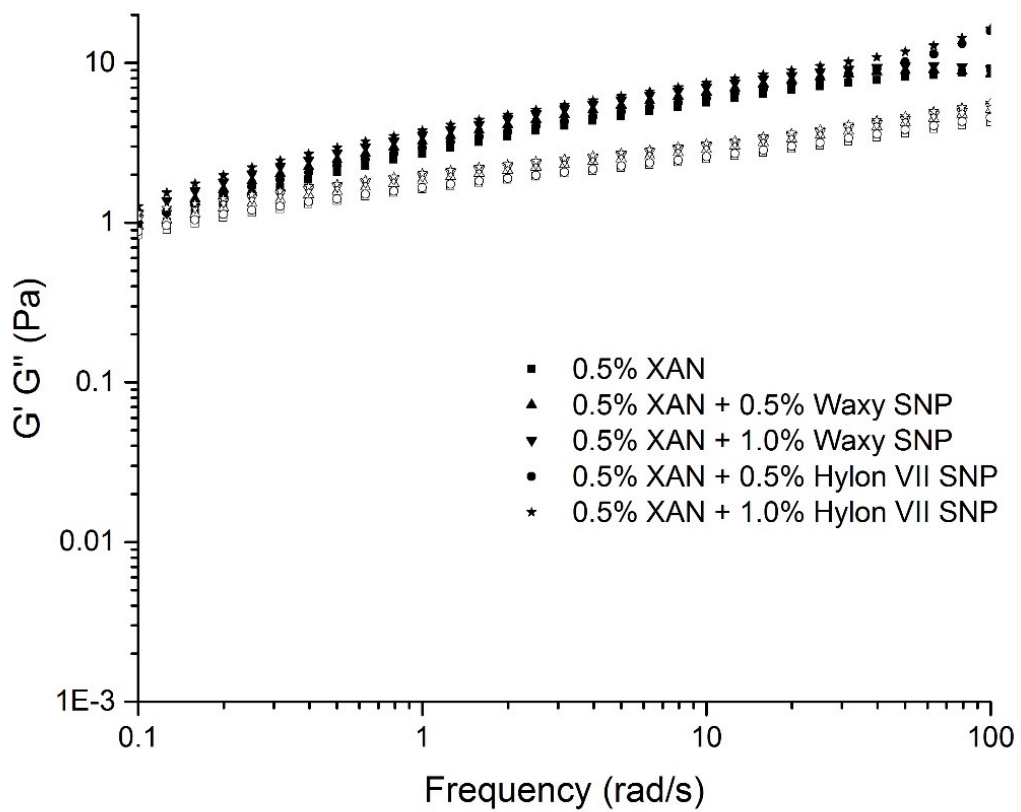


Figure 6.6 Storage modulus (G') and loss modulus (G'') of XAN-SNP blends as a function of frequency. The solid symbols represent G' and the open symbols represent G'' .

The viscoelastic behaviour of XAN-SNP blends as a function of increasing temperature were also investigated (Figure 6.7). At the initial temperature (25°C), all the blends and XAN alone behaved like an elastic gel ($G' > G''$), which transitioned to a viscous liquid ($G'' > G'$) at elevated temperatures. This corresponds to a melting behaviour, which is caused by a change in the conformational structure of xanthan gum at temperatures above 40°C. According to Milas and Rinaudo (1979) the temperature dependence of xanthan gum is attributed to a conformational change in the backbone from a helix to a coil state and a decrease in the rigidity of the linear β -(1,4)-D-glucose backbone. In all samples, the G' and G'' trend was nearly similar, however, the values for G' and G'' increased slightly with the addition of 1% hylon VII SNP. For example, at 25°C, 0.5% XAN alone had values of 1.9 and 1.2 Pa corresponding to G' and G'' , respectively, while 0.5% XAN + 1% hylon VII had 3.5 and 2.0 Pa, respectively. Regardless of the SNP source and concentration, all XAN-SNP blends showed a decreasing trend in G' and G'' with increasing temperatures of up to 75°C (Figure 6.7). Beyond this temperature, the same sharp increase in G' that was observed for the blends containing waxy SNP and CAR was also evident in the XAN-waxy samples. Again this behaviour is attributed to partial swelling, melting and solubilisation of the waxy SNP and the formation of intermolecular interactions between the depolymerized amylopectin chains (dispersed phase) and coil xanthan matrix (continuous phase). This trend was also not significantly prominent in the blends containing hylon VII SNP. Overall, the incorporation of SNP into a gum system with high viscosity such as XAN does not substantially change the elastic nature particularly at low temperatures. However, different behaviours are observed with and without the addition of SNP at elevated temperatures.

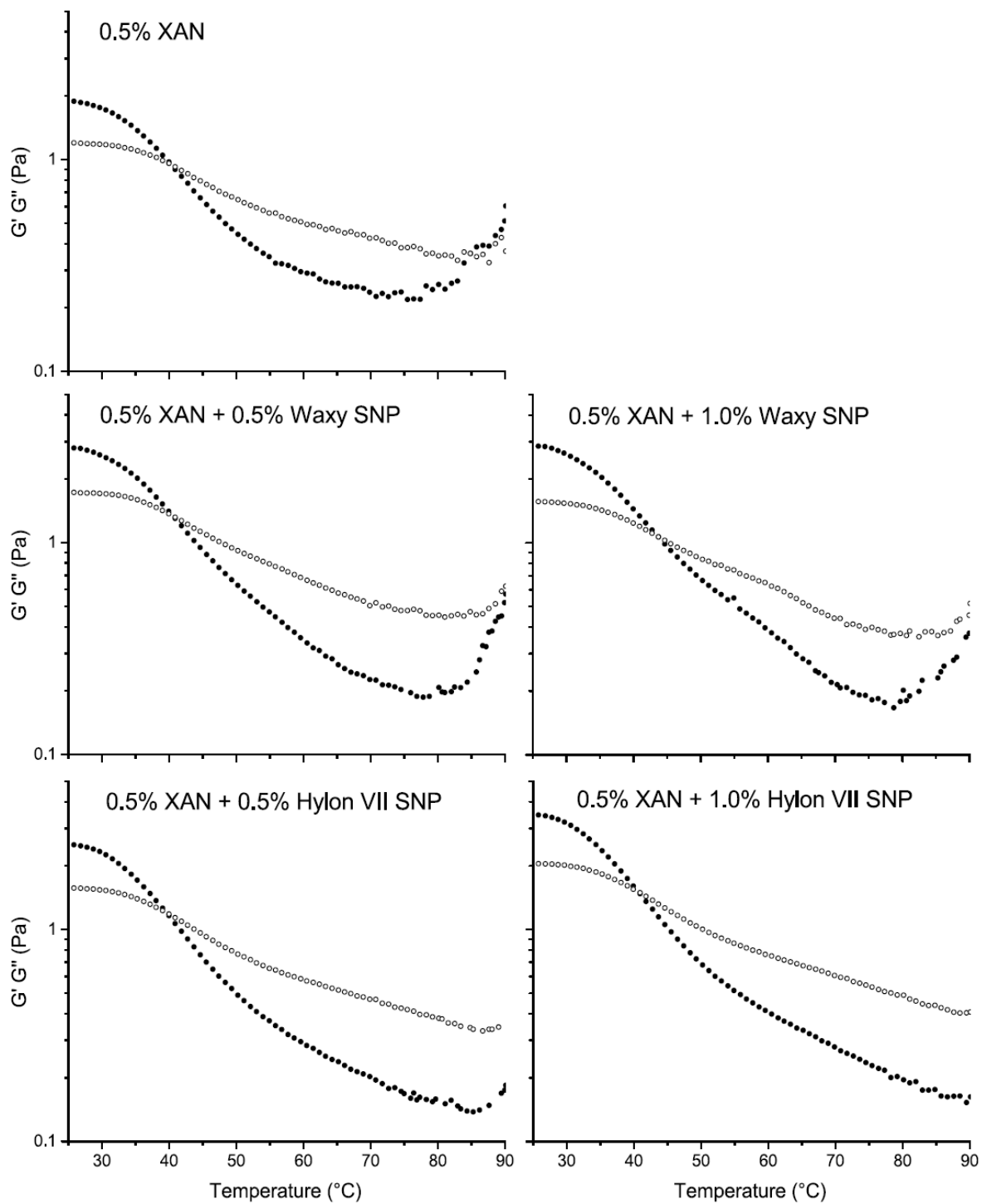


Figure 6.7 Storage modulus (G') and loss modulus (G'') of XAN-SNP blends as a function of temperature. The solid symbols represent G' and the open symbols represent G'' .

6.4. CONCLUSIONS

The SNP source, concentration and thermal stability influenced the viscosity and viscoelastic properties of the gum-SNP blends. The effect of SNP concentration varied with gum type, and was more pronounced in CAR than XAN. With some exceptions, all blends exhibited a shear thinning behaviour. The XAN-SNP blends were more elastic in nature whereas CAR exhibited a more viscous liquid behaviour. The viscoelastic properties as a function of frequency and temperature were substantially different for the CAR-SNP and XAN-SNP blends. During heating, the CAR-SNP blends exhibited a thermal gelation and the gel transition temperature differed with SNP concentration. On the contrary, the gel network of the XAN-SNP blends had a melting transition with increasing temperatures. In the presence of SNP, particularly at high concentrations of hylon VII, the blends showed a strong viscoelastic stability as a function of increasing temperatures. This was attributed to the greater thermal stability of hylon VII SNP in comparison to waxy SNP. This research represents a fundamental contribution to food science since it demonstrates a potential application of SNP as a texture modifier in food systems containing anionic gums. Further research is warranted to precisely understand the nature of molecular interactions that are taking place between SNP and the gums at both room and elevated temperatures.

CHAPTER 7 General conclusions

7.1. SUMMARY AND SIGNIFICANCE OF RESEARCH

Starch nanoparticles (SNP) represent a potential natural and environmentally friendly nanomaterial to be used in food and non-food applications. The acid hydrolysis process has been widely used for SNP production; however, shortcomings like high cost, low SNP yield, long treatment times and the complexities related to the acid handling and recycling have triggered efforts to produce SNP using other non-chemical techniques. To date, SNP from waxy maize have been subjected to intense research related to their isolation, characterization and applications especially in polymer nanocomposites and bioplastics. However, the use of non-waxy amylose containing (>20% amylose content) starches as the raw material for SNP extraction has received little attention and thus presents a research opportunity.

The present thesis addresses some of the research gaps on the use of non-waxy starches for SNP production through acid hydrolysis, and demonstrates their novel characteristics in comparison to waxy maize starch. Overall, this research demonstrated that the physicochemical properties of SNP can vary according to: 1) the starch source, 2) amylose content, 3) crystalline type, 4) morphology, 5) particle size and 6) thermal stability. The above findings confirmed there is a strong relationship between the structure and function of SNP, in particular in amylose containing starches such as maize, wheat, oat, barley and potato. Thus, selecting the raw starch material and the isolation protocol can be used to control the functionality of SNP for different food and non-food applications. With regard to the starch granule structure, this study indicated the presence of a wide variability between the blocklets (nanoscale building blocks) of different

starch granules. Subsequently, the presence and role of amylose and amylopectin within the crystalline and amorphous regions of A- and B-type crystallites was established.

In Chapter 3, SNP from maize starches of varying amylose content were obtained by acid hydrolysis. The isolation process was modified for the different starches according to the following observations. During the washing cycles, non-waxy starches (normal, hylon V and hylon VII) had suspended nanoparticles in the water washings, which was not evident in waxy maize. SEM images revealed the presence of SNP in the water-washed acid-resistant starch residue of waxy maize, whereas in non-waxy starches, the SNP appeared in the water washings used in the removal of excess acid from the acid-resistant starch residues. Variations in the amylose content among native starches influenced the yield, morphology and crystalline properties of SNP. These results were used to develop a model explaining the principle behind the release of SNP (individual blocklets) from the native starch granular structure as well as the formation of SNP through the recrystallization of depolymerized short chain amylose during the acid hydrolysis treatment of amylose containing (non-waxy) starches. The presence of discrete nanoparticles helped support the blocklet model as a level of granule organization proposed by Gallant et al. (1997) and Baldwin et al. (1998).

The molecular size distribution and amylase resistance of the SNP isolated and characterized in Chapter 3 were further investigated in Chapter 4. The weight average molecular weight (M_w) and linear chain length distribution were determined by high performance size exclusion chromatography (HPSEC) and high performance anion-exchange chromatography (HPAEC), respectively. The chromatography elution profiles, molecular size and chain length distribution of the SNP showed significant variations in the molecular composition of SNP

prepared from waxy and non-waxy starches. The results from this study provided fundamental information with regard to the amylose involvement in A- and B- type crystalline structures of native starch. The molecular characteristics before and after isoamylase debranching, and the amylose resistance of high amylose maize SNP confirmed the presence of co-crystallized amylose molecules in the crystalline lamellae of B-type starches or as retrograded amylose crystal possibly in the form of spherulites. SNP from waxy and normal (A-type) starches were composed of short branched amylopectin chains, whereas those from high amylose (B-type) starches had both low M_w linear chains and short branched amylopectin chains.

Following the in depth investigation on maize SNP discussed previously, SNP were isolated from regular starches from other botanical origins (wheat, oat, barley and potato) showing different crystalline types (Chapter 5). Variations in the morphology, particle size distribution, concentration and thermal stability between the SNP influenced their aqueous rheological properties. All SNP showed low thermal stability at temperatures above 60°C, possibly due to amylopectin crystallite melting in excess water. Suspensions of 1% SNP exhibited a thin liquid behaviour similar to water, while at 5% the SNP suspensions formed a thick paste that demonstrated a viscosity profile similar to that of lyotropic liquid crystal polymers like cellulose nanocrystals. The viscosity and viscoelastic behaviour as a function of shear, frequency and temperature significantly varied among the starch sources. A schematic diagram predicting the composition of the continuous and dispersed phases in SNP suspensions of amylose containing starches before and after heating was established. Before heating, the SNP (amylopectin blocklets and recrystallized short chain amylose) and water molecules interact at their surface through hydrogen bonds forming a stable gel network. During and after heating, some SNP may

undergo swelling and solubilization leading to a thinner, more unstable network composed of depolymerized short linear and branched chains, small heat resistant amylopectin SNP and recrystallized short chain amylose (nano-spherulites). Based on the rheological variability between the different SNP, correctly selecting the starch source is suggested to achieve the desirable rheological properties particularly in applications such as thickening and texture modification.

Although the use of SNP in food products has not been widely explored due to the lack of safety and risk assessment research, their physicochemical properties make them promising candidates as thickening, bulking and texturizing ingredients. In the food industry, gums and hydrocolloids are commonly used as texture modifiers. In Chapter 6, the rheological behaviours of waxy and high amylose maize SNP and their blends with some commercial food gums (λ -carrageenan and xanthan) were investigated. The starch source, concentration and thermal stability of the SNP influenced the viscosity and viscoelastic properties of the gum-SNP blends, in particular in the low elasticity sample such as λ -carrageenan. However, when these were incorporated into a high elasticity sample such as xanthan gum, their effect was minimal. SNP are insoluble in water; however, during heating they can undergo swelling and solubilization. In maize starches, the thermal stability of SNP positively correlates to the amylose content and the crystalline type (B-type) of the native starches. The blends containing high concentrations of high amylose maize SNP showed high viscoelastic stability as a function of increasing temperatures from 25 to 90°C possibly due to the higher thermal stability of those compared to waxy maize.

7.2. RECOMMENDATIONS FOR FUTURE WORK

More research is warranted in order to make the isolation of SNP commercially appealing. With respect to acid hydrolysis, minimizing the processing time, improving the yield to more than 15%, and reducing the acid waste and water utilization are needed to make this process economically feasible at a large scale. Since acid selectively hydrolyzes the amorphous material in native starch, increasing the crystalline content prior to isolation would improve the SNP yield. This may be achieved by incorporating a pre-treatment with annealing or heat moisture treatment (HMT). Annealing and HMT have been shown to increase the crystallinity in different starch types and promote crystal growth and stability (Hoover and Vasanthan 1994b; Tester and Debon 2000; Hoover 2010). Annealing may also reduce the amount of hydrolysis time because it can promote pores on the granules surface (Rocha et al. 2012), which may facilitate the diffusion of acid to the interior of the granule. Furthermore, in order to develop food friendly SNP, other acid alternatives which are less corrosive than sulfuric acid and more label friendly (acetic, lactic, citric), should be investigated. A possible drawback to this would be the absence of sulfonate ester groups, which provide excellent suspension stability to the current SNP. Additionally, if SNP are to be produced at a large scale, the industry would benefit from producing SNP from locally available grains to reduce costs and promote sustainability. For example in Canada, SNP could be obtained from pulse starches, especially the low value broken grains not utilized in the food industry. Finally, in the area of polymer nanocomposites, the use of chemical modifications including grafting and cross-linking have been investigated to improve the compatibility of SNP with other materials. A similar approach to this can be used to modify the surface reactive groups in SNP to promote or inhibit intermolecular interactions with different food ingredients.

REFERENCES

Angellier-Coussy, H., Putaux, J. L., Molina-Boisseau, S., Dufresne, A., Bertoft, E. and Perez, S. 2009. The molecular structure of waxy maize starch nanocrystals. *Carbohydr. Res.* 344:1558-66.

Angellier, H., Choisnard, L., Molina-Boisseau, S., Ozil, P. and Dufresne, A. 2004. Optimization of the preparation of aqueous suspensions of waxy maize starch nanocrystals using a response surface methodology. *Biomacromolecules* 5:1545-1551.

Angellier, H., Molina-Boisseau, S. and Dufresne, A. 2005a. Mechanical properties of waxy maize starch nanocrystal reinforced natural rubber. *Macromolecules* 38:9161-9170.

Angellier, H., Molina-Boisseau, S., Lebrun, L. and Dufresne, A. 2005b. Processing and structural properties of waxy maize starch nanocrystals reinforced natural rubber. *Macromolecules* 38:3783-3792.

Atkin, N. J., Abeysekera, R. M., Cheng, S. L. and Robards, A. W. 1998. An experimentally-based predictive model for the separation of amylopectin subunits during starch gelatinization. *Carbohydr. Polym.* 36:173-192.

Baker, A. A., Miles, M. J. and Helbert, W. 2001. Internal structure of the starch granule revealed by afm. *Carbohydr. Res.* 330:249-256.

Baldwin, P. M., Adler, J., Davies, M. C. and Melia, C. D. 1998. High resolution imaging of starch granule surfaces by atomic force microscopy. *J. Cereal Sci.* 27:255-265.

BeMiller, J. N. 2011. Pasting, paste, and gel properties of starch–hydrocolloid combinations. *Carbohydr. Polym.* 86:386-423.

Bertoft, E. 2004a. Lintnerization of two amylose-free starches of a- and b-crystalline types, respectively. *Starch/Stärke* 56:167-180.

Bertoft, E. 2004b. On the nature of categories of chains in amylopectin and their connection to the super helix model. *Carbohydr. Polym.* 57:211-224.

Bertoft, E. 2007. Composition of clusters and their arrangement in potato amylopectin. *Carbohydr. Polym.* 68:433-446.

Bertoft, E., Qin, Z. and Manelius, R. 1993. Studies on the structure of pea starches .4. Intermediate material of wrinkled pea starch. *Starch/Stärke* 45:420-425.

Biliaderis, C., Grant, D. and Vose, J. 1981. Structural characterization of legume starches. II. Studies on acid-treated starches. *Cereal Chem* 58:502-7.

Bogracheva, T. Y., Morris, V. J., Ring, S. G. and Hedley, C. L. 1998. The granular structure of c-type pea starch and its role in gelatinization. *Biopolymers* 45:323-332.

Boluk, Y., Lahiji, R., Zhao, L. and McDermott, M. T. 2011. Suspension viscosities and shape parameter of cellulose nanocrystals (cnc). *Colloids Surf. A.* 377:297-303.

Bouwmeester, H., Brandhoff, P., Marvin, H. J. P., Weigel, S. and Peters, R. J. B. 2014. State of the safety assessment and current use of nanomaterials in food and food production. *Trends Food Sci. Tech.* 40:200-210.

Cai, L. and Shi, Y.C. 2013. Self-assembly of short linear chains to a- and b-type starch spherulites and their enzymatic digestibility. *J. Agric. Food Chem.* 61:10787-10797.

Campo, V. L., Kawano, D. F., Silva Jr, D. B. d. and Carvalho, I. 2009. Carrageenans: Biological properties, chemical modifications and structural analysis – a review. *Carbohydr. Polym.* 77:167-180.

Cheetham, N. W. H. and Tao, L. P. 1997. The effects of amylose content on the molecular size of amylose, and on the distribution of amylopectin chain length in maize starches. *Carbohydr. Polym.* 33:251-261.

Chen, Y., Cao, X., Chang, P. R. and Huneault, M. A. 2008. Comparative study on the films of poly(vinyl alcohol)/pea starch nanocrystals and poly(vinyl alcohol)/native pea starch. *Carbohydr. Polym.* 73:8-17.

Choi, H. M. and Yoo, B. 2009. Steady and dynamic shear rheology of sweet potato starch–xanthan gum mixtures. *Food Chem.* 116:638-643.

Chung, H.-J., Min, D., Kim, J.-Y. and Lim, S.-T. 2007. Effect of minor addition of xanthan on cross-linking of rice starches by dry heating with phosphate salts. *J. Appl. Polym. Sci.* 105:2280-2286.

de Rodriguez, N. L. G., Thielemans, W. and Dufresne, A. 2006. Sisal cellulose whiskers reinforced polyvinyl acetate nanocomposites. *Cellulose* 13:261-270.

Doehlert, D. C. and Simsek, S. 2012. Variation in β -glucan fine structure, extractability, and flour slurry viscosity in oats due to genotype and environment. *Cereal Chem.* 89:242-246.

- Ehrenbergerová, J., Březinová Belcredi, N., Psota, V., Hrstková, P., Cerkal, R. and Newman, C. W. 2008. Changes caused by genotype and environmental conditions in beta-glucan content of spring barley for dietetically beneficial human nutrition. *Plant Foods Hum. Nutr.* 63:111-117.
- Evers, T. and Millar, S. 2002. Cereal grain structure and development: Some implications for quality. *J. Cereal Sci.* 36:261-284.
- French, D. 1984. Organization of starch granules. *Starch: Chemistry and technology* 2:183-247.
- Gallant, D. J., Bouchet, B. and Baldwin, P. M. 1997. Microscopy of starch: Evidence of a new level of granule organization. *Carbohydr. Polym.* 32:177-191.
- Gao, J., Vasanthan, T. and Hoover, R. 2009. Isolation and characterization of high-purity starch isolates from regular, waxy, and high-amylose hulless barley grains. *Cereal Chem.* 86:157-163.
- Gérard, C., Colonna, P., Buléon, A. and Planchot, V. 2002. Order in maize mutant starches revealed by mild acid hydrolysis. *Carbohydr. Polym.* 48:131-141.
- Ghotra, B. S., Vasanthan, T. and Temelli, F. 2009. Rheological properties of aqueous blends of high purity barley β -glucan with high purity commercial food gums. *Food Chem.* 117:417-425.
- Gidley, M. J. and Bociek, S. M. 1985. Molecular organization in starches: A carbon 13 cp/mas nmr study. *J. Am. Chem. Soc.* 107:7040-7044.
- Gidley, M. J. and Bulpin, P. V. 1989. Aggregation of amylose in aqueous systems - the effect of chain-length on phase-behavior and aggregation kinetics. *Macromolecules* 22:341-346.
- Gunaratne, A. and Hoover, R. 2002. Effect of heat-moisture treatment on the structure and physicochemical properties of tuber and root starches. *Carbohydr. Polym.* 49:425-437.
- Haaj, S. B., Magnin, A., Pétrier, C. and Boufi, S. 2013. Starch nanoparticles formation via high power ultrasonication. *Carbohydr. Polym.* 92:1625-1632.
- Hanashiro, I., Abe, J.-i. and Hizukuri, S. 1996. A periodic distribution of the chain length of amylopectin as revealed by high-performance anion-exchange chromatography. *Carbohydr. Res.* 283:151-159.
- Hizukuri, S. 1986. Polymodal distribution of the chain lengths of amylopectins, and its significance. *Carbohydr. Res.* 147:342-347.

Hizukuri, S. 1996. Starch: Analytical aspects. Pages 347-429 in: A. C. Eliasson, ed. Carbohydrates in Foods. Marcel Dekker, Inc., New York.

Hizukuri, S., Takeda, Y., Yasuda, M. and Suzuki, A. 1981. Multi-branched nature of amylose and the action of debranching enzymes. Carbohydr. Res. 94:205-213.

Hoover, R. 2000. Acid-treated starches. Food Rev. Int. 16:369-392.

Hoover, R. 2010. The impact of heat-moisture treatment on molecular structures and properties of starches isolated from different botanical sources. Crit. Rev. Food Sci. Nutr. 50:835-47.

Hoover, R. and Manuel, H. 1996. Effect of heat—moisture treatment on the structure and physicochemical properties of legume starches. Food Res. Int. 29:731-750.

Hoover, R. and Ratnayake, W. S. 2001. Determination of total amylose content of starch. Pages E:E2:E2.3 in: Current protocols in food analytical chemistry. John Wiley & Sons, Inc.

Hoover, R. and Ratnayake, W. 2002. Starch characteristics of black bean, chick pea, lentil, navy bean and pinto bean cultivars grown in Canada. Food Chem. 78:489-498.

Hoover, R. and Sosulski, F. 1991. Composition, structure, functionality, and chemical modification of legume starches: A review. Can. J. Physiol. Pharmacol. 69:79-92.

Hoover, R. and Vasanthan, T. 1994a. Effect of heat-moisture treatment on the structure and physicochemical properties of cereal, legume, and tuber starches. Carbohydr. Res. 252:33-53.

Hoover, R. and Vasanthan, T. 1994b. The flow properties of native, heat-moisture treated, and annealed starches from wheat, oat, potato and lentil. J. Food Biochem. 18:67-82.

Inouchi, N., Glover, D. and Fuwa, H. 1987. Properties of residual maize starches following acid hydrolysis. Starch/Stärke 39:284-288.

Jane, J. L. and Chen, J. F. 1992. Effect of amylose molecular-size and amylopectin branch chain-length on paste properties of starch. Cereal Chem. 69:60-65.

Jane, J.-L. and Robyt, J. F. 1984. Structure studies of amylose-v complexes and retro-graded amylose by action of alpha amylases, and a new method for preparing amylopectins. Carbohydr. Res. 132:105-118.

Jane, J.-l., Wong, K.-s. and McPherson, A. E. 1997. Branch-structure difference in starches of a- and b-type x-ray patterns revealed by their Naegeli dextrins. Carbohydr. Res. 300:219-227.

Jane, J., Chen, Y. Y., Lee, L. F., McPherson, A. E., Wong, K. S., Radosavljevic, M. and Kasemsuwan, T. 1999. Effects of amylopectin branch chain length and amylose content on the gelatinization and pasting properties of starch. *Cereal Chem.* 76:629-637.

Jansson, P.-e., Kenne, L. and Lindberg, B. 1975. Structure of the extracellular polysaccharide from *Xanthomonas campestris*. *Carbohydr. Res.* 45:275-282.

Jayakody, L. and Hoover, R. 2002. The effect of lintnerization on cereal starch granules. *Food Res. Int.* 35:665-680.

Jenkins, P. J. and Donald, A. M. 1995. The influence of amylose on starch granule structure. *Int. J. Biol. Macromol.* 17:315-321.

Ji, N., Li, X., Qiu, C., Li, G., Sun, Q. and Xiong, L. 2015. Effects of heat moisture treatment on the physicochemical properties of starch nanoparticles. *Carbohydr. Polym.* 117:605-609.

Jiang, B., Liu, C., Zhang, C., Wang, B. and Wang, Z. 2007. The effect of non-symmetric distribution of fiber orientation and aspect ratio on elastic properties of composites. *Compos. Part B: Eng.* 38:24-34.

Jiang, H., Srichuwong, S., Campbell, M. and Jane, J.-I. 2010. Characterization of maize amylose-extender (ae) mutant starches. Part iii: Structures and properties of the naegeli dextrans. *Carbohydr. Polym.* 81:885-891.

Jiang, S., Liu, C., Han, Z., Xiong, L. and Sun, Q. 2016. Evaluation of rheological behavior of starch nanocrystals by acid hydrolysis and starch nanoparticles by self-assembly: A comparative study. *Food Hydrocolloids* 52:914-922.

Jin, Y., Hengl, N., Baup, S., Pignon, F., Gondrexon, N., Sztucki, M., Romdhane, A., Guillet, A. and Aourousseau, M. 2015. Ultrasonic assisted cross-flow ultrafiltration of starch and cellulose nanocrystals suspensions: Characterization at multi-scales. *Carbohydr. Polym.* 124:66-76.

Kasemsuwan, T. and Jane, J. 1994. Location of amylose in normal starch granules .2. Locations of phosphodiester cross-linking revealed by p-31 nuclear-magnetic-resonance. *Cereal Chem.* 71:282-287.

Katzbauer, B. 1998. Properties and applications of xanthan gum. *Polym. Degrad. Stab.* 59:81-84.

Kaur, L., Singh, J., Singh, H. and McCarthy, O. J. 2008. Starch–cassia gum interactions: A microstructure–rheology study. *Food Chem.* 111:1-10.

Kim, H.-S. and Huber, K. C. 2008. Channels within soft wheat starch a- and b-type granules. *J. Cereal Sci.* 48:159-172.

Kim, H.-Y., Han, J.-A., Kweon, D.-K., Park, J.-D. and Lim, S.-T. 2013a. Effect of ultrasonic treatments on nanoparticle preparation of acid-hydrolyzed waxy maize starch. *Carbohydr. Polym.* 93:582-588.

Kim, H.-Y., Lee, J. H., Kim, J.-Y., Lim, W.-J. and Lim, S.-T. 2012. Characterization of nanoparticles prepared by acid hydrolysis of various starches. *Starch/Stärke* 64:367-373.

Kim, H.-Y., Park, D. J., Kim, J.-Y. and Lim, S.-T. 2013b. Preparation of crystalline starch nanoparticles using cold acid hydrolysis and ultrasonication. *Carbohydr. Polym.* 98:295-301.

Kim, H.-Y., Park, S. S. and Lim, S.-T. 2015. Preparation, characterization and utilization of starch nanoparticles. *Colloids Surf. B. Biointerfaces* 126:607-620.

Kim, J. C., Mullan, B. P., Simmins, P. H. and Pluske, J. R. 2003. Variation in the chemical composition of wheats grown in western australia as influenced by variety, growing region, season, and post-harvest storage. *Aust. J. Agric. Res.* 54:541-550.

Koehler, P. and Wieser, H. 2013. Chemistry of cereal grains. Pages 11-45 in: *Handbook on sourdough biotechnology*. Springer, New York.

Kozlov, S. S., Krivandin, A. V., Shatalova, O. V., Noda, T., Bertoft, E., Fornal, J. and Yuryev, V. P. 2007. Structure of starches extracted from near-isogenic wheat lines - part ii. Molecular organization of amylopectin clusters. *J. Therm. Anal. Calorim.* 87:575-584.

Kristo, E. and Biliaderis, C. G. 2007. Physical properties of starch nanocrystal-reinforced pullulan films. *Carbohydr. Polym.* 68:146-158.

Laohaphatanaleart, K., Piyachomkwan, K., Sriroth, K. and Bertoft, E. 2010. The fine structure of cassava starch amylopectin: Part 1: Organization of clusters. *Int. J. Biol. Macromol.* 47:317-324.

Le Corre, D. and Angellier-Coussy, H. 2014. Preparation and application of starch nanoparticles for nanocomposites: A review. *React. Funct. Polym.* 85:97-120.

Le Corre, D., Bras, J. and Dufresne, A. 2010. Starch nanoparticles: A review. *Biomacromolecules* 11:1139-1153.

LeCorre, D., Bras, J. and Dufresne, A. 2011. Influence of botanic origin and amylose content on the morphology of starch nanocrystals. *J. Nanopart. Res.* 13:7193-7208.

LeCorre, D., Bras, J. and Dufresne, A. 2012a. Influence of native starch's properties on starch nanocrystals thermal properties. *Carbohydr. Polym.* 87:658-666.

LeCorre, D., Vahanian, E., Dufresne, A. and Bras, J. 2012b. Enzymatic pretreatment for preparing starch nanocrystals. *Biomacromolecules* 13:132-7.

Li, C., Li, Y., Sun, P. and Yang, C. 2014. Starch nanocrystals as particle stabilisers of oil-in-water emulsions. *J. Sci. Food Agric.* 94:1802-7.

Li, C., Sun, P. and Yang, C. 2012. Emulsion stabilized by starch nanocrystals. *Starch/Stärke* 64:497-502.

Li, L. 2002. Thermal gelation of methylcellulose in water: scaling and thermoreversibility. *Macromolecules* 35:5990-5998.

Lin, N., Huang, J., Chang, P. R., Anderson, D. P. and Yu, J. 2011a. Preparation, modification, and application of starch nanocrystals in nanomaterials: A review. *J. Nanomaterials* 2011:1-13.

Lin, N., Huang, J. and Dufresne, A. 2012. Preparation, properties and applications of polysaccharide nanocrystals in advanced functional nanomaterials: A review. *Nanoscale* 4:3274-94.

Lin, N., Yu, J., Chang, P. R., Li, J. and Huang, J. 2011b. Poly(butylene succinate)-based biocomposites filled with polysaccharide nanocrystals: Structure and properties. *Polymer Composites* 32:472-482.

Lintner, C. J. 1886. Studien über Diastase. *J. Prakt. Chem.* 34:378-394.

Liu, D., Wu, Q., Chen, H. and Chang, P. R. 2009. Transitional properties of starch colloid with particle size reduction from micro-to nanometer. *J. Colloid Interface Sci.* 339:117-124.

Liu, Q. 2005. Understanding starches and their role in foods. *Food carbohydrates: Chemistry, physical properties and applications.* Taylor and Francis Group, Boca Raton, USA.

Lopez-Rubio, A., Flanagan, B. M., Gilbert, E. P. and Gidley, M. J. 2008. A novel approach for calculating starch crystallinity and its correlation with double helix content: A combined xrd and nmr study. *Biopolymers* 89:761-768.

Ma, X., Jian, R., Chang, P. R. and Yu, J. 2008. Fabrication and characterization of citric acid-modified starch nanoparticles/plasticized-starch composites. *Biomacromolecules* 9:3314-3320.

McPherson, A. E. and Jane, J. 1999. Comparison of waxy potato with other root and tuber starches. *Carbohydr. Polym.* 40:57-70.

Mewis, J. and Wagner, N. J. 2009. Current trends in suspension rheology. *J. Non-Newton. Fluid Mech.* 157:147-150.

Mewis, J. and Wagner, N. J. 2012. *Colloidal suspension rheology*. New York : Cambridge University Press, (Chapter 5).

Mihindukulasuriya, S. D. F. and Lim, L. T. 2014. Nanotechnology development in food packaging: A review. *Trends Food Sci. Tech.* 40:149-167.

Milas, M. and Rinaudo, M. 1979. Conformational investigation on the bacterial polysaccharide xanthan. *Carbohydr. Res.* 76:189-196.

Morris, E., Rees, D., Young, G., Walkinshaw, M. and Darke, A. 1977. Order-disorder transition for a bacterial polysaccharide in solution. A role for polysaccharide conformation in recognition between xanthomonas pathogen and its plant host. *J. Mol. Biol.* 110:1-16.

Morrison, W. R. and Laignelet, B. 1983. An improved colorimetric procedure for determining apparent and total amylose in cereal and other starches. *J. Cereal Sci.* 1:9-20.

Morrison, W. R., Tester, R. F., Gidley, M. J. and Karkalas, J. 1993. Resistance to acid-hydrolysis of lipid-complexed amylose and lipid-free amylose in lintnerised waxy and non-waxy barley starches. *Carbohydr. Res.* 245:289-302.

Nagahata, Y., Kobayashi, I., Goto, M., Nakaura, Y. and Inouchi, N. 2013. The formation of resistant starch during acid hydrolysis of high-amylose corn starch. *J. Appl. Glycosci.* 60:123-130.

Nägeli, W. 1874. Beiträge zur näheren Kenntniss der Stärkegruppe. *Justus Liebigs Ann. Chem.* 173:218-227.

Naguleswaran, S., Li, J., Vasanthan, T. and Bressler, D. 2011. Distribution of granule channels, protein, and phospholipid in triticale and corn starches as revealed by confocal laser scanning microscopy. *Cereal Chem.* 88:87-94.

Naguleswaran, S., Vasanthan, T., Hoover, R. and Bressler, D. 2013. The susceptibility of large and small granules of waxy, normal and high-amylose genotypes of barley and corn starches toward amylolysis at sub-gelatinization temperatures. *Food Res. Int.* 51:771-782.

Nakazawa, Y. and Wang, Y.-J. 2003. Acid hydrolysis of native and annealed starches and branch-structure of their naegeli dextrans. *Carbohydr. Res.* 338:2871-2882.

Namazi, H. and Dadkhah, A. 2008. Surface modification of starch nanocrystals through ring-opening polymerization of ϵ -caprolactone and investigation of their microstructures. *J. Appl. Polym. Sci.* 110:2405-2412.

Nasseri, R. and Mohammadi, N. 2014. Starch-based nanocomposites: A comparative performance study of cellulose whiskers and starch nanoparticles. *Carbohydr. Polym.* 106:432-439.

Park, H., Xu, S. and Seetharaman, K. 2011. A novel in situ atomic force microscopy imaging technique to probe surface morphological features of starch granules. *Carbohydr. Res.* 346:847-853.

Perera, C. and Hoover, R. 1999. Influence of hydroxypropylation on retrogradation properties of native, defatted and heat-moisture treated potato starches. *Food Chem.* 64:361-375.

Perera, C., Lu, Z., Sell, J. and Jane, J. 2001. Comparison of physicochemical properties and structures of sugary-2 cornstarch with normal and waxy cultivars. *Cereal Chem.* 78:249-256.

Pérez, S. and Bertoft, E. 2010. The molecular structures of starch components and their contribution to the architecture of starch granules: A comprehensive review. *Starch/Stärke* 62:389-420.

Phillips, G. O. and Williams, P. A. 2009. Carrageenan and furcellaran. Pages 164-185 in: *Handbook of hydrocolloids*. CRC Press, Boca Raton, FL.

Putaux, J. L., Molina-Boisseau, S., Momaur, T. and Dufresne, A. 2003. Platelet nanocrystals resulting from the disruption of waxy maize starch granules by acid hydrolysis. *Biomacromolecules* 4:1198-1202.

Rånby, B. G. and Ribí, E. 1950. Über den feinaufbau der zellulose. *Experientia* 6:12-14.

Redaelli, R., Del Frate, V., Bellato, S., Terracciano, G., Ciccoritti, R., Germeier, C. U., De Stefanis, E. and Sgrulletta, D. 2013. Genetic and environmental variability in total and soluble β -glucan in european oat genotypes. *J. Cereal Sci.* 57:193-199.

Rees, D., Steele, I. and Williamson, F. 1969. Conformational analysis of polysaccharides. Iii. The relation between stereochemistry and properties of some natural polysaccharide sulfates (1). Pages 261-276 in: *Journal of Polymer Science Part C: Polymer Symposia*. Wiley Online Library.

Ridout, M. J., Parker, M. L., Hedley, C. L., Bogracheva, T. Y. and Morris, V. J. 2003. Atomic force microscopy of pea starch granules: Granule architecture of wild-type parent, r and rb single mutants, and the rrb double mutant. *Carbohydr. Res.* 338:2135-2147.

Ring, S.G., Miles, M.J., Morris, V.J., Turner, R. and Colonna, P. 1987. Spherulitic crystallization of short chain amylose. *Int. J. Biol. Macromol.* 9:158-160.

Robin, J. P., Mercier, C., Duprat, F., Charbonniere, R. and Guilbot, A. 1975. Lintnerized starches - chromatographic and enzymatic studies of insoluble residues from acid-hydrolysis of various cereal starches, particularly waxy maize starch. *Starch/Stärke* 27:36-45.

Rocha, T. S., Felizardo, S. G., Jane, J.-I. and Franco, C. M. L. 2012. Effect of annealing on the semicrystalline structure of normal and waxy corn starches. *Food Hydrocolloids* 29:93-99.

Romdhane, A., Aourousseau, M., Guillet, A. and Mauret, E. 2015. Effect of ph and ionic strength on the electrical charge and particle size distribution of starch nanocrystal suspensions. *Starch/Stärke* 67:319-327.

Rossi, M., Cubadda, F., Dini, L., Terranova, M. L., Aureli, F., Sorbo, A. and Passeri, D. 2014. Scientific basis of nanotechnology, implications for the food sector and future trends. *Trends Food Sci. Tech.* 40:127-148.

Rubio-Hernandez, F. J., Carrique, F. and Ruiz-Reina, E. 2004. The primary electroviscous effect in colloidal suspensions. *Adv. Colloid Interface Sci.* 107:51-60.

Saibene, D. and Seetharaman, K. 2010. Amylose involvement in the amylopectin clusters of potato starch granules. *Carbohydr. Polym.* 82:376-383.

Santander-Ortega, M. J., Stauner, T., Loretz, B., Ortega-Vinuesa, J. L., Bastos-González, D., Wenz, G., Schaefer, U. F. and Lehr, C. M. 2010. Nanoparticles made from novel starch derivatives for transdermal drug delivery. *J. Control Release* 141:85-92.

Shafiei-Sabet, S., Hamad, W. Y. and Hatzikiriakos, S. G. 2012. Rheology of nanocrystalline cellulose aqueous suspensions. *Langmuir* 28:17124-17133.

Shi, A.-m., Li, D., Wang, L.-j. and Adhikari, B. 2012a. The effect of nacl on the rheological properties of suspension containing spray dried starch nanoparticles. *Carbohydr. Polym.* 90:1530-1537.

Shi, A.-m., Li, D., Wang, L.-j. and Adhikari, B. 2012b. Rheological properties of suspensions containing cross-linked starch nanoparticles prepared by spray and vacuum freeze drying methods. *Carbohydr. Polym.* 90:1732-1738.

Shi, A.-m., Wang, L.-j., Li, D. and Adhikari, B. 2013. Suspensions of vacuum-freeze dried starch nanoparticles: Influence of nacl on their rheological properties. *Carbohydr. Polym.* 94:782-790.

Singh, V. and Ali, S. Z. 2008. Properties of starches modified by different acids. *Int. J. Food Prop.* 11:495-507.

Song, D., Thio, Y. S. and Deng, Y. 2011. Starch nanoparticle formation via reactive extrusion and related mechanism study. *Carbohydr. Polym.* 85:208-214.

Song, S. W., Wang, C., Pan, Z. L. and Wang, X. F. 2008. Preparation and characterization of amphiphilic starch nanocrystals. *J. Appl. Polym. Sci.* 107:418-422.

Srichuwong, S., Isono, N., Mishima, T. and Hisamatsu, M. 2005. Structure of lintnerized starch is related to x-ray diffraction pattern and susceptibility to acid and enzyme hydrolysis of starch granules. *Int. J. Biol. Macromol.* 37:115-121.

Srinivasarao, M. 1995. Rheology and rheo-optics of polymer liquid-crystals. *Int. J. Mod. Phys. B* 9:2515-2572.

Sun, Q., Li, G., Dai, L., Ji, N. and Xiong, L. 2014. Green preparation and characterisation of waxy maize starch nanoparticles through enzymolysis and recrystallisation. *Food Chem.* 162:223-228.

Szymonska, J. and Krok, F. 2003. Potato starch granule nanostructure studied by high resolution non-contact afm. *Int. J. Biol. Macromol.* 33:1-7.

Takeda, C., Takeda, Y. and Hizukuri, S. 1993. Structure of the amylopectin fraction of amylomaize. *Carbohydr. Res.* 246:273-281.

Takeda, Y., Shitaozono, T. and Hizukuri, S. 1988. Molecular structure of corn starch. *Starch/Stärke* 40:51-54.

Tan, Y., Xu, K., Li, L., Liu, C., Song, C. and Wang, P. 2009. Fabrication of size-controlled starch-based nanospheres by nanoprecipitation. *ACS Appl. Mater. Interfaces* 1:956-959.

Tester, R. F. 1997. Starch: The polysaccharide fractions. In: *Starch structure and functionality*. P.J. Frazier, A.M. Donald, and P. Richmond eds. p. 163-171. The royal society of chemistry, Cambridge.

- Tester, R. F. and Debon, S. J. 2000. Annealing of starch—a review. *Int. J. Biol. Macromol.* 27:1-12.
- Tester, R. F., Karkalas, J. and Qi, X. 2004. Starch - composition, fine structure and architecture. *J. Cereal Sci.* 39:151-165.
- Tzoumaki, M. V., Moschakis, T. and Biliaderis, C. G. 2013. Effect of soluble polysaccharides addition on rheological properties and microstructure of chitin nanocrystal aqueous dispersions. *Carbohydr. Polym.* 95:324-331.
- Vamadevan, V. and Bertoft, E. 2015. Structure-function relationships of starch components. *Starch/Stärke* 67:55-68.
- Vamadevan, V., Hoover, R., Bertoft, E. and Seetharaman, K. 2014. Hydrothermal treatment and iodine binding provide insights into the organization of glucan chains within the semi-crystalline lamellae of corn starch granules. *Biopolymers* 101:871-885.
- Van de Velde, F., Knutsen, S. H., Usov, A. I., Rollema, H. S. and Cerezo, A. S. 2002. 1h and 13c high resolution nmr spectroscopy of carrageenans: Application in research and industry. *Trends Food Sci. Tech.* 13:73-92.
- Vasanthan, T. and Bhatt, R. 1996. Physicochemical properties of small-and large-granule starches of waxy, regular, and high-amylose barleys. *Cereal Chem.* 73:199-207.
- Waduge, R. N., Kalinga, D. N., Bertoft, E. and Seetharaman, K. 2014. Molecular structure and organization of starch granules from developing wheat endosperm. *Cereal Chem.* 91:578-586.
- Wang, C. H. and Damodaran, S. 1990. Thermal gelation of globular proteins: weight-average molecular weight dependence of gel strength. *J. Agric. Food. Chem.* 38:1157-1164.
- Wang, S., Blazek, J., Gilbert, E. and Copeland, L. 2012. New insights on the mechanism of acid degradation of pea starch. *Carbohydr. Polym.* 87:1941-1949.
- Wang, S., Jin, F. and Yu, J. 2013. Pea starch annealing: New insights. *Food Bioprocess Tech.* 6:3564-3575.
- Wang, S. J. and Copeland, L. 2015. Effect of acid hydrolysis on starch structure and functionality: A review. *Crit. Rev. Food Sci. Nutr.* 55:1079-1095.
- Wang, Y.-J., Truong, V.-D. and Wang, L. 2003. Structures and rheological properties of corn starch as affected by acid hydrolysis. *Carbohydr. Polym.* 52:327-333.

Warriner, K., Reddy, S. M., Namvar, A. and Neethirajan, S. 2014. Developments in nanoparticles for use in biosensors to assess food safety and quality. *Trends Food Sci. Tech.* 40:183-199.

Watanabe, T. and French, D. 1980. Structural features of naegeli amylopectin as indicated by enzymic degradation. *Carbohydr. Res.* 84:115-123.

Weber, F. H., Clerici, M. T. P., Collares-Queiroz, F. P. and Chang, Y. K. 2009. Interaction of guar and xanthan gums with starch in the gels obtained from normal, waxy and high-amylose corn starches. *Starch/Stärke* 61:28-34.

Wei, B., Hu, X., Li, H., Wu, C., Xu, X., Jin, Z. and Tian, Y. 2014a. Effect of pHs on dispersity of maize starch nanocrystals in aqueous medium. *Food Hydrocolloids* 36:369-373.

Wei, B., Xu, X., Jin, Z. and Tian, Y. 2014b. Surface chemical compositions and dispersity of starch nanocrystals formed by sulfuric and hydrochloric acid hydrolysis. *PloS one* 9:e86024.

Weng, L., Zhang, L., Ruan, D., Shi, L. and Xu, J. 2004. Thermal gelation of cellulose in a NaOH/thiourea aqueous solution. *Langmuir* 20:2086-2093.

Xu, Y., Sismour, E. N., Grizzard, C., Thomas, M., Pestov, D., Huba, Z., Wang, T. and Bhardwaj, H. L. 2014. Morphological, structural, and thermal properties of starch nanocrystals affected by different botanic origins¹. *Cereal Chem.* 91:383-388.

Yu, J., Ai, F., Dufresne, A., Gao, S., Huang, J. and Chang, P. R. 2008. Structure and mechanical properties of poly(lactic acid) filled with (starch nanocrystal)-graft-poly(ϵ -caprolactone). *Macromol. Mater. Eng.* 293:763-770.

Yuan, R. C., Thompson, D. B. and Boyer, C. D. 1993. Fine-structure of amylopectin in relation to gelatinization and retrogradation behavior of maize starches from 3 wx-containing genotypes in 2 inbred lines. *Cereal Chem.* 70:81-89.

Zheng, H., Ai, F., Chang, P. R., Huang, J. and Dufresne, A. 2009. Structure and properties of starch nanocrystal-reinforced soy protein plastics. *Polymer Composites* 30:474-480.

Zhu, J., Li, L., Chen, L. and Li, X. 2012. Study on supramolecular structural changes of ultrasonic treated potato starch granules. *Food Hydrocolloids* 29:116-122.

APPENDIX I

β -Glucan content, viscosity and solubility of Canadian grown oat as influenced by cultivar and growing location

INTRODUCTION

Oat (*Avena sativa* L.) is a cereal grain widely used for human and animal nutrition. Whole oat groats contain high amounts of dietary fibre, especially soluble dietary fibre (mainly β -glucan), which can form a viscous solution in water and has positive implications in human health. Many studies have shown that oat β -glucan can lower blood cholesterol levels and therefore decrease the risk of cardiovascular diseases (Anderson et al. 1990; Queenan et al. 2007; Wolever et al. 2010), lower postprandial glucose and insulin response to prevent diabetes (Wood et al. 2000; Tiwari and Cummins 2011) and assist in weight control by increasing post meal satiety (Daou and Zhang 2012). In the past two decades, oat and barley have received a vast amount of attention from the food and health industries due to their high contents of β -glucan, up to 7% w/w and 10% w/w, respectively. Cereal β -glucan is a non-starch polysaccharide comprised of D-glucopyranosyl units linked by β -(1,3) and β -(1,4) linkages. It is a molecule composed of cellotriosyl (DP3) and cellotetraosyl (DP4) segments (Staudte et al. 1983; Lazaridou and Biliaderis 2007).

*A version of this chapter has been published in *Canadian Journal of Plant Science*, 2016, 96:183-196.

Since the approval of health claims by the Food and Drug Administration (FDA) of USA, Health Canada, and the European Food Safety Authority (EFSA) for oat β -glucan for reducing the risk of cardiovascular diseases (Food and Drug Administration 1997; Health Canada 2010; European Food Safety Authority 2011), the demand for this grain in food processing has been fast growing. The exact mechanisms of how β -glucan influences human health are not very well understood. It has been suggested that cereal β -glucans can decrease the absorption of cholesterol and reduce starch digestion by increasing the viscosity of intestinal contents, thus delaying nutrient absorption and enzyme hydrolysis (Lazaridou and Biliaderis 2007; Wang and Ellis 2014). Therefore, the β -glucan content and its physicochemical properties such as solubility and viscosity are important parameters in providing human health benefits, and in determining its impact on the processing and sensory properties of the foods.

The physicochemical properties of oat β -glucan are primarily influenced by its molecular weight and concentration (Johansson et al. 2000; Lazaridou and Biliaderis 2007; Wang and Ellis 2014). Additionally, these characteristics differ between oat genotypes and are affected by the environmental growing conditions (Autio et al. 1992; Tiwari and Cummins 2009; Doehlert and Simsek 2012; Redaelli et al. 2013). Recently, Doehlert and Simsek (2012) investigated the β -glucan fine structure and viscosity of 16 oat genotypes grown in different environments and found significant genotypic variation in the slurry viscosity and an environmental influence on the contents of DP3 (degree of polymerization) and DP4 oligosaccharide fragments. The authors suggested that variations in temperature and water availability of growing locations may impact the mechanism of β -glucan synthesis and therefore alter its structural properties. Variations in the oat grain composition and physicochemical properties challenge the oat industry by

imparting considerable inconsistency in the quality of oat flour supplied to various food processors.

The objective of this study was to investigate how the cultivar, growing location and year would influence the β -glucan content of Canadian oat, as well as its solubility and viscosity. The outcome of this study is expected to facilitate a blending strategy in order to produce oat flour for a desired food application (high β -glucan or low β -beta-glucan). This information would be useful to oat producers, processors and the food industry utilizing oat as ingredient in a variety of products.

MATERIALS AND METHODS

Materials

The oat growing trials were coordinated by Viterra Inc. Canada. Eight oat cultivars (CDC Dancer, Derby, Furlong, HiFi, Jordan, Leggett, Morgan, and SW Betania) were grown in 20 locations within four western Canadian Provinces (Alberta, British Columbia, Manitoba and Saskatchewan) in 2008, 2009 and 2010 (Table 1). There were eight growing locations in Alberta/British Columbia (Beiseker, Dawson Creek, Donelly, Killam, Nampa, Neapolis, Sexsmith, and St. Albert), five in Manitoba (Brandon, Portage, Rosebank, Souris, and Winnipeg) and seven in Saskatchewan (Lake Lenore, Rosthern, Saskatoon, Valparaiso, Watrous, Wilkie, and Yorkton) (Table 1). Due to adverse climatic conditions, some field plots (cultivar*location*year) were either not grown or not successfully harvested. Missing data for certain years and locations were reported, however, all cultivars were grown at least once in each location.

Table 1. Growing locations for oat trials over three years^a.

2008	2009	2010
AB: Beiseker, Donnelly, Killam, Neapolis, Sexsmith	AB: Killam, Neapolis BC: Dawson Creek	AB: Killam, Nampa, Neapolis, St. Albert
MB: Brandon, Portage, Rosebank, Souris	MB: Brandon, Rosebank, Winnipeg SK: Lake Lenore, Saskatoon,	MB: Brandon, Winnipeg
SK: Lake Lenore, Rosthern, Valparaiso, Wilkie, Yorkton	Watrous, Yorkton	SK: Lake Lenore, Watrous, Yorkton

^aAB: Alberta, BC: British Columbia, MB: Manitoba, SK: Saskatchewan; in each location eight oat cultivars (CDC Dancer, Derby, Furlong, HiFi, Jordan, Leggett, Morgan, and SW Betania) were grown.

The geographical and climate information (mean daily temperature and mean total precipitation (mm) of growing season) are presented in Table 2. The most northern location was Nampa, Alberta (56°02'N), while the most western location was Dawson Creek, British Columbia (120°14'W), the most southern location was Rosebank, Manitoba (49°26'N), and the most eastern location was Winnipeg, Manitoba (97°1'W). The mean daily temperatures were between 11.6°C and 15.5°C while the precipitation ranged from 91- 428 mm for the growing season (Table 2). The temperature and precipitation are the mean values for the experimental years.

The oat seeds were de-hulled with an impact huller (locally fabricated), aspirated to remove most of the hulls, and further manually picked to obtain hull-free oat groat samples. Heat treatment was applied to the de-hulled oat groats. The methodology for heat treatment was established in the lab to simulate an industrial oat stabilization process (kilning). Groats (300 g) were steamed in a kitchen vegetable steamer with a lid by placing the groats on the metal shelf (layered on a cheese cloth) over boiling water for 20 min. After steaming, the samples were dried in a forced air oven at 78°C for 1 h, 63°C for 30 min and 50°C for overnight (simulating industrial process). After such a heat treatment of the groats, residual β -glucanase activity was found to be negative. The oat groats were then ground using the Udy cyclone sample mill (UDY Lab Equipment and Supplies, Ft. Collins, CO, USA) equipped with a 0.5 mm screen.

Table 2. Geographical details and climate information of the oat growing locations^a.

Growing Location	Longitude/Latitude	Mean daily temperature of 3 growing seasons (°C)	Precipitation (mm) for 3 growing seasons
Beiseker (AB)	51°23'N/113°32'W	13.6	172
Dawson Creek (BC)	55°46'N/120°14'W	12.8	n/a
Donnelly (AB)	55°43'N/117°06' W	13.7	137
Killam (AB)	52°47'N/111° 51' W	13.1	284
Nampa (AB)	56°02'N/117°08'W	12.5	151
Neapolis (AB)	51°38'N/113°53'W	12.1	254
Sexsmith (AB)	55°33'N/118°47'W	11.6	91
St. Albert (AB)	53°38'N/113°38'W	13.9	306
Brandon (MB)	49°50'N/99°57'W	14.5	380
Portage (MB)	49°58'N/98°18'W	14.9	358
Rosebank (MB)	49°26'N/98°7'W	15.0	319
Souris (MB)	49°38'N/100°15'W	14.5	380
Winnipeg (MB)	49°54'N/97°14'W	15.5	428
Lake Lenore (SK)	52° 24'N/104° 59'W	13.9	312
Rosthern (SK)	52°41'N/106°20'W	14.7	134
Saskatoon (SK)	52°10'N/106°41'W	14.2	236
Valparaiso (SK)	52°51'N/104°11'W	n/a	n/a
Watrous (SK)	51°40'N/105°28'W	13.8	278
Wilkie (SK)	52°25'N/108°42'W	13.9	217
Yorkton (SK)	51°16'N/102° 28'W	14.2	338

^aGrowing season included May, June, July, and August.

n/a: data not available. The temperature and precipitation were the mean values for the experimental years for that particular growing location.

Chemical composition

Moisture and ash contents were determined according to the AACC method 44-15A and 08-01 (AACC International 2004), respectively. Nitrogen content was determined using a Carbon/Nitrogen determination system (TruSpec[®] CN, Leco Corporation, St. Joseph, MI, USA). The protein content was calculated by multiplying the % nitrogen by a factor of 6.25. Fat content was determined by the Goldfish extraction AACC method 30-25, with petroleum ether as the solvent (AACC International 2004). Starch and β -glucan contents were determined using the total starch assay kit and the mixed-linkage β -glucan assay kit obtained from Megazyme International (Wicklow, Ireland). The contents of soluble dietary fibre (SDF) and insoluble dietary fibre (IDF)

were quantified by the enzymatic gravimetric procedures of AOAC methods 993.19 and 991.42 (AOAC International 1997), respectively, using Megazyme International total dietary fibre kit (Wicklow, Ireland).

Determination of oat β -glucan viscosity and solubility

Viscosity of oat β -glucan in the native flour was determined in duplicate at 0.5% (w/w) β -glucan concentration solubilized in deionized Milli-Q water. The 0.5% (w/w) β -glucan solution was prepared by calculating the amount of sample (g) needed to prepare a 50 g slurry, based on the initial β -glucan concentration (%). The oat flour slurry was heated to 85°C for 1 h with thermostable α -amylase (0.1% v/w), having no β -glucanase side activity (Termamyl 120 L, Novozyme North America, Franklinton, NC, USA). This step was necessary to ensure complete solubilization of β -glucan while hydrolyzing starch to minimize contribution of starch to viscosity. The slurry was then cooled to room temperature and water was added to compensate for evaporative losses during heating. The slurry was centrifuged (10 min, 3000 \times g) and the viscosity was determined at consecutive fixed shear rates of 1.29-129 s⁻¹ using a rheometer (PAAR Physica UDS 200, Glenn Allen, VA, USA) equipped with a Peltier heating system and controlled by US200 v. 2.00 programming. Viscosity tests were performed at 20°C (\pm 0.03°C) using the DG 27 cup and bob geometry with double gap. Sample size was measured by weight (7.05 \pm 0.02 g).

β -Glucan solubility was determined according to the following procedure. Oat flour samples containing 0.5 g β -glucan were mixed with 20 ml deionized Milli-Q water in 50 ml test tubes. The tubes were incubated in a shaking water bath (Memmert, type NB 14, Andreas Hettich GmbH, Tuttlingen, Germany) at 37°C for 1 h and then centrifuged (10 min, 5000 \times g). The

solubilized β -glucan in the supernatant was quantified by the mixed-linkage beta-glucan assay kit. β -Glucan solubility was calculated as the percentage ratio of solubilized β -glucan to the total β -glucan in the flour sample.

Statistical analysis

Two-way ANOVA (analysis of variance) was applied to determine the effects of oat cultivar, growing location and the growing location by cultivar interaction on the parameters investigated. In this analysis, two main factors, growing location, oat cultivar and their interaction, were considered to be fixed, whereas the effect of “year” was considered random due to missing data. Least square means (LSMeans) were determined and the least significant difference (LSD) value was used to identify the significant differences between LSMean for cultivar, growing location and the interaction of cultivar and growing location at a significance level of $p < 0.05$. Statistical analyses were performed with SAS software (v. 9.2, SAS Institute, Cary, NC) using PROC MIXED procedures. Pearson’s correlation coefficients were also calculated to show the association among the grain composition, β -glucan properties and climate information by using PROC CORR procedure in SAS.

RESULTS AND DISCUSSION

Chemical composition and β -glucan content of oat grains

The average composition of oat grains by cultivar, location and the interaction of cultivar and location is presented in Table 3. The β -glucan content of the cultivars ranged between 4 and 6%, with the lowest reported for Derby (4.37%), followed by Furlong (4.59%), CDC Dancer (4.68%) and Morgan (4.71%), then Jordan (5.03%), Leggett (5.25%), SW Betania (5.39%) and the highest

was HiFi (5.82%). The starch contents ranged from 57 to 62%, which followed the opposite trend as that of β -glucan content, the lowest was HiFi (56.8%) and the highest was Derby (61.8%). The protein content ranged from 16 to 19%, where the lowest was for Jordan (16.2%) and the highest for Leggett (18.7%). The fat content ranged between 7 and 9%, with the highest reported for HiFi (9.0%) and the lowest for Morgan (6.9%), which is higher than that found in wheat, barley and corn (Price and Parsons 1975). Leggett and HiFi showed the highest ash content (1.9%) and Derby and Jordan showed the lowest (1.8%). HiFi had the highest SDF content (7.1%) and the highest IDF content (6.6%) whereas, Derby had the lowest SDF and IDF content (5.7% and 5.5%, respectively).

β -glucan content was the lowest for oat from Donnelly (4.59%) and the highest for Rosebank and St. Albert (5.27%). Overall, the β -glucan content varied within a small range (0.67%) for the 20 locations. For all locations, the starch content was in the same range as that reported for the cultivars (Table 3). Winnipeg recorded the highest starch content (62.10%) and Donnelly, recorded the lowest (56.46%). The protein content was also similar to the cultivar 16-19% range, however two locations had values outside this range. Oat grown in Winnipeg had the lowest protein (13.92%) while oat from Nampa had the highest (20.24%). On average, crops grown at Donnelly had the highest crude fat content (9.60%), whereas crops grown at Portage showed the lowest (7.02%). Oat grown at Souris showed the highest ash content (2.18%), and at Nampa showed the lowest (1.34%). For dietary content, oat grown at Nampa gave the highest SDF (7.28%) and Sexsmith gave the lowest (5.81%). Additionally, oat from Sexsmith had the highest IDF (7.80%) and oat from Valparaiso had the lowest (5.12%).

Among the combinations of cultivars and growing locations (the interaction effect), the lowest oat β -glucan content was 3.95% (Derby grown in Neapolis) and the highest was 6.53% (Morgan grown in St. Albert) (Table 3). Derby grown at Winnipeg, showed the highest starch content (65.09%) and HiFi grown at Donnelly, showed the lowest (52.74%). Leggett grown in Nampa had the highest protein content (21.52%), while Jordan grown in Winnipeg had the lowest (12.68%). HiFi grown at Donnelly demonstrated the highest fat content (11.98%) and Morgan grown at Portage demonstrated the lowest (5.51%). Furlong grown at Dawson Creek gave the highest SDF content (8.94%), while the lowest was for Derby grown in Beiseker (4.71%), SW Betania grown in Sexsmith had the highest IDF content (9.13%) and grown in Valparaiso showed the lowest (3.91%).

The β -glucan contents found in this study are in agreement with other reported values (Welch and Lloyd 1989; Autio et al. 1992; Saastamoinen et al. 1992; Redaelli et al. 2013). In a study of 100 oat genotypes grown in the United Kingdom, the β -glucan contents were between 2.8% and 5.5% (Welch and Lloyd 1989). Similarly, the β -glucan contents of thirteen oat cultivars grown in eight locations in Finland were reported as 3.9-6.6% (Saastamoinen et al. 1992). Furthermore, the current findings are consistent with those of Peterson (1991), who found that β -glucan content was affected by the interaction between genotype and environment for 12 oat cultivars grown in nine locations. More recently, Redaelli et al. (2013) also investigated the effects of genotype and environment on total β -glucan content for 11 standard oat cultivars harvested in five locations across Europe and found that all factors, location, genotype and their interaction, had significant effects on the β -glucan content.

Table 3. The chemical composition of oat grain samples (eight cultivars) grown in twenty Canadian Prairie locations^a.

Locations	Cultivar								LSMean (location)
	CD	DB	FL	HF	JD	LG	MG	SB	
<i>β-Glucan (%)</i>									
Beiseker (AB)	4.62	4.47	5.22	5.74	4.92	5.41	4.75	5.24	5.05b-f
Dawson Creek (BC)	5.13	4.52	4.87	5.98	5.67	5.17	4.52	5.71	5.20a-c
Donnelly (AB)	4.15	4.23	4.47	4.96	5.02	4.65	4.47	4.78	4.59h
Killam (AB)	4.75	4.39	4.43	5.82	5.17	5.21	4.57	5.64	5.00d-f
Nampa (AB)	4.52	4.25	5.00	4.91	4.36	5.27	5.56	4.44	4.79gh
Neapolis (AB)	4.57	3.95	4.58	5.62	4.72	5.20	4.78	5.22	4.83g
Sexsmith (AB)	4.36	4.31	4.41	5.39	5.04	5.12	4.33	5.16	4.76gh
St. Albert (AB)	4.92	4.58	5.19	5.51	4.92	5.95	6.53	4.53	5.27ab
Brandon (MB)	4.59	4.37	4.61	6.04	5.38	5.27	4.68	5.74	5.09b-e
Portage (MB)	4.77	4.53	4.51	6.36	5.10	5.53	4.46	5.90	5.14a-d
Rosebank (MB)	4.95	4.65	4.86	6.00	5.52	5.85	4.62	5.75	5.27a
Souris (MB)	4.40	4.28	4.31	5.90	4.92	4.95	4.50	5.73	4.87fg
Winnipeg (MB)	4.63	4.49	4.43	6.46	4.90	5.09	4.26	5.47	4.97d-g
Lake Lenore (SK)	4.74	4.23	4.41	5.98	4.79	5.01	4.60	5.30	4.88fg
Rosthern (SK)	4.78	4.40	4.40	5.82	5.21	5.48	4.74	5.62	5.06b-f
Saskatoon (SK)	5.30	4.83	4.60	6.33	4.77	5.19	4.32	5.83	5.15a-d
Valparaiso (SK)	4.48	4.14	4.37	5.85	4.96	5.55	4.37	5.09	4.85fg
Watrous (SK)	4.71	4.23	4.29	6.00	4.88	5.08	4.39	5.81	4.92fg
Wilkie (SK)	4.51	4.07	4.29	6.23	5.19	4.69	4.47	5.71	4.89e-g
Yorkton (SK)	4.62	4.42	4.63	5.50	5.08	5.27	5.29	5.23	5.01c-f
LSMean (cultivar)	4.68e	4.37f	4.59e	5.82a	5.03d	5.25c	4.71e	5.39b	LSD=0.56*
<i>Starch (%)</i>									
Beiseker (AB)	59.23	61.31	59.70	57.15	60.16	59.68	60.72	56.90	59.36c-f
Dawson Creek (BC)	62.73	63.65	61.40	58.31	60.59	60.04	63.02	57.87	60.95b
Donnelly (AB)	56.00	59.46	56.35	52.74	57.60	55.40	56.97	57.14	56.46i
Killam (AB)	60.89	62.50	60.43	56.42	60.18	58.77	60.70	56.98	59.61cd
Nampa (AB)	58.16	58.09	57.22	55.24	58.52	53.95	54.27	58.23	56.71i
Neapolis (AB)	62.56	62.75	60.48	57.75	61.33	59.14	59.59	59.06	60.33b
Sexsmith (AB)	60.48	59.78	57.16	54.92	58.96	58.25	60.25	57.69	58.44h
St. Albert (AB)	63.16	62.64	61.54	59.35	61.72	58.70	56.55	63.03	60.84b
Brandon (MB)	62.11	61.77	59.30	56.30	59.69	58.37	60.67	56.61	59.35d-f
Portage (MB)	61.68	62.31	59.75	55.89	58.37	56.58	62.61	56.70	59.24c-g
Rosebank (MB)	61.40	62.36	58.66	54.97	58.66	58.55	60.67	56.56	58.98e-h
Souris (MB)	64.74	63.24	60.89	58.31	62.03	58.72	60.97	57.42	60.79b
Winnipeg (MB)	64.83	65.09	62.51	58.47	62.05	60.16	63.25	60.45	62.10a
Lake Lenore (SK)	61.87	61.90	59.99	57.28	60.22	58.37	61.42	57.71	59.84c
Rosthern (SK)	61.32	60.00	58.58	57.00	60.03	56.78	60.65	55.69	58.76f-h
Saskatoon (SK)	60.82	61.46	59.36	56.52	58.08	58.08	60.60	55.32	58.78f-h
Valparaiso (SK)	63.16	62.53	61.10	57.56	60.31	59.79	61.77	58.84	60.63b
Watrous (SK)	60.78	62.06	59.40	57.39	60.46	58.30	60.13	57.39	59.49c-e
Wilkie (SK)	61.46	61.28	57.18	56.62	59.38	56.82	59.68	55.68	58.51gh
Yorkton (SK)	61.42	61.55	60.31	56.95	59.13	58.04	60.09	57.96	59.43c-e
LSMean (cultivar)	61.44a	61.79a	59.57c	56.76f	59.87bc	58.12d	60.23b	57.66e	LSD=1.94*

Table 3. (continued)

Locations	Cultivar								LS Mean (location)
	CD	DB	FL	HF	JD	LG	MG	SB	
<i>Protein (%)</i>									
Beiseker (AB)	17.11	16.12	15.40	18.29	17.10	17.77	16.13	18.46	17.05f-i
Dawson Creek (BC)	18.87	19.32	19.55	20.47	17.69	20.60	18.63	19.76	19.36b
Donnelly (AB)	19.08	19.65	20.07	20.94	18.67	20.91	19.27	21.28	19.98ab
Killam (AB)	17.46	17.10	17.33	18.97	16.04	18.90	17.25	18.38	17.68c-e
Nampa (AB)	19.98	20.22	18.03	21.26	19.62	21.52	21.23	20.03	20.24a
Neapolis (AB)	17.01	17.32	16.52	18.27	15.91	18.25	17.76	17.56	17.33e-h
Sexsmith (AB)	17.48	18.06	17.94	18.92	16.37	19.88	17.57	19.41	18.20cd
St. Albert (AB)	16.16	17.63	15.33	18.49	16.90	17.31	17.40	16.46	16.96h-j
Brandon (MB)	17.04	17.30	17.61	19.25	16.44	19.05	16.39	18.21	17.66de
Portage (MB)	15.64	17.38	17.08	18.41	15.58	18.25	16.32	16.90	16.94hi
Rosebank (MB)	16.76	16.71	17.53	19.30	16.55	19.38	17.35	18.00	17.70c-e
Souris (MB)	16.39	16.66	15.85	17.96	15.09	18.27	15.31	16.30	16.48ij
Winnipeg (MB)	12.86	14.13	13.54	14.86	12.68	14.23	14.09	14.92	13.92k
Lake Lenore (SK)	16.03	16.69	16.45	17.95	15.09	17.64	16.04	17.50	16.67ij
Rosthern (SK)	17.00	18.12	17.89	18.50	15.57	18.74	17.99	18.04	17.73c-f
Saskatoon (SK)	15.98	16.09	15.66	17.34	15.89	20.06	16.04	21.23	17.29e-h
Valparaiso (SK)	15.21	16.01	16.44	17.24	14.74	17.86	15.86	16.52	16.23j
Watrous (SK)	15.96	17.69	17.06	17.98	15.21	18.49	16.64	17.68	17.09f-i
Wilkie (SK)	17.72	17.44	19.07	19.14	16.07	18.75	18.22	19.67	18.26c
Yorkton (SK)	16.30	17.30	16.92	19.05	17.02	18.54	16.93	18.54	17.57e-g
LSMean (cultivar)	16.8d	17.35c	17.06cd	18.63a	16.21e	18.72a	17.12cd	18.24b	LSD=1.71*
<i>Fat (%)</i>									
Beiseker (AB)	6.94	6.52	8.58	9.57	8.73	8.65	7.12	9.74	8.23bc
Dawson Creek (BC)	6.93	6.37	8.11	9.47	8.65	8.04	6.63	9.49	7.96c-e
Donnelly (AB)	9.30	9.03	10.3	12.0	10.6	9.40	6.56	9.60	9.60a
Killam (AB)	6.87	6.44	8.52	8.72	8.69	7.69	6.80	8.91	7.83d-f
Nampa (AB)	7.79	7.70	9.04	9.28	7.83	9.63	9.11	8.55	8.62b
Neapolis (AB)	7.49	8.15	9.11	9.01	9.25	8.24	7.80	9.56	8.58b
Sexsmith (AB)	8.79	8.28	9.61	10.6	9.70	8.71	7.99	10.9	9.32a
St. Albert (AB)	6.33	6.00	7.57	8.81	5.91	8.14	8.68	7.95	7.42g-j
Brandon (MB)	7.12	6.64	8.71	8.96	8.69	8.07	6.50	8.87	7.94cd
Portage (MB)	6.33	6.26	7.95	7.58	7.86	6.93	5.51	7.75	7.02j
Rosebank (MB)	7.02	6.73	8.23	8.74	8.40	7.65	6.70	8.48	7.74d-h
Souris (MB)	6.39	6.55	7.88	8.19	7.78	7.13	5.85	7.67	7.18ij
Winnipeg (MB)	6.71	6.77	8.49	8.88	8.84	7.30	6.54	8.84	7.80d-g
Lake Lenore (SK)	6.98	6.76	8.54	8.28	8.61	7.48	7.12	8.45	7.78d-g
Rosthern (SK)	6.54	6.63	8.28	8.06	8.65	7.46	6.02	8.14	7.47f-i
Saskatoon (SK)	6.53	6.10	7.92	9.65	8.53	7.13	6.09	8.49	7.55e-i
Valparaiso (SK)	7.06	6.86	7.72	8.95	8.57	7.74	6.41	8.14	7.68d-h
Watrous (SK)	6.46	6.29	8.09	8.48	8.55	7.21	6.56	8.32	7.50g-i
Wilkie (SK)	6.88	6.79	8.77	8.53	8.56	7.62	6.89	8.54	7.82c-h
Yorkton (SK)	7.01	7.21	7.83	7.58	7.60	7.65	6.82	8.04	7.47hi
LSMean (cultivar)	7.07e	6.90e	8.46c	8.96a	8.50bc	7.89d	6.88e	8.72ab	LSD=1.09*

Table 3. (continued)

Locations									LS Mean
	CD	DB	FL	HF	JD	LG	MG	SB	(location)
<i>Ash (%)</i>									
Beiseker (AB)	1.94	1.84	1.84	1.87	1.87	1.99	1.94	2.05	1.92d-h
Dawson Creek (BC)	1.62	1.62	1.57	1.60	1.58	1.70	1.60	1.58	1.61j
Donnelly (AB)	1.42	1.39	1.50	1.61	1.49	1.48	1.44	1.64	1.50k
Killam (AB)	1.91	1.85	1.92	2.03	1.85	2.02	1.97	1.88	1.93d-f
Nampa (AB)	1.36	1.33	1.29	1.44	1.36	1.32	1.37	1.23	1.34l
Neapolis (AB)	1.81	1.83	1.84	1.91	1.83	1.98	1.91	1.87	1.87gh
Sexsmith (AB)	1.33	1.31	1.39	1.40	1.35	1.40	1.34	1.31	1.35l
St. Albert (AB)	1.86	1.78	1.84	2.00	1.91	1.96	1.94	1.80	1.89e-h
Brandon (MB)	1.74	1.63	1.75	1.78	1.74	1.87	1.83	1.75	1.76i
Portage (MB)	1.98	2.04	2.09	2.11	1.99	2.15	1.93	2.17	2.06b
Rosebank (MB)	1.85	1.85	1.97	2.05	2.00	2.11	2.08	2.04	1.99bc
Souris (MB)	2.14	2.13	2.02	2.32	2.17	2.25	2.14	2.24	2.18a
Winnipeg (MB)	2.08	1.92	2.07	2.17	1.95	2.14	1.98	2.02	2.04b
Lake Lenore (SK)	1.97	1.89	1.95	2.05	1.89	2.03	1.96	1.96	1.96cd
Rosthern (SK)	1.93	1.93	2.04	2.03	1.89	2.11	2.10	2.03	2.01bc
Saskatoon (SK)	1.87	1.90	2.00	2.06	1.86	2.02	2.00	2.05	1.97b-e
Valparaiso (SK)	1.90	1.75	1.96	2.06	1.81	2.10	1.85	2.05	1.94c-g
Watrous (SK)	1.90	1.88	1.91	1.96	1.85	2.02	1.91	1.89	1.92d-h
Wilkie (SK)	1.83	1.72	1.76	1.79	1.80	2.04	1.85	1.94	1.84h
Yorkton (SK)	1.89	1.81	1.81	1.85	1.93	1.98	1.98	1.90	1.89f-h
LSMean (cultivar)	1.82de	1.77f	1.83c-e	1.90ab	1.81ef	1.93a	1.86cd	1.87bc	LSD=0.20*
<i>SDF (%)^b</i>									
Beiseker (AB)	5.00	4.71	7.20	7.86	4.78	6.49	4.82	7.53	6.05f-i
Dawson Creek (BC)	5.49	5.86	8.94	8.88	8.82	5.87	6.11	6.73	7.09ab
Donnelly (AB)	5.21	6.34	5.57	7.18	6.62	5.76	5.59	6.39	6.08f-i
Killam (AB)	5.63	5.53	5.61	7.15	6.39	5.78	6.08	6.48	6.08g-i
Nampa (AB)	6.96	6.79	6.85	6.75	6.70	8.65	7.98	7.55	7.28a
Neapolis (AB)	5.73	6.26	6.81	7.50	6.80	6.66	6.40	7.23	6.68b-e
Sexsmith (AB)	5.03	4.91	5.58	6.86	6.90	5.88	5.87	5.46	5.81hi
St. Albert (AB)	4.95	4.76	5.49	4.90	6.19	7.20	7.10	6.47	5.88hi
Brandon (MB)	5.10	5.92	5.57	6.34	6.96	6.95	6.57	6.66	6.26f-h
Portage (MB)	6.16	6.36	7.27	7.55	6.66	6.93	5.42	8.19	6.82a-d
Rosebank (MB)	5.93	6.20	6.24	7.17	6.30	5.03	6.55	6.81	6.28f-h
Souris (MB)	5.89	5.96	5.93	8.04	6.80	5.83	5.80	6.55	6.35c-h
Winnipeg (MB)	5.85	5.17	5.43	6.43	6.33	5.95	5.91	6.67	5.97hi
Lake Lenore (SK)	5.56	5.39	4.87	5.68	7.26	5.93	5.70	6.16	5.82i
Rosthern (SK)	5.91	5.70	6.76	7.68	6.97	6.67	5.54	7.04	6.53b-g
Saskatoon (SK)	6.23	5.72	7.15	8.16	7.56	6.37	6.73	7.56	6.94a-c
Valparaiso (SK)	6.66	5.61	5.03	6.29	7.35	5.54	6.63	6.89	6.25e-i
Watrous (SK)	5.33	5.26	5.64	6.52	6.78	5.97	6.11	6.79	6.05g-i
Wilkie (SK)	5.81	5.12	5.79	8.40	6.27	6.60	5.05	6.65	6.21e-i
Yorkton (SK)	5.80	6.00	6.33	7.06	6.60	7.01	6.13	6.43	6.42d-f
LSMean (cultivar)	5.71d	5.68d	6.20c	7.12a	6.75b	6.35c	6.10c	6.81b	LSD=1.35*

Table 3. (continued)

Locations	CD	DB	FL	HF	JD	LG	MG	SB	LS Mean (location)
<i>IDF (%)^c</i>									
Beiseker (AB)	8.70	6.18	4.61	6.32	5.65	6.63	7.88	5.91	6.49c
Dawson Creek (BC)	5.96	5.01	5.18	5.85	6.44	6.01	5.19	5.67	5.66e-h
Donnelly (AB)	6.83	6.27	7.65	7.42	6.91	7.14	7.09	7.23	7.07b
Killam (AB)	5.29	5.36	5.05	5.87	5.14	5.95	4.87	5.56	5.39hi
Nampa (AB)	5.45	4.92	5.54	6.23	5.67	6.65	6.67	5.91	5.88d-f
Neapolis (AB)	5.49	4.92	4.91	6.07	5.21	5.59	5.46	5.71	5.42g-i
Sexsmith (AB)	7.50	7.62	8.54	8.05	7.40	6.21	7.97	9.13	7.80a
St. Albert (AB)	5.38	5.38	5.67	5.86	5.25	6.34	6.79	5.61	5.78d-g
Brandon (MB)	6.05	5.16	5.55	6.73	5.58	5.75	5.34	6.26	5.80ef
Portage (MB)	4.97	5.17	5.09	5.54	5.07	5.50	5.52	5.48	5.29hi
Rosebank (MB)	5.85	6.40	5.15	7.57	6.45	5.58	6.06	6.32	6.17cd
Souris (MB)	4.62	5.16	5.18	5.44	4.91	6.55	5.33	6.38	5.44f-i
Winnipeg (MB)	5.49	5.11	4.71	7.10	5.91	6.43	4.85	6.83	5.80ef
Lake Lenore (SK)	5.69	5.01	4.65	6.19	4.71	5.41	4.92	7.23	5.48g-i
Rosthern (SK)	6.42	5.14	6.50	5.17	4.50	6.77	6.17	5.49	5.77e-g
Saskatoon (SK)	5.73	5.19	4.59	7.78	5.59	6.40	4.63	5.95	5.73e-h
Valparaiso (SK)	4.31	4.74	6.14	8.03	4.07	5.38	4.40	3.91	5.12i
Watrous (SK)	5.42	5.05	4.77	7.62	5.10	5.71	5.03	6.30	5.63e-h
Wilkie (SK)	6.57	6.58	7.36	5.95	5.85	5.12	5.48	4.85	5.97de
Yorkton (SK)	5.39	5.33	5.47	6.67	5.40	6.14	6.31	5.77	5.81ef
LSMean (cultivar)	5.85bc	5.49d	5.62cd	6.57a	5.54d	6.06b	5.80c	6.07b	LSD=1.07*

^aCD, CDC Dancer; DB, Derby; FL, Furlong; HF, HiFi; JD, Jordan; LG, Leggett; MG, Morgan; and SB, SW Betania are the oat cultivars.

^bSDF, soluble dietary fibre.

^cIDF, insoluble dietary fibre.

LSMeans within cultivar or location with different letters are significantly different ($p < 0.05$).

*LSD is the least significant difference for the interaction of cultivar and growing location at $p < 0.05$.

Aqueous solubility of oat β -glucan at 37°C

Detailed results showing the effects of growing location, oat cultivar and the location by cultivar interaction for β -glucan solubility are presented in Table 4. The β -glucan solubility in water was evaluated at 37°C to reflect physiological conditions. Solubilization of β -glucan from the flour matrix is dictated by its molecular weight, the ratio of β -(1,3) to β -(1,4) linkages as well as its interactions with the other components (Wang and Ellis 2014; Zhao et al. 2014). The β -glucan solubility for all cultivar and location combinations ranged from 22.30-40.94% (Table 4).

Based on the growing location only, oat grown in Donnelly had the highest β -glucan solubility (36.45%) and oat grown in Watrous had the lowest (26.48%). With respect to cultivar, the highest β -glucan solubility was for HiFi (34.28%) while the lowest was for Furlong (28.44%) (Table 4). It is interesting to note that based on the cultivar effect, HiFi had both the highest β -glucan content and solubility while for the location effect, oat grown in Donnelly, had the lowest β -glucan content but the highest β -glucan solubility. β -Glucan solubility was significantly influenced by growing location, oat cultivar and the location by cultivar interaction. In a review by Tiwari and Cummins (2009), genotype, environmental conditions and food processing operations, are all factors that have an effect on the solubility properties of β -glucan. Moreover, the water solubility of β -glucan is influenced by the presence of β -(1,3) linkages. According to Doehlert and Simsek (2012), both environment and genotype had a significant influence in the fragment frequencies of DP3 and DP4, which consequently can change the functional properties of β -glucan such as solubility.

Viscosity of oat β -glucan in a flour slurry

β -Glucan viscosity was evaluated by consecutive fixed speed tests at shear rates of 1.29 s^{-1} to 129 s^{-1} . Oat β -glucan dispersions exhibit a non-Newtonian fluid behavior known as pseudoplastic or shear thinning (Ryu et al. 2012; Zhao et al. 2014). This behavior is reflected in the decrease in apparent viscosity with increasing shear rates. In this study, the power-law or Ostwald de Waele model was used to determine the flow behavior index (n) and the consistency coefficient (k) in order to describe the β -glucan flow behavior. The power-law model is given by the following equation (Lee and Inglett 2007):

$$\tau = k \dot{\gamma}^n \quad (\text{Eq. 1})$$

where τ is the shear stress (Pa), $\dot{\gamma}$ is the shear rate (s^{-1}), k is the consistency coefficient ($Pa\ s^n$) and n is the flow behavior index. According to this model, dispersions with a value of $n < 1$ show a shear thinning behavior, those with $n > 1$ are fluids with shear thickening behavior and $n = 1$ are Newtonian fluids (Chhabra 2008). According to Zhao et al. (2014), the molecular weight of β -glucan is closely related to the consistency coefficient and flow behavior index. The authors reported that as the molecular weight of β -glucan increased, the consistency coefficient (k) increased, however, the flow index (n) decreased.

The viscosities (mPa-s) of oat β -glucan dispersions based on oat cultivar, growing locations and the interaction of cultivar and growing location at shear rates of $1.29\ s^{-1}$, $12.9\ s^{-1}$ and $129\ s^{-1}$ are presented in Table 4. Results show that oat cultivar, growing location, and shear rate influence the viscosity of oat β -glucan dispersions. The influence of oat cultivar on viscosity was similar to that of solubility (Table 4). On average, HiFi had the highest β -glucan viscosity while Furlong had the lowest for all shear rates. Although β -glucan viscosity is mainly influenced by oat cultivar, growing location and the interaction also have a significant effect on this property (Table 5). Oat grown in Rosebank recorded the highest viscosity (1150 mPa-s) measured at $1.29\ s^{-1}$ and oat grown in St. Albert recorded the lowest viscosity (736 mPa-s) (Table 4). At shear rate $12.9\ s^{-1}$, the highest viscosity was for Portage oat (335 mPa-s), and the lowest for Wilkie oat (234 mPa-s) while at $129\ s^{-1}$, the highest was also for Portage (79 mPa-s) and the lowest for Beiseker (59 mPa-s).

The flow behavior index (n) and consistency coefficient (k) of 0.5% (w/w) β -glucan dispersions at $20^\circ C$ are also shown in Table 4. According to the values reported for n (0.39 - 0.49), all β -glucan dispersions showed shear thinning fluid behavior. These numbers are considerably

lower than those reported for pure gum systems (Ghotra et al. 2009). HiFi showed the lowest flow behavior index ($n = 0.39$), which represents a higher degree of shear thinning. Furlong, on the other hand, had the highest flow behavior index ($n = 0.48$), which corresponds to a lower degree of shear thinning. The shear thinning behavior is exhibited by the decrease in viscosities with increasing shear rates (Table 4). For example, the viscosity of HiFi decreased from 1422 mPa-s to 82 mPa-s as shear rate increased from 1.29 s^{-1} to 129 s^{-1} , while that for Furlong, only decreased from 633 mPa-s to 55 mPa-s. Furthermore, the consistency coefficient also varied between oat cultivars. According to the flow behavior index and consistency coefficient, it is possible to suggest that the β -glucan from HiFi has a higher molecular weight than that of Furlong. The flow behavior index (n) of oat β -glucan dispersions as influenced by growing locations had a smaller range (0.42-0.49) than that of cultivar influence. In accordance with other studies, the aqueous oat β -glucan solutions exhibit a shear thinning behavior (Lazaridou et al. 2004; Ryu et al. 2012; Zhao et al. 2014). The consistency coefficient also differed among oat grown in different locations; however, a comparison of k values is only possible when n values are the same (Nguyen and Nguyen 2012). For example, oat grown in Beiseker, Brandon, and Portage had an n value of 0.43, therefore a comparison of their k values (consistency coefficient) is possible. The k values reported are 1.09, 1.28 and 1.43 for Beiseker, Brandon and Portage respectively (Table 4) and the LSD value of k for the location effect is 0.19. Therefore, we can conclude that β -glucan from Portage grown oat had a higher molecular weight than those of Beiseker and Brandon.

Table 4. The solubility, viscosity and flow behavior of β -glucan dispersions^a.

Locations	Cultivar								LSMean (location)
	CD	DB	FL	HF	JD	LG	MG	SB	
<i>Solubility (%)</i>									
Beiseker (AB)	35.51	24.78	26.68	37.90	28.36	29.95	28.26	39.60	31.38c-e
Dawson Creek (BC)	32.16	30.51	29.50	35.86	31.06	39.84	31.72	32.30	32.87bc
Donnelly (AB)	40.94	37.29	34.36	37.05	32.20	38.45	30.66	40.67	36.45a
Killam (AB)	32.71	30.81	28.48	35.87	31.64	29.21	30.12	27.97	30.85de
Nampa (AB)	36.66	38.07	29.88	38.18	31.11	29.37	38.37	29.22	33.86b
Neapolis (AB)	30.67	31.30	27.73	31.30	26.11	29.65	29.26	29.32	29.42fg
Sexsmith (AB)	32.62	34.29	30.02	37.11	29.08	38.03	28.82	34.18	33.02bc
St. Albert (AB)	36.04	31.83	28.61	33.69	28.84	33.94	38.23	30.34	32.69bc
Brandon (MB)	30.78	29.64	27.07	32.84	27.16	28.52	26.39	30.30	29.09g
Portage (MB)	28.22	28.69	28.45	33.23	31.53	27.86	29.58	27.12	29.33e-h
Rosebank (MB)	25.83	24.89	26.95	34.23	25.82	27.49	25.92	27.74	27.36i
Souris (MB)	27.58	27.87	27.53	32.36	26.22	27.18	31.35	22.57	27.83g-i
Winnipeg (MB)	27.03	25.47	26.23	33.28	26.50	29.31	23.79	25.41	27.13i
Lake Lenore (SK)	25.23	27.21	25.95	31.38	23.91	28.58	22.30	36.51	27.63hi
Rosthern (SK)	29.05	29.11	29.05	34.22	26.57	28.32	29.20	29.99	29.44e-g
Saskatoon (SK)	29.23	26.85	25.97	35.12	30.05	34.87	26.48	30.57	29.89d-g
Valparaiso (SK)	34.99	28.22	27.29	34.41	31.89	32.03	27.58	33.24	31.21c-f
Watrous (SK)	27.50	25.79	23.92	31.36	23.96	26.05	23.83	29.41	26.48i
Wilkie (SK)	31.49	29.64	35.41	30.47	32.23	35.11	28.35	33.56	32.03b-d
Yorkton (SK)	33.36	30.72	29.80	35.78	29.18	33.06	31.01	28.88	31.47cd
LSMean (cultivar)	31.38b	29.65c	28.44d	34.28a	28.67cd	31.34b	29.06cd	30.94b	LSD=5.17*
<i>β-glucan viscosity at shear rate 1.29 s⁻¹(mPa s)</i>									
Beiseker (AB)	871	668	669	1316	762	659	710	1434	886d-i
Dawson Creek (BC)	510	789	484	1416	579	556	692	1263	786f-i
Donnelly (AB)	1014	755	841	1275	995	750	714	1488	979b-e
Killam (AB)	826	624	583	1424	698	577	468	1166	796g-j
Nampa (AB)	687	645	753	702	555	1171	1189	697	800e-i
Neapolis (AB)	731	724	561	1048	648	787	802	883	773i
Sexsmith (AB)	809	639	516	1241	833	504	608	1140	786f-i
St. Albert (AB)	843	609	699	595	366	1214	1137	377	730i
Brandon (MB)	976	823	770	1638	1014	769	734	1520	1031bc
Portage (MB)	989	1003	865	1983	1152	818	996	1371	1147ab
Rosebank (MB)	1041	759	768	2086	1125	842	1154	1453	1153a
Souris (MB)	820	873	652	1687	758	682	713	1224	926c-g
Winnipeg (MB)	572	580	540	1774	950	830	511	1391	894d-h
Lake Lenore (SK)	851	772	521	1617	720	784	522	1750	942c-e
Rosthern (SK)	879	874	695	1722	950	770	558	1732	1022a-d
Saskatoon (SK)	773	600	582	1488	1090	935	640	1651	970b-e
Valparaiso (SK)	858	842	518	1571	910	432	547	1920	950c-f
Watrous (SK)	654	636	502	1632	888	726	458	1765	908d-h
Wilkie (SK)	650	555	536	1018	613	983	577	1108	755h-j
Yorkton (SK)	820	655	735	1344	770	971	802	1198	912d-f
LSMean (cultivar)	809cd	721de	640e	1429a	819c	788cd	727cde	1327b	LSD=416*

Table 4. (continued)

Locations	Cultivar								LSMean (location)
	CD	DB	FL	HF	JD	LG	MG	SB	
<i>β-glucan viscosity at shear rate 12.9 s⁻¹(mPa s)</i>									
Beiseker (AB)	255	198	191	343	220	205	211	385	251g-k
Dawson Creek (BC)	192	262	183	376	188	205	244	357	251h-k
Donnelly (AB)	322	250	262	364	289	255	235	426	300b-d
Killam (AB)	270	218	203	383	219	206	166	325	249ij
Nampa (AB)	236	226	234	241	192	343	328	235	255f-j
Neapolis (AB)	236	236	191	308	207	246	241	264	241j
Sexsmith (AB)	269	223	191	344	252	187	210	345	253f-j
St. Albert (AB)	266	211	221	208	142	364	358	147	240ij
Brandon (MB)	297	258	242	422	273	246	231	391	295c
Portage (MB)	314	302	277	537	326	270	302	387	339a
Rosebank (MB)	357	233	237	508	311	274	329	386	329ab
Souris (MB)	277	277	213	471	240	233	232	354	287c-h
Winnipeg (MB)	200	196	188	443	266	263	179	367	263e-j
Lake Lenore (SK)	273	246	179	418	218	259	185	435	276c-h
Rosthern (SK)	276	263	219	429	273	246	192	446	293c-e
Saskatoon (SK)	255	204	201	411	289	295	216	441	289c-g
Valparaiso (SK)	264	262	177	387	274	162	186	468	272c-i
Watrous (SK)	216	218	179	392	257	245	171	442	265e-i
Wilkie (SK)	215	192	189	292	191	309	195	324	238ij
Yorkton (SK)	258	217	227	361	236	289	242	341	271d-h
LSMean (cultivar)	262b	235c	210d	382a	243bc	255b	233c	363a	LSD=87*
<i>β-glucan viscosity at shear rate 129 s⁻¹(mPa s)</i>									
Beiseker (AB)	62	51	48	73	54	53	53	83	60hi
Dawson Creek (BC)	54	66	51	79	49	56	63	79	62f-i
Donnelly (AB)	80	66	65	82	68	68	61	94	73bc
Killam (AB)	67	58	55	83	55	56	47	74	62hi
Nampa (AB)	62	59	57	63	50	79	74	61	63e-i
Neapolis (AB)	60	61	52	72	53	63	60	63	60i
Sexsmith (AB)	70	62	55	76	62	54	58	82	65d-i
St. Albert (AB)	65	55	55	56	43	84	85	44	61g-i
Brandon (MB)	73	65	61	89	62	62	59	83	69cd
Portage (MB)	78	73	70	111	75	70	74	85	79a
Rosebank (MB)	73	59	59	101	71	69	77	83	74b
Souris (MB)	73	70	58	102	62	63	63	81	71bc
Winnipeg (MB)	56	53	52	92	64	67	51	81	65e-h
Lake Lenore (SK)	68	62	49	88	54	66	52	90	66d-f
Rosthern (SK)	69	65	57	88	65	63	54	93	69b-e
Saskatoon (SK)	65	54	54	87	64	72	57	92	68c-e
Valparaiso (SK)	65	66	50	79	66	49	52	95	65e-i
Watrous (SK)	56	58	49	81	62	63	48	91	64e-i
Wilkie (SK)	57	55	53	68	50	76	53	75	61g-i
Yorkton (SK)	65	57	58	78	59	70	60	78	65e-g
LSMean (cultivar)	66b	61c	55d	82a	59c	65b	60c	80a	LSD=14*

Table 4. (continued)

Locations	Cultivar							LSMean (location)	
	CD	FL	HF	JD	LG	MG	SB		
<i>n – the β-glucan flow behavior index</i>									
Beiseker (AB)	0.44	0.46	0.44	0.38	0.44	0.46	0.45	0.39	0.43fg
Dawson Creek (BC)	0.49	0.46	0.49	0.39	0.45	0.48	0.47	0.41	0.45b-f
Donnelly (AB)	0.46	0.48	0.45	0.41	0.43	0.49	0.48	0.41	0.45c-f
Killam (AB)	0.46	0.49	0.52	0.38	0.46	0.50	0.52	0.4	0.47bc
Nampa (AB)	0.48	0.49	0.43	0.48	0.50	0.39	0.37	0.48	0.45b-f
Neapolis (AB)	0.46	0.47	0.48	0.43	0.46	0.46	0.44	0.46	0.46b-d
Sexsmith (AB)	0.48	0.50	0.53	0.40	0.44	0.53	0.50	0.43	0.48ab
St. Albert (AB)	0.44	0.49	0.44	0.50	0.63	0.40	0.42	0.62	0.49a
Brandon (MB)	0.46	0.47	0.48	0.38	0.40	0.46	0.45	0.37	0.43fg
Portage (MB)	0.46	0.44	0.46	0.37	0.42	0.47	0.44	0.40	0.43fg
Rosebank (MB)	0.43	0.45	0.45	0.36	0.41	0.46	0.43	0.39	0.42g
Souris (MB)	0.49	0.46	0.49	0.40	0.47	0.49	0.48	0.42	0.46b-e
Winnipeg (MB)	0.49	0.47	0.48	0.35	0.41	0.44	0.49	0.37	0.44e-g
Lake Lenore (SK)	0.45	0.46	0.50	0.37	0.45	0.47	0.51	0.35	0.45d-f
Rosthern (SK)	0.46	0.45	0.47	0.36	0.43	0.47	0.50	0.37	0.44d-g
Saskatoon (SK)	0.46	0.46	0.47	0.40	0.40	0.44	0.46	0.39	0.44e-g
Valparaiso (SK)	0.45	0.46	0.51	0.36	0.44	0.54	0.50	0.35	0.45c-f
Watrous (SK)	0.47	0.47	0.51	0.34	0.42	0.47	0.51	0.35	0.44d-f
Wilkie (SK)	0.48	0.51	0.51	0.42	0.47	0.45	0.49	0.42	0.47a-c
Yorkton (SK)	0.45	0.47	0.45	0.41	0.45	0.43	0.45	0.43	0.44d-f
LSMean (cultivar)	0.46b	0.47ab	0.48a	0.39e	0.45c	0.47ab	0.47ab	0.41d	LSD=0.06*
<i>k – the β-glucan consistency coefficients</i>									
Beiseker (AB)	1.07	0.81	0.81	1.65	0.93	0.81	0.87	1.80	1.09d-j
Dawson Creek (BC)	0.62	0.98	0.59	1.79	0.71	0.68	0.86	1.59	0.98f-j
Donnelly (AB)	1.26	0.93	1.04	1.60	1.24	0.93	0.89	1.88	1.22b-e
Killam (AB)	1.03	0.77	0.72	1.79	0.86	0.71	0.58	1.45	0.99g-j
Nampa (AB)	0.86	0.81	0.93	0.87	0.69	1.46	1.47	0.87	1.00e-j
Neapolis (AB)	0.90	0.89	0.69	1.31	0.80	0.97	0.99	1.10	0.96j
Sexsmith (AB)	1.00	0.79	0.64	1.56	1.04	0.62	0.75	1.43	0.98f-j
St. Albert (AB)	1.05	0.76	0.87	0.74	0.46	1.52	1.43	0.48	0.91ij
Brandon (MB)	1.21	1.02	0.95	2.06	1.25	0.95	0.90	1.90	1.28bc
Portage (MB)	1.23	1.24	1.08	2.46	1.43	1.01	1.23	1.73	1.43ab
Rosebank (MB)	1.33	0.93	0.95	2.64	1.39	1.05	1.44	1.82	1.44a
Souris (MB)	1.01	1.08	0.80	2.13	0.93	0.84	0.87	1.53	1.15c-g
Winnipeg (MB)	0.69	0.70	0.66	2.21	1.16	1.02	0.62	1.72	1.10d-i
Lake Lenore (SK)	1.05	0.95	0.64	2.02	0.89	0.97	0.64	2.19	1.17c-e
Rosthern (SK)	1.09	1.08	0.85	2.16	1.18	0.95	0.68	2.18	1.27a-d
Saskatoon (SK)	0.95	0.73	0.71	1.89	1.35	1.16	0.78	2.09	1.21b-e
Valparaiso (SK)	1.06	1.04	0.63	1.98	1.13	0.53	0.67	2.41	1.18c-f
Watrous (SK)	0.81	0.78	0.62	2.02	1.09	0.90	0.56	2.21	1.12d-h
Wilkie (SK)	0.80	0.68	0.66	1.27	0.75	1.22	0.71	1.39	0.94h-j
Yorkton (SK)	1.01	0.80	0.90	1.70	0.95	1.20	0.98	1.51	1.13d-f
LSMean (cultivar)	1.00cd	0.89de	0.79e	1.79a	1.01c	0.98cd	0.90cde	1.66b	LSD=0.52*

^aCD, CDC Dancer; DB, Derby; FL, Furlong; HF, HiFi; JD, Jordan; LG, Leggett; MG, Morgan; and SB, SW Betania are the oat cultivars. LSMeans within cultivar or location with different letters are significantly different ($p < 0.05$).

*LSD is the least significant difference for the interaction of cultivar and growing location at $p < 0.05$.

Effects of cultivar, growing location, their interaction and growing year on grain composition and β -glucan properties

The effects of cultivar, growing location, their interaction and growing year on the chemical composition of oat groats and their β -glucan properties are presented in Table 5. The growing year and oat cultivar were the dominant effects for the β -glucan content and contributed to 84.7% and 14.2% of the variation, respectively ($p < 0.01$) (Table 5). This variation is in contrast to that observed by Andersson and Börjesdotter (2011) who reported a 23% variation in β -glucan content due to cultivar, 42% due to the environmental effects and 11% accounted for their interaction. (Saastamoinen et al. 2008) also reported that β -glucan content was mainly influenced by oat cultivar. However, Brunner and Freed (1994) reported β -glucan content was mainly influenced by crop year, while cultivar effect was not significant. The greatest proportion of variation for starch content was attributed to cultivar (81.1%, $p < 0.01$) and year effect was negligible. Cultivar and growing location contributed similarly for protein content and the sum of their effects contributed less than the year effect. For β -glucan properties, year effect was dominant and accounted for over 50% of the variation, followed by cultivar ($< 41\%$) (Table 5). These results can explain the year to year variation in oat flour properties often reported by oat food processors. Additionally, selecting particular oat cultivars instead of the growing location will have a bigger effect in obtaining desirable flour properties.

Correlation between oat grain composition and β -glucan properties

β -glucan content negatively correlated to starch ($r = -0.38$, $p < 0.001$), but positively correlated to protein ($r = 0.39$, $p < 0.001$), fat ($r = 0.28$, $p < 0.001$), ash ($r = 0.27$, $p < 0.001$), SDF ($r = 0.33$,

p<0.001) and IDF (r=0.28, p<0.001) (Table 6). Since β -glucan is a valuable and healthful component of oat, increasing its content through breeding efforts and developing new high β -glucan cultivars is of interest to the industry. It is important to note that, for these particular cultivars this may increase the crude fat content, which can lead to a decrease in the shelf life of oat foods. Furthermore, a positive correlation exists between solubility and viscosity, for all shear rates 1.29 s^{-1} (r=0.51), 12.9 s^{-1} (r= 0.52) and 129 s^{-1} (r=0.53) at p<0.001 (Table 6).

Table 5. Effect of cultivar, growing location, and the interaction of the cultivar and growing location on chemical composition of oat grains and β -glucan properties^a

Characteristics	Cultivar	Growing location	Interaction of Cultivar and Growing location	
			Year	
<i>Chemical composition of oat groats</i>				
β -glucan	14.2*	0.7*	0.3*	84.7*
Starch	81.1*	16.4*	1.4*	0.5ns
Protein	24.6*	23.1*	0.6ns	51.1*
Fat	68.1*	14.2*	1.3*	15.8*
Ash	10.6*	63.2*	0.7ns	24.6*
SDF	31.8*	8.2*	2.4*	56.1*
IDF	28.4*	28.4*	5.3*	36.3*
<i>β-glucan properties</i>				
β -glucan solubility	18.2*	13.1*	1.8*	66.0*
Viscosity at 1.29 s^{-1}	41.0*	3.1*	1.2*	54.3*
Viscosity at 12.9 s^{-1}	29.7*	2.5*	0.9*	66.5*
Viscosity at 129 s^{-1}	22.8*	2.4*	0.8*	73.7*
n^b	40.6*	5.1*	2.9*	50.4*
k^c	40.0*	2.9*	1.1*	55.4*

^aThe results were expressed as percentage of total mean square.

^b n , flow behavior index.

^c k , consistency coefficient.

*Significance levels $p < 0.05$; ns, not significant.

Table 6. Pearson's correlation coefficients (r) for all the variables^a.

	1	2	3	4	5	6	7	8	9	10	11	12	13	14	15
1-Temperature	1.00														
2-Precipitation	0.43***	1.00													
3-BG	-0.00	0.41***	1.00												
4-Starch	0.12**	0.26***	-0.38***	1.00											
5-Protein	-0.30***	-0.16***	0.39***	-0.49***	1.00										
6-Fat	-0.24***	-0.21***	0.28***	-0.51***	0.24***	1.00									
7-Ash	0.39***	0.53***	0.27***	0.11**	-0.17***	-0.27***	1.00								
8-SDF	-0.00	-0.00	0.33***	-0.27***	0.25***	0.37***	0.06	1.00							
9-IDF	-0.07	-0.18***	0.28***	-0.43***	0.26***	0.26***	-0.24***	-0.12**	1.00						
10-BG solubility	-0.13**	-0.36***	-0.04	-0.34***	0.35***	0.29***	-0.24***	0.13**	0.22***	1.00					
11-BG Vis (1.29s ⁻¹)	0.26***	-0.09	0.12**	-0.46***	0.12**	0.33***	0.11*	0.29***	0.25***	0.51***	1.00				
12-BG Vis (12.9s ⁻¹)	0.26***	-0.15***	0.01	-0.45***	0.11*	0.27***	0.08	0.25***	0.24***	0.52***	0.98***	1.00			
13-BG Vis (129s ⁻¹)	0.26***	-0.19***	-0.07	-0.42***	0.11*	0.22***	0.07	0.20***	0.22***	0.53***	0.94***	0.99***	1.00		
14-n ^b	-0.25***	0.06	-0.16***	0.42***	-0.04	-0.35***	-0.08	-0.31***	-0.22***	-0.43***	-0.90***	-0.88***	-0.83***	1.00	
15-k ^c	0.25***	-0.10*	0.11**	-0.47***	0.12**	0.33***	0.10*	0.28***	0.25***	0.51***	1.00***	0.98***	0.94***	-0.90***	1.00

^aSignificance levels: * p<0.05, ** p<0.01, *** p<0.001; Vis, viscosity.

^bn, flow behavior index.

^ck, consistency coefficient.

As shown in Table 4, the oat cultivars with the highest and lowest solubility (HiFi and Furlong, respectively) were also those with the highest and lowest viscosities. This is expected since β -glucan in the cell walls of the grain needs to solubilize before viscosity can develop in the aqueous phase. β -Glucan solubility was not correlated with β -glucan content, but negatively correlated with starch and positively correlated with protein (Table 6). Since the functional properties of β -glucan are known to influence its human health benefits, it is important that oat cultivars with the highest solubility and viscosity be recommended for food use.

Effect of climatic factors on grain composition and β -glucan properties

Climatic factors including daily average temperature and precipitation amount during the growing season were tested for their effects on the grain composition and β -glucan properties (Table 6). Starch, ash, β -glucan viscosity, and the flow consistency coefficient positively correlated with the daily average temperature, whereas, protein, fat, β -glucan solubility, and flow behavior index were negatively correlated with the daily average temperature. In addition, β -glucan content, starch and ash were positively correlated to the precipitation amount during the growing season. On the other hand, protein, fat, IDF, β -glucan solubility, viscosity (12.9-129s⁻¹) and consistency coefficient were negatively correlated with the precipitation amount. Similar to Andersson and Börjesdotter (2011), no correlation was found between β -glucan content and the mean growing season temperature. This is in contrast to other studies, which show that high growth temperature yields a higher β -glucan content (Saastamoinen 1995).

CONCLUSIONS

A significant effect of growing location, oat cultivar, and their interaction “location x cultivar”, as well as growing year, was observed for most of the properties measured in this study, specifically β -glucan content, its solubility and viscosity. Inconsistent rheological behaviors between oat cultivars with similar β -glucan contents have been a challenge for the food processing industry. This may be attributed primarily to variations in the viscosity characteristics of β -glucan resulting from variations in its solubility. HiFi, Leggett, and SW Betania showed relatively higher values of β -glucan content/properties across most growing locations. However, it is important to note that each of these three cultivars, when grown at certain locations, show significantly lower than average values for the above mentioned properties. Since β -glucan viscosity is the key factor attributed to human health benefits of oat, understanding how cultivar and location (environmental conditions) influence β -glucan viscosity is important to ensure consistency in the human physiological efficacy of oat-based food products. The present study clearly suggests that in order to supply oat flour with consistent composition and physicochemical properties, there needs to be an oat grain “binning and blending” strategy established based on β -glucan content, aqueous solubility and viscosity. Furthermore, contract grain production outside the blending approach is also recommended for those products specifically targeted to meet the requirements for including a health claim on the package regarding the risk reduction for cardiovascular diseases.

References

AACC International 2004. Approved methods of the aacc. AACC International, St. Paul, MN, USA.

AOAC International 1997. The official methods of analysis of aoac international. AOAC International, Rockville, MD, USA.

Anderson, J. W., Spencer, D. B., Hamilton, C. C., Smith, S. F., Tietzen, J., Bryant, C. A. and Oeltgen, P. 1990. Oat-bran cereal lowers serum total and ldl cholesterol in hypercholesterolemic men. *Am. J. Clin. Nutr.* 52:495-499.

Andersson, A. A. and Börjesdotter, D. 2011. Effects of environment and variety on content and molecular weight of β -glucan in oats. *J. Cereal Sci.* 54:122-128.

Autio, K., Myllymaki, O., Suortti, T., Saastamoinen, M. and Poutanen, K. 1992. Physical properties of (1-3), (1-4)-beta-d-glucan prepartes isolated from finnish oat varieties. *Food Hydrocolloids* 5:513-522.

Brunner, B. and Freed, R. 1994. Oat grain β -glucan content as affected by nitrogen level, location, and year. *Crop Sci.* 34:473-476.

Chhabra, R. P. 2008. Non-newtonian flow and applied rheology : Engineering applications, 2nd ed. Butterworth-Heinemann, Oxford.

Daou, C. and Zhang, H. 2012. Oat beta-glucan: Its role in health promotion and prevention of diseases. *Compr. Rev. Food Sci. Food Saf.* 11:355-365.

Doehlert, D. C. and Simsek, S. 2012. Variation in β -glucan fine structure, extractability, and flour slurry viscosity in oats due to genotype and environment. *Cereal Chem.* 89:242-246.

European Food Safety Authority. 2011. Scientific opinion on the substantiation of health claims related to beta-glucan from oats and barley and maintenance of normal blood ldl-cholesterol concentrations (id 1236, 1299), increase in satiety leading to a reduction in energy intake (id 851, 851), reduction of post-prandial glycaemic responses (id 821, 824), and "digestive function" (id 850) pursuant to article 13(1) of regulation (ec) no 1924/2006. Page 2207. *European Food Safety Authority Journal*

Food and Drug Administration. 1997. 21 cfr part 101. Food labeling: Health claims; soluble dietary fiber from certain foods and coronary heart disease. Federal register 70:76150-76162.

Ghotra, B. S., Vasanthan, T. and Temelli, F. 2009. Rheological properties of aqueous blends of high purity barley beta-glucan with high purity commercial food gums. *Food Chem.* 117:417-425.

Health Canada. 2010. Summary of assessment of a health claim about oat products and blood cholesterol lowering. Bureau of Nutritional Sciences, Food Directorate, Health Products and Food Branch. .

Johansson, L., Virkki, L., Maunu, S., Lehto, M., Ekholm, P. and Varo, P. 2000. Structural characterization of water soluble beta-glucan of oat bran. *Carbohydr. Polym.* 42:143-148.

Lazaridou, A. and Biliaderis, C. G. 2007. Molecular aspects of cereal β -glucan functionality: Physical properties, technological applications and physiological effects. *J. Cereal Sci.* 46:101-118.

Lazaridou, A., Biliaderis, C. G., Micha-Screttas, M. and Steele, B. R. 2004. A comparative study on structure–function relations of mixed-linkage (1 \rightarrow 3), (1 \rightarrow 4) linear β -d-glucans. *Food Hydrocolloids* 18:837-855.

Lee, S. and Inglett, G. 2007. Effect of an oat β -glucan-rich hydrocolloid (c-trim30) on the rheology and oil uptake of frying batters. *J. Food Sci.* 72:E222-E226.

Nguyen, Q.-H. and Nguyen, N.-D. 2012. Incompressible non-newtonian fluid flows. Pages 42-47 in ed. *Continuum mechanics-progress in fundamentals and engineering applications*. Intech Publications, Rijeka, Croatia.

Peterson, D. M. 1991. Genotype and environment effects on oat beta-glucan concentration. *Crop Sci.* 31:1517-1520.

Price, P. B. and Parsons, J. G. 1975. Lipids of 7 cereal-grains. *J. Am. Oil Chem. Soc.* 52:490-493.

Queenan, K. M., Stewart, M. L., Smith, K. N., Thomas, W., Fulcher, R. G. and Slavin, J. L. 2007. Concentrated oat beta-glucan, a fermentable fiber, lowers serum cholesterol in hypercholesterolemic adults in a randomized controlled trial. *J. Nutr.* 6.

Redaelli, R., Del Frate, V., Bellato, S., Terracciano, G., Ciccoritti, R., Germeier, C. U., De Stefanis, E. and Sgrulletta, D. 2013. Genetic and environmental variability in total and soluble β -glucan in european oat genotypes. *J. Cereal Sci.* 57:193-199.

Ryu, J.-H., Lee, S., You, S., Shim, J.-H. and Yoo, S.-H. 2012. Effects of barley and oat β -glucan structures on their rheological and thermal characteristics. *Carbohydr. Polym.* 89:1238-1243.

Saastamoinen, M. 1995. Effects of environmental factors on the β -glucan content of two oat varieties. *Acta Agric. Scand. Sect. B* 45:181-187.

Saastamoinen, M., Hietaniemi, V. and Pihlava, J.-M. 2008. β -glucan contents of groats of different oat cultivars in official variety, in organic cultivation, and in nitrogen fertilization trials in Finland. *Agric. Food Sci.* 13:68-79.

Saastamoinen, M., Plaami, S. and Kumpulainen, J. 1992. Genetic and environmental variation in beta-glucan content of oats cultivated or tested in Finland. *J. Cereal Sci.* 16:279-290.

Staudte, R. G., Woodward, J. R., Fincher, G. B. and Stone, B. A. 1983. Water-soluble (1 \rightarrow 3), (1 \rightarrow 4)- β -D-glucans from barley (*Hordeum vulgare*) endosperm. iii. Distribution of cellotriosyl and cellotetraosyl residues. *Carbohydr. Polym.* 3:299-312.

Tiwari, U. and Cummins, E. 2009. Factors influencing β -glucan levels and molecular weight in cereal-based products. *Cereal Chem.* 86:290-301.

Tiwari, U. and Cummins, E. 2011. Meta-analysis of the effect of beta-glucan intake on blood cholesterol and glucose levels. *Nutrition* 27:1008-1016.

Wang, Q. and Ellis, P. R. 2014. Oat β -glucan: Physico-chemical characteristics in relation to its blood-glucose and cholesterol-lowering properties. *Br. J. Nutr.* 112:S4-S13.

Welch, R. W. and Lloyd, J. D. 1989. Kernel (1-3) (1-4)-beta-D-glucan content of oat genotypes. *J. Cereal Sci.* 9:35-40.

Wolever, T. M., Tosh, S. M., Gibbs, A. L., Brand-Miller, J., Duncan, A. M., Hart, V., Lamarche, B., Thomson, B. A., Duss, R. and Wood, P. J. 2010. Physicochemical properties of oat β -glucan influence its ability to reduce serum LDL cholesterol in humans: A randomized clinical trial. *Am. J. Clin. Nutr.* 92:723-732.

Wood, P. J., Beer, M. U. and Butler, G. 2000. Evaluation of role of concentration and molecular weight of oat beta-glucan in determining effect of viscosity on plasma glucose and insulin following an oral glucose load. *Br. J. Nutr.* 84:19-23.

Zhao, Q., Hu, X. Z., Guo, Q. B., Cui, S. W., Xian, Y. S., You, S. P., Chen, X. Y., Xu, C. and Gao, X. 2014. Physicochemical properties and regulatory effects on db/db diabetic mice of beta-glucans extracted from oat, wheat and barley. *Food Hydrocolloids* 37:60-68.

APPENDIX II

Apparent amylose determination

The starch samples (20.0 ± 0.1 mg) were weighed into round bottom glass screw cap tubes. Similarly, mixtures of pure potato amylose and amylopectin (0%, 10%, 20%, 40%, 50%, 60%, 70%, 80%, 90%, 100%) for the calibration curve were weighed into round bottom glass screw cap tubes. All tubes were treated with 8 ml of 90% DMSO, mixed vigorously for 2 min and then heat treated in a water bath at 85°C for 15 min with intermittent mixing in order to completely solubilize the starch. The samples were allowed to cool to room temperature for 45 min before diluting to 25 ml with distilled water in a volumetric flask. An aliquot of 1 ml of the diluted solution was then quantitatively transferred and mixed with 40 ml of distilled water in a 50 ml volumetric flask and 5 ml of iodine solution (0.0025 M I₂/0.0065 M KI) were added. The volume was adjusted to 50 ml with distilled water, mixed vigorously and allowed to sit for 15 min for color development. The absorbance of the blue solutions was measured at 600 nm against a reagent blank using a Jenway UV/Vis Spectrophotometer (6320D spectrophotometer, Bibby Scientific, Stone, U.K.). The reagent blank contains all the reagents in the same amounts without the starch. The apparent amylose content of each sample was calculated from the standard curve obtained with pure potato amylose and amylopectin (Sigma-Aldrich, Saint Louis, MO, USA).

Particle size distribution of native starch granules and fractions 2 and 3

METHODOLOGY

The particle size of native starch granules and fraction 3 were determined by laser light scattering with a Mastersizer 3000 system (Malvern Instruments Ltd.) and a Hydro EV pump and stirrer to avoid particle sedimentation. Suspensions containing native starch granules and fraction 3 were diluted until an obscuration rate between 2-10% was achieved. Measurements were conducted at a temperature of 25°C. Three measurements were performed for each run and the mean of triplicated are reported.

The particle size of fraction 2 in suspension were determined by dynamic light scattering with a Zetasizer Nano-S system (Malvern Instruments Ltd.). The fraction 2 suspensions were diluted to 0.1% (w/v) with milliQ water and left to equilibrate at room temperature overnight. Measurements were conducted at a scattering angle 173° in a temperature regulated cell at 25°C. Eleven measurements were performed for each run and the mean of triplicates are reported.

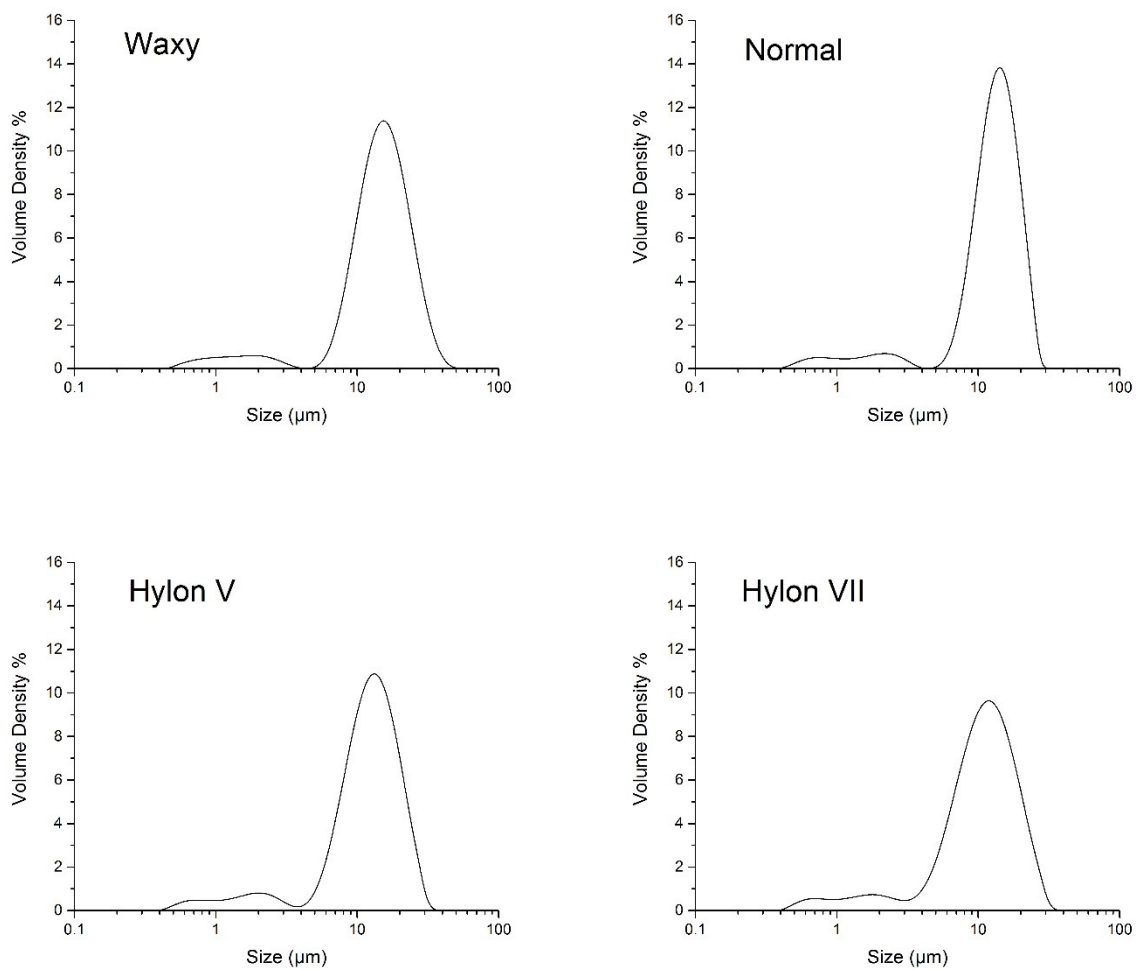


Figure 1. Particle size distribution of native maize starch granules varying in amylose content.

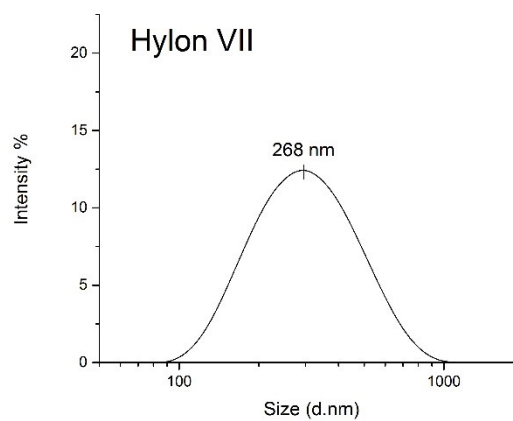
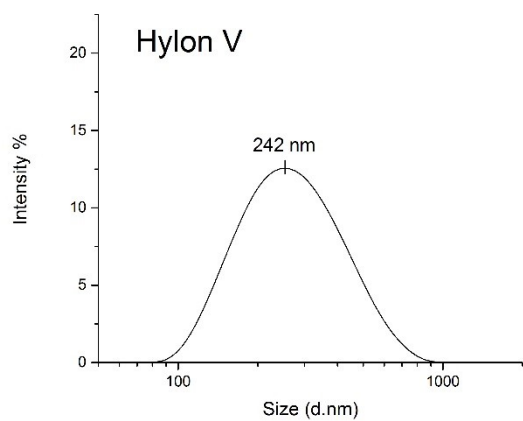
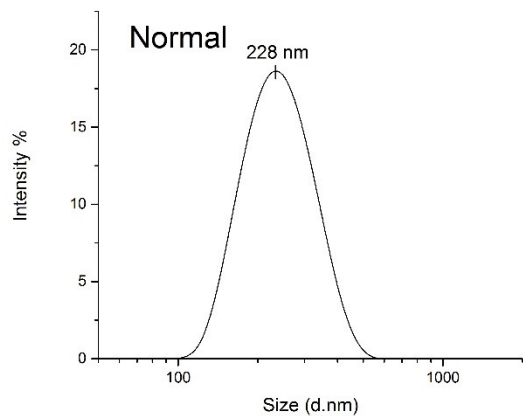


Figure 2. Particle size distribution of fraction 2 collected after 6 days of acid hydrolysis.

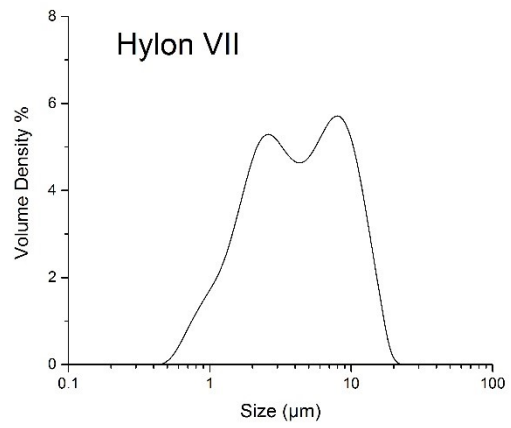
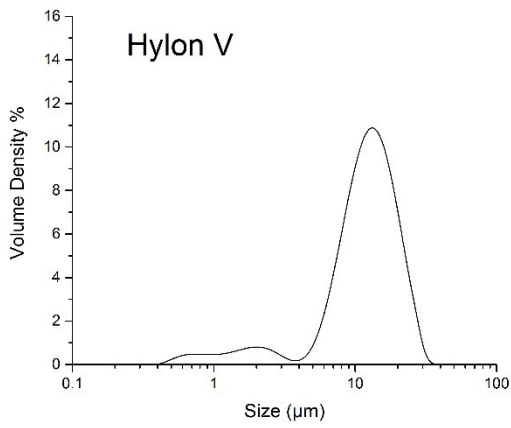
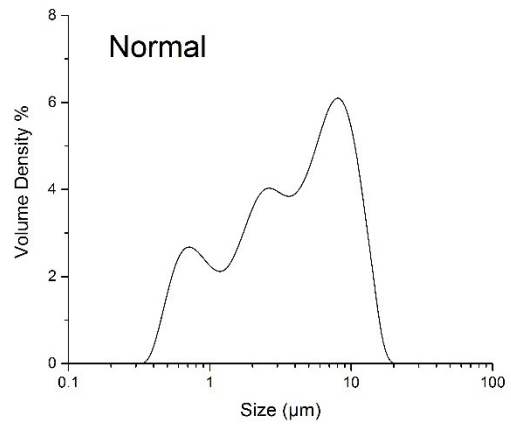
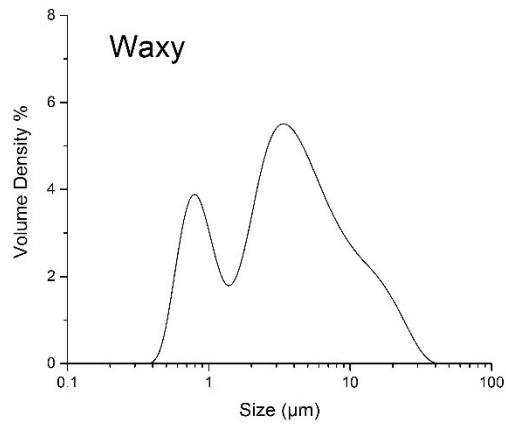


Figure 3. Particle size distribution of fraction 3 collected after 6 days of acid hydrolysis.

Starch isolation from wheat grains

Wheat grains were ground into flour in a Retsch mill (Model ZM 200, Haan, Germany) using a ring size with an aperture size of 0.5 mm. The traditional dough development method was used to isolate pure starch from the whole grain flour. The dough was prepared by combining 75 g of wheat flour with 45 ml deionized water in a dough mixer (Kitchen Aid Professional 600, Canada) at low speed for 10 min, then kneaded for an additional 10 min and allowed to sit for 5 min. The dough ball was placed inside a cheesecloth, washed under dropwise running water and the starch-water slurry collected. The slurry was then filtered using a sieve with an aperture size of 75 μm (W.W. Tyler, ON, Canada) and the fibre residue on the top of the sieve discarded. The filtrate was centrifuged (3000 xg for 15 min), the supernatant was removed and the upper brown layer (tailing protein) was scraped with a spatula and discarded. The bottom layer (starch) was re-suspended in 150 ml of deionized water, centrifuged (3000 xg for 15 min) and the supernatant and brown layer was carefully scraped and discarded. This procedure was repeated two more times, until the brown layer was no longer observed. The pure starch pellet was dried in a 40°C oven overnight and ground using a pestle and mortar.

Starch isolation from barley and oat grains

Barley and oat grains were ground into flour in a Retsch mill (Model ZM 200, Haan, Germany) using a ring size with an aperture size of 0.5 mm. A combination of aqueous alcohol and aqueous extraction was used to isolate the pure starch from barley and oat flour. Ground flour was mixed with 50% ethanol (1:4.5 w/v) in a beaker and gently stirred for 30 min. The slurry was sieved through a 63 μm screen (filtrate 1). The fiber residue on the screen was reslurried with 50% ethanol (1:2.5 w/v) and sonicated (Sonic 300 dismembrator, Systems Corporation, Farmingdale, NY, U.S.A.) with 90% amplitude for 30 min under continuous stirring. The slurry was filtered again through a 63 μm screen (filtrate 2). The fiber residue on the screen was again reslurried again with 50% ethanol (1:2 w/v), homogenized at 30,000 rpm for 10 min (PT 2000, Kinematica AG LITTAU, Switzerland) followed by filtration through a 63 μm screen once again (filtrate 3). Filtrates 1, 2 and 3 were pooled and centrifuged (1500 xg for 10 min). The supernatant was discarded and crude starch collected as the pellet. The crude starch was reslurried with water (1:2 w/v) and sodium dodecyl sulfate (0.25% w/w according to the original flour weight), and sonicated for 30 min with constant stirring. The slurry was centrifuged (7500 xg for 10 min) and the supernatant and upper gray layer (protein) carefully removed with a spatula. The bottom white layer (starch) was washed three more times with distilled water and a final wash with 95% ethanol. The pure starch was dried in a 40°C oven overnight and ground using a pestle and mortar.

APPENDIX III

Comparison of geometry types for rheological tests

BACKGROUND

All rheological tests in this thesis were performed using the rheometer HR-3 from TA Instruments (DE, U.S.A.), with the following geometries available: cone and plate (40 mm diameter, 2° angle, 53 µm gap, steel), parallel plate (40 mm diameter, 1000 µm gap, steel) and cup and bob (concentric cylinder cup radius 15 mm, DIN rotor radius 14 mm, aluminium). Ideally, it is expected that measuring the same sample with different geometries should yield similar results. However, the selection of the geometry type is usually done considering a variety of limitations including the materials consistency, presence or absence of solid particles, and test modes. For example, concentric cylinders (cup and bob) are ideal when working with fluids showing a very low viscosity due to the large shear surface area; however, a drawback is the need for a very large sample size (approx. 22 ml). Cone and parallel plate geometries are available in different diameters usually ranging from 20 to 60 mm. If a variety of sizes are available, higher diameters are recommended when analyzing low viscosity fluids.

GOAL AND OBJECTIVE

This study investigated which geometry is the most suitable for the rheological tests performed. The objective was to determine the variability in the data when using different

geometry types to evaluate a low viscosity (0.5% λ -carrageenan) and a high viscosity (0.5% xanthan) system under continuous shear, frequency sweep and temperature ramp tests.

INSTRUMENT CALIBRATIONS

The following rheometer and geometry calibration were conducted to improve the quality of the data. A geometry calibration known as rotation mapping was performed before each continuous shear test in order to minimize the error when the torque values of the samples fall below 1 $\mu\text{N}\cdot\text{m}$ (close to machine limits). This calibration is particularly important when evaluating very low viscosity samples and the calibration is recommended each time the geometry is removed for cleaning. Prior to conducting dynamic rheological tests, a series of calibrations including oscillatory mapping, geometry inertia and gap temperature compensation were performed. Oscillatory mapping is an instrument calibration recommended when samples with low torque and low displacement are being analyzed. Geometry inertia is particularly important during high frequency oscillations and low viscosity samples. During heating and cooling, thermal expansion and contraction of the upper and lower geometries can result in incorrect rheological measurements unless the equipment is correctly calibrated. The gap temperature compensation calibration allows the stage to move according to the expansion coefficient of the geometry during any temperature ramp and temperature sweep tests. The cone and parallel plate geometries were calibrated for the gap temperature compensation using a heating rate of $2^\circ\text{C}/\text{min}$ from 25°C to 90°C . The expansion coefficients were $0.569 \mu\text{m}/^\circ\text{C}$ and $0.757 \mu\text{m}/^\circ\text{C}$, respectively. Since the gap size in the cone and plate ($53 \mu\text{m}$) is much smaller than that of the parallel plate ($1000 \mu\text{m}$), incorrectly calibrating the geometry can lead to large error.

MATERIALS AND METHODOLOGY

The λ -carrageenan (Ticaloid 750) and xanthan (Tixacan pre-hydrated rapid-3) powders were provided by TIC Gums (White Marsh, MD, U.S.A). The experiments were performed at a gum concentration of 0.5% (w/v). The gums were solubilized in milli-Q water at room temperature and mixed until they appeared homogenous. Before each rheological test, the samples were allowed to equilibrate at 25°C for 2 min. The apparent viscosity was determined by a continuous shear test from 0.01-100 s⁻¹ and at a temperature of 25°C. The viscoelastic properties as a function of frequency (0.1-100 rad/s) were evaluated at 25°C and an oscillating strain of 2% (linear viscoelastic region). The viscoelastic properties as a function of temperature (25 to 90°C, heating rate of 2°C/min) were evaluated at an oscillating strain of 2% and frequency of 1 rad/s. All necessary calibrations were performed and precautions were taken to adjust for geometry expansion as well as to prevent moisture evaporation while testing at elevated temperatures.

RESULTS AND DISCUSSION

Apparent viscosity as a function of shear rate

Figure 1 shows the apparent viscosity vs shear rate between different geometry types. When evaluating a low viscosity system (as is 0.5% λ -carrageenan), the cup and bob has better sensitivity at lower shear rates because it is not affected by the surface tension. On the other hand, the cone and parallel plate are unable to accurately detect the viscosity at very low shear rates when the torque values of the samples fall below 1 μ N.m (close to machine limits). Above the shear rate of 1 s⁻¹, the apparent viscosity of 0.5% λ -carrageenan was nearly similar between

the cone and parallel plate geometries. In the high viscosity system (0.5% xanthan), all three geometries showed comparable results (Figure 1).

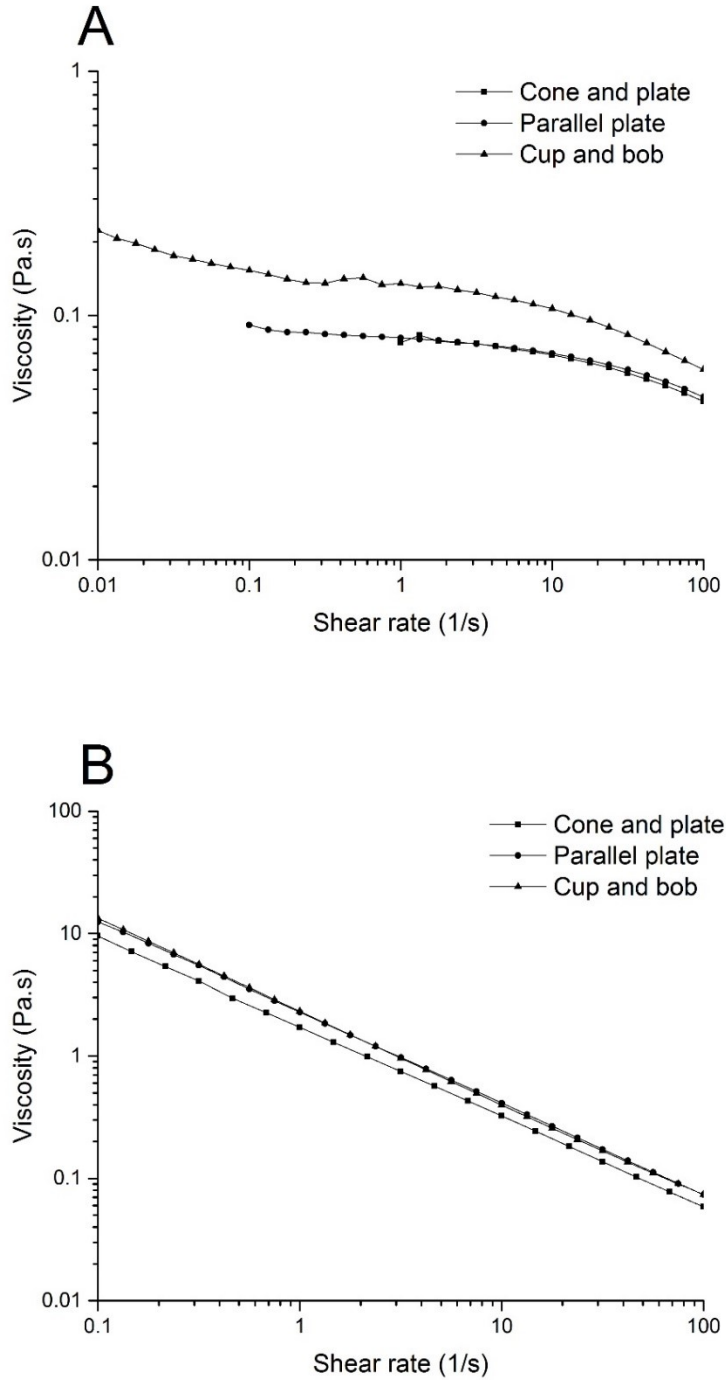


Figure 1. Apparent viscosity of (A) 0.5% CAR; (B) 0.5% XAN using different geometry types.

Viscoelastic properties as a function of frequency

The storage modulus (G') and loss modulus (G'') of 0.5% λ -carrageenan and 0.5% xanthan using different geometry types is presented in Figure 2. Regardless of the geometry, the viscoelastic properties of 0.5% λ -carrageenan were highly frequency dependent and the curves showed similar trends. Furthermore, between 1-2 rad/s, the storage modulus for all geometry types were comparable. For 0.5% xanthan, all samples behaved like an elastic gel ($G' > G''$) and were more stable to frequency changes. G' and G'' were nearly identical for cone and parallel plate, while some deviation was observed in the cup and bob geometry.

Viscoelastic properties as a function of temperature

The storage modulus (G') and loss modulus (G'') of 0.5% λ -carrageenan and 0.5% xanthan as a function of temperature using different geometry types is presented in Figure 3. All three geometries had a solvent trap (with silica oil) and a solvent trap cover, which were used to create a stable environment and prevent moisture loss during heating. Moreover, the gap temperature compensation feature was enabled when using the cone and parallel plate geometries. A large variation was observed in the viscoelastic properties of 0.5% λ -carrageenan, evaluated using different geometries. However, cone and plate and cup and bob both showed a similar transition point, which was not detected in the parallel plate. Data obtained using the parallel plate were significantly noisier and had lower reproducibility than compared to the other two geometries. In 0.5% xanthan, the same curve trend and transition point was observed regardless of the geometry type. The storage modulus (G') and loss modulus (G'') values for cone and parallel plate were nearly similar while the values for cup and bob were significantly higher.

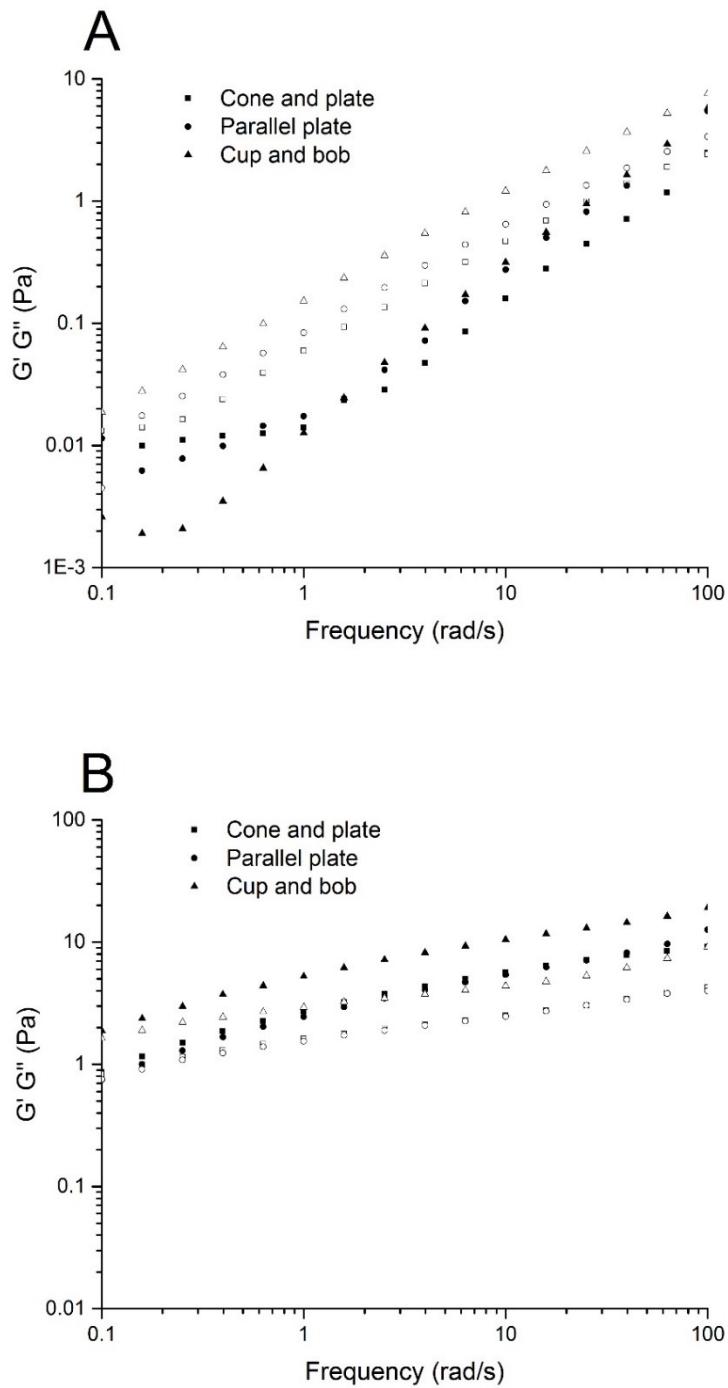


Figure 2. Storage modulus (G') and loss modulus (G'') of (A) 0.5% CAR; (B) 0.5% XAN as a function of frequency evaluated using different geometry types. The solid symbols represent G' and the open symbols represent G'' .

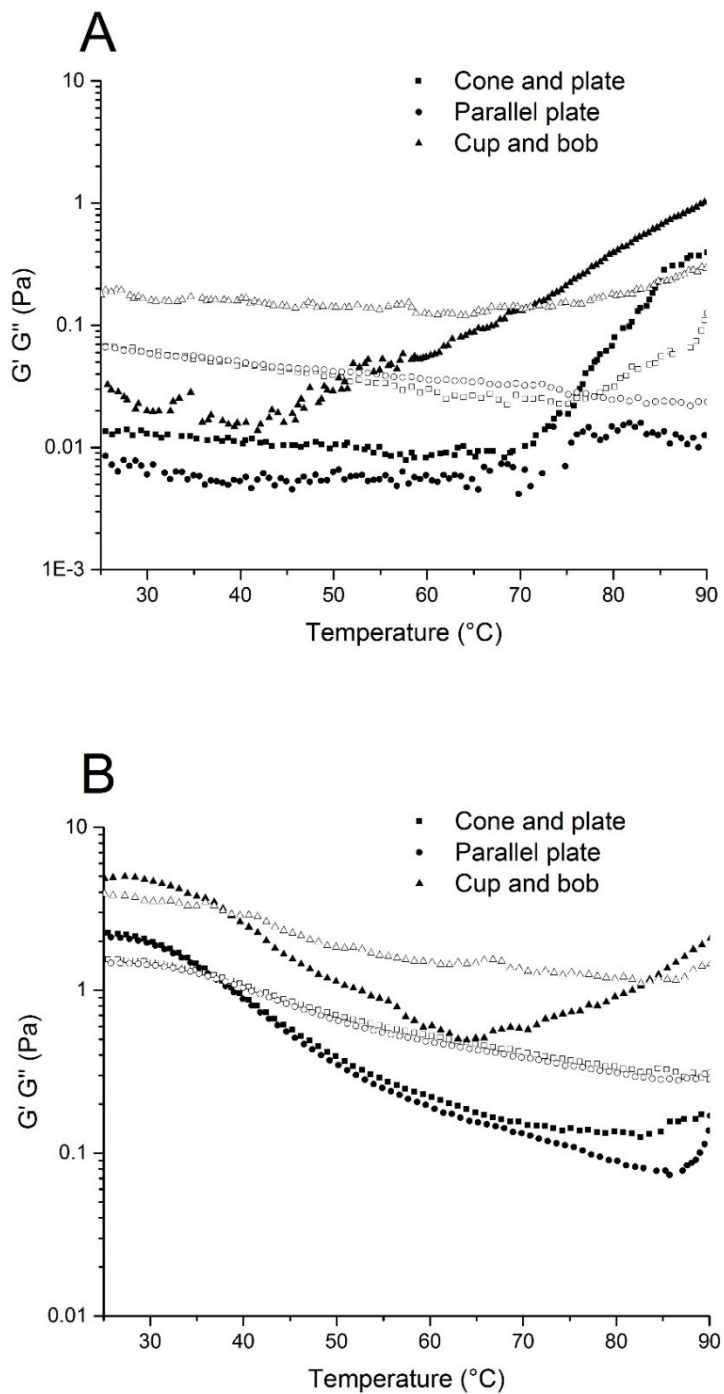


Figure 3. Storage modulus (G') and loss modulus (G'') of (A) 0.5% CAR; (B) 0.5% XAN as a function of temperature evaluated using different geometry types. The solid symbols represent G' and the open symbols represent G'' .

Typically heating ramps are not done with the cone geometry due to the very small gap size (53 μm) used in comparison to the parallel plate (1000 μm). The cone and plate geometry used in this study has an expansion coefficient of 0.569 $\mu\text{m}/^\circ\text{C}$, therefore by heating from 25 to 90 $^\circ\text{C}$, the gap size can change by up to 37 μm . This is a substantial change that can lead to very significant rheological errors. In comparison, using the parallel plate (expansion coefficient, 0.757 $\mu\text{m}/^\circ\text{C}$) heating from 25 to 90 $^\circ\text{C}$ would lead to a gap change of 49 μm . Since the gap is originally 1000 μm , a reduction of 49 μm is not that significant, and thus can be used without the need of a gap adjustment. In order to prevent this, modern rheometers have a gap temperature compensation feature, which can be enabled to adjust the gap size with any temperature change. If available, this is recommended when any thermal testing is done with either the cone or the parallel plate geometries. Figure 4 shows the gap size variability during the temperature ramp test when this feature was enabled. In both geometries, the gap size values remain within ± 0.05 μm of the original gap size and thus the error due to a gap reduction is minimized.

CONCLUSIONS

The cone and plate was selected as the most appropriate geometry for the following reasons: 1) small sample size required (less than 1 ml), 2) good data reproducibility 3) comparable results with cup and bob geometry (ideal for low viscosity) and 4) visibly lower moisture loss during temperature treatments in comparison to parallel plate.

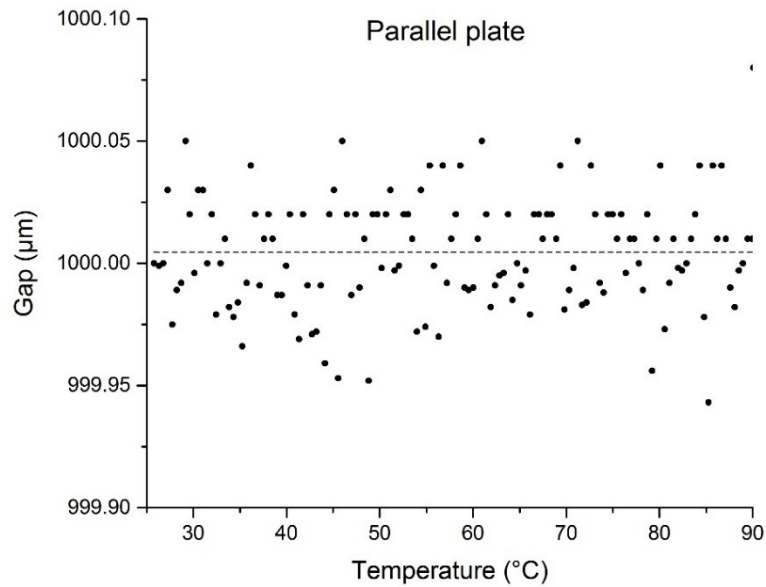
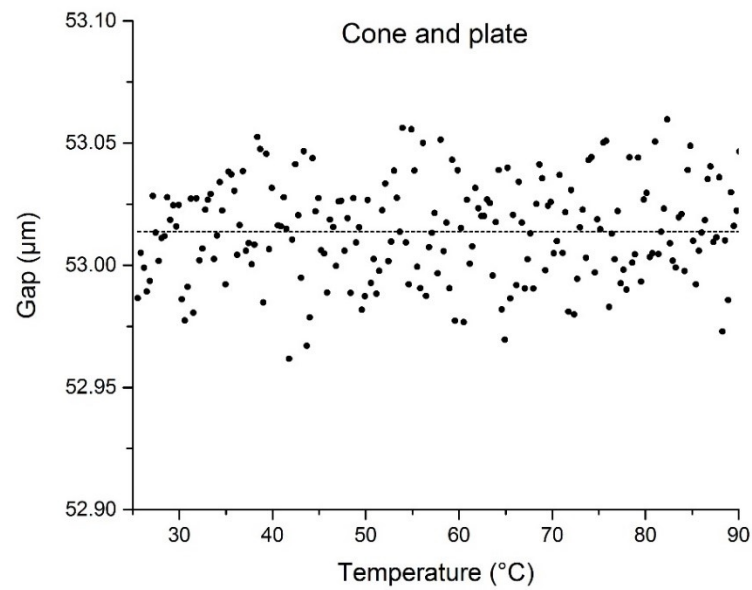


Figure 4. Gap size variability during the temperature ramp test using the cone and plate, and parallel plate geometries. Dashed line is the average gap size.